

**DISEQUILIBRIUM OF NATURALLY OCCURRING
RADIONUCLIDES AND DISTRIBUTION OF TRACE
ELEMENTS IN A HIGHLY MINERALISED ZONE**

By

**ADITI CHAKRABARTY PATRA
BHABHA ATOMIC RESEARCH CENTRE**

*A Thesis submitted to the
Board of Studies in Chemical Science Discipline*

*In partial fulfillment of requirements
For the Degree of*

**DOCTOR OF PHILOSOPHY
of
HOMI BHABHA NATIONAL INSTITUTE**



June, 2010

Homi Bhabha National Institute

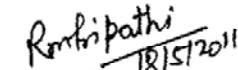
Recommendations of the Viva Voce Board

As members of the Viva Voce Board, we certify that we have read the dissertation prepared by Smt. Aditi Chakrabarty Patra entitled "Disequilibrium of Naturally Occurring Radionuclides and Distribution of Trace Elements in a Highly Mineralised Zone" and recommend that it may be accepted as fulfilling the dissertation requirement for the Degree of Doctor of Philosophy.

Chairman - Prof. Y.S. Mayya

Date:  18/5/11

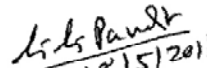
Convener - Prof. R. M. Tripathi

Date:  18/5/2011

External Examiner – Prof. N. Karunakara

Date:  18/05/11

Member 1 - Prof. G. G. Pandit

Date:  18/5/2011

Member 2 - Prof. M. P. Chougankar

Date:  18/5/11

Member 3 - Prof. B. K. Sapra

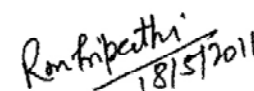
Date:  18/5/11

Final approval and acceptance of this dissertation is contingent upon the candidate's submission of the final copies of the dissertation to HBNI.

I hereby certify that I have read this dissertation prepared under my direction and recommend that it may be accepted as fulfilling the dissertation requirement.

Date: 18-05-2011

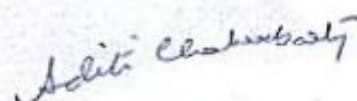
Place: Trombay, Mumbai

 18/5/2011
Guide – Prof. R. M. Tripathi

STATEMENT BY AUTHOR

This dissertation has been submitted in partial fulfillment of requirements for an advanced degree at Homi Bhabha National Institute (HBNI) and is deposited in the Library to be made available to borrowers under rules of the HBNI.

Brief quotations from this dissertation are allowable without special permission, provided that accurate acknowledgement of source is made. Requests for permission for extended quotation from or reproduction of this manuscript in whole or in part may be granted by the Competent Authority of HBNI when in his or her judgment the proposed use of the material is in the interests of scholarship. In all other instances, however, permission must be obtained from the author.



Aditi Chakrabarty Patra

DECLARATION

I, hereby declare that the investigation presented in the thesis has been carried out by me. The work is original and has not been submitted earlier as a whole or in part for a degree / diploma at this or any other Institution / University.



Aditi Chakrabarty Patra

Dedicated to my Family

ACKNOWLEDGEMENTS

It is indeed a great opportunity for me to express my sincere gratitude and profound respect to my supervisor, Prof. R. M. Tripathi, for his constant guidance, ceaseless encouragement and continuous support during my research work. If I should thank one most for being able to submit my thesis from this Institute it would be my supervisor; any word to express my gratitude towards him would fall short.

It is my great privilege to acknowledge Shri. H. S. Khushwaha and Shri. V. D. Puranik for their kind help and support.

Chairman (Prof. Y. S. Mayya) and members (Prof. G. G. Pandit, Prof. M. P. Chougankar and Prof. B. K. Sapra) of the doctoral committee are gratefully acknowledged for their critical review, suggestions and help during the progress review, comprehensive review and pre-synopsis viva-voce.

It is my great pleasure to acknowledge the help and encouragement rendered by all the members of EAD and RPS (NF). Members of UCIL and HPU, Jaduguda are also gratefully acknowledged for their valuable suggestions and help. I wish to thank my colleagues Shri. S. K. Sahoo, Smt. S. J. Sartandel, Smt. S. Mohapatra, Shri. S. Chinnaesakki, Shri. C. J. Sumesh, Shri. P. Lenka, Smt. S. Kadam and Kum. K. S. Shrimal for their suggestions, support and encouragement during the course of this research work.

I wish to express my sincere gratitude and indebtedness to my grandparents, parents, in-laws, sister, sister-in-law, uncle and other family members and all well wishers for their love, blessings and support. The help and encouragement received from my friends is also gratefully acknowledged.

Finally I would like to thank my husband Abhijit for his relentless support and affection. I am grateful to have him as my best friend since the last seven years; without his help, patience and understanding, it would hardly be possible to come out with this thesis.

Aditi Chakrabarty Patra

CONTENTS

	Page No.
SYNOPSIS	xi-xx
LIST OF FIGURES	xxi-xxvi
LIST OF TABLES	xxvii-xxix
CHAPTER 1	
INTRODUCTION	
1.1. Natural radioactivity and radioactive disequilibrium in a mineralised region	1-2
1.1.1. Natural radioactivity, its sources, types and distribution	
in environment	2-8
1.1.2. Occurrences and geochemistry of radionuclides	8-14
1.1.3. Radioactive equilibrium and disequilibrium condition	
in environment	14-19
1.2. Trace elements in environment	
1.2.1. Origin, distribution and association	20-26
1.2.2. Variation with physicochemical parameters	27-29
1.3. Extraction and Leaching	
1.3.1. Definition and methods	29-35
1.3.2. Variation with physical conditions of leaching	36-38
1.4. Physiography of the region	38-39
1.4.1. Climate	39-39
1.4.2. Geology	40-43
1.5. Scope of the present thesis	43-44

CHAPTER 2

SAMPLING AND ANALYTICAL TECHNIQUES

2.1. Sampling	45-45
2.1.1. Criteria for selection of sampling locations and matrices sampled	46-46
2.1.2. Sampling methodology and sample collection	46-50
2.1.3. Sample processing and preservation	50-53
2.2. Analytical techniques	53-54
2.2.1. High Resolution Gamma Spectrometry	54-70
2.2.2. Instrumental Neutron Activation Analysis	70-82
2.2.3. Laser Fluorimetry	82-87
2.2.4. Quality control	88-90

CHAPTER 3

EXPERIMENTAL STUDIES AND SALIENT OBSERVATIONS

3.1. Physicochemical characterisation of samples	91-91
3.1.1. Particle size distribution	91-94
3.1.2. Moisture Content	94-95
3.1.3. Organic matter content	95-95
3.1.4. pH	95-96
3.1.5. Cation exchange capacity	96-98
3.1.6. Humic acid content	98-100
3.2. Measurements through High Resolution Gamma Spectrometry	100-102
3.2.1. Distribution of radionuclides in soils	102-108
3.2.2. Distribution of radionuclides in host rocks	108-110
3.2.3. Distribution of radionuclides in uranium bearing rocks	110-115

3.2.4. Distribution of radionuclides in wastes	115-121
3.3. Measurements through Instrumental Neutron Activation Analysis	121-122
3.3.1. Distribution of elements in soils	122-128
3.3.2. Distribution of elements in host rocks	128-130
3.3.3. Distribution of elements in uranium bearing rocks	130-132
3.3.4. Distribution of elements in wastes	132-136
3.4. Leaching experiments	136-138
3.4.1. Methodology of semi-dynamic and dynamic leaching experiments	139-140
3.4.2. Variation of different physical conditions	141-141
3.4.3. Variations in uranium concentrations	141-150

CHAPTER 4

RESULTS AND DISCUSSIONS

4.1. Activity and activity ratios of uranium and thorium series radionuclides	151-152
4.1.1. Soils	152-159
4.1.2. Host rocks	159-162
4.1.3. Uranium bearing rocks	162-171
4.1.4. Wastes	171-172
4.2. Trace elemental concentrations and distributions	172-175
4.2.1. Variation with particle size	175-180
4.2.2. Correlation with elements and physicochemical properties	180-185
4.3. Uranium leaching	
4.3.1. Semi-dynamic leaching experiments	
4.3.1.1. Cumulative leach fraction	185-187
4.3.1.2. Controlling Leaching mechanism	187-189
4.3.1.3. Apparent diffusion coefficient	190-191

4.3.1.4. Bulk release	191-192
4.3.2. Dynamic leaching: cumulative leach fraction and associated leaching rate	
4.3.2.1. Effect of pH of leachant	193-196
4.3.2.2. Effect of particle size of sample	196-198
4.3.2.3. Effect of temperature	198-201
CHAPTER 5	
CONCLUSIONS	
5.1. Conclusions	202-205
5.2. Future prospects	206-206
REFERENCES	207-237
LIST OF PUBLICATIONS	238-239

SYNOPSIS

Introduction

A mineralised zone is marked by the presence of elevated levels of certain minerals, which are associated with heavy metals. The extent and nature of mineralisation is highly dependent on the geological setting of the area. Due to the presence of mineral deposits of economically viable grades, mining and extraction of metals are carried out in such mineralised zones. This is also true in the case of naturally occurring radionuclides; mining and extraction are carried out where the minerals of the element of interest for the nuclear energy sector are found in abundance. With these activities, the region gets industrialised and has the potential to pollute the surrounding environment if sufficient safety measures are not taken.

Due to the rapid depletion of reserve fossil fuels, there has been an increasing demand for nuclear power generation and as such there is an endeavour to increase production of uranium; the fuel for nuclear reactors. This has necessitated the identification of prospective uranium mineralised regions, enhanced uranium ore production and optimal performance of the uranium mining and milling processes. For smooth and safe operation of these processes and safe disposal of wastes generated, it is extremely important to understand the environmental distribution and behaviour of elements in these mineralised regions.

Geochemical processes like weathering and leaching, influence the distribution of elements in different environmental matrices and lead to the transport of elements from one location to another with groundwater or surface waters. Study of the environmental levels of radionuclide and trace elements is therefore very important. The environmental distribution of elements can also be employed to identify underlying trends directing towards elemental behaviour or possible environmental pollution.

Apart from the levels of occurrences, transport of elements in the environment is also equally important. Transport/leaching of elements from any matrix by environmental processes is a function of (1) the amount and form of the element, (2) the physicochemical properties and composition of the solid phase and (3) the composition of the liquid phase. Natural radioactive equilibrium/disequilibrium has found wide applicability in transport and migration studies and their timescales, which reflect the openness of a system with respect to geochemical changes. Natural radioactive equilibrium is essentially associated with the uranium and thorium radioactive series present in the environment. Radionuclide mobility can also be assessed through laboratory based leaching studies. Such studies are regularly used for the quantification of rate of leaching of elements from a bulk solid. Another major objective of these studies is to examine the effect of different physical conditions on the rate of leaching. Leaching studies carried over a long time can also be used to ascertain the extent of elemental leaching over geological timescales.

The highly mineralised Singhbhum Shear Zone in Jharkhand state of Eastern India is known for hosting vein/disseminated type of uranium deposits. Mining and processing of low-grade uranium ore commenced in the mid-sixties and is being carried out at different locations in this region. Mostly Archaean or Precambrian formations of granites, schists, quartzites and gneisses are present in this area. Apart from uranium, the region is known for its widespread mineral deposits including copper, nickel and manganese of economically viable grades. The mining and milling operations at the uranium deposits in this region have the potential to redistribute environmentally noxious elements in the surrounding environment if adequate safety measures are not taken during operation of these processes and waste disposal. Distribution and transport of elements in this mineralised region and their leaching characteristics is therefore an important subject area for research.

Scope of the present work

Elements have been present in the environment since the evolution of the earth. Their concentrations vary from region to region depending on the geological formation and geochemistry of the elements. Anthropogenic activities have the potential to disperse elements in the environment, increasing their levels over and above the natural background. Hence it is important to study the distribution of radionuclide and trace and major elements in environmental matrices in the mineralised Singhbhum Shear Zone where mining and milling facilities are operational. Assessment of radionuclide mobility using natural radioactive disequilibrium and leaching experiments will also assist in predicting the possibility of an element to reach groundwater, get transported and subsequently enter the food chain.

The thesis has been divided into five chapters. The contents of each chapter are given in brief in the following sections.

Chapter-I

Introduction

This chapter draws an outline of the thesis. It is divided into three major parts.

The first part addresses the issue of natural radioactivity, properties of radionuclides, their environmental behaviour, their distribution in the environment and natural radioactive series equilibrium/disequilibrium condition. The factors affecting the radioactive equilibrium condition are also described.

The second part of the chapter deals with trace elements, their association and distribution in the environment and their variation with physicochemical parameters.

In the third part, different leaching methodologies and their utility have been discussed. Influence of different physical conditions on the extent of leaching is also covered. An account of the available literature has also been provided in all the aforementioned parts.

The present thesis provides insights on the relatively less explored but significantly important area of radionuclide transport and behaviour in the Singhbhum Shear Zone. A brief discussion on the uranium mineralised region of Singhbhum East district in Jharkhand along with its physiography and geology has also been included.

Chapter-II

Sampling and Analytical techniques

This chapter, divided in two parts, discusses the sampling methodologies and experimental techniques employed in this thesis.

The first part reviews the basic criteria for selection of sampling locations, methods of sampling, sample processing, preservation and storage.

The second part discusses the analytical techniques like High Resolution Gamma Spectrometry, used for the quantification of radionuclides in the sampled matrices; Instrumental Neutron Activation Analysis (INAA), used for the quantification of stable elements in the sampled matrices; and Laser Fluorimetry (LF), used for estimation of total uranium in liquid samples. The part also discusses the necessary steps taken for the accuracy and precision of the results and quality control procedures used during analysis of the elements.

Chapter-III

Experimental studies and salient observations

This chapter gives a brief summary of all the important investigations and findings during the course of this study. It is divided into four major parts.

Physicochemical characterisation of the samples through laboratory based standard protocols is discussed in the first part.

The second part deals with the distribution of radionuclides in different matrices around the operating uranium mines in the region.

The third part covers the distribution of trace elements in different environmental matrices. The distribution of elements in the environment depends on the geography of the area, operating geochemical forces and various anthropogenic activities which may cause dispersion and redistribution of the metals in the environment.

The fourth part discusses the methodology of leaching experiments and the variation and effect of various physical conditions/parameters that can affect the leaching process.

Chapter-IV

Results and Discussions

This chapter discusses the findings of the studies carried out and described in the previous chapter. Activity ratios of radionuclides, employed in natural radioactive disequilibrium studies, have been discussed in the first part of this chapter. They have been applied to study the openness of a system to geochemical changes and also acquire an idea of radionuclide mobility from different matrices.

In the second part of this chapter variation of trace elemental concentrations with respect to particle size, inter-elemental relationships and correlation of elemental concentrations with physicochemical properties are elucidated.

The third part of this chapter discusses the results from semi-dynamic and dynamic leaching experiments and the associated rate of leaching. Effects of variation in the physical conditions on the rate of leaching are also examined.

Salient features of the findings

1. Heterogeneous distribution of radionuclide activity in matrices was observed due to their crustal nature of origin.
2. Radionuclide activity concentrations were found to be nearly constant and the lowest in Turamdih among the uranium deposits. Radionuclide activity concentrations in soils were observed to be of disseminated type and are not solely dependent on proximity to uranium deposits but mainly dependent on the regional geology and elemental geochemistry.
3. Average ^{238}U , ^{226}Ra and ^{232}Th activity concentrations were observed to be 4457 ± 2179 Bq/kg, 4940 ± 2478 Bq/kg and 30.4 ± 20.2 Bq/kg in ore samples from the uranium deposits of Jaduguda, Bhatin, Narwapahar and Turamdih; 107.8 ± 37.1 Bq/kg, 107.1 ± 37.6 Bq/kg and 59.8 ± 25.7 Bq/kg in non-uranium bearing rocks; 76.1 ± 59.6 Bq/kg, 81.5 ± 53.3 Bq/kg and 65.1 ± 22.7 Bq/kg in surface soils and 640.9 ± 101.1 Bq/kg, 1713.4 ± 75.7 Bq/kg and 38.3 ± 4.3 Bq/kg in uranium tailings.
4. The activity and activity ratios do not show a very clear trend with depth, in the deposits. No inference could be drawn on the enhancement or reduction in the mobility of radionuclides with increasing depth.
5. The $^{226}\text{Ra}/^{238}\text{U}$ daughter–parent pair was observed to be in secular equilibrium condition in the uranium deposits, especially Turamdih while $^{231}\text{Pa}/^{235}\text{U}$, $^{227}\text{Ac}/^{235}\text{U}$ and $^{228}\text{Th}/^{228}\text{Ra}$ daughter–parent pairs are not in secular equilibrium in most samples

from the deposits. The activity ratios of $^{226}\text{Ra}/^{230}\text{Th}$ suggest that the deposits were not closed to groundwater movement for a maximum time period of 8ky.

6. The Thiel plot of $^{234}\text{U}/^{238}\text{U}$ vs. $^{230}\text{Th}/^{238}\text{U}$ activity ratios indicates uranium accumulation and complex processes of uranium redistribution, but an overall slight shift from secular equilibrium.
7. The analysis of uranium in soils show deviation from secular equilibrium and it is attributed to the system being open. On the other hand, deviation from secular equilibrium in the case of uranium bearing tailings is attributed to the fact that the tailings are chemically treated. Non-uranium bearing rocks are in secular equilibrium, indicating that these are unfractured rocks which have not been affected by groundwater movements.
8. The analyses of various samples indicates that the Cu and Ba concentrations ranged from hundreds to thousands of ppm; Ni, Cu, Cr, U, La and Sm ranged from tens to hundreds of ppm and Sc, Co, Th and As concentrations were in tens of ppm in uranium ores. The Co, Sc, Ni, Cs, Sb, Th and Rb concentrations were in tens of ppm; Ce, La and Cu ranged from tens to hundreds of ppm in surface soils. The Co, Ba, Cr, Cu, U, Ni range from tens to hundreds of ppm; As, Hg, Th, Cd, Sb, Se, Sc range from sub ppm to ppm concentrations in uranium tailings. The Zn, Rb, Cr and Co concentrations range from tens to hundreds of ppm; Ni, Cu, Th and As concentrations were in tens of ppm; Se, U in ppm; Hg, Cs, Cd, Sb and Sc in sub-ppm to ppm range in non-uranium bearing rocks. Major elements, like Fe, Ca etc. indicate the presence of calcite in soils and pyrite nature of uranium tailings.
9. Different extents of negative Ce and Eu anomaly in uranium and non-uranium bearing rocks reflected uranium mineralisation in the uranium bearing rocks; La/Sm ratio

indicates light rare earth element fractionation and fractional condensation at the time of solidification of magma

10. Trace elements in soils and uranium tailings concentrate in smaller particle sizes due to their association with minerals like kaolinite, chlorite, vermiculite etc. in the smaller particles; Mass balance of total elemental concentrations and sum of elemental concentrations in particle size fractionated samples shows a good match.
11. The siderophile elements Ni-Co are well-correlated; the chalcophile elements Se-Hg and Cd-Hg were found to be well correlated in non-uranium bearing rocks. This is due to the elemental properties and subsequent association with minerals in the environment. The Na and K concentrations are positively correlated with trace elements and negatively correlated with uranium concentrations in uranium bearing rocks, indicating the mineralogical association of the elements with primary minerals of Na and K, like plagioclase, feldspar etc.
12. The cation exchange capacity (CEC) is positively correlated with moisture content, pH, clay content and Humic acid content in soils, showing the dependence of these properties on each other.
13. The leaching of uranium from soils, ores and tailings was very slow, being faster in the initial stage and then attaining a near steady state condition in laboratory experiments under semi-dynamic conditions carried over a long time. The apparent diffusion coefficient (cm^2/s) ranged from 10^{-10} to 10^{-11} .
14. In dynamic conditions of leaching, cumulative percent of U leached from soils was highest under basic pH conditions, varying from 5-16%, 7-45% and 42-70% in neutral, acidic and basic pH, respectively. For U tailings cumulative percent of U leached varied from 0.8-2.8%, 1.9-17.2% and 0.4-0.8% in the neutral, acidic and basic pH, respectively. Leaching rate ranged from $6 \times 10^{-4} \text{ h}^{-1}$ to $1.8 \times 10^{-3} \text{ h}^{-1}$, $8 \times 10^{-4} \text{ h}^{-1}$ to

$6 \times 10^{-3} \text{ h}^{-1}$ and $5 \times 10^{-3} \text{ h}^{-1}$ to $1 \times 10^{-2} \text{ h}^{-1}$ from soils and $2 \times 10^{-4} \text{ h}^{-1}$ to $4 \times 10^{-4} \text{ h}^{-1}$, $1.4 \times 10^{-3} \text{ h}^{-1}$ to $2.3 \times 10^{-3} \text{ h}^{-1}$ and $1 \times 10^{-4} \text{ h}^{-1}$ to $4 \times 10^{-4} \text{ h}^{-1}$ from uranium tailings in the neutral, acidic and basic pH, respectively.

15. The leaching rate was observed to be variable for the different particle sizes, being higher in the lower particle sizes. This is due to the different reactive surface area of the different particle sizes.
16. With the increase in temperature the cumulative fraction of U leached increases; equilibrium condition is reached in the case of soil samples but not for U tailings samples in the time period of nearly 100hrs. The cumulative percent of U leached varied from 0.9-11.9%, and 2.5-14.2% for soils and 0.3-0.6% and 0.7-1.2% for U tailings at 25°C and 60°C respectively. The leach rate varies in same order of magnitude at 25°C and 60°C.
17. The leach rate under all the experimental conditions is observed to be low, indicating less mobility of uranium in the studied environment.

Chapter-V

Conclusions and future prospects

This chapter summarises the main results from the thesis and proposes future work that can be carried out. The thesis presents an idea of the distribution of radionuclides and trace elements in a mineralised region in the vicinity of natural uranium deposits. It also elucidates the status of radioactive equilibrium in the environment and assesses the mobility of uranium present therein. Some of the matrices display complex uranium redistribution and show a slight shift from near secular equilibrium whereas others are in near secular equilibrium condition. Trace elements are observed to concentrate in smaller particle sizes and their interrelationships are a function of their nature and association.

The extent of uranium leached from the matrices is relatively low with considerably low leach rates, indicating less elemental mobility in this mineralised environment

In future, studies will be carried out on the depth profile of radionuclides, trace element concentrations and the equilibrium status of the natural radioactive series in soils and uranium tailings ponds to get a better idea of interaction of the same with groundwater. Disequilibrium studies will also be applied to ground water and soil pore water in this area. Since the environmental behaviour of an element is dependent on parameters like its oxidation state, chemical environment/ chemical association in the matrix, such information will be of aid in assessing its mobility, toxicity and geochemical behaviour. Studies on the chemical forms of uranium in different matrices using single extraction (using specific solvents) and sequential extraction techniques have already been carried out in our lab. Preliminary investigations have yielded interesting results, making this an important avenue for further exploration in future.

LIST OF FIGURES	Page No.
Fig. 1. Contribution of different sources to radiation in the environment	3
Fig. 2. Distribution of uranium in soil-water environment	11
Fig. 3. Uranium species in aqueous medium as a function of pH	12
Fig. 4. ^{238}U decay scheme	15
Fig. 5. ^{232}Th decay scheme	16
Fig. 6. Geochemical cycle of elements	23
Fig. 7. Single and sequential extraction schemes for assessing elemental mobility	34
Fig. 8. Location map of the Singhbhum region (with uranium deposits) in India	39
Fig 9. Geological map of Singhbhum Shear Zone with the uranium deposits at Bhatin, Narwapahar, Jaduguda and Turamdih	41
Fig. 10. Random sampling approach	47
Fig. 11. Degree of error in laboratory sample preparation relative to other activities	52
Fig. 12. Analytical techniques available for chemical analysis	53
Fig. 13. Interaction of gamma rays with matter (a) Photoelectric effect, (b) Compton scattering and (c) Pair production	57
Fig. 14. HPGe detector in Pb shielding to minimize background and along with computer and MCA	58
Fig. 15. Block diagram of HPGe Gamma spectrometry system	60
Fig. 16. Energy calibration graph for HPGe detector	63
Fig. 17. Efficiency Calibration Graph For 100% n-Type HPGe	65
Fig. 18. Gamma spectrum of (a) RGU-I standard, (b) RGTh-I standard	69
Fig. 19. Background gamma spectrum of 100% n-type HPGe	70
Fig. 20. Neutron capture by a target nucleus followed by the emission of gamma rays	72

Fig. 21. A typical reactor neutron energy spectrum	74
Fig. 22. Typical gamma-ray spectrums showing (a) short-lived elements and (b) and (c) medium and long lived elements	78
Fig. 23. Gamma Spectrometric setup for INAA	80
Fig. 24. Laser uranium analyser	84
Fig. 25. Block diagram of Laser uranium analyser	85
Fig. 26. Typical standard addition curve for Laser uranium analyzer	86
Fig. 27. Soil texture triangle	92
Fig. 28. Particle size fractions of sample (a) to (d) soil, (e) copper clinker ash, (f) copper tailings and (g) uranium tailings	94
Fig. 29. Overview of the IHSS Humic acid separation procedure	100
Fig. 30. Distribution of (a) ^{238}U , ^{226}Ra and ^{232}Th , (b) ^{40}K and (c) ^{137}Cs in soils	105
Fig. 31. Box-Whisker plots of radionuclide concentrations in soils	106
Fig. 32. Distribution fits for radionuclide concentrations in soils	107
Fig. 33. Distribution of ^{238}U , ^{226}Ra and ^{232}Th in host rocks	109
Fig. 34. Box-Whisker plots of radionuclide concentrations in host rocks	109
Fig. 35. Distribution fits for radionuclide concentrations in host rocks	110
Fig. 36. Distribution of (a) ^{238}U and ^{226}Ra and (b) ^{232}Th in uranium bearing rocks	112
Fig. 37. Box-Whisker plots of radionuclide concentrations in (a) Bhatin, (b) Narwapahar, (c) Jaduguda and (d) Turamdih deposit	114
Fig. 38. Distribution fits for radionuclide concentrations in (a) Bhatin, (b) Narwapahar, (c) Jaduguda and (d) Turamdih deposit	115
Fig. 39. Distribution of (a) ^{226}Ra , (b) ^{238}U and (c) ^{232}Th in waste samples	118
Fig. 40. Box-Whisker plots of radionuclide concentrations in (a) TP3, (b) TP1 and (c) copper tailings and (d) copper clinker ash	119

Fig. 41. Distribution fits for radionuclide concentrations for (a) TP3, (b) TP1 and (c) copper tailings and (d) copper clinker ash	120
Fig. 42. Concentrations of (a) Major element oxides and (b) to (d) Trace element in soils	124
Fig. 43. Mass balance of major and trace elements – soil 4	125
Fig. 44. Mass balance of major and trace elements – soil 7	126
Fig. 45. Contribution of particle sizes towards total elemental concentrations, soil 4	127
Fig. 46. Contribution of particle sizes towards total elemental concentrations, soil 7	128
Fig 47. Concentrations of (a) major oxides and (b) and (c) trace elements in host rocks	130
Fig 48. Concentrations of (a) major oxides and (b), (c) and (d) trace elements in uranium bearing rocks	132
Fig 49. Concentrations of (a) major oxides and (b) and (c) trace elements in waste samples	134
Fig. 50. Mass balance of major and trace elements – uranium tailings	135
Fig. 51. Contribution of particle size fractions towards total elemental concentrations, TP	136
Fig. 52. Evolution of uranium concentrations in semi-dynamic leaching, using water	142
Fig. 53. Evolution of uranium concentrations in semi-dynamic leaching, 0.1N NaNO ₃	142
Fig. 54. Evolution of uranium concentrations in semi-dynamic leaching tests	143
Fig. 55. Evolution of uranium concentrations in dynamic leaching tests-neutral pH	143
Fig. 56. Evolution of uranium concentrations in dynamic leaching tests-acidic pH	144
Fig. 57. Evolution of uranium concentrations in dynamic leaching tests-basic pH	144
Fig. 58. Evolution of uranium concentrations at different pH (a) TP1 and (b)TP3	145

Fig. 59. Evolution of uranium concentrations at different pH (a) copper tailings and (b) copper clinker ash	145
Fig. 60. Evolution of uranium concentrations for different particle sizes (a) soil 1, (b) soil 4, (c) soil 7 and (d) soil 11	147
Fig. 61. Evolution of uranium concentrations for different particle sizes in uranium tailings	148
Fig. 62. Evolution of uranium concentrations at different temperatures in (a) soil 1 and (b) soil 11	148
Fig. 63. Evolution of uranium concentrations at different temperatures in (a) TP 1, (b) TP3, (c) copper tailings and (d) copper clinker ash	149
Fig. 64. The (a) $^{226}\text{Ra}/^{238}\text{U}$ and $^{208}\text{Tl}/^{228}\text{Ac}$, (b) $^{235}\text{U}/^{238}\text{U}$ and (c) $^{234\text{m}}\text{Pa}/^{238}\text{U}$ and $^{227}\text{Th}/^{235}\text{U}$ activity ratios in some soils	159
Fig 65. The (a) $^{226}\text{Ra}/^{238}\text{U}$ and $^{208}\text{Tl}/^{228}\text{Ac}$ and (b) $^{235}\text{U}/^{238}\text{U}$ activity ratios in soils	161
Fig. 66. Distribution of radionuclides with mine depth in (a) Narwapahar, (b) Jaduguda and (c) Bhatin deposits	163
Fig. 67. Thiel diagram of uranium decay series of the ore samples from the deposits of Bhatin, Narwapahar and Jaduguda, drawn from the data presented in table 40. I: U leaching region, II: U accumulation region, III: forbidden region for any single process and IV: forbidden region for any single continuous process. The boxed-in area indicates secular equilibrium condition.	169
Fig 68. Activity ratios of various daughter-parent pairs, plotted with U concentration. Error bars correspond to 10% error.	170
Fig. 69. Variation of $^{226}\text{Ra}/^{238}\text{U}$, $^{231}\text{Pa}/^{235}\text{U}$ and $^{227}\text{Ac}/^{235}\text{U}$ Activity Ratios with mine depth levels for (a) Narwapahar, (b) Jaduguda and (c) Bhatin mines	171

Fig. 70. Activity ratios of various daughter-parent pairs for (a) uranium tailings, TP1, (b) uranium tailings, TP3, (c) copper tailings and (d) copper clinker ash.	172
Fig. 71. Chondrite normalised REE diagram for (a) uranium bearing rocks and (b) host rocks	175
Fig. 72. Minerals in different particle sizes	176
Fig. 73. Trace element concentration sin different particle size classes: (a) to (c) Soil 4 and (d) to (f) Soil 7.	178
Fig. 74 . Trace element concentrations in different particle size classes: uranium tailings	178
Fig. 75. Power law fitting of trace elements for soil 4	179
Fig. 76. Power law fitting of trace elements for soil 7	179
Fig. 77. Power law fitting of trace elements for uranium tailings	180
Fig. 78. Cumulative fraction of uranium leached with (a) water and (b) 0.1N NaNO ₃	186
Fig. 79. CLF of uranium leached with (a) water and (b) 0.1N NaNO ₃	187
Fig. 80. IF of uranium leached with (a) water and (b) 0.1N NaNO ₃	188
Fig 81. Linear regression for log CLF vs. log t for (a) water and (b) 0.1N NaNO ₃	189
Fig. 82. Cumulative fraction of U leached from soils under different pH conditions (a) neutral, (b) acidic and (c) basic pH	194
Fig. 83 . Cumulative fraction of U leached from wastes under different pH conditions (a) neutral, (b) acidic and (c) basic pH	195
Fig. 84 . Cumulative fraction of U leached from wastes under different particle sizes (a) soil 1, (b) soil 4 (c) soil 7 and (d) soil 11	197
Fig. 85. Cumulative fraction of U leached from wastes under different	

particle sizes of uranium tailings	198
Fig. 86 . Cumulative fraction of U leached from (a) soil 1 and (b) soil 11 at different temperatures	199
Fig. 87 . Cumulative fraction of U leached from (a) U tailings TP1, (b) U tailings TP3, (c) Cu tailings and (d) Cu clinker ash at different temperatures	200

LIST OF TABLES

Page No.

Table 1. Information of radionuclides generated by modified sources	3
Table 2. Information on common cosmogenic radionuclides	4
Table 3. Information on certain primordial radionuclides	6
Table 4. Concentration of radionuclides in various environmental matrices	7
Table 5. Global emissions of trace metals from natural sources ($\times 10^6$ kg/yr).	21
Table 6. Global emissions of trace metals from anthropogenic sources ($\times 10^6$ kg/yr).	22
Table 7 . Abundances of some elements in the Earth's crust and Granitic rocks in $\mu\text{g/g}$.	23
Table 8. Average abundances of trace elements in soil, Earth's crust, sediment and igneous rocks in ppm.	24
Table 9. Elements accumulated in different rocks.	24
Table 10. Mean contents of certain heavy metals in major rock types ($\mu\text{g/g}$)	24
Table 11. Relative mobilities of elements in the environment	26
Table 12. Parameters affecting leaching	36
Table 13. Different methods used for radioactivity quantification	55
Table 14. Efficiency values for different geometries	66
Table 15. MDL values for different geometries	67
Table 16. Sensitivities for determination of elements using INAA	81
Table 17. Comparison of different analytical techniques for U measurement	83
Table 18. Reference Materials used in Environmental Analysis in this study	89
Table 19. Quality Assurance of Metal Analysis in Soil	89
Table 20. Particle size fractions of the collected samples	94
Table 21. Moisture content of the collected samples	95
Table 22. Organic matter content of the collected samples	95

Table 23. pH of the collected samples	96
Table 24. Cation exchange capacity of the collected samples	98
Table 25. Humic acid content of the collected samples	99
Table 26. Radionuclides analysed by gamma spectrometry, with energies and gamma ray intensities	101
Table 27. Activity concentrations of radionuclides of the ^{238}U and ^{232}Th series, ^{40}K and ^{137}Cs in surface soil samples	103
Table 28. Activity concentrations of ^{238}U series and ^{232}Th in host rocks	108
Table 29. Activity concentrations of ^{238}U series and ^{232}Th in uranium bearing rocks	111
Table 30. Activity concentrations of ^{238}U series and ^{232}Th in waste samples	116
Table 31. Stable elements and the gamma energies and half lived of their corresponding radioisotopes formed	121
Table 32. Average elemental contribution (%) of particle size fractions, soil 4	127
Table 33. Average elemental contribution (%) of particle size fractions, soil 7	128
Table 34. Average weighted elemental contribution (%) of particle size fractions, TP	136
Table 35. ^{238}U and ^{232}Th activity concentrations in soil samples from worldwide studies	154
Table 36. ^{238}U and ^{232}Th activity concentrations in rock samples from other studies	160
Table 37. ^{238}U activity concentrations in rock samples compared with other studies	162
Table 38. U and Th contents in the samples and the corresponding activity ratios	168
Table 39. Activity concentrations of uranium series radionuclides measured in some of the samples.	169
Table 40. Activity ratios of the uranium series daughters.	169
Table 41. Correlation matrix for trace elements in host rock samples	181
Table 42. Correlation matrix for trace elements in host rock samples	181
Table 43. Correlation matrix for trace elements in soil samples	183

Table 44. Correlation matrix for trace elements in soil samples	184
Table 45. Correlation matrix for trace elements in uranium bearing rock samples	185
Table 46. Mean apparent diffusion coefficients (D in cm^2/s) for U release from the studied matrices using different solvents	191
Table 47. The bulk release values, R_i ($\mu\text{g}/\text{m}^2$), for U release from the studied matrices using different solvents	192
Table 48. Leaching rate of uranium from soils under different pH conditions	194
Table 49. Leaching rate of uranium from wastes under different pH conditions	196
Table 50. Leaching rate of uranium from different particle sizes of soil	197
Table 51. Leaching rate of uranium from different particle sizes of uranium tailings	198
Table 52. Leaching rate of uranium from soils at different temperatures	199
Table 53. Leaching rate of uranium from wastes at different temperatures	200

CHAPTER 1

INTRODUCTION

Scope

Elevated concentrations of certain minerals and associated elements mark a highly mineralised region. Such regions host mineral deposits of economically viable grades and industries related to mining and extraction of these minerals. Due to the rapid industrial development and consequent demand for energy and resources these industries are constantly growing. This growth is marked by a parallel increase in waste production and hence an increase in potential for environmental pollution unless sufficient safety measures are taken. The distribution and transport of elements in such environments is hence essential to assess the environmental degradation, if any, and to reach at a plausible solution to existing environmental problems.

This chapter gives a brief overview of natural radioactivity, properties of radionuclides, their environmental behaviour, distribution in the environment and natural radioactive series equilibrium/disequilibrium condition. The factors affecting radioactive equilibrium condition are also covered. This chapter also addresses association and distribution of trace elements in the environment and their variation with physicochemical parameters. Different leaching methodologies, their application in assessing elemental transport and influence of different physical conditions on the extent of leaching is also described. A brief discussion on the uranium mineralised region of Singhbhum East district in Jharkhand along with its physiography and geology has also been included.

1.1. Natural radioactivity and radioactive disequilibrium in a mineralised region

In view of the rapid depletion of reserve fossil fuels, there has been an increased demand for nuclear energy in the civilian economics. Hence, there has been an endeavour to increase uranium production. This necessitates the identification of prospective uranium mineralised

regions, enhanced uranium ore production and optimal performance of the uranium mining and milling processes. Such mineralised zones are marked by higher concentrations of naturally occurring radionuclides and associated trace elements compared to background locations. The extent and nature of mineralisation is highly dependent on the geological setting of the area. Geochemical processes, like weathering and leaching, also influence the distribution of radionuclides in different environmental matrices. Such environmental forces also lead to the transport of radionuclides from one location to another.

The highly mineralised Singhbhum Shear Zone of Jharkhand state in India has long been identified by Atomic Minerals Directorate. Uranium occurs here in disseminated form in the copper mineralisation area of this shear zone. There are seven uranium mines, viz. Jaduguda, Narwapahar, Bhatin, Turamdih, Bandhuhurang, Bagjata and Mohuldih in the study region in different stages of operation and development. The central uranium ore processing facilities was located at Jaduguda which process the ores from all operating the uranium mines [1]. Of late, the new ore processing plant at Turamdih process the ores from Turamdih and Bandhuhurang uranium mines. Mining activities in the region involves the transport of ores, waste products and other low radioactive materials.

1.1.1. Natural radioactivity, its sources, types and distribution in environment

Natural radiation is a fact of life. All living organisms are continuously exposed to ionizing radiation, which always existed naturally. The predominant part of the natural radiation in our environment is due to the primordial radionuclides. Fig. 1, adapted from NCRP 1987 [2], shows the contribution of different sources to radiation in the environment.

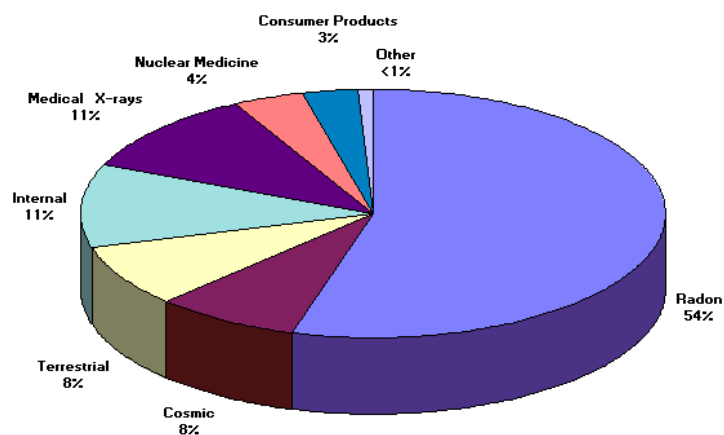


Fig. 1. Contribution of different sources to radiation in the environment

Natural radioactivity present in the earth's crust belongs to virgin and modified sources. Virgin sources are cosmogenic or primordial (terrestrial) and have existed in the earth since primordial times. Modified sources are formed due to human activities like mining activities, usage of fossil fuel, production of fertilizers or naturally occurring radioactive materials used for building construction. Release of low levels of natural and artificial radionuclides can also occur in the environment during the normal operations of nuclear facilities like nuclear ore processing, uranium enrichment, fuel fabrication, reactors, particle accelerators and the production and application of radioisotopes in the fields of nuclear medicine, industry, research and agriculture [3]. Some radionuclides produced or enhanced by human activities are given in Table 1.

Table 1. Information of radionuclides generated by modified sources

Nuclide	Half-life	Source
^3H	12.3 yr	Produced from weapons testing and fission reactors
^{131}I	8.04 days	Fission product produced from weapons testing and fission reactors, used in medical treatment of thyroid problems
^{129}I	1.57×10^7 yr	Fission product produced from weapons testing and fission reactors

^{137}Cs	30.17 yr	Fission product produced from weapons testing and fission reactors
^{90}Sr	28.78 yr	Fission product produced from weapons testing and fission reactors
^{99}Tc	2.11×10^5 yr	Decay product of ^{99}Mo , used in medical diagnosis

An important source of radiation is cosmic rays, which come from outer space and from the surface of the sun. Cosmic rays are the dominant source of ionisation in the atmosphere at higher altitudes [4]. This component consists of 85% high- energy protons (3-30GeV), 10% alpha particles and the rest of neutrinos, photons, electrons and heavier particles. At the top of the Earth's atmosphere, low energy charged particles are deflected back into outer space because of Earth's magnetic field and only the particles with energy more than $19.2 \cos^4 \lambda$ (GeV) at a latitude (λ) only enter the Earth's atmosphere [5]. When primary cosmic rays enter the atmosphere, those with higher energy undergo nuclear reactions (spallation reactions), whereas those with lower energy lose their energy by ionisation. Cosmogenic radionuclides like, ^3H , ^7Be , ^{14}C and ^{22}Na , are produced by primary cosmic rays (heavy charged particles coming from outer space), upon interaction with the atoms present in the atmosphere, like, nitrogen, oxygen, argon etc. [4, 6]. Apart from the cosmogenic nuclides, neutrons, protons, pions and kaons are also produced, which form secondary cosmic rays. Many of the secondary particles have sufficient energy to initiate whole sequences of further nuclear reactions with nitrogen and oxygen nuclei. Some other cosmogenic radionuclides are ^{10}Be , ^{26}Al , ^{36}Cl , ^{80}Kr , ^{14}C , ^{32}Si , ^{39}Ar , ^{22}Na , ^{35}S , ^{37}Ar , ^{33}P , ^{32}P , ^{38}Mg , ^{24}Na , ^{38}S , ^{31}Si , ^{18}F , ^{39}Cl , ^{38}Cl , $^{34\text{m}}\text{Cl}$ [4, 6]. Information on some common cosmogenic radionuclides is given in Table 2.

Table 2. Information on common cosmogenic radionuclides

Nuclide	Half-life	Source
---------	-----------	--------

^{14}C	5730 yr	Cosmic-ray interactions, $^{14}\text{N}(\text{n,p})^{14}\text{C}$
^3H	12.3 yr	Cosmic-ray interactions with N and O, spallation from cosmic-rays, $^6\text{Li}(\text{n}, \alpha)^3\text{H}$
^7Be	53.28 days	Cosmic-ray interactions with N and O

The primordial radionuclides, present since the creation of the Earth, are typically long lived, with half-lives often in the order of hundreds of millions of years. During the early highly molten stage of the Earth, there was a major segregation of the elements, with the more dense and compressible elements like iron, nickel and platinum moving towards the centre and the less dense and less compressible elements like oxygen and potassium moving towards the surface. Elements that combine readily with oxygen, such as thorium and uranium, were swept upwards with oxygen, which forms half of the surface rocks. This radial differentiation or segregation, which may still be going on today at an ever decreasing rate, formed the geo-spheres [7].

The most important primordial radionuclides are those in the decay series starting with ^{238}U , ^{232}Th and ^{235}U , and also ^{40}K [4]. These primordial radionuclides are supposed to have formed together with the stable, nonradioactive nuclides at least five billion years ago [7]. The average abundance of U, Th and K in the Earth's crust is 32.36, 40.6 and 1% respectively [8]. Some other primordial radionuclides are ^{50}V , ^{87}Rb , ^{113}Cd , ^{115}In , ^{123}Te , ^{138}La , ^{142}Ce , ^{144}Nd , ^{147}Sm , ^{152}Gd , ^{174}Hf , ^{176}Lu , ^{187}Re , ^{190}Pt , ^{192}Pt and ^{209}Bi [6]. Some basic information on common primordial radionuclides is given in Table 3.

^{232}Th having the half-life of 1.4×10^{10} yrs, has decayed the least with the result that the ^{232}Th to ^{238}U (half-life of 4.5×10^9 yrs) ratio has increased. In the nearly five billion years history of the Earth, ^{235}U (half-life of 7.1×10^8 yrs) had been a significant source of ionizing radiation in the

early part of history, but is a minor factor today. Three distinct processes affect the concentrations of U, Th and K in the environment. These processes are partial melting, assimilation and fractional crystallisation or differentiation [7]. As a result of various geological processes these radionuclides tend to concentrate in a variety of ways to produce six types of radioactive anomalies: Monazite sands and other placers, Alkaline intrusives and granites, Bauxite and intensely weathered soils, Uraniferous phosphate rock (and soils), Ground waters enriched in radium and radon and Black shales and related organic accumulations [9].

Table 3. Information on certain primordial radionuclides

Nuclide	Half-life	Natural Activity
^{235}U	7.1×10^8 yr	0.71% of all natural uranium [10]
^{238}U	4.47×10^9 yr	99.28% of all natural uranium [10]; Global concentration level 33 Bq/kg [4]; In Indian context 31 Bq/kg [11]
^{232}Th	1.41×10^{10} yr	7.2 ppm in crust [12]; Global concentration level 45 Bq/kg [4]; In Indian context 63 Bq/kg [11]
^{226}Ra	1.60×10^3 yr	48 Bq/kg in igneous rocks [13]
^{40}K	1.28×10^9 yr	Present in soil at 100.0 mBq/g activity concentration [13]

The primordial radionuclides are present in bedrock, soil, building materials, water, air and in the human body. The contents of the natural radioactive substances vary widely between different rocks and soil types, due to the different ways in which they are formed. The contents of uranium and thorium, and therefore of their daughter products, also vary considerably between, and within, rocks, often even in the same area. Locally, the uranium and thorium contents can be very high, several percent, as is the case in ores and in occurrences of uranium and thorium. Certain types of rocks commonly have higher contents of uranium and thorium than others. Examples of such rocks are certain types of granites, acidic gneiss, pegmatites, carbonatites and

black shales [15]. Concentrations of radionuclides in various environmental matrices are given in Table 4 [13]. In India, regions of Maharashtra and South Gujarat covered by the Deccan lava basalt are found to have low radioactivity content. Gangetic alluvial regions covering parts of Uttar Pradesh, Bihar and West Bengal have higher natural radioactivity, while the granite region of Andhra Pradesh exhibits higher levels of primordial radioactivity [14].

Table 4. Concentration of radionuclides in various environmental matrices

<i>Environmental Matrix</i>	^{238}U	^{226}Ra	^{40}K
Igneous rock (Bq/g)	0.04	0.048	1.2
Phosphate rock (Bq/g)	1.60	1.50	0.4
Lime stone (mBq/g)	16.0	5.0 – 20.0	30.0 – 150.0
Soil (mBq/g)	37.0	16.0	100.0
Air ($\mu\text{Bq/m}^3$)	1.2	1.5	22.0
Surface water (mBq/l)	0.18 – 62.9	0.4 – 111.0	$3.7 \times 10^2 - 2.4 \times 10^5$
Ocean surface water (mBq/l)	44.4	1.3 – 3.1	1.1×10^4
Ocean bottom water (mBq/l)	40.0	3.0 – 5.6	1.1×10^4

The weathering and erosion of parent rocks and variable extents of pedogenesis lead to the formation of soils. The physical characteristics of soils, such as grain-size distribution and permeability, are governed by factors like parent rock material, mode of formation of the minerals, the means and distance of transport, and the depositional environment. Soil formation processes modify the weathered rock material and eventually give soil the characteristics that distinguish it from the source material. For example, podzols typically develop on coarse (sandy) material in granitic/gneissic environments [16].

The final distribution of natural radioactivity in soils is affected by the radionuclide content of the parent rock, and recent physical and chemical events (i.e. chemical leaching, transport with

water, and precipitation/adsorption effects). In this process certain elements are enriched compared to their content in the source rock. Gravel, sand, silt and clay are soil types, which are transported by water and then settle, also show depletion or enrichment of a particular radionuclide. For gravel and coarse sand, the contents of radioactive substances depend on the rocks from which they originated. Sand and silt have consistently low contents of uranium and thorium since the radioactive elements are carried away with the water. The clays adsorb uranium, radium and thorium from the water and they have often higher contents of these substances than sand and silt [15]. As soil develops from carbonate bedrock in Pennsylvania, U and Th are concentrated by a factor of about 10, whereas in soils developing from other parent materials (particularly sandstone) the nuclides are generally enriched only about 1.5-2 times [17]. Greeman et al. [18] found, in soils developed from carbonate rock, both Ra and U enriched 10-12 times, while Th, Al and Fe were enriched 20 times. Weathering also mobilises U and Ra out from the rock. They are subsequently redeposited, primarily through adsorption onto Fe oxides, organic material and secondary minerals. U and Ra may also be adsorbed or precipitated on the surface of grains or pore space surfaces [19, 20]. Wanty et al. [19] assumed Ra to be tightly bound to the solid phase, either through adsorption to mineral surfaces or by co-precipitation with Fe oxides.

1.1.2. Occurrences and geochemistry of radionuclides

Uranium

Naturally occurring uranium consists of three isotopes with mass numbers 238, 235 and 234. The ^{238}U isotope constitutes 99.28% of the natural uranium, which is in equilibrium with ^{234}U (0.0058%). The ^{235}U isotope, the progenitor of the Actinium series is present in the amount 0.71% [10]. Uranium occurs in ore as uraninite (UO_2) or pitchblende (U_3O_8) or as secondary

minerals (complex oxides, silicates, phosphates, vanadates). Uranium oxide precipitates out from uranium-bearing ground waters as they enter a reducing environment. It can be mobilised (redissolved) in situ by oxygenated leach solution.

Average crustal abundance of U is 1.8 ppm [12]. Uranium is present in ppm levels in the earth's crust, rocks and soils [21, 22, 23] and ranges from thousands of ppm to a few percentages in minerals/ rocks used in the mining industry. Radionuclides like uranium, thorium and radium are often non-homogeneously distributed in rock material. The distribution depends primarily on the rock type (igneous, metamorphic, or sedimentary) and the extent of weathering. U and Th distributions differ due to their different chemical properties.

In igneous rocks, U concentration increases with degree of differentiation, very low U concentrations occur in ultrabasic rocks (0.014 ppm) whereas they are higher in granites (2-15 ppm) [24] and pegmatites. Uranium does not easily fit into the mineral lattice of rock-forming minerals. A major portion of it is deposited as separate minerals or at grain boundaries during the cooling of the magma. This explains high uranium concentrations in pegmatites, which are formed from residual hydrothermal solutions.

Tieh et al. [25] attribute U occurrences in rocks to the following modes:

1. Background U: Usually low concentration levels of uranium in major rock-forming minerals (quartz, feldspar, biotite and amphibole).
2. Resistate U: Uranium in accessory minerals, such as zircon, apatite, sphene etc. Uranium is probably included in these through crystal lattice substitution [26]. Morawska and Phillips [27] point out that the radioactivity in granites is located in microscopic heavy minerals like uranium oxide, which are concentrated along grain boundaries, in microcracks and at alteration sites.

Wathen [28] noted that accessory minerals provide U with a crystal position, making it less leachable than uranium that is deposited as coatings on grains.

3. Interstitial U: Interstitial uranium is concentrated along grain boundaries and fractures in noncrystalline phases; formed during deuteric alteration and early weathering. Non-crystalline phases are amorphous Fe, Mn and Ti oxides and clay minerals [29]. Gabelman [30] specifies that one third of the U in granites is placed in interstitial oxides, which are easily leached. Guthrie and Kleeman [31] concluded from their data regarding effects of chemical weathering, that:

1. Depletion of background U occurs as uranium is liberated from primary phases and accumulated within secondary aggregates as interstitial U.
2. Interstitial U increases during early weathering. During intense leaching, interstitial U is decreased. Uranium atoms that are situated at grain boundaries are easily accessible for leaching when the material is exposed to water.
3. U content in weathering resistant accessory minerals is not affected, but the abundance of mineral grains is decreased. Accessory minerals that are not weathering resistant are removed or altered. Guthrie and Kleeman [31] discovered no net loss of U in moderately weathered granites; however weathering results in mobilisation of U, providing for U mineralisation elsewhere.

In metamorphic rocks the abundance and distribution of U and Th is dependent on the source rock. The contents of both generally decrease with increasing degree of metamorphism, U concentration generally varying from 0.2-11 ppm (Rogers and Adams, 1969). In sedimentary rocks uranium concentration increases with content of clay, phosphorus and organic matter. Sandstones, shales and limestones generally have low U contents, while phosphorites often contain >50 ppm U. The uranium content of black shales can be as high as 1200 ppm [24] and is often correlated to the content of organic material and abundance of colloidal size grades [12].

Elevated uranium concentrations are also associated with deposits that contain heavy minerals, such as placer deposits [32].

The chemical behaviour of an element is dependent not only on its electronic structure but also on its chemical environment. Uranium has six valence states, viz. U^{+1} , U^{+2} , U^{+3} , U^{+4} , U^{+5} and U^{+6} . The most important in these are U^{+4} and U^{+6} [33]. Fig. 2 is a schematic representation of uranium distribution in soil-water system. Uranium becomes immobile if present in a precipitated form or adsorbed to immobilised solid media and mobile if present in dissolved phase or associated with mobile colloids. The association of uranium with solid phases and its mobility is dependent on site-specific conditions. At high dissolved carbonate concentrations, formation of uranyl-carbonate species increases the uranium mobility. High phosphate concentrations lead to the precipitation of uranium as insoluble uranyl phosphate minerals. The sorption of a variety of heavy metals to natural porous media can be attributed to the $Fe(OH)_3$ component.

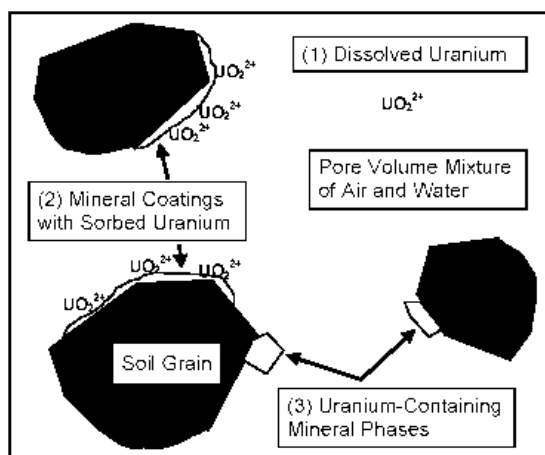


Fig. 2. Distribution of uranium in soil-water environment

In reducing environments, uranium occurs as U(IV), and is immobile due to the insoluble nature of uraninite (UO_2) and coffinite ($USiO_4$). Under these conditions, the uranium concentration in water is less than 10^{-13} M. Under oxidizing conditions, U(IV) is oxidised to U(VI), which greatly enhances solubility. U(VI) forms uranyl ion complexes (e.g., UO_2^{2+} , $UO_2(CO_3)$, $UO_2(CO_3)_2^{2-}$ or

$\text{UO}_2(\text{CO}_3)_3^{4-}$, $\text{UO}_2(\text{HPO}_4)_2^{2-}$ etc.) that are highly stable [33, 34]. The uranyl ion (UO_2^{2+}) and its complexes have a high solubility and can be transported to long distances in groundwater under certain environmental conditions. Between pH 5 and pH 8.5 uranyl minerals limit the U concentration to $\sim 10^{-9}\text{M}$ [33]. Since the uranyl ion does not bond strongly with most anions, it forms few insoluble compounds. The various species of uranium in aqueous medium at different pH are shown in fig. 3.

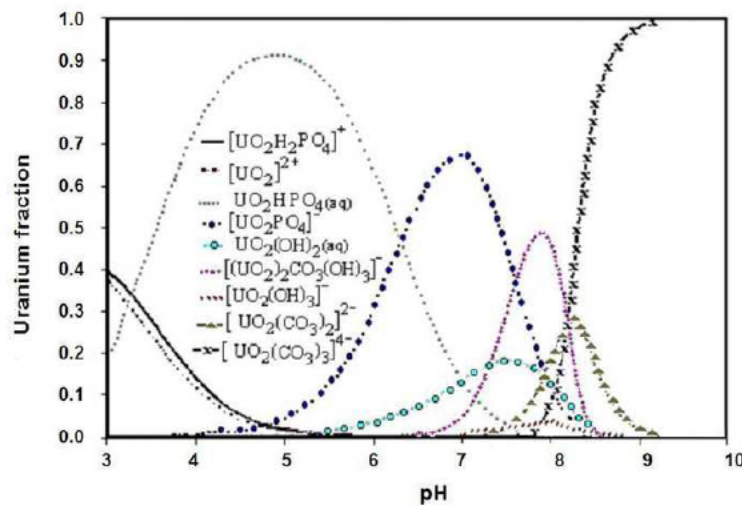


Fig. 3. Uranium species in aqueous medium as a function of pH

Uranium and its daughter isotopes are also redeposited from groundwater. Uranium is reduced by organic material, i.e., carbonaceous or bituminous shales and lignites [34], Fe (producing Fe oxides), sulphide [30], or adsorbed onto mineral surfaces or organic matter. Phosphate rocks are also enriched in uranium, due to co-precipitation of U with Ca^{2+} [34]. The uranium concentration in natural waters is primarily controlled by sorption [33, 19]. Between pH 5 - 8.5, sorption occurs on organic matter, Fe, Mn and Ti oxides, zeolites and clays. Uranium sorption can be inhibited by carbonate complexation of the uranyl ion [35]. Concentrated deposits of uranium in the environment occur in uraninite, UO_2 . During the weathering of uraninite, a series of secondary minerals including uranium (VI) oxyhydroxides, phosphates, silicates, sulfates, and carbonates

are precipitated [36]. The secondary minerals then constitute source phases for uranium mobilisation.

Thorium

Average crustal abundance of Th is 7.2 ppm [12]. In rocks thorium occurs at similar sites as uranium, as a trace constituent in phosphate, oxide and silicate minerals. A large part of naturally occurring Th is found substituting for Zr in zircon. Zircon and many other minerals containing Th are resistant to weathering [37].

Like uraninite in case of uranium, thorianite is a principal mineral of thorium. These are classified under the MO_2 type of oxides. Both uraninite and thorianite are found in intrusive igneous rocks, particularly granites, syenites and related pegmatites. Thorianite is most common in pegmatites. Thorium has very low solubility in almost all aqueous environments due to the high ionic potential of Th^{4+} . It remains in solution for a short while before being precipitated as hydroxylates or being adsorbed on clay surfaces. Due to its large ionic radius, high electronegativity and valence, it occurs in association with igneous rocks, often crystallizing in the later stages of differentiation in accessory minerals. In the sedimentary cycle the greatest thorium and uranium separation takes place. Thorium varies from 3-50 ppm in granites and pegmatites and from 1-3 ppm in basalts and other basic rocks.

Radium

Radium in rocks is generated by the decay of U. It is not affected by long-term processes, due to its continuous production and relatively short half-life of 1600 years. If no separation of radionuclide mothers and daughters takes place for 8000 years, ^{226}Ra geochemistry is governed entirely by ^{230}Th [38]. However, in nature even short term equilibrium may not be reached because of the selective leaching of radium or thorium, or due to uranium enrichment [34].

Radium geochemistry is relatively simple, due to singular valence state (+II), and as behaviour of Ra is similar to the other alkaline earth elements. The Ra^{2+} ion is moderately soluble in natural waters, and may precipitate as sparingly soluble salts (sulphate, carbonate and chromate salts), but due to the low natural abundance (4×10^{-18} M), the Ra concentration in water is primarily controlled by co-precipitation with other elements and adsorption to active surfaces of all kinds [34]. The adsorption efficiency of Ra onto ferric oxyhydroxide is significant, even though it is about two orders of magnitude lower than for sorption of U [35]. Ames et al. [35] found that Ra in general was more efficiently sorbed onto secondary minerals, such as illite, kaolinite and montmorillonite than U, the most efficient Ra sorbers being those with the highest cation exchange capacity. To summarise, radium is less efficiently sorbed onto iron oxides and more efficiently sorbed onto secondary minerals with high cation exchange capacity, than uranium.

1.1.3. Radioactive equilibrium and disequilibrium condition in environment

Radioactive disequilibrium is the disruption of the state of secular radioactive equilibrium in the natural radioactive series. It occurs when one or more decay products in a decay series are completely or partially removed or added to a system [39]. Radioactive disequilibrium arises due to geochemical processes, like leaching and erosion, operating in the environment. Depending on the half-lives of the radioisotopes involved, it may take days to millions of years for equilibrium to be restored [40]. The three natural radioactive series, with uranium, thorium and actinium as their parent radionuclides, contain chemically and physically different elements. The uranium and thorium decay series are given in fig. 4 and 5.

Z→ A↓	82	83	84	85	86	87	88	89	90	91	92
238	Long lived α emitters ²³⁸ U, ²³⁴ U, ²³⁰ Th, ²²⁶ Ra and ²¹⁰ Po Radon Progeny ^{Po} ²¹⁸ , ^{Pb} ²¹⁴ , ^{Bi} ²¹⁴ , ^{Po} ²¹⁴ and ^{Pb} ²¹⁰			Significant γ Emissions ²¹⁴ Pb – 295 keV (19%), 77 keV (10%) ²¹⁴ Bi – 1238 keV (6%), 609 keV (46%), 1764 keV (16 %), 1120 keV (15%) Others: ²³⁸ U, ²³⁴ Th, ²³⁴ U, ²³⁰ Th, ²²⁶ Ra & ²¹⁰ Pb							²³⁸ U (4.5 E 9 y)
234									²³⁴ Th (24.1 d)	^{234m} Pa (1.18 m)	²³⁴ U (2.48 E 5 y)
230									²³⁰ Th (8.0 E 4 y)		
226							²²⁶ Ra (1620 y)				
222					²²² Rn (3.825 d)						
218			²¹⁸ Po (3.05 m)					Legend → β ⁻ - emission, ↙ α - emission			
214	²¹⁴ Pb (26.8 m)	²¹⁴ Bi (19.7 m)	²¹⁴ Po (164 μs)	Radon progeny							
210	²¹⁰ Pb (19.4 y)	²¹⁰ Bi (5.01 d)	²¹⁰ Po (138.4 d)								
206	²⁰⁶ Pb (Stable)										

Fig. 4. ^{238}U decay scheme

$Z \rightarrow$ $A \downarrow$	81	82	83	84	85	86	87	88	89	90
232										^{232}Th (1.4×10^{10} y)
228								^{228}Ra (5.8 y)	^{228}Ac (6.13 h)	^{228}Th (1.91 y)
224								^{224}Ra (3.64 d)		
220						^{220}Rn (52 s)				
216				^{216}Po (0.15 s)				Legend \rightarrow β^- - emission, \nwarrow α - emission		
212		^{212}Pb (10.64 h)	^{212}Bi (60.6 m)	^{212}Po (3×10^{-7} s)						
208	^{208}Tl (3.1 m)	^{208}Pb (Stable)						^{212}Bi is both α (36%) and β (64%) emitter.		
210										

Fig. 5. ^{232}Th decay scheme

If a chemical system behaves as isolated and closed for chemical exchanges for a long period of time, in relation to the longest half-life of daughters of the radioactive series present in the system, the radioactive series reaches secular radioactive equilibrium. Thorium rarely occurs in disequilibrium condition in nature, and there are no disequilibrium problems with potassium. But in the uranium decay series disequilibrium is common. The unique geochemical behaviour of uranium and the contrasting behaviour of its daughter isotopes provide a variety of tools in geochemistry and hydrogeology, ranging from global cycling of the elements to tracing of water in the hydrologic cycle [41]. Disequilibrium in the uranium series can occur at several positions in the ^{238}U decay series: ^{234}U can be selectively leached relative to ^{238}U ; ^{230}Th and ^{226}Ra can be selectively removed from the decay chain; and finally ^{222}Rn (radon gas) is mobile and can escape from soils and rocks into the atmosphere. The mechanisms giving rise to radioactive disequilibrium are:

1.Elemental fractionation

This arises due to the greater mobility of uranium in comparison with its less soluble daughters ^{230}Th and ^{226}Ra . ^{230}Th is found at very low concentrations in most ground waters. Whereas, ^{226}Ra is quite soluble in waters with high Cl^- concentration but relatively immobile in waters with high SO_4^{2-} concentrations, due to the formation of sparingly soluble radium sulphate.

2.Isotopic fractionation

^{234}U - ^{238}U disequilibria, which is very common in the environment occurs due to the direct α -recoil or leaching of ^{234}U . This results in the preferential enrichment of ^{234}U in the groundwaters and ^{238}U in the solid matrix. When α -decay occurs, the crystal lattice is damaged by the recoil tracks, which may enhance leaching of the daughter isotopes. Atoms that have been produced

through α -decay will then be more easily leached than atoms that have settled into crystal lattice position at the time of crystallisation [42, 43].

Radioactive disequilibrium between ^{226}Ra and ^{238}U can have several causes. Thorium is generally less soluble and less mobile than U, partly due to a stronger adsorption of Th than U. During migration of U, Th, and Ra in solution, their different sorption behaviours also enhance radioactive disequilibrium. Several other causes of disequilibrium have been discussed by many researchers. Greeman et al. [18], Hogue et al. [43] and Vanden Bygaart [44] suggested that Ra is kept in the surface layers by cycling in vegetation. Åkerblom et al. [46] noted that uranium minerals have a tendency to disintegrate due to their own radioactivity, which facilitates radon escape and thereby the onset of radioactive disequilibrium. In uranium minerals, the Ra atom generated by decay is much larger than the original U atom, thus Ra is metastable in the structure of uranium minerals, e.g., uraninite and coffinite. The loss of Ra occurs by diffusion in the original host mineral and by diffusion through the water layer adsorbed on the grain surface, and hence into solution [34]. Radioactive disequilibrium between ^{234}U and ^{238}U (due to the α -recoil effect) exists in certain rocks, and ^{234}U is enriched compared to ^{238}U in seawater. Kigoshi [45] argues that selective dissolution of ^{234}U is probably not the only explanation, and suggests that ejection of ^{234}Th into groundwater also contributes to the excess ^{234}U in water. Ek and Ek [20] performed a Swedish study of the radium distribution in soils, by analysing the radioactive disequilibrium between ^{226}Ra and ^{238}U . They used grain-size separated material from two different samples. In a radioactive granite sample the activity ratio between ^{226}Ra and ^{238}U was as large as 8.3 in the grain-size fraction <0.063 mm. They concluded that this was because the radium had been leached from the primary minerals and then adsorbed onto the surface of mineral particles in the soil, while uranium was oxidised to a more soluble form during leaching,

and thus was not adsorbed to the same extent. In another sample, which contained uraniferous alum shale and carbonaceous slates, ^{226}Ra and ^{238}U were in more radioactive equilibrium, probably because the Ra was enclosed in primary uranium minerals, which in turn were enclosed in kerogenic compounds, and thus less affected by weathering. Greeman et al. [18] examined the $^{226}\text{Ra}/^{238}\text{U}$ ratio in different soil phases. They found the largest disequilibrium in soil organic matter, a $^{226}\text{Ra}/^{238}\text{U}$ ratio of up to 30, while the ratio in Fe-oxides and in the C-horizon of deeply weathered soils was lower, 1.8 and 1.5, respectively. The soil mineral matter was Ra-poor ($^{226}\text{Ra}/^{238}\text{U}=0.73$). In vegetation the disequilibrium was even larger, with a ratio of up to 65.

It is hence apparent that natural radioactive series disequilibrium has been investigated by many researchers in various fields for diverse applications [40, 38, 41, 47-50]. Thiel et al.[51]; Condomines et al., [38]; Min et al., [48]; Rekha et al., [49] have investigated uranium series disequilibrium in sedimentary, carbonate and metamorphic deposits. These studies were used to assess elemental mobility in these deposits and their timescales of migration. Ibraheim, [53] and El-Dine, [47] have carried out disequilibrium studies and observed deviation from secular equilibrium condition in several rock samples from Eastern and North Eastern desert of Egypt. Volcanic rocks and mid ocean ridge basalts have also been extensively studied for radioactive disequilibrium [54-59]. Dosseto and co-workers [60-63] have carried out extensive studies on weathering rates in drainage basins employing natural radioactive series disequilibrium. Hence radioactive disequilibrium investigations were used as a tool to assess the mobility and transport of elements in the mineralised Singhbhum region in this thesis.

1.2. Trace elements in environment

1.2.1. Origin, distribution and association

Elements are intrinsic, natural constituents of our environment. They are present in the environment since the evolution of the earth and are present in trace or ultra trace levels in environmental matrices. They occur as ions, compounds, complexes and in a variety of other forms. Elements in a matrix can be categorised into major and trace elements based on their concentration. Usually, major elements are primary constituents of identifiable minerals, while trace elements only exist in minerals due to isomorphous substitution or surface sorption [64-66]. Higher trace element contents are observed in primary silicate minerals, primary Fe and Ti oxides, secondary Fe and Mn nodules, pieces of charcoal and fragments of plant material.

The sources of elements can be broadly classified into natural and anthropogenic ones. Natural sources include dust raised by winds, volcanic activity, forest fires, vegetation and sea salt sprays etc. Anthropogenic sources include mining, smelting and industrial processing of ores and metals, fossil fuel combustion and automobile exhaust etc. Although development of modern science and technology has led to an enhanced commercial use of metals, the environmental pollution from mining of metal ores and smelter emissions reached significant levels long before the onset of the industrial revolution. There is also an increasing worldwide trend to land-apply sewage sludge, industrial wastes and other residues, which could pose higher environmental risks if incinerated, buried or discharged to water [67]. Table 5 and 6 below lists the different natural and anthropogenic sources of elements and their global emissions.

Table 5. Global emissions of trace metals from natural sources ($\times 10^6$ kg/yr).

Data from Nriagu [68]

Source category	As	Cd	Co	Cr	Cu	Hg	Mn	Mo	Ni	Pb	Sb	Se	V	Zn
Wind blown dusts	2.6	.2	4.1	27	8.0	.05	221	1.3	11	3.9	.78	.18	33	19
Seasalt spray	1.7	.06	.07	.7	3.6	.02	.86	.22	1.3	1.4	.56	.55	3.1	.44
Volcanoes	3.8	.82	.96	15	9.4	1.0	42	.40	14	3.3	.71	.95	5.6	9.6
Forest fires	.19	.11	.31	.09	3.8	.02	23	.57	2.3	1.9	.22	.26	1.8	7.6
Biogenic: Continental particulates	.26	.15	.52	1.0	256	.02	27	.40	.51	1.3	.20	.12	.92	2.6
Continental volatiles	1.3	.04	.06	.05	.32	.61	1.3	.06	.10	.20	.04	2.6	.13	2.5
Marine	2.3	.05	.08	.06	.39	.77	1.5	.08	.12	.24	.05	4.7	.16	3.0
Total emission	12	1.3	6.1	44	28	2.5	317	3.0	30	12	2.4	9.3	28	45

Table 6. Global emissions of trace metals from anthropogenic sources ($\times 10^6$ kg/yr).

Data from Nriagu [68]

Source category	As	Cd	Cr	Cu	Hg	Mn	Mo	Ni	Pb	Sb	Se	Sn	V	Zn
Coal combustion	2.0	.53	11	5.2	2.1	11	2.7	14	8.2	1.3	1.8	1.0	7.9	11
Oil combustion	.06	.14	1.4	1.9	-	1.4	.55	27	2.4	-	.48	3.3	76	1.4
Non ferrous metals: Mine operation	.06	-	-	.48	-	.62	-	.80	2.6	.10	.10	-	-	.46
Pb production	1.2	.12	-	.27	.01	-	-	.33	21	.29	.29	-	.06	.33
Cu/Ni production	11	2.6	-	22	.12	2.6	-	7.6	16	1.1	.85	1.1	-	6.4
Zn production	.46	2.8	-	.48	-	-	-	-	8.5	.07	.16	-	-	64
Secondary non-ferrous metals	-	-	-	.11	-	15	-	-	.76	.02	.02	-	-	.86
Iron and steel Manufacture	1.4	.16	16	1.5	-	-	-	3.7	7.6	-	-	-	.74	20
Refuse incineration	.31	.75	.84	1.6	1.2	8.2	-	.36	2.4	.67	.06	.81	1.2	5.9
Phosphate fertilizers	-	.17	-	.41	-	-	-	.41	.16	-	-	-	-	4.1
Plant production	.53	.27	1.3	-	-	-	-	.49	7.1	-	-	-	-	9.8
Fuel wood combustion	.18	.12	-	.90	.18	-	-	1.2	2.1	-	-	-	-	3.6
Miscellaneous sources	2.0	-	-	-	-	-	-	-	253**	-	-	-	-	3.2
Total Emission	19	7.6	30	35	3.6	38	3.2	56	332	3.5	3.8***	6.2	86	132

A blank in the table denotes an insignificant contribution from a particular source.

Mostly from automobile tailpipes; *Particulate Se only, the total (volatile and particulate)

flux is 6.3×10^6 kg/yr.

The distribution and overall migration of elements in the various environmental matrices can be explained by the geochemical cycle of elements. In the lithosphere this begins with the initial crystallisation of the magma, proceeds through the weathering and alteration of igneous rock and then transport, deposition and diagenesis to produce sedimentary rocks. Sedimentary rocks further give rise to metamorphic rocks which by anatexis and paligenesis again generates magma. This cycle is depicted in fig. 6 [69]. The average abundances of elements in the Earth's

crust and granitic rocks are given in Table 7. Brooks has also listed average abundances of some trace elements soil, sediment and igneous rocks, as listed in Table 8. The elements, namely, Fe, Ni, S (or possibly O) comprises most of the Earth's core and O, Si, Al, Ca, Fe, K, Na and Mg comprises most of the Earth's crust [69, 70].

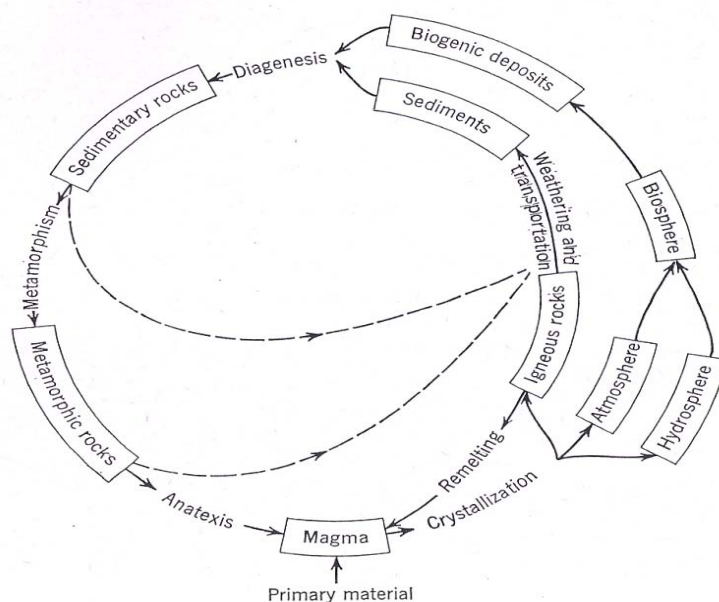


Fig. 6. Geochemical cycle of elements

Table7 . Abundances of some elements in the Earth's crust and Granitic rocks in $\mu\text{g/g}$ [69, 70].

Element	Crustal average	Granite	Element	Crustal average	Granite
H	1400	400	Fe	50000	13700
Li	20	24	Co	25	2.4
Be	2.8	3	Ni	75	2
B	10	2	Cu	55	13
C	200	200	Zn	70	45
N	20	8	As	1.8	0.8
O	466000	485000	Cd	0.2	0.06
Na	28300	24600	Sb	0.2	0.4
Mg	20900	2400	La	30	120
Al	81300	74300	Sm	6.0	11
Si	277200	339600	Lu	0.5	0.1
K	25900	45100	Hg	0.08	0.2
Ca	36300	9900	Pb	13	49

Cr	100	22	Th	7.2	52
Mn	950	230	U	1.8	3.7

Table 8. Average abundances of trace elements in soil, Earth's crust, sediment and igneous rocks in ppm [71].

Element	Soil	Sediment	Igneous rock
Mn	850	760	1000
Cr	200	130	117
Z	50	80	80
Ni	40	95	100
Cu	20	57	70
Pb	10	20	16
Co	10	22	18
Cd	0.5	0.2	0.13

Again, the distribution of elements within different rocks is also variable. This depends on the rock type and hence the process of formation of the rock (geochemical cycle). For example the acid rocks (granites) are different from the ultrabasic rocks (peridotites, dunites) and basic rocks (gabbro, basalts) in elemental abundances, as shown in Table 9. The mean contents of certain heavy metals in major rock types are given in Table 10.

Table 9. Elements accumulated in different rocks [72].

Elements accumulated in basic and ultrabasic rocks	Elements accumulated in acid rocks
Ti, V, Cr, Mg, Ni, Cu, Co, Fe, Zn, Sc	Ca, Be, Si, Ce, Mo, W, Nb, Ta, Sn, Li, Zr, Hf, Y, U, Th, Sr, Pb, K, Ba, Rb, Tl, Cs

Table 10. Mean contents of certain heavy metals in major rock types ($\mu\text{g/g}$) [73 and references therein].

Element	Igneous rocks			Sedimentary rocks		
	Ultrabasic	Basic	Granitic	Limestone	Sandstone	Shales
As	1	1.5	1.5	1	1	13
Cd	0.12	0.13	0.09	0.028	0.05	0.22
Co	110	35	1	0.1	0.3	19

Cr	2980	200	4	11	35	90
Cu	42	90	13	5.5	30	39
Hg	0.004	0.01	0.08	0.16	0.2	2.6
Mn	1040	1500	400	620	460	850
Ni	2000	150	0.5	7	9	68
Zn	58	100	52	20	30	120
Pb	14	3	24	5.7	10	23
Sb	0.1	0.2	0.2	0.3	0.05	1.5
Se	0.13	0.05	0.05	0.03	0.01	0.5
U	0.03	0.43	4.4	2.2	0.45	3.7

Glodschmidt in 1932 classified elements based on their geochemically different behaviour, into siderophile, chalcophile, lithophile and atmophile elements with affinities for metallic iron, sulphide, silicate and for the atmosphere respectively. In general, this classification refers to the behaviour of an element in liquid-liquid equilibria between melts [69,73]. Typical examples of siderophile, chalcophile, lithophile and atmophile elements are Ni, Co, Pt, Au, Mo; Se, As, Zn, Cd, Cu, Ag, (Au), Pb, Sb, Tl; Al, Na, K, Ca, V, Cr, Mn and N, Ar respectively. In order to understand more about the behaviour of elements in the environment, it is vital to study their mechanism of distribution in the Earth. Under natural conditions the metals are mobilised in two ways: hypogene and supergene mobility. The former implies the crystallisation of liquid magma and distribution in various rock types in a definite pattern. Thereafter, the weathering process sets in and the elements are mobilised in the secondary environment by supergene mobility [71]. Elements get concentrated in certain type of geochemical formations, known as ores, by the process of primary dispersion. During crystallisation of rocks from the cooling and solidifying melt, the prevailing temperatures and pressures govern the sequence of minerals formed by the primary elements. The physicochemical properties of elements like ionic radii, valence state and electronegativity affect these processes. Secondary dispersion occurs by physical and chemical weathering, whereby elements are mobilised from the bedrock to the surrounding environment.

Physical weathering breaks rocks into smaller particles, thus increasing the reactive surface area. Chemical weathering, occurring in the presence of water and oxygen, change the primary minerals into phases that are stable in surface conditions of low temperature and pressure. The newly formed phases are particulate and colloidal material, with physical properties intermediate of bedrock, water and minerals resistant to weathering. The behaviour of these aqueous species (ionic potential, hydrated ion diameter etc.) determines the fate of elements.

Depending on these factors an element may be leached from weathered material; precipitated from solution as hydroxide, carbonate, sulphate, phosphate etc. or adsorbed onto the charged surfaces of clay particles or organic matter [74]. Conductivity, pH and stability of host minerals are important parameters for weathering processes. The relative mobilities of elements and their pH dependence are given in Table 11 [71]. It is evident from the table that U, Se, V, Mo are more mobile in the environment in higher oxidation states.

Table 11. Relative mobilities of elements in the environment

Relative mobility	Environmental conditions			
	Oxidising	Acidic	Neutral to alkaline	Reducing
Very high	Cl, Br, I, S, B	Cl, Br, I, S, B	Cl, Br, I, S, B, Mo, V, U, Se, Re	Cl, Br, I
High	Mo, V, U, Se, Ca, Na, Mg, Ra, Zn	Mo, V, U, Se, Ca, Na, Mg, Ra, Zn, Cu, Co, Ni, Hg, Au, Ag	Mg, Ra, Ca, Na	Mg, Ra, Ca, Na
Medium	Cu, Co, Ni, Hg, Cd, As	As, Cd	As, Cd	
Low	Si, P, Pb, K, Cs, Bi, Be, Ba	Si, P, Pb, K, Cs, Bi, Be, Ba	Si, P, Pb, K, Cs, Bi, Be, Ba	Si, P, K, Fe, Mn
Very low to immobile	Fe, Mn, Al, Ti, Cr, Zn, REE	Ti, Al, Cr, Sn, REE	Ti, Al, Cr, Sn, REE	Ti, Al, Cr, Sn, REE

1.2.2. Variation with physicochemical parameters

There are several factors that influence the enrichment of major and trace elements in a matrix, such as mineralogical composition, weathering, particle size, pH, redox condition, organic matter content, leaching and human activities.

Weathering processes affect the mineral makeup of a matrix is affected by the weathering process which in turn affects the distribution of elements. Primary minerals are generally resistant to weathering due to their lower temperature of initial crystallisation. Minerals that are most stable at high temperatures, and therefore crystallize first from the molten magma, are the least stable at low temperatures and hence are least resistant to weathering [75]. The minerals in igneous rocks and metamorphic rocks can be arranged in an increasing order with respect to their resistance to weathering [75], as given below:

Olivine<Hypersthene<Augite< Biotite mica<K feldspar<Muscovite mica<Quartz

Ca plagioclase<Ca-Na plagioclase<Na-Ca plagioclase<Na plagioclase<K feldspar<Muscovite mica<Quartz

Low pH values, presence of complexing ligands, warm temperatures and high leaching potential lead to mineral weathering [76]. Element concentrations are related to the size of the soil particles. Thus, the loss or gain in clay, silt and sand size fractions of soil by eolian or hydrological transport causes differences in element enrichment in regional or local scales. Generally the elements that are resistant to leaching and are associated with the easily weathered minerals tend to accumulate in the clay size fraction. Quartz is generally a primary mineral absent in the clay size (<2 μ) fraction of soils. This is because quartz mineral grains reduced to clay size dimensions have sufficient free energy (from unsatisfied chemical bonds) that enhances their solubility and reduces their longevity in the geological time scale. Apart from association

with particle size, some elements are related with iron and manganese oxides during the early stages of rock weathering.

Migration of elements from a matrix is dependent on the hydrogen ion concentration in the aqueous solution, i.e. the pH of the matrix. The pH of acidic soils may reach values of 2, and that of alkaline soils can vary up to 11. The acidity of normal soils varies from 5-7 pH units. Many of the elements form difficultly soluble hydroxides at higher pH values and hence their mobility is reduced [72].

The redox potential of a system shifts the natural oxidation-reduction reaction of multivalent elements in one direction or another [72]. For example, arsenic is known to commonly exist as As^{+3} and As^{+5} . The As^{+3} is believed to be more mobile and more toxic than the As^{+5} . As a result, arsenic will leach from a material at a higher rate under reduced conditions. Chromium typically exists either as Cr^{+3} or Cr^{+6} . Trivalent chromium has low solubility in water and therefore is less mobile, while hexavalent chromium is more mobile and toxic. Under oxidizing conditions, trivalent chromium is converted into hexavalent chromium, resulting in enhanced toxicity and mobility in the environment. In alkaline zones, at high pH, the oxidation potential decreases and oxidation proceeds more rapidly [72]. Oxidizing conditions prevail in hot, arid regions, while swampy, peat containing, high moisture content regions have reducing conditions.

The organic matter content, also called humus, is formed by the decomposition of dead plant organisms, fallen leaves and needles. The organic material, under certain conditions, forms soluble complex compounds with elements and thereby enhance their mobility. In other conditions they may fix some elements like As, Se, Cu, Zn etc. and reduce their environmental mobility [72]. Humic, fulvic and other organic acids are some examples of complexing agents naturally present in the environment.

Elements can redistribute in a matrix due to geological processes like leaching. Cations, especially alkali and alkaline earth elements tend to be influenced by leaching processes.

Organisms, particularly plant organisms, are also effective in mobilising, extracting and dissolving many elements in the environment [72].

Elements generated due to anthropogenic activities are, on the other hand, adsorbed onto metal oxides/hydroxides, clay minerals and humic substances. All three of these substances are abundant in the clay size fraction of soils.

From the above discussions it can be inferred that the study of elemental distributions and their variations due to different physico chemical parameters of the matrices can aid in understanding elemental behaviour. Rare earth elements have long been used in similar studies [77-80] to understand the genesis of soils and rocks and thereby predict elemental behaviour in the same. Hence the concentration distribution of elements in various environmental matrices of this highly mineralised environment and their relation with physico chemical parameters of the matrices studied is important to predict the environmental behaviour of elements in this region.

1.3. Extraction and Leaching

1.3.1. Definition and methods

Geochemical processes, like interaction with water (leaching and erosion), lead to the mobility of an element in the environment and its presence in the aqueous medium. Elemental physicochemical mobility and leaching to groundwater is dependent on several factors like pH, redox potential, concentration of complexing anions, porosity of the medium, temperature, presence of organic and inorganic compounds, amount of water available for leaching and microbial activity [81-84]. For instance, heavy metals are mobilised into soil solution by a

decrease in pH and by decomposition of humus [85]. It is very important to consider the mobility of an element, apart from their total content in any soil, sediment, waste or rock, to assess the impact of that matrix on the environment. Because the leaching process is very complex, no one single leaching test or single set of leaching conditions is appropriate for a wide variety of leach testing objectives and applications [86]. For this reason, several leaching tests have been developed in order to evaluate the different leaching parameters and conditions being tested. These tests simulate the chemical reactions that can occur in soils, sediments, wastes, rocks etc and provide a relative empirical measurement of the amounts of elements that may be mobilised from a sample and become available for plant uptake at the time of the measurement, or over a longer period of time. Following deposition and/or discharge, the distribution of pollutants between soil solution and soil solid phases gradually reaches equilibrium and may become associated with soil–plant nutrient cycling processes. The rate at which equilibrium is reached depends on the form of the original pollution, and on soil characteristics; this process may take years [85]. Once elements enter the soil, their forms change as they interact with other soil components [87]. Initially, the mobility and bioavailability of elements is influenced by the physico-chemical form of the fallout [87]. Thereafter, the form/speciation of the elements can change with time due to dynamic biological and biochemical soil processes including organic and mineral cation exchange, complex formation, leaching and mineral weathering.

There are two groups of leaching tests that can be used for studies on leaching and extraction: equilibrium tests and dynamic tests. Equilibrium tests are designed to evaluate the release of constituents in the limiting case when the material is in chemical equilibrium with its surroundings; dynamic tests are designed to evaluate the release of constituents as a function of time. Equilibrium testing offers the advantage of greater reproducibility and simpler design;

dynamic testing provides more realistic simulation of leaching processes that occur in field conditions [88-94].

Equilibrium tests were developed to study the equilibrium between a solid phase and a leachant solution. There are several approaches to equilibrium tests, including single batch extractions with and without pH control, single batch extractions with some form of complexation by organic constituents and single batch extractions at low liquid: solid ratios [94]. As a general rule for equilibrium tests, the material is in contact with the leaching solution and the variables include: contact time, agitation rate, pH of the leachant solution and liquid: solid ratio. Equilibrium leaching tests have been discussed extensively elsewhere [86]. The goal of equilibrium batch testing is to represent constituent solubility and release over a range of conditions by varying one parameter (e.g., pH, liquid: solid ratio) [86]. Dynamic tests include multiple or serial batch test, and percolation and flow through (i.e., column) tests. While serial batch testing can provide leaching information of heavy metals for a given material, it is not possible to rely on serial batch testing for predicting the movement of these metals through the ground. Column tests typically consist of a leachant (e.g., deionised water, acidified water) percolating through a column packed with the material of study. Hence column leaching tests provide a better way of evaluating the soil sorption performance and the effects of partial soil saturation [95]. These tests give an indication of the time-dependent leaching behavior, and can be useful to quantify the retention of the element of interest in the matrix relative to the inert constituents of the matrix. Kosson et al. developed a framework for evaluation of leaching from materials that provides specific leaching test methods and a hierarchical approach to testing and evaluation [96]. Batch tests proposed in this framework are designed to measure the intrinsic leaching properties of a material, including aqueous-solid equilibrium partitioning of

constituents, and evaluate the release of constituents in the limiting case when the material is in chemical equilibrium with its surroundings.

As the environmental processes operate for a long time, it is very important to study the behaviour of a solid, in contact with a liquid over a long period. Long-term leaching behaviour has been used to assess the environmental risk or impact associated with fly ash for land fill purposes [97, 98]. Semi-dynamic leaching tests or static leaching tests are generally used to understand the slow environmental processes by researchers [97, 99-101]. Such tests simulate the slow and long-term environmental processes and are used mainly for waste matrices. The trend of the release of uranium during weathering and leaching processes can be used to understand the solid-water interactions. Ettler et al. [102] have investigated the leaching behaviour of metallurgical slags from lead smelting to understand the slag-water interactions. The knowledge of the trends of release of metals and other contaminants due to geochemical processes like weathering and leaching are essential to predict their mobility and possibility to reach groundwater. Also, the determination of reaction rates from leaching experiments has important applications in the management and remediation of contaminated sites. Reaction mechanisms and reaction rate constants can be incorporated into hydrogeochemical reactive transport models for contaminant mobility. Reaction rates are also key parameters for the design of water treatment and site remediation strategies.

Any leaching (dissolution) process comprises of three main stages [103]. The first stage is approach of the leachant to the solid surface through either molecular diffusion or convection. At the second stage, chemical reactions at the solid - liquid interface take place, and at the third stage, the ions or molecules of the sample being dissolved are withdrawn to the solution bulk. If the whole process rate is limited by the rate of the first or third stage, the course of the process is

governed by the laws of diffusion kinetics. If the second stage is the rate-limiting stage, the process follows the laws of chemical kinetics. Some processes obey mixed kinetics. The rate of dissolution and leaching of minerals and other solids is determined, in most cases, by the rate of diffusion [104, 105]. The extraction processes of the forms of elements are, most often, also diffusion-controlled.

Apart from the leaching procedures discussed earlier, many single and sequential leaching procedures have also been developed [85, 106, 107] to identify the chemical forms and evaluate the mobility and bioavailability of elements from soil, sediment etc. and hence to assess the risk associated with the solid. Heavy metals and radionuclides associated with exchangeable phases, as measured by extractants, are assumed to be easily mobilised by soil–soil solution ion exchange reactions. Pollutants associated with oxidisable phases, as measured by more chemically aggressive extractants, are assumed to remain in soil for longer periods but may be mobilised by decomposition processes like weathering and microbial activity. However, reactions taking place in the laboratory during extraction are non-selective. They are likely to be influenced by the length of extraction time and the soil mass: volume ratio used. Therefore, elemental concentrations measured in the extract solution are defined by the extractant and the experimental protocol [108, 109].

A range of single extractants are used to bring elements associated with particular soil fractions into solution, some of them are shown in fig. 7 [85, 110]. Apart from the single extractants mentioned in the Fig, few other extractants are, H_2O ; CaCl_2 , $\text{CH}_3\text{COONH}_4$, NH_4NO_3 , NaNO_3 , BaCl_2 , MgCl_2 ; CH_3COOH , CH_3COONa ; EDTA, DTPA; $\text{NH}_2\text{OH.HCl}$; $\text{K}_4\text{P}_2\text{O}_7$ used for the elemental water soluble fraction; exchangeable fraction; carbonate bound fraction; non-silicate bound fraction; reducible fraction and fraction bound to organic matter and sulphides

respectively [85, 110 and references therein]. Apart from single extraction procedures, sequential extraction procedures like Community Bureau of Reference (BCR) (refer fig. 5) and Tessier method are also used. In Tessier method the phases are operationally defined as water soluble (H_2O), exchangeable (1 M MgCl_2), carbonate bound (1 M NaOAc adjusted to pH 5 with AcOH), bound to Fe–Mn oxides (0.04 M NH_4OH , HCl in 25% v/v AcOH), bound to organic matter (H_2O_2 adjusted to pH 2 with HNO_3) and residual (HF – HClO_4 digestion). The increasing strength of extractants down the extract series can be used to predict pollutant soil associations and hence potential mobility and bioavailability. Hence elemental concentrations measured in sequential extraction solutions can be used to differentiate between short and long term soil radionuclide and heavy metal bioavailability.

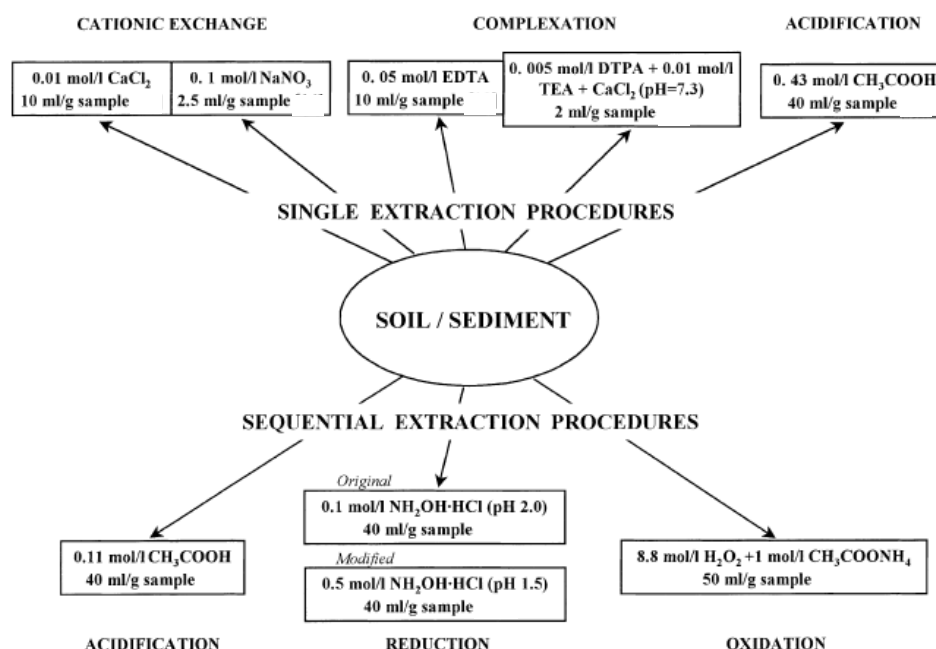


Fig. 7. Single and sequential extraction schemes for assessing elemental mobility

Any laboratory leaching method can only be used to determine a few extremely important elements of leaching. The mass of easily mobilised elements can be determined using a leaching test with a short equilibration time. Again, a comparison of bulk concentrations of elements with

their leachate concentrations can be used for estimating the mobilisation of various elements with respect to time. The evolution of leachate concentrations can be determined with multi-equilibration time long-term leaching experiments. But it has to be kept in mind that, laboratory leaching cannot provide an estimation of the concentration of elements in leachates under natural conditions with a very high degree of accuracy. The concentration of chemical constituents under natural leaching conditions will be a product of several factors that are not easily duplicated in laboratory leaching.

The environmental pollution by the mining industry and wastes generated thereby can be a potential source of contamination both in soil and water. Hence it is very important to characterize them physically and chemically and also study their behaviour in contact with liquids. Water plays a dual role in the environmental processes by triggering a sequence of reactions and by carrying contaminants away from the waste site [111]. Water infiltration through these waste piles presents a potential hazard to the underground aquifers [111]. Hence, it is important to estimate the leaching of uranium from tailings that acts as the major migration and transfer processes caused by ingress of water into tailings piles [112]. The leaching of the toxic constituents however becomes prominent when the tailings are in loose form. This is due to the acid generating process of pyrite, a major constituent of the tailings [111]. The radioactive elements and toxic heavy metals may travel from the waste mass to the pore water [111], where they may be mobilised. This mobilisation in soil solution of the contaminants may lead to their uptake by plants or transport in groundwater and hence finally they may reach the human food chain.

1.3.2. Variation with physical conditions of leaching

Factors influencing elemental leaching from waste material include pH, particle size, complexation with organic or inorganic chemicals, liquid: solid ratio, leaching (or contact) time, kinetics, redox conditions and chemical speciation of pollutants of interest [113]. Table 12 below lists some of the important physical and chemical-biological parameters.

Table 12. Parameters affecting leaching

Physical factors	Chemical-biological factors
Particle size, contact time, homogeneity, liquid to solid ratio, porosity, sorption, temperature, type of flow, partitioning	pH, redox condition, precipitation, organic carbon content, precipitation, alkalinity, common ion effect

pH

One of the significant factors influencing the release of elements from any solid material is pH. The leach rate in leaching experiments is not only controlled by the pH of the leachant but also by a number of reactions. Many metals are widely known to have the tendency to leach more at extreme pH values [114, 94, 115]. To evaluate pH effect on metal leaching, a pH static test is commonly employed over a broad range of pH.

Particle Size

Particle size of a material determines its surface area exposed to the leaching solution. Whenever leaching tests are carried out on size-reduced material, a larger surface area is exposed to the leaching solution, resulting in more chance of transfer of an element from the material into the solution.

Oxidation Reduction Condition

Oxidation and reduction conditions may play a significant role in chemical leaching from a solid substance. To measure oxidation and reduction condition in a given chemical system, oxidation reduction potential is measured to determine electron availability. Oxidation reduction potential indicates the intensity of oxidation or reduction in the chemical system. For some heavy metals, it directly changes the oxidation state of the metals and consequently determines their mobility in the environment, as discussed earlier. Biologically active environments can create reducing conditions, resulting in heavy metals being substantially immobilised within the solid material through precipitation with sulfides and complexation with organic acids.

Liquid-to-Solid (L/S) Ratio

The L/S ratio is defined as the amount of a leaching solution in contact with the amount of solid material used for the leaching experiment (e.g., liter/kg). In batch tests, L/S ratios typically range from 20 to 10, while relatively low L/S ratios are used in a column (or field) test. In general, chemical concentrations are greater at lower L/S and decrease as the L/S increases because of less dilution of waste material with leaching solution. Grimshaw, [116] recommended that the best soil: extractant ratio for nutrient studies is one such that doubling or halving the ratio makes no difference to the final result. He suggested that high ratios were better, recommending 1: 25 for extractants used to measure nutrient concentrations. A number of radioecologists have opted for 1: 10 when extracting for radionuclides [117, 118]. Others do not provide clear information about the ratios used or refer to Tessier, [119] who used a ratio of 1: 8 for their heavy metal work with aquatic sediments. If the solid mass to extractant volume ratio is kept very low, for example 1:5, there is a possibility of radionuclide and heavy metal re-adsorption and in such cases the solid-extractant equilibrium condition may not be attained [85].

Contact Time

The amount of time during which a leaching solution is in contact with waste material may influence the quantity of contaminant leached unless equilibrium conditions are established. The amount of contaminant released may depend upon contact (or leaching) time. In extraction batch tests, the contact time is equal to the duration of the test. For this reason, contact time for extraction tests should run until equilibrium conditions are reached for the contaminants of interest. Batch leaching tests such as TCLP and SPLP are based on the assumption that kinetic equilibrium or local equilibrium is reached. Since the tests may not give sufficient time for equilibrium to be reached, attempts should be made to ensure that kinetic equilibrium is reached during the testing period. It is important that the shaking time is fixed, and that the time is sufficient to allow a steady state to be established between the soil and the extractant but not so long that dissolution of other soil fractions occurs [85]. In practice, the contact time needs to be a minimum of 1h to 17h. Where only gentle or intermittent shaking is used it may be necessary to extend this up to 24 h [85].

From the foregoing discussion it is clear that the leaching and extraction studies of toxic, trace and heavy elements are very important from the environmental point of view to predict their mobility and availability in the environment. Extensive studies in this regard have been carried out globally [101, 81, 97, 102, 120, 112, 85, 100, 121, 107, 122, 113, 106]. Hence it was considered important to study the leaching behaviour of uranium from different environmental matrices in this highly mineralised study area, hosting natural uranium deposits.

1.4. Physiography of the Region

Studies were carried out at locations around uranium deposits in the Singhbhum region of Jharkhand state in Eastern India. Fig. 8 shows the location of this region. Uranium mineralisation

has taken place discontinuously here, along the 200 km long Singhbhum copper-uranium belt, concentration being more in the central part [112]. Apart from uranium, the region is known for its widespread mineral deposits including Cu, Ni, Mo of economically viable grades [123].

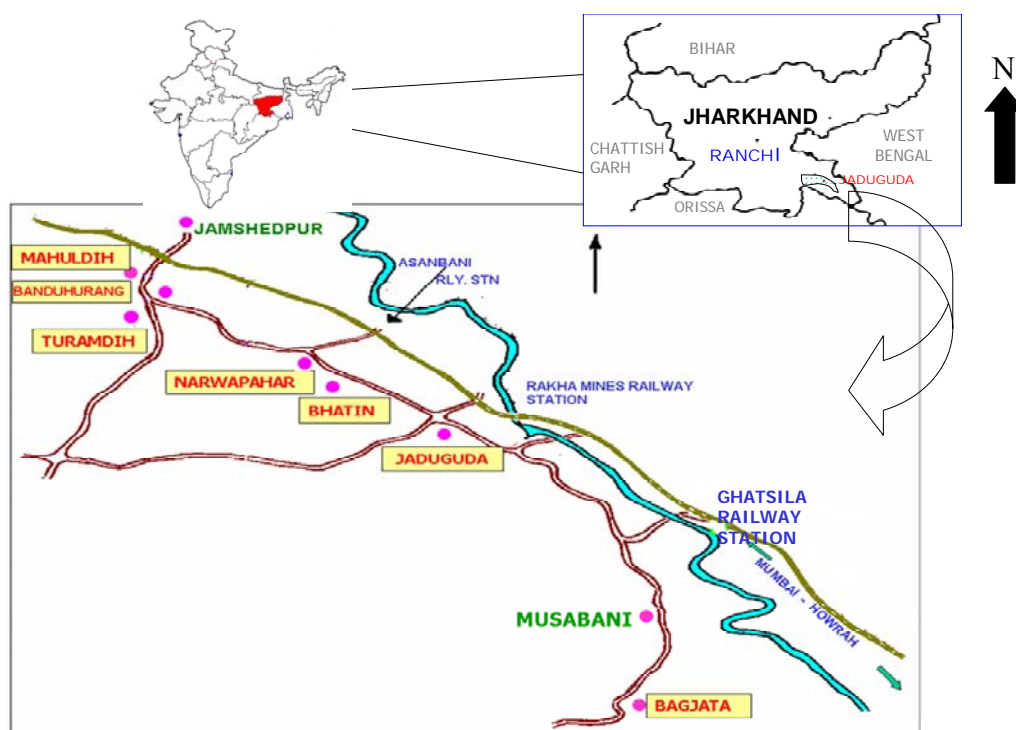


Fig. 8. Location map of the Singhbhum region (with uranium deposits) in India

1.4.1. Climate

The annual rainfall in the area is around 1200 mm and the area is naturally well vegetated. The agricultural land is fertile and crops are irrigated by stream or river waters. The area experiences three climatic seasons, a hot season from March to May, a rainy season from June to September and a cold season from November to February. The Tropic of Cancer crosses through the state, so that the area experiences true tropical climate. Maximum temperatures of 39-42°C is observed during the summer months, Average temperatures in the winter months come down to 9-15°C. Relative humidity ranges from nearly 50% in the summer to 85% in the monsoons [124].

1.4.2. Geology

This mineralised region, hosting underground uranium deposits, is located in the hilly and undulating terrain within the Singhbhum Shear Zone, in East Singhbhum district of Jharkhand. Mostly Arachaeon or Precambrian formations of schists, phillites, quartzites, gneisses and altered tuffs are present in this area, as shown in the geological map of the region in fig. 9 [125]. The rock types are classified under two stages: the older Chaibasa stage and the younger Dhanjori stage. The older rocks of Chaibasa stage have been thrust upon the younger rocks of Dhanjori stage. The thrust contact itself was severely sheared and brecciated. Uranium occurs in this brecciated zone in finely disseminated form. The mineralisation is structurally controlled and is confined to shears [125]. The major shear zone, called the Singhbhum Copper belt divides the Arachaeon rocks of Singhbhum into an unmetamorphosed one in the South and a metamorphosed one in the North. Uranium mineralisation occurs discontinuously in the metasediments at several places in this Copper belt, which runs for more than 160km and is 2-5km wide [126]. Wide-spread uranium mineralisation is found to be associated with copper, nickel, molybdenum and other sulphides. The south-eastern part of the shear zone is rich in copper mineralisation, whereas the central part between Jaduguda–Bhatin–Nimidihi, Narwapahar–Garadihi–Turamidihi and Mahuldihi are rich in uranium [127]. The shear zone was active over a long time period of 2000 to 700 Ma and has been the centre for volcanism and emplacement of basic intrusives and granites rich in potassium and sodium [127].

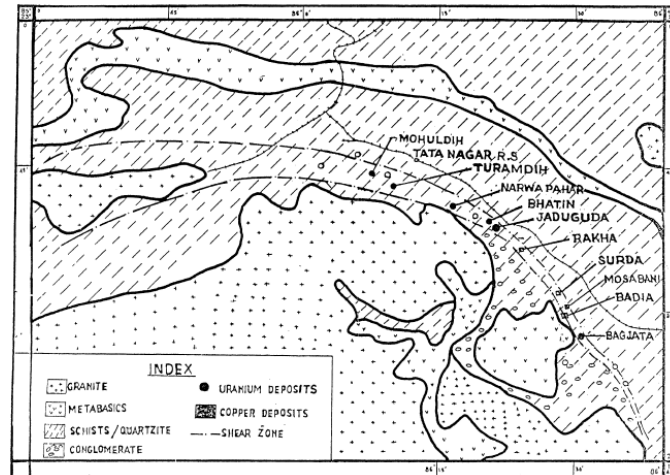


Fig 9. Geological map of Singhbhum Shear Zone with the uranium deposits at Bhatin, Narwapahar, Jaduguda and Turamdih

The mineralisation in the uranium deposits at Singhbhum (India) is mainly within the narrow cracks in metamorphic rocks, also filled with pitchblende and are hence named vein type deposits [128]. In vein deposits, the major part of the mineralisation fills fractures with highly variable thickness. The veins consist mainly of gangue material (e.g. carbonates, quartz) and ore material, mainly pitchblende [128]. The early Proterozoic rocks which contain the mineralisation are chlorite-biotite bearing quartz schists, with apatite, magnetite, and tourmaline as accessories; quartz-chlorite schist containing apatite and magnetite; biotite-chlorite schist; brecciated quartzites and soda (silica) metasomatites. The sheet-like orebodies, sometimes occurring more than one at a place, are conformable with the compositional banding and schistosity in the host rocks [112].

The average grade of the uranium ore from the Singhbhum Belt is $< 0.01\% \text{ U}_3\text{O}_8$ [112]. The principal ore mineral, uraninite, occurs as disseminated grains and crystals. Other primary uranium-bearing minerals are sooty pitchblende, a complex U-Ti oxide, allanite, sphene, xenotime, davidite, pyrochlore-microlite, clarkeite, schoepite, and rare monazites [129 and

references therein, 130]. Secondary uranium minerals occur as autunite, potassium autunite, uranophene, torbernite, uraniferous iron oxides and rare interstitial uraninite or pitchblende. The antecedent of these secondary minerals is ilmenite. The minerals namely, magnetite, ilmenite, martite, uraninite, rutile, chalcopyrite, pyrrhotite, marcasite, pyrite, machinawite, pentlandite, violanite, tellurbismuth, tetradyne, cubanite and molybdanite have been identified in the uranium ore. The dominance of uraninite over pitchblende, the presence of several percents of REE in uraninite, the development of hematite-bearing quartz and sodic oligoclase at places, the local association of uranium mineralisation and Ni(-Co)-Mo-S(-As-Se) mineralisation and the continuation of some of the ore veins to considerable depth suggest these ores formed at moderately high temperatures. The age of mineralisation is 1500 to 1600 Ma (IAEA, 1986).

The Singhbhum uraninite is low in thorium ($\text{UO}_2/\text{ThO}_2 = 70\text{-}150$), high in lead ($\text{PbO} = 14\text{-}15\%$) [131] and moderate in REE content [132]. Chlorite, biotite, tourmaline, apatite, magnetite, and quartz in the ore have been found to be radioactive. The source of radioactivity is uranium in the structural sites of these minerals or as inclusions of uraninite, or both [133].

Until now the most important deposit of the belt is located at Jaduguda where mining has been in progress for more than a decade. Jaduguda uranium deposit is a sodium metasomatic uranium deposit [128]. Other regions with similar deposits are Kirovograd Ore District (Ukraine), Beaverlodge (Canada), Itatiaia (Brazil) and Kokchetav Massif (Kazakhstan) [128]. Such deposits are related to alkaline metasomatites of sodium or potassium series. The metasomatites are developed in ancient shields and median masses, where they form stockworks controlled by long-lived ancient faults. Sodium metasomatites are predominantly albite in composition, usually with minor carbonate and alkaline amphiboles and pyroxenes — albitites and eisites [128]. There is evidence on all scales that deformation has outlasted ore mineralisation in this deposit. The

zones of intense copper and uranium mineralisation do not coincide [112]. The adjoining Bhatin deposit is more or less similar except that the mineralisation was less intense. Jaduguda and Bhatin deposits are separated by a post-mineralisation transverse fault [112]. At Narwapahar exists a low grade but large tonnage deposit extending for a strike length of over 3 km. There are two subparallel orebodies in this deposit, conformable to the dominant planar structures of the host rock. The average grade is 0.058% U_3O_8 . The host rock is sericitic chlorite schist with abundant introduced quartz and some feldspar. Dusty hematite in quartz and feldspar can be seen at places [112]. At Turamdih uranium deposit, south of Tatanagar, the uranium mineralised zone exists 30 m above the zone of copper mineralisation. The deposit occurs in sericitised chlorite schists. Its average grade is 0.04% U_3O_8 [112]. Vinogradov et al. [72] and Rao et al. [134] studied the Pb-isotope geochronology of these ores from several places in the belt. The age obtained from the $^{207}Pb/^{206}Pb$ ratio and the Concordia method suggest that most of the Singhbhum uranium has an age of 1500 to 1600 Ma, an age not much different from the uranium of vein-type deposits in parts of the Precambrian shields of Canada and Australia (1700 - 1800 Ma [112]).

1.5. Scope of the present thesis

Efforts have been made to incorporate relevant literature in each chapter of the thesis. However, a brief account of literature has also been presented earlier in this chapter. From the earlier discussions it can be concluded that studies on distribution and environmental behaviour of elements in this highly mineralised study area, hosting natural uranium deposits, is of prime importance.

Extensive geological studies have been carried out in this area since the last few decades [129 and references therein]. Physical characteristics of the tailings (particle size), leachability of radium and associated radioactivity have been reviewed by Markose [135] in the study area. Jha et al., have also carried out studies concerning radon and its daughters in this region [136-138]. Sengupta, Mahur and co-workers have also carried out experiments on radon and subsequent dose from the rocks in this region [139-142, 127]. Jha and co-workers have carried out studies on heavy metal uptake from uranium tailings, from this area and the radiological environment in this area [143, 144]. Mishra et al., [146] have also carried out some studies on distribution coefficients for stream sediments from this area.

The present thesis provides insights on the relatively less explored but significantly important area of radioactive disequilibrium, radionuclide transport and behaviour in the Singhbhum Shear Zone. The distribution of radionuclides and trace elements has been studied in various environmental matrices and natural radioactive disequilibrium has been investigated in the same to investigate elemental mobility. Leaching of uranium from different matrices has also been studied to understand its environmental behaviour. Effect of physico-chemical properties of samples on elemental distribution and leaching behaviour has been examined.

CHAPTER 2

SAMPLING AND ANALYTICAL TECHNIQUES

Scope

In order to draw a proper scientific conclusion from measurements on natural matrices practical considerations like sample collection, processing and preservation, methods of estimation, availability of equipment and skill of the concerned individual have to be taken into account. Calibration and standardisation of the instruments using Certified Reference Materials are also of vital importance. To ascertain that the quality of output from any measurement technique, continuous quality control exercises need to be carried out. The overall objective is to produce a quality output with improved level of accuracy and precision, which can be used for arriving at meaningful scientific conclusions.

This chapter discusses the sampling methodologies, experimental techniques employed in this thesis and quality control involved.

2.1. Sampling

The basic principle of environmental sampling to be studied before actual sample collection involve site selection, development of investigation plan, collection and review of background information, selection of sampling parameters, selection of sampling approach, selection of sampling points, selection of monitoring equipment and analytical sampling equipment.

During and after sampling the following steps have to be kept in mind:

Sample collection, sample number, sample volume, removal of extraneous material, physical characterisation of the sample, sample sieving, sample homogenisation, sample splitting and sample preparation.

2.1.1. Criteria for selection of sampling locations and matrices sampled

The basic criterion for the selection of sampling sites is that each sampling location should represent the area for the study. The following points should be considered while selecting the sampling locations.

Location of area should be representative of the region of interest

Site should be potentially impacted by different types of sources

It should not be located very near to a particular source

Easy accessibility and safety of the instrument is also important

2.1.2. Sampling methodology and sample collection

How a sample is collected can affect its representativeness. The greater the number of samples collected from a site and the larger the volume of each sample, the more representative the analytical results can be. However, sampling activities are often limited by sampling budgets and project schedules.

The approaches existing for collection of representative soil samples include judgmental, random, systematic grid, systematic random, search and transect sampling. Judgmental sampling is the subjective selection of sampling locations at a site, based on historical information, visual inspection, and on best professional judgement of the sampling team [146]. Random sampling is the arbitrary collection of samples within the defined boundaries of the area of concern. The arbitrary selection of sampling points requires each sampling point to be selected independent of the location of all other points, and results in all locations within the area of concern having an equal chance of being selected. Systematic grid sampling involves subdividing the area of concern by using a square, triangular or herringbone grid and collecting samples from the nodes. The

distance between sampling locations in the systematic grid is determined by the size of the area to be sampled and the number of samples to be collected. Systematic random sampling is a useful and flexible design for estimating the average pollutant concentration within grid cells and is sometimes also referred to as stratified random sampling. The area of concern is subdivided using a square or triangular grid and samples are collected from within each cell using the random selection procedures. Search sampling utilizes either a systematic grid or systematic random sampling approach to search for areas where contaminants exceed applicable clean-up standards. Transect sampling involves establishing one or more transect lines across the surface of a site. Samples are collected at regular intervals along the transect lines. The length of the transect line and the number of samples to be collected determine the spacing between sampling points [146].

In this thesis random sampling approach, as shown in fig. 10 has been employed for sample collection.

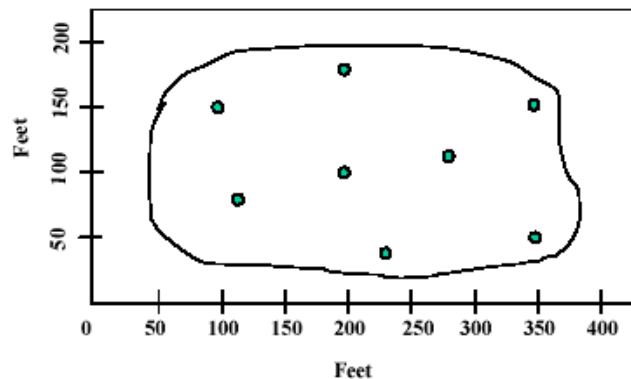


Fig. 10. Random sampling approach

Soil sample collection

Soil is a heterogeneous material which shows significant variation in chemical and physical properties even in a small site due to different geophysical formations,

topography, farming procedure, soil type, drainage, etc. It is one of the ultimate targets for all kinds of contaminants dispersed within the natural environment through human activities. Topsoil is a particularly difficult matrix for environmental pollution studies as it is generally composed of a multitude of geological and biological materials resulting from weathering and degradation including particles of different sizes with varying surface and chemical properties. There are many different soil types categorised according to their content of biological matter, from sandy soils to loam and peat soils, which make analytical characterisation even more complicated.

Representative soil sample is important for knowing the chemical composition of soil sample that represents the entire area under study. Representative soil sampling helps the location and identification of potential sources of contamination, defines the extent of contamination and helps the formulation of treatment options. The tools required for sampling include an auger, a spade and a trowel. For shallow sampling of disturbed material, a scoop or trowel is sufficient to gather material. Then the sample is placed in a polythene bag, sealed and clearly labeled with a permanent marker. Depth sampling can be carried out either by using augers or spades.

In this study, mostly topsoil / surface soil were collected, as an indicator of metal pollution in that area, using scoop. The soil samples were collected in polythene bags, sealed properly and labeled neatly. The details of the sample, for eg. sample code, sampling location, latitude and longitude of the location, date of collection etc. were registered.

Waste sample collection

The principal wastes produced in large quantities from uranium milling process that are

to be dealt with in the long term are the uranium tailings. The nature of tailings depends on the mineralogy of ore and host rock. The quantity depends on the ore body configuration and mining methods [112]. The amount of sludge produced is nearly the same as that of the ore milled. The uranium mill tailings management system, in Singhbhum, at present comprises of treatment of barren liquor from the ion exchange columns in uranium mill with lime stone slurry followed by addition of lime slurry to raise the pH to 10-10.5 and mixing with the barren cake slurry, obtained after filtration of the dissolved uranium. A final pH of 9.5 - 10 is maintained to keep the residual uranium, radium, other radionuclide and chemical pollutants in precipitate form with the solid tailings. The treated slurry is classified into coarse and fine fractions. The coarse material, forming nearly 50% of the total mass, is backfilled in mines. The fine tailings are pumped to engineered tailings ponds for permanent containment. The slimes with the precipitates settle down, the clear liquid is decanted and sent to the Effluent Treatment Plant.

In this study, surface uranium and copper tailings were collected from the tailings ponds, using a scoop. Copper clinker ash samples were also collected from the surface of the wastes around a copper smelter. The samples were collected in polythene bags, sealed properly and labeled neatly. Sample code, sampling location, latitude and longitude of the location, date of collection etc. were registered.

Uranium bearing rock collection

The uranium bearing rocks were collected from operational underground uranium deposits located in the Singhbhum Shear Zone of Eastern India. This 200 km arcuate belt in Jharkhand state of India is known for hosting vein/disseminated type of uranium deposits [129]. Uranium bearing rocks were collected from the deposits at Jaduguda,

Bhatin, Narwapahar and Turamdih in this region.

The uranium bearing rock samples were collected from UCIL, Jaduguda. The collected samples were obtained in fine powdered form. The details of the samples, for example, name of the deposit, depth of collection of the sample, date of collection of sample, location of sample collection etc. were noted down.

Non-uranium bearing rock collection

Mostly Archaean or Precambrian formations of schists, phillites, quartzites, gneisses and altered tuffs are present in the Singhbhum Shear Zone. The rock types are classified under: the older Chaibasa stage and the younger Dhanjori stage.

Non-uranium bearing metamorphic host rocks were collected from the Singhbhum Area in Jharkhand. The details of the samples, for example, date of collection of sample, location of sample collection etc. were noted down.

After sampling, all the samples, namely soils, uranium tailings, uranium bearing rocks and non-uranium bearing rocks, were brought back to the Environmental Assessment Division laboratory at BARC Hospital, Anushaktinagar, Mumbai for further processing and analysis, where all the analytical facilities are available.

2.1.3. Sample Processing and preservation

The samples were subjected to the following processes in the laboratory: removal of extraneous materials, sample drying, sieving. Extraneous materials are not relevant or vital for characterizing the sample or the site, since their presence may introduce an error in the sampling or analytical procedures. Examples of extraneous material in samples include glass pieces, stones, large roots, twigs or leaves [146]. These materials were first identified and discarded from the sample. The collected samples were then oven dried (at

105°C). The dried samples were first lightly ground to break big lumps and then sieved to <2mm particle size. Sieving is the process of physically sorting a sample to obtain uniform particle sizes. Sub-sampling was then carried out to obtain a small representative sample of finely ground sample. The purpose of this process is to obtain a sample suitable for the analytical technique and yet still remain representative of the original bulk sample. One of the most popular methods of sample homogenisation or sub-sampling the dried sample to obtain a representative sample for subsequent analysis is “coning and quartering” technique [147]. This technique was adopted in this thesis. In this procedure, the dried sample is thoroughly mixed and poured onto a clean sheet of polythene to form a cone. The cone is then divided into four quarters and opposite quarters taken and the procedure is repeated for at least five times for obtaining a representative sample.

Soil and uranium tailings sample were processed as given above. Uranium bearing rocks and non-uranium bearing rocks were in dry fine powder form and hence were homogenised and a sub-sample separated for further analysis.

Precautions in sample processing and sample storage

Sampling design, sampling methodology, sample handling, sample preparation, storage and analytical procedures are important steps causing uncertainty in analysis [146]. However reliable and sensitive the analytical technique may be, the quality of the data is lost if sufficient care is not taken regarding the sampling, pretreatment and storage. Trip blanks, field blanks and replicate samples are generally used to identify error due to sampling methodology and sample handling procedures [146]. As a general rule, the error in sampling and sample preparation stage portion of an analytical procedure is considerably higher than that in the methodology itself, as is evident in fig. 11 [148].

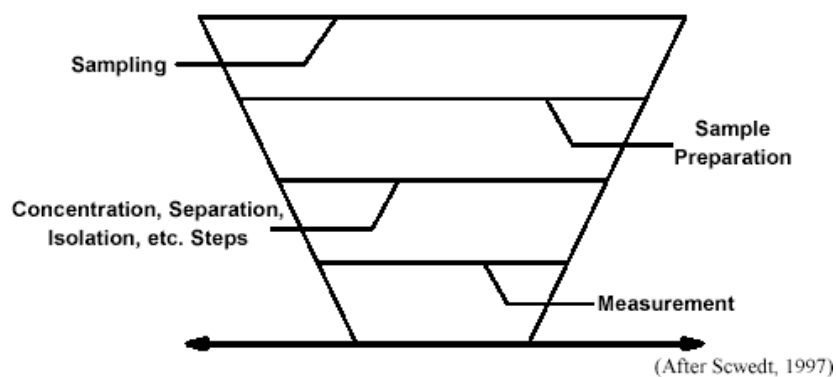


Fig. 11. Degree of error in laboratory sample preparation relative to other activities

Problems of cross-contamination and loss of elements are present at every stage of elemental analysis. This problem is especially relevant for lower concentration of analyte and small sample size. Adeloju et al. [149] have observed that airborne particulate can contribute significantly to elemental contamination from the environment. Therefore, attention was paid to containers, laboratory conditions and clean habits of the analyst.

There is a tendency for metals to get adsorbed on the walls of the containers, if they are not pretreated. On the other hand, acid treated samples may leach some of the metals from the containers itself. Quartz, teflon and high purity polyethylene containers are generally suitable for storing any solution. Several investigators [150, 151] have studied the interactions between trace elements in dilute solutions and container materials. Stumpler, [152] has studied the adsorption characteristics of Ag, Pb, Cd, Zn and Ni, on Borosilicate glass, polyethylene and polypropylene container surfaces. The adsorption losses can be prevented by using the containers of non-wettable walls (Teflon, Polyethylene etc.). The surface conditioning of quartz and glass containers can be carried out by dilute mineral acids, such as nitric acid (HNO_3) and hydrochloric acid (HCl), followed by thorough rinsing with distilled water.

In the present study, all laboratory wares used in sample collection, analysis and storage were soaked in 10% HNO₃ for several days and then rinsed thoroughly with distilled and double distilled water, respectively before use, according to EPA[153].

2.2. Analytical techniques

Analytical chemistry can be split into two main types, qualitative and quantitative. Most of the modern analytical chemistry is quantitative. Quantitative analysis can be further split into different areas of study. There are many techniques for the analysis of materials on the basis of spectroscopic, electrochemical, mass, thermal and separation parameters. Some of the most common techniques used in environment analysis are given in Fig. 12.

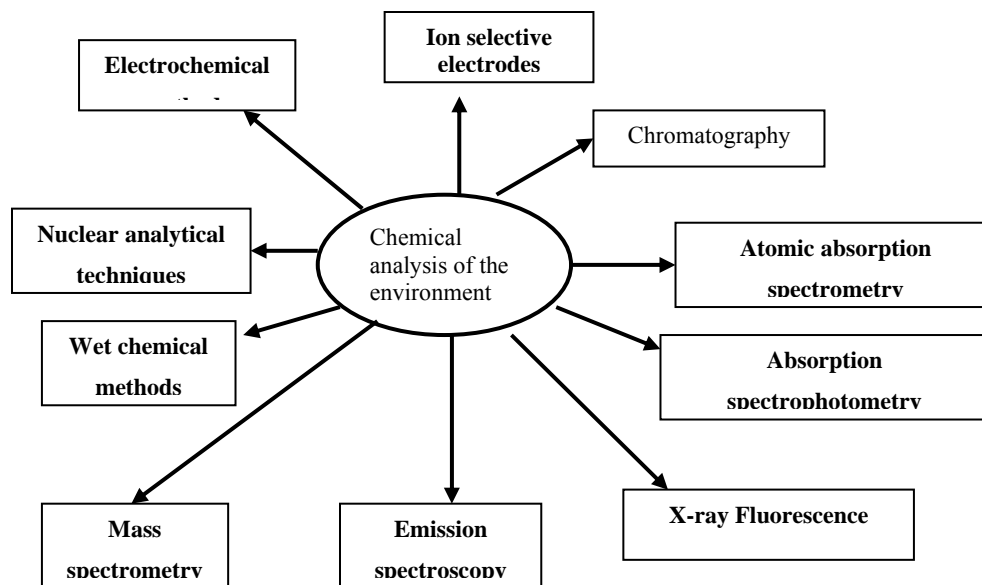


Fig. 12. Analytical techniques available for chemical analysis

The determination of elements in environmental samples is quite difficult due to the low concentrations, unknown constituents and interferences due to different chemical species present. Concentration of some of elements in environmental samples is very low, ranging from ppb to sub ppb range, which are near the detection limits of most of the

conventional techniques. Therefore analytical methods suitable for quantitative estimation at such low levels have to be selected based on the following criteria:

1. High sensitivity at low concentrations
2. Good precision and accuracy
3. High selectivity
4. Simple to operate and maintain
5. Minimum contamination problem
6. Independent of matrix effects and chemical interference
7. Simultaneous multi-elemental capability
8. Large sample throughput
9. High linear dynamic range

Besides the above criteria the speed of the method, number of samples that can be analysed, nature of the sample, cost per analysis and availability of the instrumentation and methodology are also to be considered. Being idealistic, no analytical method currently in use for environmental analysis satisfies all the above criteria. In the present study the techniques adapted, however meet most of them for elemental analysis and sensitivities attained are often much higher than from the other methods.

The details of the analytical techniques used in this study are explained below.

2.2.1. High Resolution Gamma Spectrometry

Spectrometry is the technique of analyzing the energy spectrum of a material and identifying the elements of interest in the same. Gamma ray spectrometry is one of the techniques used for isotopic estimation of gamma emitting radionuclides. It measures the energy and intensity of gamma photons, which in turn helps in determining the

radioactive contents of the sample. It is a nondestructive technique used for qualitative and quantitative determination of low level artificial and natural radioactivity in environmental or other samples through their gamma ray emission. Emission of gamma radiation is always associated with emission of alpha and beta particles. The estimation of natural radioactivity and radionuclides in any sample can hence be done by alpha spectrometry, beta counting and gamma spectrometry. The three techniques are compared in table 13.

Table 13. Different methods used for radioactivity quantification

Alpha spectrometry	Beta counting	Gamma spectrometry
Involves radiochemical separation	Involves radiochemical separation	Does not involve radiochemical separation
Tracers required	Tracers required	Certified reference standards required
Time consuming	Time consuming	Fast
Destructive	Destructive	Non-destructive

Due to the advantages of the gamma spectrometric technique being non-destructive, simultaneous multi-element, relatively faster and not involving radiochemical separations, it was the method of choice in this thesis.

Interaction of radiation with matter

A gamma ray photon is uncharged and creates no direct ionisation or excitation of the material through which it passes. The detection of gamma rays is therefore critically dependent on causing the gamma ray photon to undergo an interaction that transfers all or part of the photon energy to an electron in the absorbing material. Because the primary gamma ray photons are “invisible” to the detector, it is only the fast electrons created in

gamma ray interactions that provide any clue to the nature of incident gamma rays. These electrons have a maximum energy equal to the energy of the incident gamma ray photon and will slow down and lose their energy in the same manner as beta particle. Energy loss is therefore through ionisation and excitation of atoms within the absorber material and through bremsstrahlung emission. In order for a detector to serve as a gamma ray spectrometer, it must carry out the distinct functions of acting as a conversion medium in which incident gamma rays have a reasonable probability of interacting to yield one or more fast electrons and functioning as a conventional detector for these secondary electrons.

Gamma rays interact with matter in a number of ways. The three interactions which play a major role in the measurement of radiation are, photoelectric absorption, Compton scattering and pair production, as shown in fig. 13 (a), (b) and (c).

Photoelectric absorption is an interaction of the gamma photon with a bound electron, in which the incident gamma ray photon disappears. In its place, a photoelectron is produced from one of the electron shells of the absorber atom with a kinetic energy given by the incident photon energy $h\nu$ minus the binding energy of the electron in its original shell. Photoelectric absorption is an ideal process if one is interested in measuring the energy of the original gamma ray.

In Compton scattering the gamma photon interacts with a free or nearly free electron in a medium, due to elastic collisions of the photons with the electrons and leads to the emission of a recoil electron and scattered gamma photon. In normal circumstances, all scattering angles will occur in the detector. Therefore a continuum of energies can be transferred to the electron, ranging from zero up to a maximum.

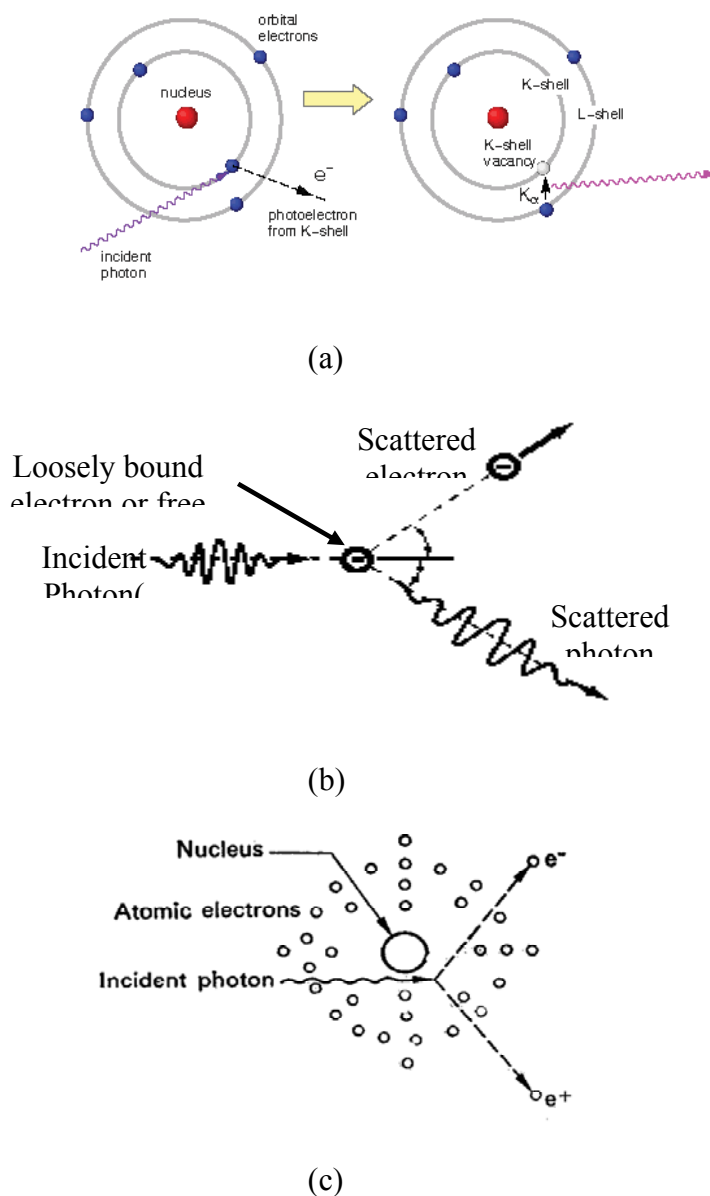


Fig. 13. Interaction of gamma rays with matter (a) Photoelectric effect, (b) Compton scattering and (c) Pair production

The pair production process occurs in the field of a nucleus of the absorbing material and corresponds to the creation of an electron-positron pair at the point of complete disappearance of the incident gamma ray photon. Because energy of $2 m_0 c^2$ is required to create the electron-positron pair, minimum gamma-ray energy of 1.02 MeV is required to make the process energetically possible. If the incident gamma-ray energy exceeds this

value, the excess energy appears in the form of kinetic energy shared by the electron–positron pair.

High purity germanium detector

The most advanced detector in the field of gamma spectrometry is high purity germanium detector. With the advancement in the growth technology of high purity, germanium is now available in the impurity concentration of 10^9 to 10^{10} atoms/cm³. This level of purity is achieved by zone refining technique. These large volume diode detectors are commonly referred to as high purity germanium (HPGe) detectors or intrinsic germanium detectors. The major advantage of HPGe detectors is that because of the absence of lithium drifting, they can be stored at room temperature when not in use. However, they can be operated only at liquid nitrogen temperature because noise due to thermal excitation at room temperature in germanium is very high. These detectors are made both in planar and co-axial configuration. Fig. 14 shows a co-axial HPGe detector housed in an aluminium casing inside a Pb shield, in our laboratory.

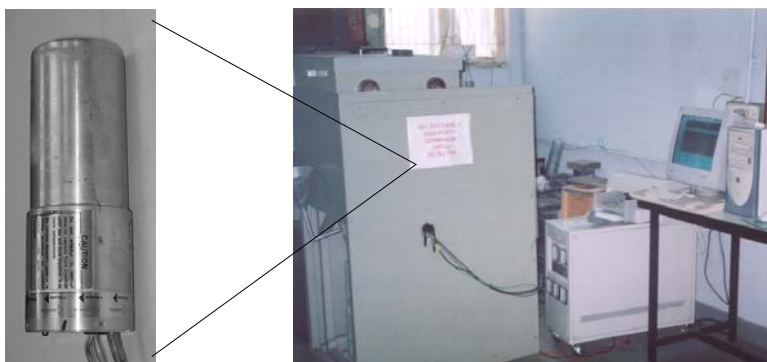


Fig. 14. HPGe detector in Pb shielding to minimize background and along with computer and MCA

For gamma ray spectroscopy we need detectors of large volume. To get detector of large volume, they are constructed in cylindrical or coaxial geometry. In this case, one electrode is fabricated at the outer cylindrical surface of a long cylindrical crystal. A

second cylindrical contact is provided by removing the core of the crystal and placing a contact over the inner cylindrical surface. Because crystals can be made long in the axial direction, much large active volumes can be produced (presently crystal up-to volume of 400 cm^3 are produced commercially). When photon enters the depletion region, it interacts with the germanium atom and breaks the strong covalent bond and raises the electrons to the conduction band leaving out holes. Thus many charge carriers are produced and they are swept towards the electrodes due to application of electric field. These charges are converted into a voltage pulse by a charge sensitive preamplifier and processed by the further electronics to produce the spectrum.

Instrumentation

High resolution gamma spectrometry system consists mainly of a detector, a preamplifier, multichannel analyzer and read out device. Fig. 15 shows the block diagram of a high resolution gamma spectrometry system. Radiation detectors generally used for gamma spectrometry are made up of solid and dense materials. The detector either produces a scintillation or charge particle after interaction with gamma rays. Multichannel analyzer (MCA) is an instrument, which separates out and stores pulses according to energy from the detector. Since the size distribution of the electric pulse produced is proportional to the energy, output from the MCA system gives selective detection of radioisotopes and hence the computation of their activity. The gamma ray line spectra are displayed on a PC connected to a printer, the readout device.

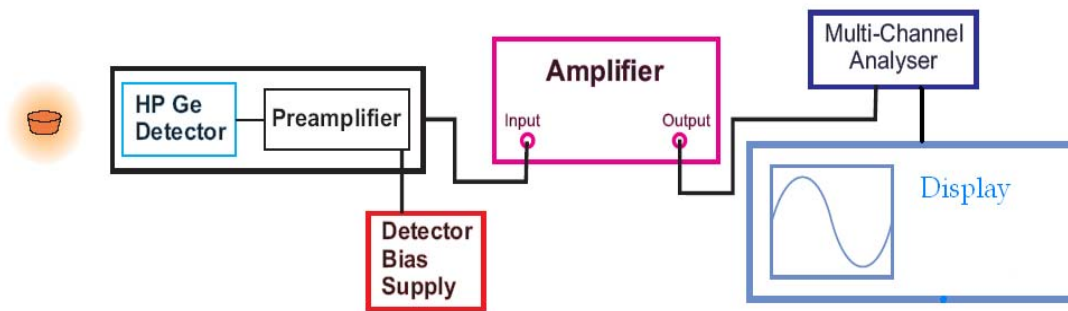


Fig. 15. Block diagram of HPGe Gamma spectrometry system

Detector bias and high voltage supply

High voltage supplied to the detector is very stable and detector bias for semiconductor detector is free of ripples or noise. In the semiconductor detectors bias supply is raised or lowered slowly in order to prevent any damage to low noise FET present in the preamplifier of the detector. Generally in the detector bias unit the protection is provided so that the bias goes down slowly even in case of sudden power failures.

Preamplifier

The output of all radiation detectors operating in pulse mode is a burst of charge Q . In semiconductor devices however the charge is so small that voltage pulse produced by it cannot be further processed without amplification step. The first element in a signal-processing chain is therefore often a preamplifier provided as an interface between the detector and the pulse-processing and analysis electronics that follow. The preamplifier is usually located as close as possible to the detector. Its main functions are:

- To terminate the capacitance quickly and hence maximizes the S/N ratio.
- Serves as an impedance matcher
- Provides a means for supplying voltage to the detector, since it is very convenient.
- To act as an interface between the detector and pulse processor.

Amplifier

The pulse amplifier or spectroscopy amplifier receives voltage pulses with sharp rise time and long tails from the pre-amplifier. It shapes them into an output pulse suitable for the ADC. During the process of amplification and shaping the pulse height and rise time information of the input pulse is preserved. The main functions of the amplifier are baseline restoration, pulse shaping, pole zero cancellation, pile-up rejection and amplification.

Multichannel analyzer

Multichannel analyzers are also called pulse height analyzers. They are special purpose systems, which perform variety of functions like data acquisition, storage, display and interpretation of information from random events. MCAs are generally used in two distinct data analysis modes, namely, pulse height analysis mode (PHA) and multichannel scaling mode (MCS).

Of the above two, the pulse height analysis mode is predominantly used in nuclear research. In the pulse height analysis mode, the system is used for accumulating spectrum of frequency distribution of the energies from a range of photons. The desired spectrum is accumulated by measuring the amplitude of each input event and converting it into a number that is proportional to the pulse height called channel number. The frequency of repetition of pulses corresponds to the counts in each channel. This is displayed on the system's CRT by the vertical displacement of the channel. MCS mode is generally for the determination of half life period of fast decaying radio nuclides events.

Analog to digital converter

The basic function of an ADC in an MCA is to provide a number proportional to the amplitude of the pulse presented at the inputs. It is the most important functional block of the MCA. It determines the quality of the MCA. An ADC having $< \pm 1\%$ differential non linearity and $< \pm 0.025\%$ analog non-linearity gives satisfactory performance. Computer based MCA have built in features to do the most part of the data processing needed for a normal gamma spectrum analysis work. Some commonly available features of this type of MCAs are energy calibration, efficiency calibration, spectrum smoothing, spectrum stripping, location of peaks, net area computation of the peak, isotope identification and qualitative analysis.

Calibration of counting system

The aim of calibration is to identify the radionuclide and the activity present in an unknown material (sample). The basic requirements for source of calibration are:

- The sources selected must have long half life so that the frequency of changing of standards can be avoided.
- The geometry must be same for both sample and standard measurements.
- The detector to sample distance should be constant for a given calibration.

Energy calibration

Energy calibration is carried out to ensure linear relationship between energy and number of channels corresponding to that energy and to determine energy of each channel in a spectrum. The amplitude of the signal at the output of a pre amplifier / amplifier is directly proportional to the energy absorbed by the detector of the incident radiation. In MCA, the events (signals) are stored in a particular channel depending on the height of the pulse.

Energy calibration is carried out by using sources of known distinct gamma energy. The spectrum is acquired for a reasonable time so that photo peaks have sufficient counts for analysis. The region of interest and the centroid peak channel numbers are identified. Then the slope of the straight line plot of channel no. vs. energy represents the energy calibration factor. Fig. 16 shows the energy calibration graph for HPGe detector.

Energy of any channel can be determined with the straight-line equation

$$\text{Energy} = m * \text{channel number} + c \quad (1)$$

where, c = intercept and m = slope of the straight line.

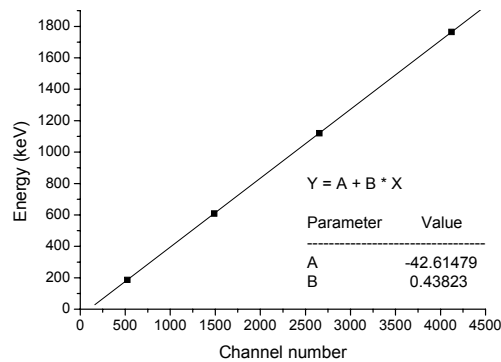


Fig. 16. Energy calibration graph for HPGe detector

Generally for calibration of HPGe detector a source like ^{137}Cs , ^{60}Co , ^{54}Mn is used. Energy calibration for HPGe is around 0.4 keV/ch.

Efficiency calibration

The efficiency of the detector system is defined as the number of pulses recorded for a given number of gamma, alpha or beta rays. Various kinds of efficiencies are:

Absolute efficiency: The ratio of number of counts produced by the detector to the number of gamma rays produced by the source (in all directions).

Intrinsic efficiency: The ratio of number of pulses produced by the detector to the number of gamma rays striking at the detector (solid angle).

Relative efficiency: Efficiency of one detector relative to another. Commonly the efficiency of the detector is specified relative to that of 3" x 3" NaI crystal at 25 cm from a point source and specified at 1.33MeV only.

$$\text{Relative efficiency of the detector} = \frac{\text{Absolute efficiency of HPGe at 1.33 MeV}}{\text{Absolute efficiency of 3" x 3" NaI(Tl)}} \quad (2)$$

Full energy or photo peak efficiency: The ratio of number of counts at a particular energy to that of gamma rays emitted by the source at that energy.

$$\text{Photo peak efficiency} = \frac{\text{Counts per second at the peak energy}}{\text{Disintegrations per second}} \quad (3)$$

Above efficiency can be defined anywhere in the spectrum.

In order to arrive at the net radioactivity of a particular radionuclide identified in the spectrum, the Compton corrected net peak intensity must be corrected for the efficiency of the detector for that energy. For this purpose the detector efficiency vs. energy curve is generated experimentally using standard sources.

For a particular energy, the efficiency is calculated as shown.

$$\eta \% = (\text{Area /s}) \times 100 \times 100 / (\text{dps} \times \text{A}\%) \quad (4)$$

where, $\eta \%$ = percentage efficiency, Area /s = net area (background subtracted) per second, dps = source strength in dps (Bq), A% = abundance of the radionuclide.

While doing efficiency calibration it has to be kept in mind that same sample to detector geometry is maintained and the same radionuclide standards are used as far as possible.

Alternately efficiency vs. energy curve has to be drawn, as shown in fig. 17. As far as possible, standard calibration source should have same or similar physical properties as the sample. Efficiency calibration of the system is necessary for calculation of the disintegration rate or activity of a particular nuclide in the sample. By dividing the area

under the photo peak by absolute efficiency one can calculate the actual number of photons emitted from the source. Efficiency calibration has to be done for specific geometries for which samples are being counted. IAEA certified reference standards RGU and RGTh were counted on the detector for 60,000 sec and the efficiency calibration carried out. The efficiency of the detector for different sample geometries are given in Table 14.

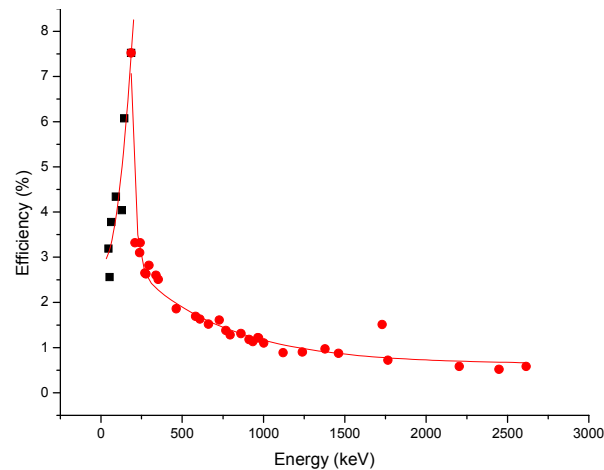


Fig. 17. Efficiency Calibration Graph For 100% n-Type HPGe

Detector efficiency depends on the energy of the measured radiation, the solid angle between sample and detector crystal, and the active volume of the crystal. A larger volume detector will have a higher efficiency. In general, detector efficiency is measured relative to a 3" x 3" sodium iodide detector using a ^{60}Co source (1332 keV gamma ray) at a distance of 25 cm from the crystal face. A general rule of thumb for germanium detectors is 1 percent efficiency per 5 cc of active volume.

Minimum Detection Limit (MDL)

MDL is the smallest amount of activity that can be determined by the system. The MDL were estimated for high resolution gamma spectrometer using the statistical laws and the

background count rate of the instruments for specific energy and are listed in Table 15.

For 95% degree the presence of activity, MDL is expressed as:

$$\text{MDL (Bq/kg)} = 4.66 * \sqrt{B} / (T \times \gamma \times \eta \times W) \quad (5)$$

where, B = Background counts, T = sample counting time in seconds, γ = gamma abundance, η = detector efficiency, W = weight of sample (kg).

The two most important performance characteristics requiring consideration when purchasing a new HPGe detector are resolution and efficiency [154]. Other characteristics to consider are peak shape, peak-to-Compton ratio, crystal dimensions or shape, and price. The detector's resolution is a measure of its ability to separate closely spaced peaks in a spectrum. In general, detector resolution is specified in terms of the full width at half maximum (FWHM) of the 122 keV photopeak of ^{57}Co and the 1332 keV photopeak of ^{60}Co .

Table 14. Efficiency values for different geometries

Radionuclide	Energy (keV)	Full Cylindrical container at contact geometry (6.5cm dia X 7.5cm height)	Half cylindrical container at contact geometry (6.5cm dia X 3.5cm height)	Quarter cylindrical container at contact geometry (6.5cm dia X 1.75cm height)
		Efficiency (%)	Efficiency (%)	Efficiency (%)
^{210}Pb (^{238}U Series)	46.5	3.19	5.5	7.88
^{226}Ra (^{238}U Series)	186.2	7.52	12.1	18.65
^{212}Pb (^{232}Th series)	238.6	3.1	5.59	7.2
^{208}Tl (^{232}Th series)	583.2	1.69	2.51	3.07
^{214}Bi (^{238}U Series)	609.3	1.63	2.48	2.95
^{137}Cs	661.6	1.52	2.38	2.74
^{228}Ac (^{232}Th series)	911.2	1.18	1.77	2.17

^{234m}Pa (^{238}U Series)	1001.03	1.1	1.68	2.06
^{40}K	1460.8	0.87	1.24	1.7
^{208}Tl (^{232}Th series)	2614.5	0.58	0.86	1.03

Table 15. MDL values for different geometries

Radionuclide	Energy (keV)	Full Cylindrical container at contact geometry (6.5cm dia X 7.5cm height)	Half cylindrical container at contact geometry (6.5cm dia X 3.5cm height)	Quarter cylindrical container at contact geometry (6.5cm dia X 1.75cm height)
		MDL (Bq)	MDL (Bq)	MDL (Bq)
^{210}Pb (^{238}U Series)	46.5	2.04	1.2	0.83
^{226}Ra (^{238}U Series)	186.2	0.73	0.46	0.29
^{212}Pb (^{232}Th series)	238.6	0.15	0.08	0.06
^{208}Tl (^{232}Th series)	583.2	0.29	0.2	0.16
^{214}Bi (^{238}U Series)	609.3	0.24	0.16	0.13
^{137}Cs	661.6	0.12	0.09	0.07
^{228}Ac (^{232}Th series)	911.2	0.41	0.27	0.22
^{234m}Pa (^{238}U Series)	1001.03	7.96	5.21	4.25
^{40}K	1460.8	3.91	2.19	2
^{208}Tl (^{232}Th series)	2614.5	1	0.68	0.56

Sample preparation and measurement

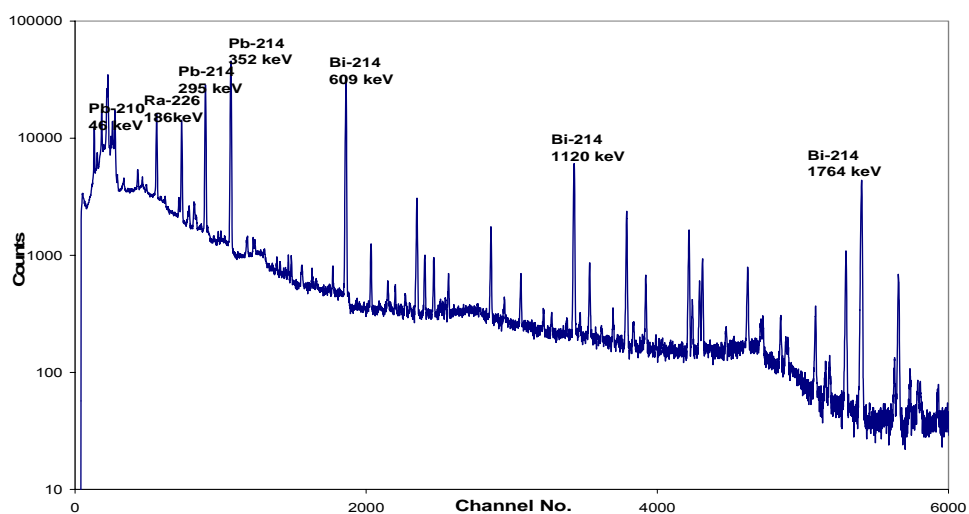
Sample preparation for high resolution gamma spectrometry (HRGS) involved, firstly, accurately weighing (about 300g) previously dried, ground and homogenised samples and standards in plastic containers of standard geometries (6.5 cm diameter and 7.5 cm

height). Samples were sealed and kept for one month so as to ensure the attainment of secular equilibrium between ^{226}Ra and its daughter products. The containers were filled to full capacity so that the daughter products of ^{222}Rn and ^{220}Rn achieve uniform distribution throughout the sample and to avoid their accumulation in the space at the top.

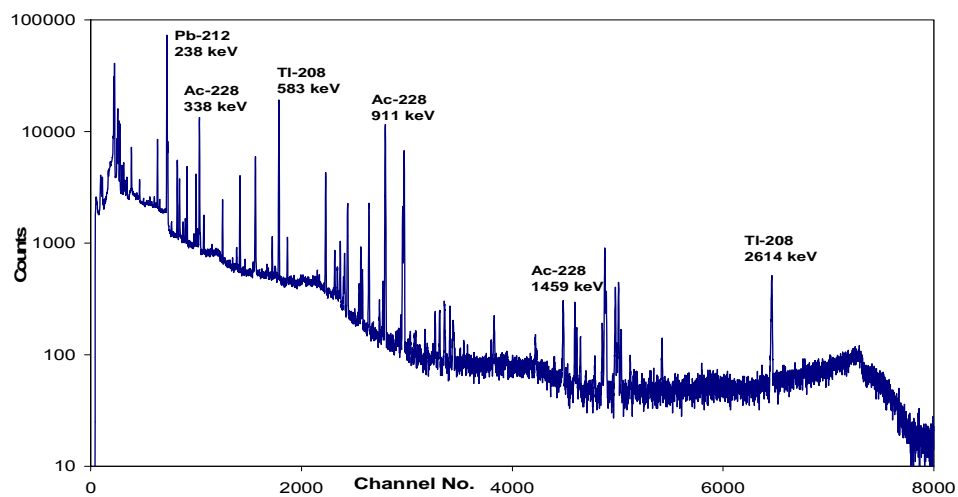
A high-purity vertical Germanium detector was used for all the HRGS measurements carried out in this thesis. The HRGS System consisted of an n-type detector (DSG, Germany) having 100% relative efficiency with respect to 7.6 cm X 7.6 cm NaI(Tl) detector at 1332 keV of ^{60}Co gamma energy measured at 25 cm and associated electronics coupled with 8K MCA. Spectrum analysis was done by PHAST software (Electronics Division, BARC). The detector was surrounded by 7.5 cm thick lead shield with inside dimensions 36 cm (l), 35 cm (b) and 36 cm (h). IAEA Certified Reference Materials, RGU-I and RGTh-I, were used for the energy and efficiency calibration of the HRGS System [155]. Spectrums of RGU-I and RGTh-I are shown in fig. 18 (a) and (b).

In order to determine the contribution of ambient background due to naturally occurring radionuclides around the detector, an empty container of the same dimensions of 6.5 cm diameter and 7.5 cm height with the same geometrical conditions as the sample was counted on the detector. Sample and background spectrum were all acquired for 60,000 seconds. The background spectra recorded were used to correct the net γ -ray photopeak areas for the isotopes of interest. A typical background spectrum is shown in fig. 19. The lower γ energies are attenuated by the sample matrix itself. Hence a self-absorption correction factor is required in the low (<150 keV) energy region [38]. The correction is especially important when the density of the sample and standard are different. This factor was taken care by using CRMs of the same density as the samples and maintaining same

sample geometry. This ensured that the sample and the CRM had similar attenuation properties.



(a)



(b)

Fig. 18. Gamma spectrum of (a) RGU-I standard, (b) RGTh-I standard

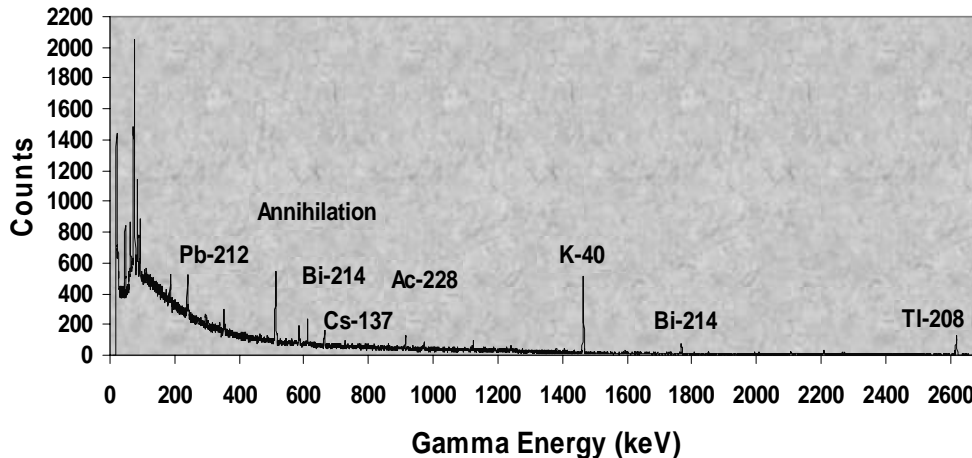


Fig. 19. Background gamma spectrum of 100% n-type HPGe

Isotope identification and quantification

The sample in which the radionuclides were analysed, were taken in geometry similar to that of the standard. Efficiency calibration of the detector was carried out for the specified geometry. The spectrum was acquired for a preset time.

The activity of a radionuclide was then calculated using the formula

$$\text{Activity (Bq/unit weight or volume)} = \frac{N \times 100 \times 100}{(T \times \gamma \times \eta \times W \text{ or } V)} \quad (6)$$

where, N= Background subtracted net counts, T = Counting time (sec), γ = Gamma emission probability in %, η = Efficiency for the particular gamma energy in % and W or V is the weight or volume of the sample.

2.2.2. Instrumental Neutron Activation Analysis

Neutron Activation Analysis (NAA) is a sensitive analytical technique useful for performing both qualitative and quantitative multi-element analysis of 25-30 major,

minor, and trace elements in samples from almost every conceivable field of scientific or technical interest. For many elements and applications, NAA offers sensitivities that are superior to those attainable by other methods, in the order of parts per billion or better. Because of its accuracy and reliability, NAA is recognised as the "referee method" when new procedures are being developed or when other methods yield results that do not agree.

The basic essentials required to carry out an analysis of samples by NAA are a source of neutrons, instrumentation suitable for detecting gamma rays and a detailed knowledge of the reactions that occur when neutrons interact with target nuclei.

Principle of NAA

In NAA, samples are activated by neutrons. During irradiation the naturally occurring stable isotopes of most elements that constitute the samples are transformed into radioactive isotopes by neutron capture. Then the activated nucleus decays according to its characteristic half-life; some nuclides emit particles only, but most nuclides emit gamma-quanta, too, with specific energies and the radiation can be used both to identify and accurately quantify the elements in the sample. The sequence of events occurring during the most common type of nuclear reaction used for NAA, namely the neutron capture or (n, gamma) reaction, is illustrated in fig. 20. When a neutron interacts with the target nucleus via a non-elastic collision, a compound nucleus is formed in an excited state. The excitation energy of the compound nucleus is due to the binding energy of the neutron with the nucleus. The compound nucleus will almost instantaneously de-excite into a more stable configuration through emission of one or more characteristic prompt gamma rays. In many cases, this new configuration yields a radioactive nucleus which

also de-excites (or decays) by emission of one or more characteristic delayed gamma rays, but at a much slower rate according to the unique half-life of the radioactive nucleus. Depending upon the particular radioactive species, half-lives can range from fractions of a second to several years.

In principle, therefore, with respect to the time of measurement, NAA falls into two categories: (1) prompt gamma-ray neutron activation analysis (PGNAA), where measurements take place during irradiation, or (2) delayed gamma-ray neutron activation analysis (DGNA), where the measurements follow radioactive decay. The latter operational mode is more common; thus, when one mentions NAA it is generally assumed that measurement of the delayed gamma rays is intended. About 70% of the elements have properties suitable for measurement by NAA.

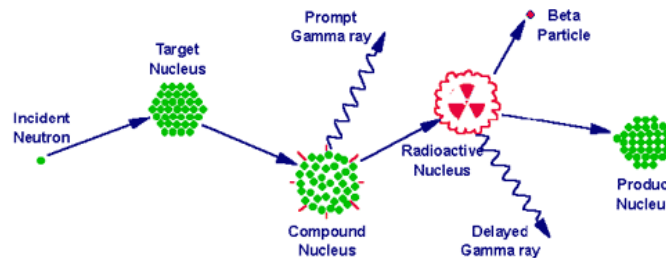


Fig. 20: Neutron capture by a target nucleus followed by the emission of gamma rays

Types of NAA

The fast neutron component of a neutron spectrum (energies above 0.5MeV) consists of the primary fission neutrons which still have much of their original energy following fission. Fast neutrons contribute very little to the (n, gamma) reaction, but instead induce nuclear reactions where the ejection of one or more nuclear particles, (n, p), (n, n'), and (n, 2n), are prevalent. In a typical reactor irradiation position, about 5% of the total flux

consists of fast neutrons. An NAA technique that employs nuclear reactions induced by fast neutrons is called fast neutron activation analysis (FNAA).

As mentioned earlier, the NAA technique can be categorised according to whether gamma rays are measured during neutron irradiation (PGNAA) or at some time after the end of the irradiation (DGNAA). The PGNAA technique is generally performed by using a beam of neutrons extracted through a reactor beam port. Fluxes on samples irradiated in beams are of the order of one million times lower than on samples inside a reactor but detectors can be placed very close to the sample compensating for much of the loss in sensitivity due to flux. The PGNAA technique is most applicable to elements with extremely high neutron capture cross-sections (B, Cd, Sm, and Gd), elements which decay too rapidly to be measured by DGNAA, elements that produce only stable isotopes, or elements with weak decay gamma-ray intensities. DGNAA (sometimes called conventional NAA) is useful for the vast majority of elements that produce radioactive nuclides. The technique is flexible with respect to time, such that if the sensitivity for a long-lived radionuclide that suffers from interference by a shorter-lived radionuclide can be improved by waiting for the short-lived radionuclide to decay. This selectivity is a key advantage of DGNAA over other analytical methods.

With the use of automated sample handling, gamma-ray measurement with solid-state detectors, and computerised data processing it is generally possible to simultaneously measure more than thirty elements in most sample types without chemical processing. The application of purely instrumental procedures is commonly called instrumental neutron activation analysis (INAA) and is one of NAA's most important advantages over other analytical techniques. If chemical separations are done to samples after irradiation

to remove interferences or to concentrate the radioisotope of interest, the technique is called radiochemical neutron activation analysis (RNAA). The latter technique is performed infrequently due to its high labour cost.

Neutron sources

Although there are several types of neutron sources (reactors, accelerators and radioisotopic neutron emitters) one can use for NAA, nuclear reactors with their high fluxes of neutrons from uranium fission offer the highest available sensitivities for most elements. Different types of reactors and different positions within a reactor can vary considerably with regard to their neutron energy distributions and fluxes due to the materials used to moderate (or reduce the energies of) the primary fission neutrons. However, as shown in fig. 21, most neutron energy distributions are quite broad and consist of three principal components (thermal, epithermal and fast).

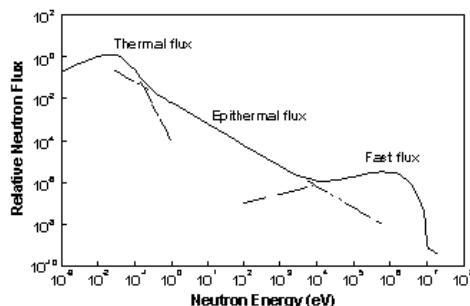


Fig. 21: A typical reactor neutron energy spectrum

The thermal neutron component consists of low-energy neutrons (energies below 0.5eV) in thermal equilibrium with atoms in the reactor moderator. At room temperature, the energy spectrum of thermal neutrons is best described by a Maxwell-Boltzmann distribution with a mean energy of 0.025eV and a most probable velocity of 2200 m/s. In most reactor irradiation positions, 90-95% of the neutrons that bombard a sample are

thermal neutrons. In general, a one-megawatt reactor has a peak thermal neutron flux of approximately 10^{13} neutrons per square centimeter per second.

The epithermal neutron component consists of neutrons (energies from 0.5eV to about 0.5MeV) which have been only partially moderated. A 1 mm thick cadmium foil absorbs all thermal neutrons but will allow epithermal and fast neutrons above 0.5eV energy to pass through. In a typical unshielded reactor irradiation position, the epithermal neutron flux represents about 2% of the total neutron flux. Both thermal and epithermal neutrons induce (n, gamma) reactions on target nuclei. An NAA technique that employs only epithermal neutrons to induce (n,gamma) reactions by irradiating the samples being analysed inside either cadmium or boron shields is called epithermal neutron activation analysis (ENAA).

Methods of INAA

In INAA, the activity induced in a sample is measured by the emitted gamma rays, with the help of a gamma spectrometric system. Induced activity is calculated according to the following equation:

$$A = N * \sigma * \phi * (1 - e^{-\lambda t}) * e^{-\lambda t_d} \quad (7)$$

Where, A is the activity induced of a particular radioisotope produced from a particular isotope of an element, N is the number of target atoms of that element in the sample, σ is the thermal neutron absorption cross section in barns, ϕ in the thermal neutron flux in $\text{cm}^2\text{sec}^{-1}$, λ is the decay constant of the radionuclide produced, t is the time of irradiation of the sample (or the particular element in it) and t_d is the time of decay after irradiation.

Absolute method

In the absolute method of INAA, parameters like σ , ϕ , λ , t and t_d are known or calculated for a particular radioisotope. Activity induced, A , is measured by gamma spectrometry. Hence the only unknown term in the above equation is N , the number of atoms of the element in the sample. Hence the concentration of a particular element in the sample can be arrived at by using eqn. 7.

Comparator method

In the comparator method of INAA a suitable standard is packed, irradiated and counted with each batch of sample. Hence the parameters like σ , ϕ , λ , t and t_d become for the same stable element- produced radioisotope pair. The only unknowns are N and A , of which the latter is counted by gamma spectrometry and hence the former can be arrived at, by using the equation:

$$\frac{A_{\text{sam}}}{A_{\text{std}}} = \frac{m_{\text{sam}} * (e^{-\lambda T})_{\text{sam}}}{m_{\text{std}} * (e^{-\lambda T})_{\text{std}}} \quad (8)$$

where, A =activity of sample (sam) and standard (std), m =mass of the element, λ =decay constant for the isotope, and T =decay time.

k_0 method

The k_0 based INAA involves the simultaneous irradiation of a sample and a single comparator, such as gold, instead of multi-element standards and the use of a composite nuclear constant called k_0 [156]. The single comparator needs to have suitable nuclear properties [157]. This method uses reactor and detector based input parameters for calculation of concentration of elements. The input parameters for the determination of concentrations of elements by this method are, net peak area, sub-cadmium to epi-thermal

neutron flux ratio (f), epi-thermal neutron flux shape factor (α), absolute/relative efficiency of the detector (ϵ) and nuclear constants k_0 and Q_0 [158].

Sample preparation

In this thesis INAA has been used for elemental concentration measurements in soils, rocks and uranium tailings samples. Since INAA technique does not require any chemical treatment of the samples, the sample preparation process is very convenient. Sample preparation involved, firstly, accurately weighing previously dried, ground and homogenised samples and standards in small plastic packets. Then each of the small plastic packets were sealed. A blank was also included in each batch of sample and standard. The plastic packets containing samples, standard and blank were then sealed in a larger plastic packet and checked for any leakage. Such batches were then sent to the Apsara reactor for irradiation.

Measurement of Gamma Rays

The instrumentation used to measure gamma rays from radioactive samples consists of a semiconductor detector, associated electronics, and a computer-based, multi-channel analyzer (MCA/computer). The detector used was a hyperpure germanium (HPGe) detector which operated at liquid nitrogen temperatures (77K). The detector parts comprise of a germanium crystal present in a vacuum cryostat, thermally connected to a copper rod or "cold finger". Although HPGe detectors come in many different designs and sizes, the most common type of detector is the coaxial detector which in NAA is useful for measurement of gamma-rays with energies over the range from about 60 keV to 3.0 MeV. Typical gamma ray spectrums for short, medium and long lived isotopes are shown in fig. 22.

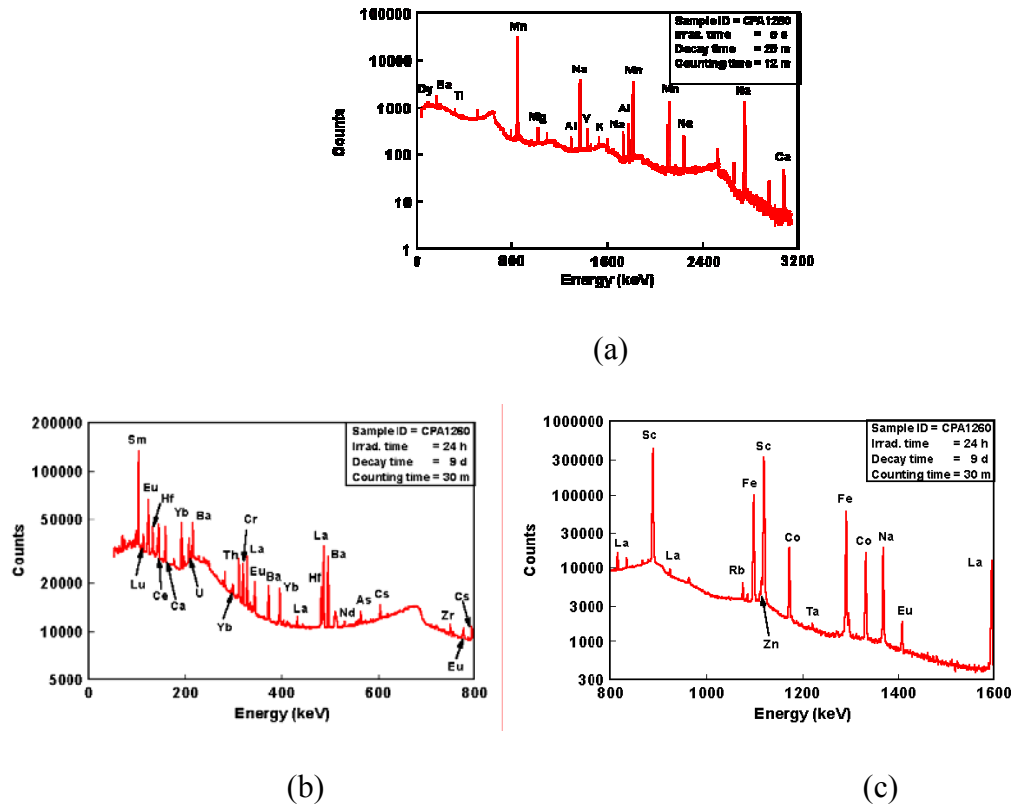


Fig. 22: Typical gamma-ray spectrums showing (a) short-lived elements and (b) and (c) medium and long lived elements

For most NAA applications, a detector with 1.0 keV resolution or below at 122 keV and 1.8 keV or below at 1332 keV is sufficient. As detector volume increases, the detector resolution gradually decreases. For most NAA applications, an HPGe detector of 15-30 percent efficiency is adequate.

Using Gamma-ray Counts to Calculate Element Concentration

When the gamma rays of a radioisotope formed by irradiation of an element enter a suitable detector, their energy can be converted to an electrical signal that is processed as a count in an energy spectrum. The accumulation of gamma counts at a particular energy will generate a curve, the area of which is proportional to the radioactivity of the characteristic radionuclide. The quantity of element is determined by measuring the

intensity of the characteristic gamma-ray lines in the spectra. By irradiating and counting standards containing known amounts of various elements, it is possible to establish a relationship between the radioactivity of the standard and the radioactivity of the sample, which in turn helps to determine the concentration of a particular element.

For these measurements a gamma-ray detector and special electronic equipment are necessary. As the irradiated samples contain radionuclides of different half-lives, different isotopes can be determined at various time intervals.

In this thesis APSARA reactor, BARC, Mumbai, with a thermal neutron flux of 10^{12} neutrons.cm⁻².s⁻¹ was used for 7 hr sample irradiation. The samples were allowed a cooling time of 3 days for decay of short-lived radioactivity. Subsequently, 3 sequential measurements were carried out on a 50% p-type HPGe after a time period of 3 days, 14 days and 30 days for each sample along with the standard and blank. Counting time was 1000 seconds, 10000 seconds and 24 hours, respectively in the three measurements.

The procedure generally used to calculate concentration of an element in an unknown sample was to irradiate the unknown sample and a comparator standard, containing a known amount of the element of interest, together in a reactor. The unknown sample and the comparator standard are both measured on the same detector and the difference in decay between the two was corrected. One usually decay corrects the measured counts (or activity) for both samples back to the end of irradiation using the half-life of the measured isotope. The equation 8 was used to calculate the mass of an element in the unknown sample relative to the comparator standard. When performing short irradiations, the irradiation, decay and counting times are normally same for all samples and standards such that the time-dependent factors cancel. Thus the above equation simplifies into:

$$C_{\text{sam}} = \frac{C_{\text{std}} * W_{\text{std}} * A_{\text{sam}}}{W_{\text{sam}} * A_{\text{std}}} \quad (9)$$

where, C = concentration of the element and W=weight of the sample and standard.

The gamma spectrometric system used for measurement consisted of a p-type coaxial high purity germanium semiconductor detector (relative efficiency of 50%) connected to PC based multichannel analyser and PHAST software, developed by Electronics Division, BARC, used for evaluation and calculation. Fig. 23 shows the general gamma spectrometric setup for INAA.

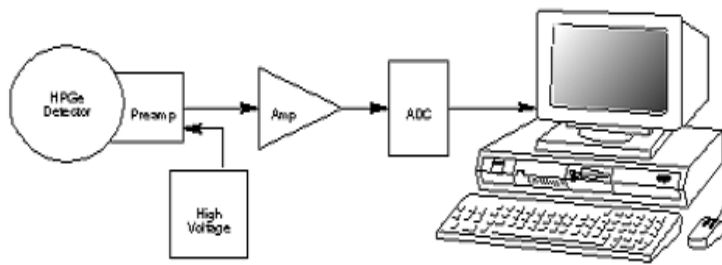


Fig 23. Gamma Spectrometric setup for INAA

Sensitivities Available by NAA

The sensitivities for NAA are dependent upon the irradiation parameters (i.e., neutron flux, irradiation and decay times), measurement conditions (i.e., measurement time, detector efficiency) nuclear parameters of the elements being measured (i.e., isotope abundance, neutron cross-section, half-life, and gamma-ray abundance). Element sensitivities varied from 10^{-3} to 10^{-10} grams per gram of sample. The accuracy of an individual NAA determination usually ranged between 1 to 10 percent of the reported value. Table 1 lists the approximate sensitivities for determination of elements assuming interference free spectra.

Table 16. Sensitivities for determination of elements using INAA

Sensitivity (picograms)	Elements
1	Dy, Eu
1–10	In, Lu, Mn
10–100	Au, Ho, Ir, Re, Sm, W
100–1E+3	Ag, Ar, As, Br, Cl, Co, Cs, Cu, Er, Ga, Hf, I, La, Sb, Sc, Se, Ta, Tb, Th, Tm, U, V, Yb
1E+3–1E+4	Al, Ba, Cd, Ce, Cr, Hg, Kr, Gd, Ge, Mo, Na, Nd, Ni, Os, Pd, Rb, Rh, Ru, Sr, Te, Zn, Zr
1E+4–1E+5	Bi, Ca, K, Mg, P, Pt, Si, Sn, Ti, Tl, Xe, Y
1E+5–1E+6	F, Fe, Nb, Ne
1E+7	Pb, S

There are several advantages of INAA. Liquids, solids, suspensions, slurries or gases can be analysed by INAA. The chemical or physical form of the sample does not pose a problem. No pre-treatment or chemical treatment of the sample, like, sample digestion, extraction, volume reduction or dilution is required. The technique is free of analytical blank. INAA offers high sensitivity and accuracy especially in respect of some trace elements. It is highly precise. Reproducibility of quality controls over long periods of time (years) is often better than 2% relative standard deviation (RSD). This is a simultaneous multielement method in that many elements can be analysed simultaneously in a given sample without changing or altering the apparatus as is necessary in atomic absorption. INAA is a nondestructive process and therefore, does not suffer from the errors associated with yield determinations. This method detects the total elemental content, regardless of oxidation state, chemical form or physical location. Since neutrons

have no charge and pass through most materials without difficulty. Therefore the middle of the sample becomes just as activated as the outer surface and the potential for matrix effects is reduced or even eliminated. INAA is time efficient for a large number of samples, as many samples can be irradiated at a given time and counted later on a given decay schedule. INAA permits the analysis of samples ranging in volume from 0.1 ml to 20 ml, and in mass from ~0.001 gram to 10 grams depending on sample density.

The major disadvantages of INAA are, INAA using reactor is the most competitive but availability of the same is difficult. The equipment needed for the analysis is rather expensive and requires special laboratory and a highly qualified staff.

Quality Assurance in INAA

Certified elemental standards, standard reference material (SRM) controls, method blanks and sample duplicates were processed along with samples to maintain a high degree of quality assurance. To check the quality of results on a long term Shewart control charts were constructed [159].

Minimum detection Level (MDL)

The minimum detection level for trace elements by INAA ranges from sub ppm to ppm ranges. The MDL values obtained, in the present set-up of INAA, for As, Ba, Ce, Cr, Co, Cs, Eu, Gd, Hf, La, Rb, Sb, Sc, Sm, Th, U, Yb were 0.1, 14, 0.5, 1, 0.04, 0.08, 0.4, 1, 0.05, 0.2, 2, 0.06, 0.02, 0.06, 0.2, 0.2 and 0.1 ppm, respectively. For the major elements it ranged from few hundreds of ppm to thousands of ppm levels.

2.2.3. Laser Fluorimetry

Laser fluorimetry is an analytical technique that can measure mass concentration of uranium in trace and ultra trace level in aqueous medium. There are many analytical techniques for uranium analysis, for example: Gamma spectrometry, alpha spectrometry, atomic absorption spectroscopy, fission track, ICP-MS, voltametry etc. Each method has got certain advantages and disadvantages of its own. Many methods require a tedious and time consuming chemical sample preparation for the analysis. Laser fluorimetry is the easiest and fastest technique to measure uranium. Table 17 gives a comparison of parameters associated with different techniques for uranium measurements.

Table 17. Comparison of different analytical techniques for U measurement

Method	Volume (ml) of sample	Counting time (s)	Accuracy (%)	Analysed Isotopes	MDA (mg.l ⁻¹)
Gamma Spectrometry	1000 - 5000	86,400 - 216000	14	²³⁵ U & ²³⁸ U	0.19
Alpha Spectrometry	200 – 1000	216000 – 432000	25	²³⁴ U, ²³⁵ U & ²³⁸ U	0.016
Laser Fluorimetry	0.05 – 0.07	120	90	Total uranium	0.0002
ICP - MS	25 - 50	400 - 600	10	²³⁴ U, ²³⁵ U & ²³⁸ U	

Principle

Laser fluorimetry works on the principle of measurement of fluorescence of uranyl complex (uranyl phosphate). This complex is formed by addition of a fluorescence enhancement reagent like Fluran (Sodium pyrophosphate) to an aqueous solution containing uranium. The excitation is done by 337.1 nm laser pulse.

Fluorescence is based on the Lambert Beer's law. For a solution of unit concentration the relationship can be expressed as:

$$A = abc \quad (10)$$

where a is the absorptivity of the liquid, c is the concentration of liquid and b is the optical path length.

Instrumentation

The laser uranium analyzer was developed by Laser instrumentation section, Instrumentation and Control Division, Center for Advanced technology, Indore, India. It is shown in fig. 24. It is a compact analytical instrument to measure uranium in trace and ultra trace level in aqueous environmental samples, since the concentration of uranium in aquatic environment is very low, may be in ppb or sub-ppb level.



Fig. 24. Laser uranium analyser

Laser fluorimetry is one of the quick, sensitive and reliable methods of estimating ultratrace uranium concentrations, though it has the difficulties of measurements in higher concentrations and is devoid of isotopic determination [160]. The instrument contains a nitrogen laser, as radiation source, sample compartment and a photomultiplier tube, as a radiation transducer, and the three are in a right-angle optical configuration, as shown in fig. 25. The detector is present at right angle to the radiation source, thus the

background signal due to the source will be negligible and a lower detection level can be achieved than atomic absorption or emission techniques. The sealed-off nitrogen laser is the excitation source lasing at 337.1 nm. The laser source emits the intense pulsed ultra violet radiation carrying energy of 20 micro joules of pulse width of 7 nano seconds at a repetition rate of 10 pulses per second [161]. The pulsed intense laser light is focused onto the sample cell, a quartz cuvette of 9 ml. The emitted fluorescence of uranyl phosphate complex is measured by a photomultiplier tube (PMT), which measures fluorescence from both, U complex and organic matter in the sample cell.

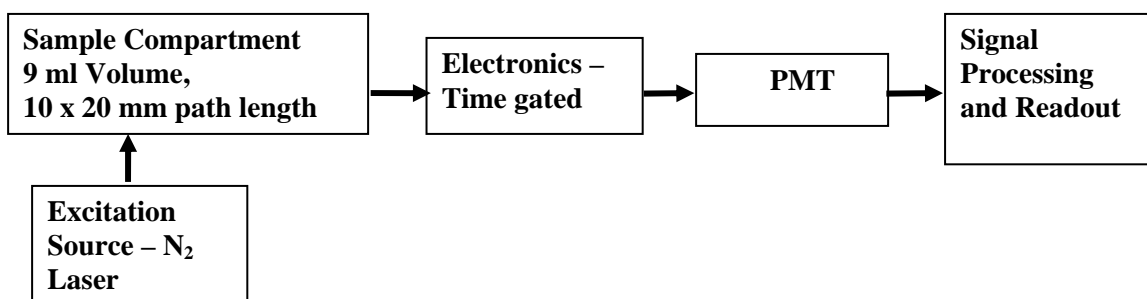


Fig. 25. Block diagram of Laser uranium analyser

Most organic matters present in natural waters fluorescence when excited by the nitrogen laser, but have very short life time (<100 ns). The fluorescence of uranyl complex has a longer life time (~ 200 μ s). The delayed fluorescence signals are measured only for a 100 μ s period starting from 30 μ s after the laser pulse and fluorescence signals from the PMT are integrated for 4 s and then displayed [161]. Thus the fluorescence due to organic compounds dies down and only the fluorescence of uranium isotopes are collected by the time gated PMT. The fluorescence is proportional to concentration of uranium in aqueous medium. Otherwise the fluorescence peak of organic matters is around 400 nm and that of uranium in complexing media are 494, 516, 540 and 565 nm, maximum around 510 nm [162]. Therefore, using an optical filter at 450 nm, the contribution of organic matters

is nullified. Thus the fluorescence interference due to organic matters is corrected by using proper optical filter, fixed electronic delay and gating technology [163].

The technical features of laser uranium analyzer are: detection limit : 0.2 ppb of uranium, range : 0.2 - 20 ppb, excitation source : sealed-off nitrogen laser, wavelength : 337 nm, pulse energy : 20 μ joule, pulse duration : 7 nano second, frequency : 10 Hz and sample size : 3-5 ml.

Sample preparation and analysis

Liquid samples measured by laser fluorimetry need to be in aqueous medium at neutral pH. The quenching effect may be encountered due to the presence of high concentration of acid (up to 2 M) during analysis. Hence pH adjustment was carried out prior to analysis.

The samples were analysed using laser uranium analyzer by standard addition method, to avoid matrix effects, as shown in fig. 26. Standard addition was carried out by successive introduction of increments of the standard to a single measured volume of the sample. Measurements were made on the original sample and on the sample plus the standard after each addition. A standard stock solution of 0.973 g.l⁻¹ uranium (Aldrich make) was diluted to working concentrations for regular calibration of the system. Sodium pyrophosphate (5%) was used as the fluorescence enhancement agent and for the formation of uranyl complex since uranyl phosphate complexes are stable [164].

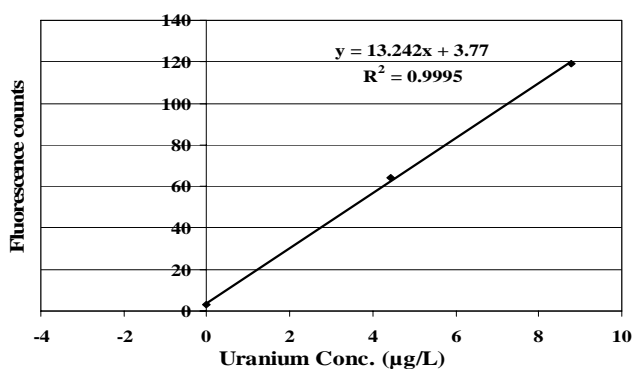


Fig. 26. Typical standard addition curve for Laser uranium analyser

About 5 ml of sample was taken in a dry and clean quartz cell. To the sample 0.5 ml of fluorescence enhancement reagent (pH ~ 7) was added and measured. The instrument was calibrated with standard uranium solution of a known concentration. Few micro liter of a known concentration of uranium standard (500µg/L) was added to the same cell and readings noted subsequently. The details of the optimisation of method and analysis protocol are given elsewhere [165-167]. Both micropipettes and analytical balance were used to avoid any measurement uncertainty while pipetting [164].

The concentration of uranium (µg/L) in samples was calculated by using the formula

$$U (\mu\text{g/L}) = D_1 / (D_2 - D_1) \times (V_1 C / V_2) \quad (11)$$

Where

D_1 – fluorescence due to sample only

D_2 – fluorescence due to sample and U-standard spiked

V_1 – volume of U-standard added (ml)

V_2 - volume of sample taken (ml)

C - Concentration of U-standard solution (µg/L)

All laboratory glass wares used for sample processing were soaked in 10% nitric acid for 15 days and then rinsed thoroughly with distilled and double distilled water, respectively before use. Reagent blank was taken along with each batch of sample preparation and concentrations observed in the reagent blank were subtracted from the same batch of samples. Various precautions were taken in order to achieve a dust free laboratory environment and a steady temperature.

2.2.4. Quality control

Quality assurance and quality control of analytical data is of prime importance in case of environmental sample matrices, because of their compositional characteristics, concentration variability and chemical state, requiring accurate and precise measurement protocols. Quality assurance of trace metals in any matrix by any method in general is maintained by following the steps given below:

1. Analysis of standard reference materials
2. Replicate analysis
3. Spike recovery
4. Cross method checks (by comparing with other instruments)
5. Low blanks (pure chemicals)
6. Clean laboratories

Employing Standard Reference Materials [SRMs] provided by the International Atomic Energy Agency [IAEA] and National Institute for Standards and Technology [NIST] is one of the validation methods in QA/QC. As far as possible, relevant standard reference materials closely matching with the sample matrix need to be selected. Our experience with the use of SRMs indicate that the measurements agree within $\pm 5-10\%$ with certified values. The various standard reference material for different analytes are summarised in Table 18. The validity of the method is also ascertained by employing parallel or independent method checks, spike recovery and replicate analysis. Standard reference materials have also been analysed by INAA and compared with the certified values in Table 19. It can be seen that the values show good conformity.

Table 18. Reference Materials used in Environmental Analysis in this study

Type of Analyte	Matrix	Code	Source	Reference Analyte
Elemental analysis	Soil	Soil-7	IAEA	Number of major and trace elements - 45
Radioactivity analysis	Ore	IAEA-RG-U-1, IAEA-RG-Th-1	IAEA	^{40}K , ^{235}U , ^{238}U , ^{232}Th

Table 19. Quality Assurance of Metal Analysis in Soil 7

Metals	Unit	IAEA-SOIL-7	
		Observed Value (n=6)	Certified value
Cd	$\mu\text{g g}^{-1}$	1.4 (1.0 - 1.9)	1.3 (1.1 – 2.7)
Co	$\mu\text{g g}^{-1}$	8.2 (7.6 - 8.5)	8.9 (8.4 – 10.1)
Cr	$\mu\text{g g}^{-1}$	54 (51 - 62)	60 (49 – 74)
Cu	$\mu\text{g g}^{-1}$	11.8 (11.2 - 12.5)	11 (9 – 13)
Fe	mg g^{-1}	25.6 (25.1 - 26.1)	25.7 (25.2 – 26.3)
Li	$\mu\text{g g}^{-1}$	32 (28 - 34)	31 (15 – 42)
Mn	$\mu\text{g g}^{-1}$	625 (620 - 632)	631 (604 – 650)
Na	mg g^{-1}	2.42 (2.32 - 2.54)	2.4 (2.3 – 2.5)
Ni	$\mu\text{g g}^{-1}$	26.5 (24.5 - 28.0)	26 (21 – 37)
Pb	$\mu\text{g g}^{-1}$	59.5 (58 - 62)	60 (55 – 71)
Zn	$\mu\text{g g}^{-1}$	103 (101 - 107)	104 (101 – 113)

To test consistency of data over a long time Control Charts were plotted. These charts are used either to assess the performance of a measurement system or to monitor the stability of a system [168, 169]. This helps to develop a control for each of the processes that are carried out in the entire exercise. Shewart control charts or Quality control charts were plotted to check the deviation of data values from the median value. The results from any

measurement process are expected to lie in between the control limits due to random fluctuations in the instrumental conditions [170]. The control limits were estimated from the data generated previously by the instrument. As long as the data values were in between the control limits, the system was considered to be in a state of statistical control.

CHAPTER 3

EXPERIMENTAL STUDIES AND SALIENT OBSERVATIONS

Scope

The physicochemical characteristics of a matrix play a major role in determining the behaviour of elements present in it. These physicochemical parameters are determined through standard protocols. The distribution of elements and radionuclides in various matrices of the mineralised Singhbhum Shear Zone gives an idea of their spatial variability. This distribution is dependent on the geography of the area, operating geochemical forces and various anthropogenic activities which may cause dispersion and redistribution of the metals in the environment. Again, the leaching of an element from a matrix is more important than its level in the same. The leaching methodology and the physical parameters associated with it are hence important.

This chapter discusses the physicochemical characterisation of the samples, radionuclide and trace elemental distribution in the matrices and the uranium concentrations obtained from leaching experiments and effects of the various physical conditions/ parameters.

3.1. Physicochemical characterisation of samples

Physicochemical properties of a matrix have important influences on the distribution and behaviour of an element in the environment. Hence it is necessary to carry out physicochemical characterisation of samples. Particle size distribution, moisture content, organic matter content, pH, cation exchange capacity and humic acid content have been studied in the collected samples, in this thesis.

3.1.1. Particle size distribution

Particle size distribution of a sample is useful for judging its texture. Soil texture is the percentage of sand, silt and clay in the soil. Sand is the coarsest (0.06-2mm), silt is intermediate (0.002-0.06mm) and clay is the finest (<0.002mm). Soils with specific ratios

of these particle types are usually represented by a texture triangle as shown in Fig. 27 below. An ideal soil texture would be 40% sand, 40% silt and 20% clay.

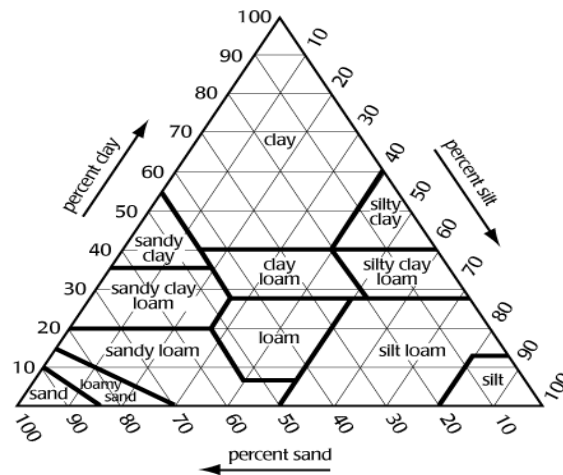
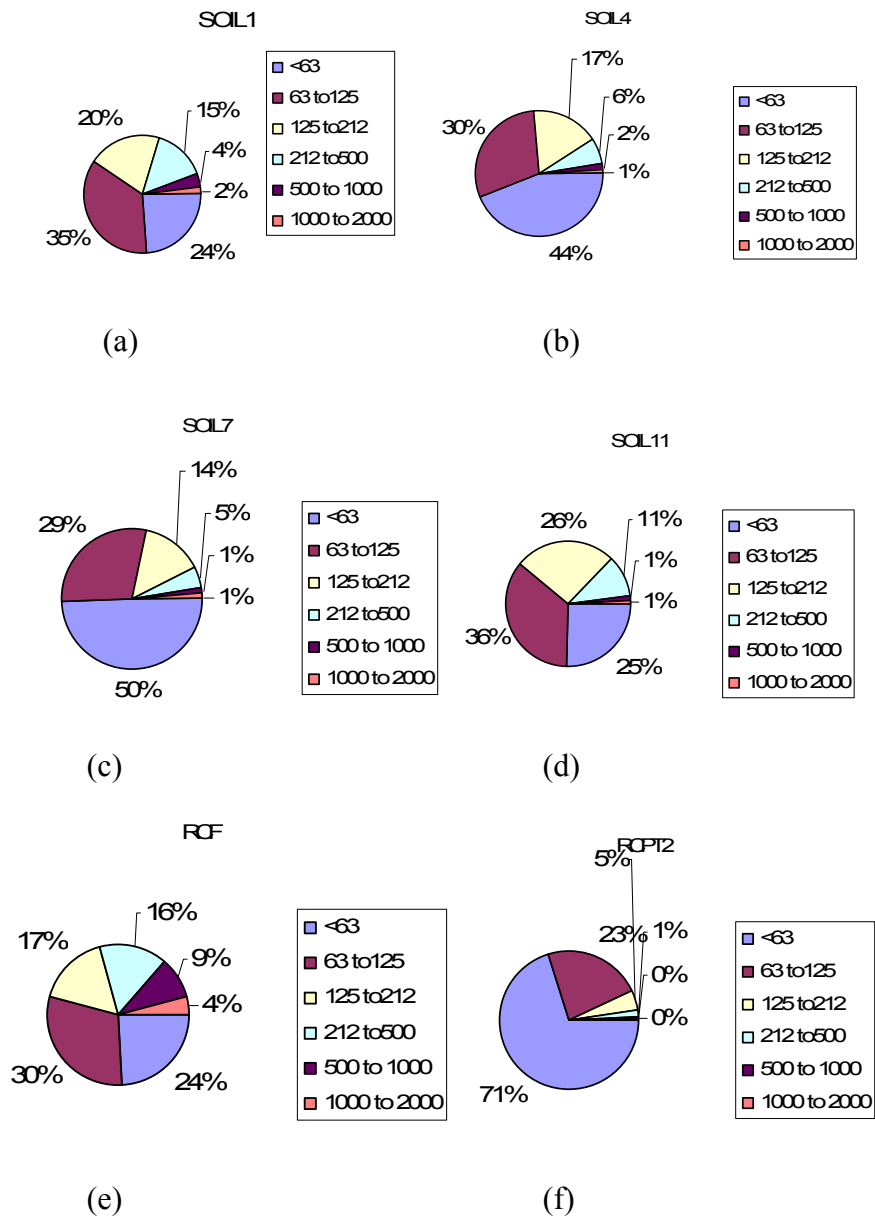


Fig. 27. Soil texture triangle

The dried samples were ground softly by porcelain mortar pestle and around one kg of sample was taken for size separation by electromagnetic sieve shaker (EMS 8). The sample was shaken continuously for a period of 40 minutes. Soil > 2 mm size was removed and not used for further analysis. The soil samples were fractionated into the following size fractions: fine gravel (2000 μm to 1000 μm), coarse sand (1000 μm to 500 μm), middle sand (500 μm to 212 μm), fine sand (212 μm to 125 μm), coarse silt (125 μm to 63 μm) and fine silt + clay fraction (< 63 μm to 2 μm). The clay fraction (< 2 μm) of the samples was later separated by the sedimentation method, using Stoke's law for the settling velocity of spherical particles. The clay particles were allowed to settle and were then collected along with the solution, dried and weighed. Hence the clay% for a given sample was measured.

The fig. 28 below shows the particle size distribution of some of the soils, copper clinker ash, copper tailings and uranium tailings samples collected. Uranium bearing and non-uranium bearing rock samples were received in powdered form and hence were not

subjected to particle size fractionation. The average sand%, silt% and clay% for the samples are shown in table 20 below. From the figure and table it is evident that the silt fraction is higher in soils, copper clinker ash, copper tailings and uranium tailings samples than the other particle size classes. From texture triangle it can be concluded that the soils, copper clinker ash, copper tailings and uranium tailings fall mainly in the silt loam, silt loam, silt and silt loam classes, respectively.



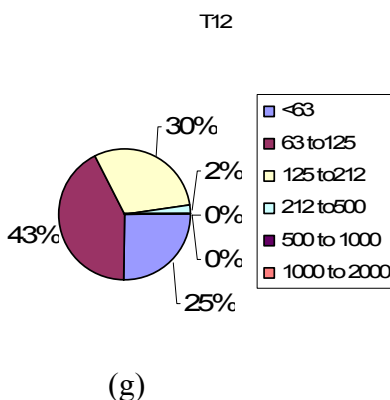


Fig. 28. Particle size fractions of sample (a) to (d) soil, (e) copper clinker ash, (f) copper tailings and (g) uranium tailings

Table 20. Particle size fractions of the collected samples

Fraction	Soil		Cu tailings		Cu clinker ash		U tailings	
	Mean	SD	Mean	SD	Mean	SD	Mean	SD
Sand %	30.6	9.1	4.8	3.1	45.7	12.2	32.6	16.5
Silt %	65.7	9.7	90.4	3.9	51.9	9.6	66.9	13.1
Clay %	3.7	1.6	4.8	0.8	2.4	1.0	0.5	0.6

3.1.2. Moisture Content

A matrix, like soil, that exists in loose form is made up of air, water and solid. The part of water present in a solid is defined by its moisture content. Moisture content was determined in the samples immediately after collection. Sample was taken in an Al boat and placed in a MA100 Satorius moisture analyzer, which gave the initial weight of the sample. The instrument works on the principle of heating, and thereby removing the moisture in a sample and gives the moisture content in percentage. The moisture content of the soils, copper clinker ash, copper tailings and uranium tailings samples are given in table 21 below.

Table 21. Moisture content of the collected samples

Moisture content %	Soil		Cu tailings		Cu clinker ash		U tailings	
	Mean	SD	Mean	SD	Mean	SD	Mean	SD
	12.57	6.23	2.51	1.22	1.72	0.57	2.65	0.82

3.1.3. Organic matter content

The organic matter present in a matrix is formed by the decay of plant and animal litter.

The organic matter then breaks down into stable humic substances, which resist further decomposition, called humus. Humus increases the cation exchange capacity of soils and hence the ability to store nutrients by chelation increases. Hence the fertility of soils is ranked based on their organic matter content.

The organic matter content of the samples was determined by heating in a muffle furnace at a temperature of 450°C for 36hrs. The organic matter content of the soils, copper clinker ash, copper tailings and uranium tailings samples are given in the table below.

Table 22. Organic matter content of the collected samples

Organic matter content %	Soil		Cu tailings		Cu clinker ash		U tailings	
	mean	sd	mean	sd	mean	sd	mean	sd
	2.44	0.56	1.12	1.04	0.87	0.21	1.37	1.13

3.1.4. pH

The pH of a medium is the negative logarithm of the H^+ ion concentration. The pH was determined by a pH meter (pH meter, Mettler Toledo) at 1:2.5 ratio of soil: water. 20gm soil was taken in a 100ml beaker to which 50 ml distilled water was added. The suspension was shaken for a period of 30 minutes in a horizontal shaker and then pH was recorded. The suspension must be stirred well just before electrode is immersed. The pH value usually increases with the increase in volume of water used. The increase in pH is

caused by the dilution of the H^+ ion concentration in the solution [171]. The pH of the soils, copper clinker ash, copper tailings and uranium tailings samples are given in table 23 below.

Table 23. pH of the collected samples

pH	Soil		Cu tailings		Cu clinker ash		U tailings	
	mean	sd	mean	sd	mean	sd	mean	sd
	4.76	0.64	5.46	2.24	5.81	2.45	6.58	1.49

3.1.5. Cation exchange capacity

The cation exchange capacity (CEC) of a soil is a measure of the quantity of sites on soil surfaces that can retain positively charged ions (cations) by electrostatic forces. CEC is normally expressed in units of charge per unit weight. Two different, but numerically equivalent sets of units are used: meq/100 g (milliequivalents of charge per 100 g of dry soil) or cmol/kg (centimoles of charge per kilogram of dry soil). Cation exchange sites are found primarily on clay and organic matter (OM) surfaces. Normal CEC ranges in soils would be from < 3 cmol_c/kg, for sandy soils low in OM, to >25 cmol_c/kg for soils high in certain types of clay or OM.

For a very precise measure of CEC, the $BaCl_2$ -compulsive exchange procedure [172-174] was used. Determining CEC by compulsive exchange is the method recommended by the Soil Science Society of America [175] because it is a highly repeatable, precise and direct measure of a soil's CEC.

First, 30 ml centrifuge tubes were weighed to the nearest mg and then 2.00 g of soil, 20 ml of 0.1 M $BaCl_2 \cdot 2H_2O$ were added and shaken for 2 hours on a horizontal shaker. The mixture was centrifuged at about 10,000 rpm and decanted carefully. Then 20 ml of 2

mM $\text{BaCl}_2 \cdot 2\text{H}_2\text{O}$ was added and shaken for 1 hour. The mixture was then centrifuged and the supernatant discarded. The two steps of addition of $\text{BaCl}_2 \cdot 2\text{H}_2\text{O}$ were repeated twice and before the third centrifugation, the pH of the slurry was measured. After the third decantation of 2 mM $\text{BaCl}_2 \cdot 2\text{H}_2\text{O}$, 10.00 ml of 5 mM MgSO_4 was added and shaken gently for one hour. The conductivity of a 1.5 mM MgSO_4 solution was determined. If conductivity of the sample solution was not 1.5 times this value, 0.100 ml increments of 0.1 M MgSO_4 were added until it attained the desired conductivity. The pH of the solution was determined. If it was not within 0.1 units of the previous measure, 0.05 M H_2SO_4 was added drop wise until pH was in appropriate range. Then distilled water was added, with mixing, until the solution conductivity was same as that of the 1.5 mM MgSO_4 . Solution pH and conductivity were alternately adjusted until the endpoints were reached. The outside of the tube was wiped dry and then weighed.

The CEC was calculated as given below:

1. Total solution (mls) [assuming 1 ml weighs 1 g] = final tube weight (g) - tube tare weight (g) - 2 g [weight of soil used]
2. Mg in solution (meq) = total solution (mls) \times 0.003 (meq/ml) [1.5 mM MgSO_4 has 0.003 meq/ml]
3. Total Mg added (meq) = 0.1 meq [meq in 10 mls of 5 mM MgSO_4] + meq added in 0.1 M MgSO_4 [mls of 0.1 M $\text{MgSO}_4 \times 0.2$ meq/ml (0.1 M MgSO_4 has 0.2 meq/ml)]
4. CEC (meq/100g) = (Pt. 3 – Pt. 2) \times 50 [Total Mg added - Mg in final solution; 50 is to convert from 2 g of soil to 100 g].

The CEC of the soils, copper clinker ash, copper tailings and uranium tailings samples are given in table below.

Table 24. Cation exchange capacity of the collected samples

CEC (meq/100g)	Soil		Cu tailings		Cu clinker ash		U tailings	
	mean	sd	mean	sd	mean	sd	mean	sd
	41.18	11.67	4.52	2.45	5.41	1.42	3.27	1.49

3.1.6. Humic acid content

Humic substances in soils and sediments can be divided into three main fractions: humic acids (HA or HAs), fulvic acids (FA or FAs) and humin. The HA and FA are extracted from soil and other solid phase sources using a strong base (NaOH or KOH). Humic acids are insoluble at low pH, and they are precipitated by adding strong acid (adjust to pH 1 with HCl). Humin cannot be extracted with either a strong base or a strong acid. Humic acid is one of the major components of humic substances which are dark brown and major constituents of soil organic matter humus that contributes to soil chemical and physical quality.

Humic substances (HS) are major components of the natural organic matter (NOM) in soil and water as well as in geological organic deposits such as lake sediments, peats, brown coals and shales. Humic substances are very important components of soil that affect physical and chemical properties and improve soil fertility. In aqueous systems, like rivers, about 50% of the dissolved organic materials are HS that affect pH and alkalinity. In terrestrial and aquatic systems HS affect the chemistry, cycling and bioavailability of chemical elements, as well as transport and degradation of xenobiotic and natural organic chemicals. Humic substances are complex and heterogeneous

mixtures of polydispersed materials formed by biochemical and chemical reactions during the decay and transformation of plant and microbial remains (a process called humification). Plant lignin and its transformation products, as well as polysaccharides, melanin, cutin, proteins, lipids, nucleic acids, fine char particles, etc., are important components taking part in this process.

The procedure used for separation and purification of HA was based on the method described by International Humic Substances Society (IHSS) [176-177]. An overview of the IHSS isolation and purification procedure (IHSS-N₂ method) is given in Fig. 29. In the IHSS method, 1000 cm³ volume of extract is used for extraction of 100g of soil containing below 3.3 % of organic carbon. The amount of sample and extractant used are also found to be sufficient according to Nagoya procedure [176]. The extraction with NaOH was carried out under nitrogen atmosphere. The humic acid content of the soils, copper clinker ash, copper tailings and uranium tailings samples are given in table 25 below.

Table 25. Humic acid content of the collected samples

Humic acid %	Soil		Cu tailings		Cu clinker ash		U tailings	
	mean	sd	mean	sd	mean	sd	mean	sd
	1.04	0.67	0.67	0.25	0.24	0.11	0.79	0.18

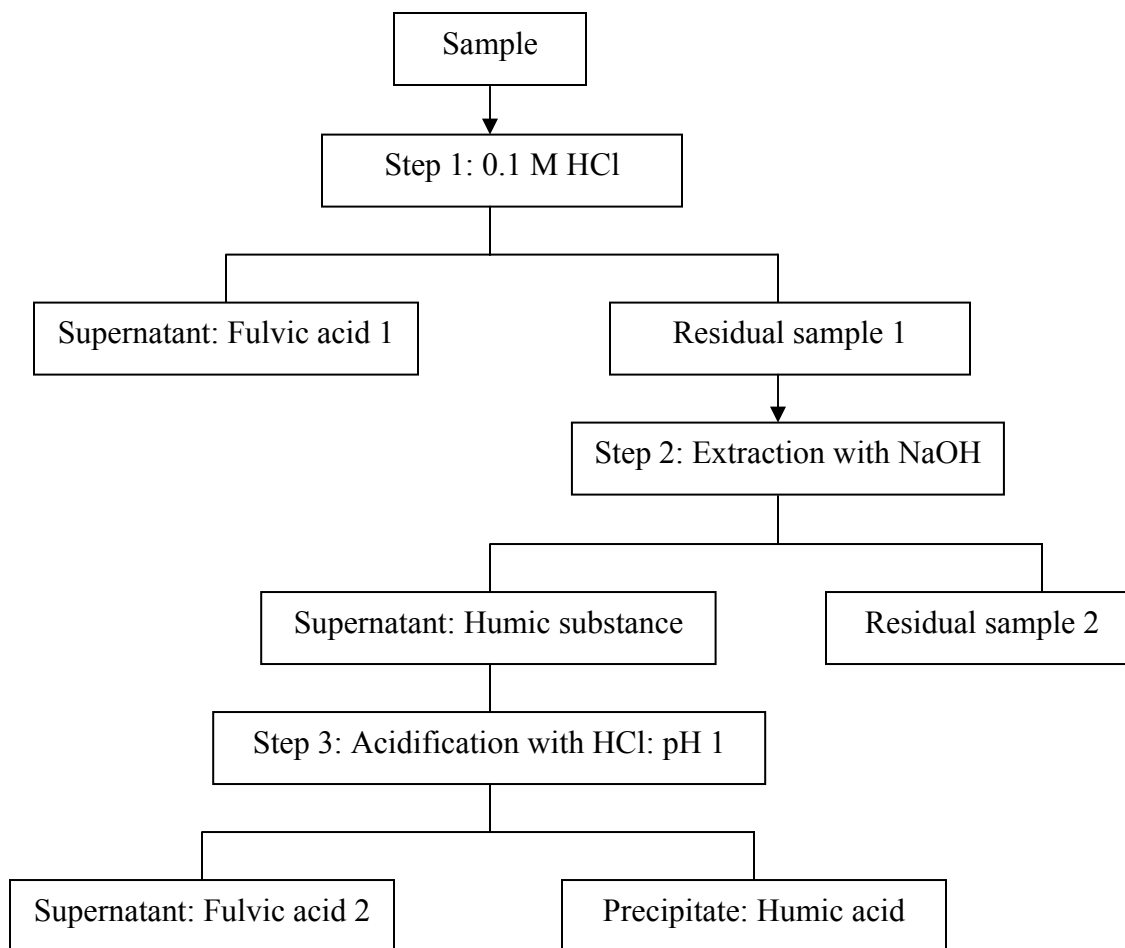


Fig 29. Overview of the IHSS Humic acid separation procedure

3.2. Measurements through High Resolution Gamma Spectrometry

As mentioned in the earlier chapter, a high-purity vertical Germanium detector was used for all the HRGS measurements carried out in this thesis. Details of the setup are given in the earlier chapter.

Since ^{238}U emits a very weak low energy γ photon (49.56 keV, 0.064%), it is difficult to detect. It can be measured by the two γ rays of its immediate daughter product ^{234}Th at 63.29 keV and 92.59 keV. The 92.59 keV peak was not considered for calculations since it is a doublet (92.4 + 92.8 keV) and cannot be resolved with the present resolution of the

HRGS. García- Talavera [178] and Morillon et al. [179] have summarised all the photons appearing in the 92-96 keV energy region. The 63.29 keV energy has some contribution from 63.3 keV γ (4.8 %) from ^{234}Th , 63.9 keV γ (0.023 %) from ^{231}Th and 63.9 keV γ (0.255 %) from ^{232}Th . However, these contributions can be neglected [38, 178]. The selection of 63.29 keV peak is supported by the equality in ^{238}U activities obtained by alpha spectrometry and ^{234}Th activities by gamma spectrometry, using the 63.3 keV γ rays from ^{234}Th [180]. The ^{234}Th and $^{234\text{m}}\text{Pa}$ gamma rays are best suited for the estimation of ^{238}U , since their short half-lives (24.1 d for ^{234}Th and 1.17 min for $^{234\text{m}}\text{Pa}$) allow them to achieve secular equilibrium with ^{238}U . Estimation of ^{238}U concentration in uranium ore and other samples containing high concentration of U by these energies has already been proven [181]. The very low abundance (0.837 %) of $^{234\text{m}}\text{Pa}$ makes ^{238}U estimation by this energy difficult for environmental samples.

For this thesis, ^{238}U was estimated through 63.29 keV gamma of its immediate daughter ^{234}Th . The ^{226}Ra 186.2 keV peak has interference from 185.7 keV peak of ^{235}U . The ^{226}Ra was determined by its direct 186.2 keV peak after correcting for ^{235}U contribution and compared with the activities obtained from ^{214}Pb and ^{214}Bi gamma energies. Radionuclides of the ^{232}Th series, namely ^{208}Tl , ^{228}Ac and ^{212}Pb were measured by the γ energies as given in table 26 along with the gamma energies used for the measurement of the other radionuclides.

Table 26. Radionuclides analysed by gamma spectrometry, with energies and gamma ray intensities

Radionuclide	Measured nuclide	Energy (keV)	Branching Intensity (%)
^{238}U	^{234}Th	63.29	4.82

²²⁶ Ra	²²⁶ Ra	186.2	3.59
²¹⁴ Pb	²¹⁴ Pb	295.2	19.3
²¹⁴ Pb	²¹⁴ Pb	351.9	37.6
²¹⁴ Bi	²¹⁴ Bi	609.3	46.1
²¹⁰ Pb	²¹⁰ Pb	46.54	4.25
²²⁷ Th	²²⁷ Th	256.2	7.0
²⁰⁸ Tl	²⁰⁸ Tl	583.2	30.4
²⁰⁸ Tl	²⁰⁸ Tl	2614	35.6
²²⁸ Ac	²²⁸ Ac	911.2	25.8
²¹² Pb	²¹² Pb	238.63	43.3
⁴⁰ K	⁴⁰ K	1460.83	10.7
¹³⁷ Cs	¹³⁷ Cs	661.6	85.1

Activity concentration of each radionuclide was calculated using the following equation:

$$A \text{ (Bq/kg)} = C / (E * \gamma * M * T) \quad (12)$$

Where, C is the background subtracted net counts of the sample, E is the efficiency of the detector for the specific gamma ray energy, γ is the absolute transition probability of that specific gamma decay, M is the mass of sample in kg and T is the counting time in seconds.

3.2.1. Distribution of radionuclides in soils

The average activity concentrations, in Bq/kg, of the radionuclides of the ²³⁸U series, ²³²Th, ⁴⁰K and ¹³⁷Cs measured in the surface soil samples are given in table 27. These statistical parameters are based on thirty samples collected from this mineralised region. The activity concentration of ²³⁵U series radionuclides was very low and was observed to follow the constant ratio of 0.04658 with ²³⁸U. Skewness and kurtosis have been calculated to gain an idea of the distribution of the data values for a specific radionuclide.

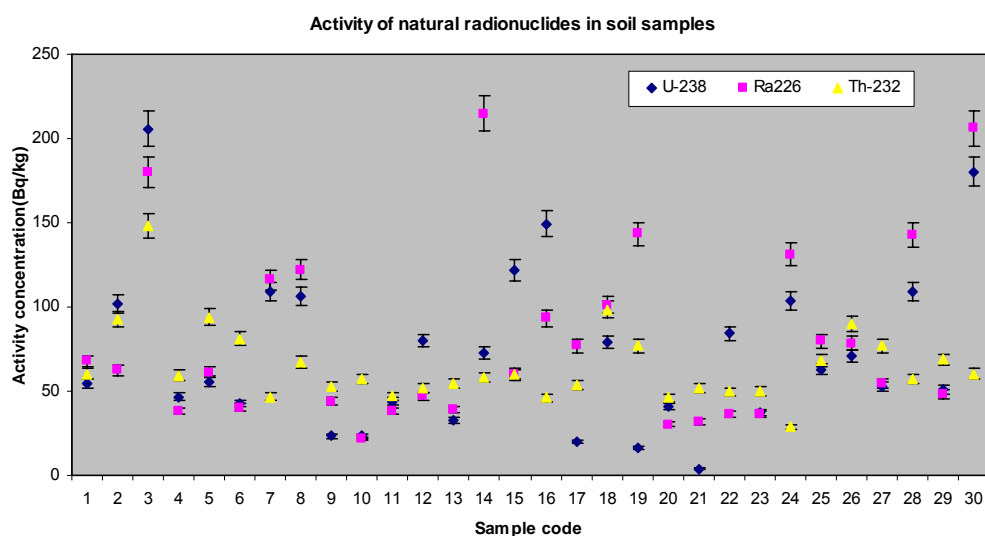
Skewness characterises the degree of asymmetry of a distribution around its mean. Positive skewness indicates a distribution with an asymmetric tail extending toward more positive values. Negative skewness indicates a distribution with an asymmetric tail extending toward more negative values. Kurtosis characterizes the relative peakedness or flatness of a distribution compared with the normal distribution. Positive kurtosis indicates a relatively peaked distribution. Negative kurtosis indicates a relatively flat distribution.

Table 27. Activity concentrations of radionuclides of the ^{238}U and ^{232}Th series, ^{40}K and ^{137}Cs in surface soil samples

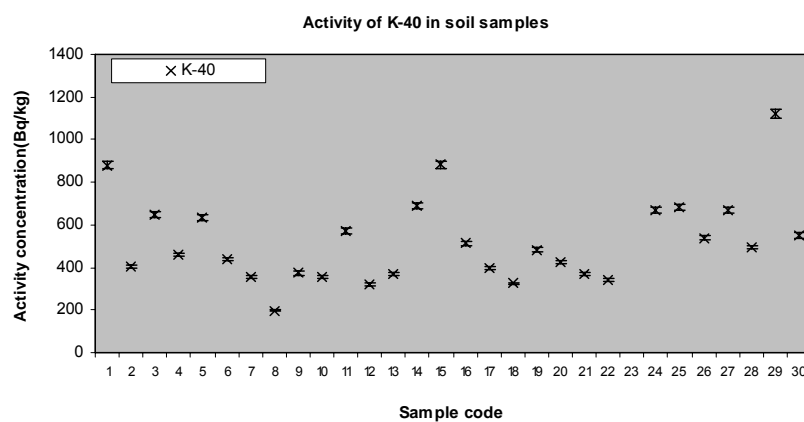
Activity concentration (Bq/kg)	^{238}U	^{226}Ra	^{232}Th	^{40}K	^{137}Cs
Min	4.0	21.6	28.7	197.7	1.8
Max	205.6	215.0	148.2	1121.4	7.5
Mean	72.8	81.5	65.1	522.8	4.2
Standard deviation	48.0	53.3	22.7	201.8	1.5
Skewness	1.08	1.18	1.84	1.13	0.15
Kurtosis	1.08	0.58	5.08	1.53	-0.79

From the table above it can be observed that the distributions of ^{238}U , ^{226}Ra , ^{232}Th and ^{40}K are positively skewed, indicating a log-normal distribution, whereas that of ^{137}Cs is near normal. The kurtosis values of the radionuclides indicate that the distributions of ^{238}U and ^{40}K are moderately peaked; ^{232}Th distribution is highly peaked; ^{226}Ra distribution is near normal whereas ^{137}Cs distribution is less peaked than a normal distribution.

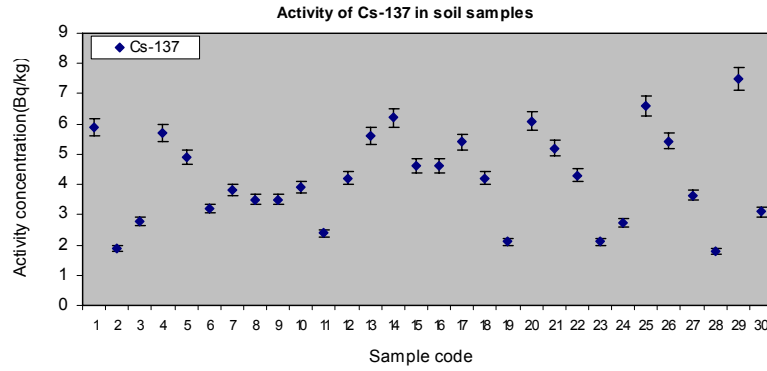
The distribution of the activity concentrations of the radionuclides are plotted in fig. 30 (a), (b) and (c) below. The standard deviations associated with the data points is the counting error due to gamma spectrometric counting of the samples. From fig. 30 it can be observed that the ^{232}Th distribution is rather uniform and varies within a smaller range as compared to the distribution of ^{238}U and ^{226}Ra . The concentration of the primordial radionuclide ^{40}K varies in a wide range whereas that of the anthropogenic radionuclide ^{137}Cs varies within a narrow range.



(a)



(b)



(c)

Fig 30. Distribution of (a) ^{238}U , ^{226}Ra and ^{232}Th , (b) ^{40}K and (c) ^{137}Cs in soils

The fig. 31 below shows the box-whisker plots of the data. These plots are useful for studying symmetry, checking distributional assumptions, and detecting outliers in a given dataset. In such plots, the data are divided into four areas of equal frequency. A box encloses the middle 50 percent, where the median is represented as a vertical line inside the box and the mean is plotted as a point. Horizontal lines, called whiskers, extend from each end of the box; the lower whisker, from the lower quartile to the smallest point within 1.5 interquartile range from the lower quartile and the other whisker, from the upper quartile to the largest point within 1.5 interquartile range from the upper quartile. Values that fall beyond the whiskers, but within 3 interquartile ranges (suspect outliers), are plotted as individual points and outliers are distinguished by a special character.

From the fig. 31 it is observed that ^{137}Cs values are normally distributed and nearly symmetrical. The ^{226}Ra values are not normally distributed and have no outlier values. The ^{238}U , ^{232}Th and ^{40}K values have one suspect outlier each, on the higher side of the distribution. These higher activity concentrations have been obtained near the mining deposits, where higher mineralisation occurs.

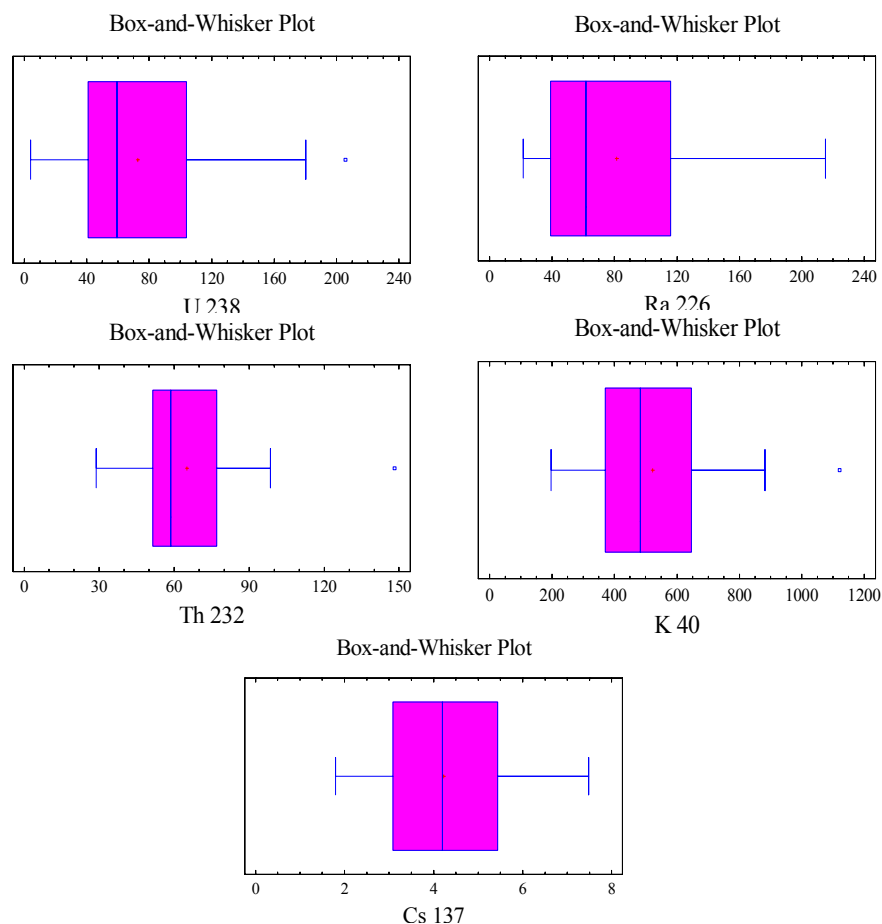


Fig. 31. Box-Whisker plots of radionuclide concentrations in soils

The distribution fitting for the data of radionuclide concentrations are shown in Fig. 32 below. The distribution fitting has been done with the help of Statgraphics Plus software. Kolmogorov-Smirnov test, Chi-square test and Shapiro Wilks test were used to identify the underlying distribution of the radionuclide data. The Kolmogorov-Smirnov test is a non-parametric test that computes the maximum distance between the cumulative distribution of the detector and the cumulative distribution function of the fitted distribution. The chi-square test divides the range of the detector into a number of equally probable classes and compares the number of observations in each class to the number expected. The Shapiro-Wilks test is based upon comparing the quantiles of the fitted normal distribution to the quantiles of the data. The test is recommended in several EPA

guidance documents [153,182] and in different texts [183, 184]. These tests rejected the hypothesis that the data sets for ^{238}U , ^{226}Ra , ^{232}Th and ^{40}K come from a normal distribution with 95%, 99%, 99% and 95% confidence, respectively. But for ^{137}Cs the tests could not reject the hypothesis that the data set came from a normal distribution with 90% or higher confidence.

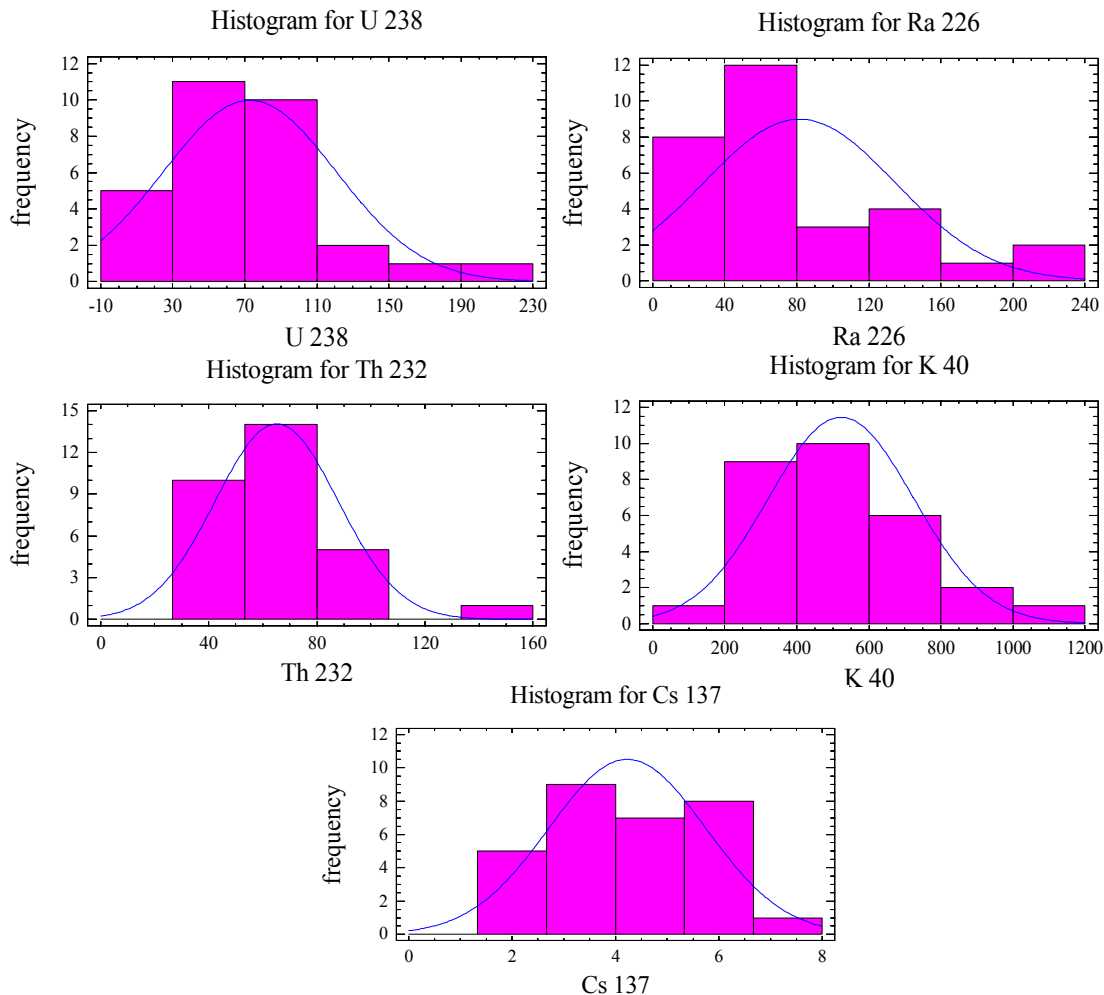


Fig. 32. Distribution fits for radionuclide concentrations in soils

Several surface soil samples were collected around the uranium deposits at Jaduguda, Bhatin, Narwapahar and Turamdih and also from locations near to the road connecting Turamdih to Jaduguda, as shown in fig. 8. Slightly higher activity concentrations were observed at few locations near the uranium deposits. This may be due to the fact that

these locations may lie in the mineralised zones. But, for many locations, in spite of being located close to the uranium deposits, they showed somewhat lower activity concentrations of ^{238}U series isotopes. This indicates that the mineralisation in this area may be occurring in pockets as no clear trend in spatial distribution is evident. Again, radionuclide concentration in these soils is not solely dependent on the proximity to uranium deposits and is of disseminated type.

3.2.2. Distribution of radionuclides in host rocks

The average activity concentrations, in Bq/kg, of the radionuclides of the ^{238}U series and ^{232}Th measured in the metamorphic host rock samples are given in table 28. These statistical parameters are based on twelve host rock samples collected from this mineralised region.

Table 28. Activity concentrations of ^{238}U series and ^{232}Th in host rocks

Activity concentration (Bq/kg)	U-238	Ra-226	Th-232
Min	62.35	59.48	31.23
Max	172.62	176.46	111.54
Mean	107.82	108.18	59.83
Standard deviation	37.02	38.23	25.72
Skewness	0.50	0.35	0.60
Kurtosis	-0.77	-0.64	-0.38

From the table above it can be observed that the distributions of ^{238}U and ^{226}Ra seem to be in near equilibrium condition in the samples. The data for all the radionuclides are very slightly positively skewed, indicating slight deviation from normal distribution. The kurtosis values of the radionuclides indicate that the distributions are less peaked than a normal distribution.

The distribution of the activity concentrations of the radionuclides are plotted in fig. 33 below. The standard deviations associated with the data points is the counting error due to gamma spectrometric counting of the samples. From Fig it can be observed that ^{238}U and ^{226}Ra are in near equilibrium condition in the samples . The ^{232}Th data values are less scattered and vary within a smaller range as compared to the distribution of ^{238}U and ^{226}Ra .

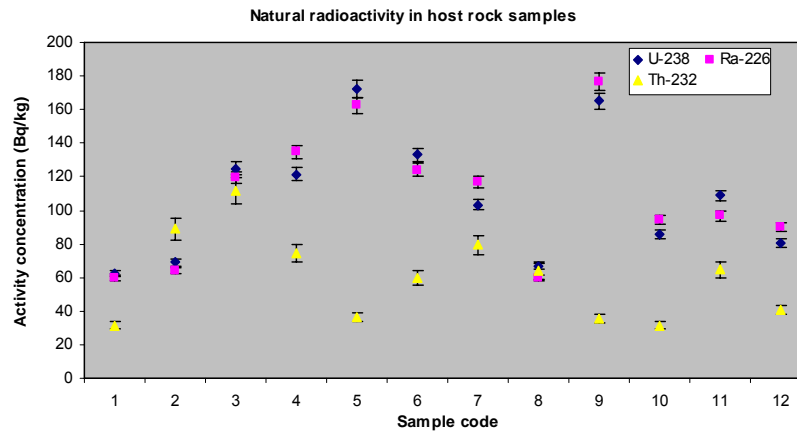


Fig 33. Distribution of ^{238}U , ^{226}Ra and ^{232}Th in host rocks

The Fig. 34 below shows the box-whisker plots of the data. The radionuclide concentrations are not exactly normally distributed, are right skewed and have no outlier values.

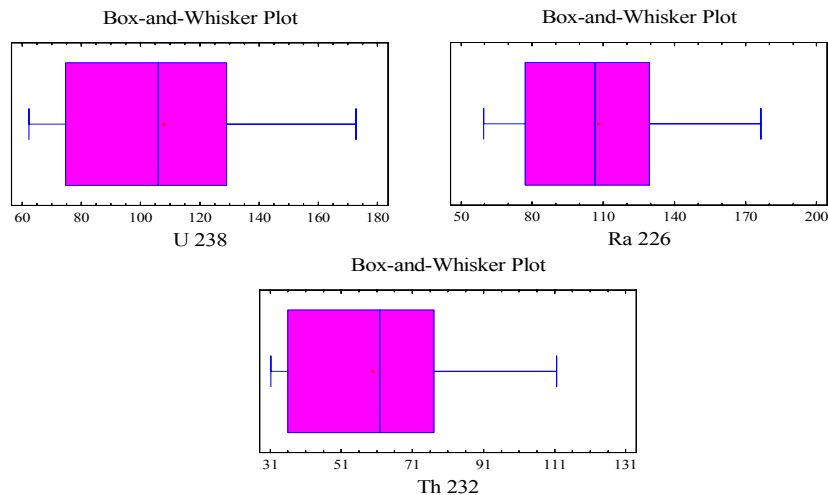


Fig. 34. Box-Whisker plots of radionuclide concentrations in host rocks

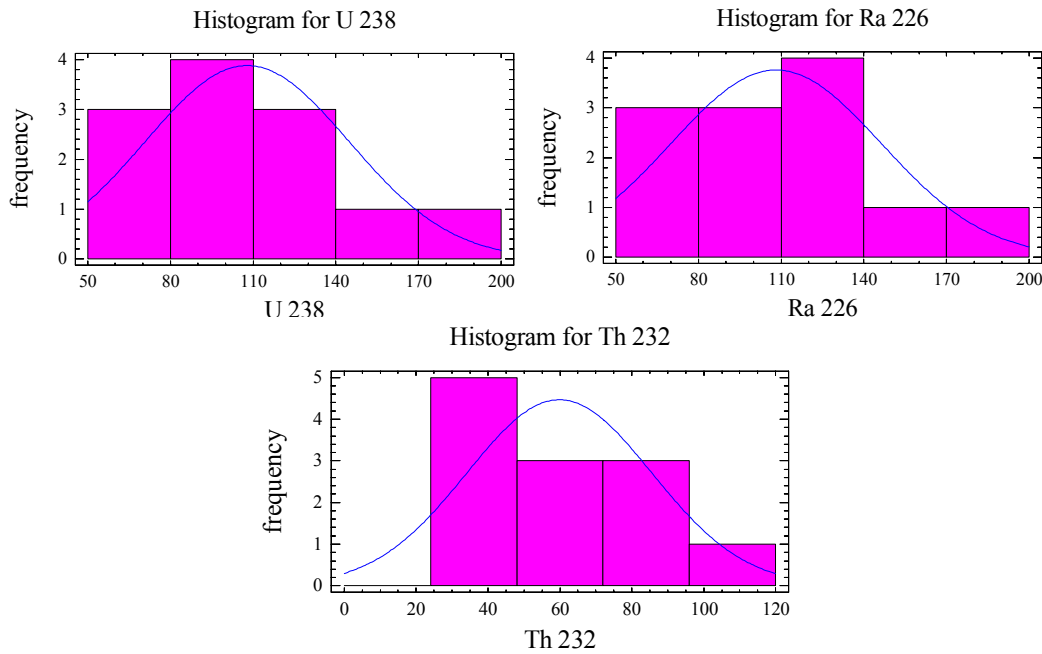


Fig 35. Distribution fits for radionuclide concentrations in host rocks

The distribution fitting for the data of radionuclide concentrations are shown in fig. 35. Kolmogorov-Smirnov test, Chi-square test and Shapiro Wilks test were used to identify the underlying distribution of the radionuclide data. These tests could not reject the hypothesis that the data sets for ^{238}U , ^{226}Ra and ^{232}Th come from a normal distribution with 90% confidence or more.

3.2.3. Distribution of radionuclides in uranium bearing rocks

The average activity concentrations, in Bq/kg, of the radionuclides of the ^{238}U series and ^{232}Th measured in the uranium bearing rock samples are given in table 29. These statistical parameters are based on twenty five samples collected from the uranium deposits in this mineralised region. From the table it can be seen that the ^{232}Th concentrations are two orders of magnitude lower than the ^{238}U and ^{226}Ra concentrations.

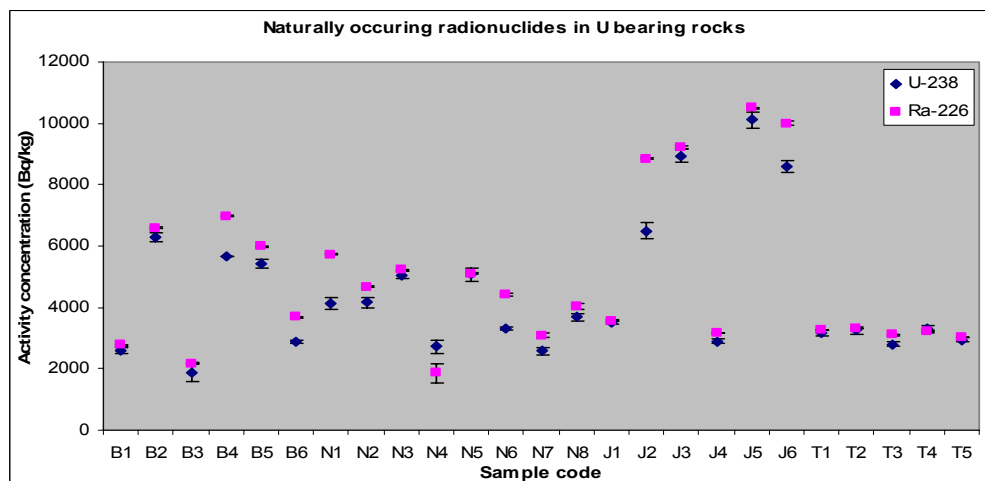
The ^{238}U and ^{226}Ra activity concentrations are the highest in Jaduguda deposit, accompanied by the highest standard deviations, compared to other deposits.

Table 29. Activity concentrations of ^{238}U series and ^{232}Th in uranium bearing rocks

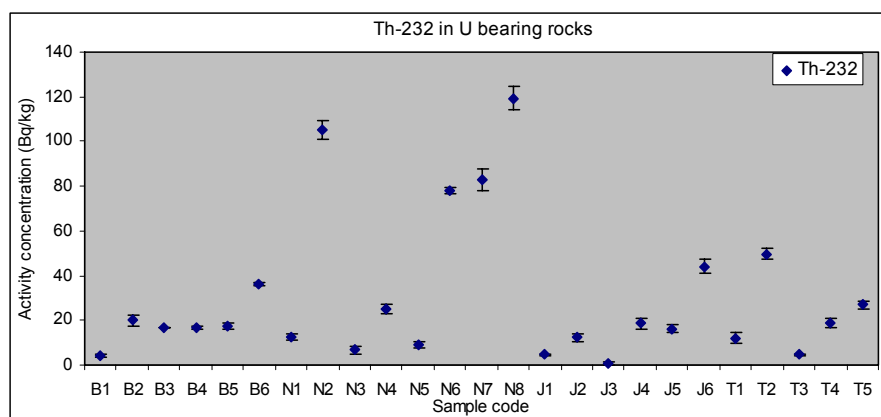
Mine	Activity concentration (Bq/kg)	^{238}U Bq/kg	^{226}Ra Bq/kg	^{232}Th Bq/kg
Bhatin	Mean	4126	4695	18
	SD	1887	2076	10
	Skewness	-0.03	-0.12	0.69
	Kurtosis	-2.70	-2.57	2.53
Narwapahar	Mean	3837	4265	55
	SD	949	1264	47
	Skewness	0.05	-1.03	0.23
	Kurtosis	-1.28	0.69	-2.08
Jaduguda	Mean	6756	7550	16
	SD	2996	3296	15
	Skewness	-0.42	-0.84	1.41
	Kurtosis	-1.96	-1.83	2.53
Turamdih	Mean	3089	3184	22
	SD	215	113	17
	Skewness	-0.70	-0.55	1.09
	Kurtosis	-1.91	-1.99	1.24

Most of the data sets on radionuclide concentration are deviant from an ideal normal distribution as observed from their skewness values. Slight deviation is observed for ^{238}U and ^{226}Ra concentrations in Bhatin deposit and ^{238}U and ^{232}Th concentrations in Narwapahar deposit. The kurtosis values indicate that the datasets are either peaked or flattened with respect to the ideal normal distribution to a high degree.

The distribution of the activity concentrations of the radionuclides are plotted in fig. 36. From the figure it can be observed that ^{238}U and ^{226}Ra are in not in ideal secular equilibrium condition in the samples. The ^{238}U and ^{226}Ra concentrations vary within a small range in samples from Turamdih deposit. The ^{232}Th data values are more uniform and vary within a smaller range in the deposits of Bhatin, Jaduguda and Turamdih.



(a)

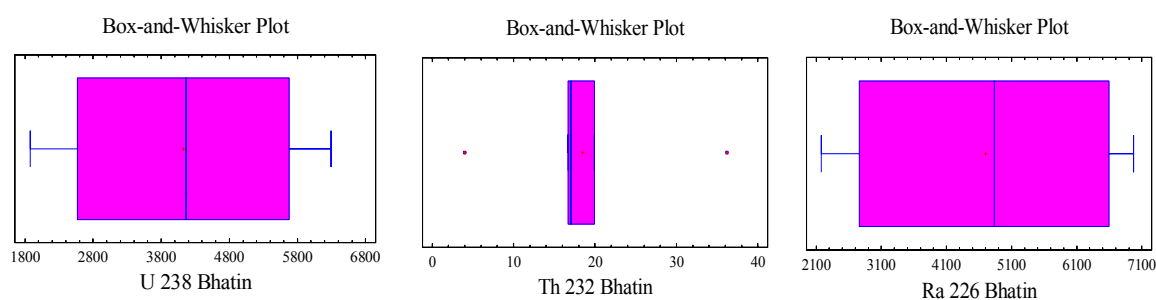


(b)

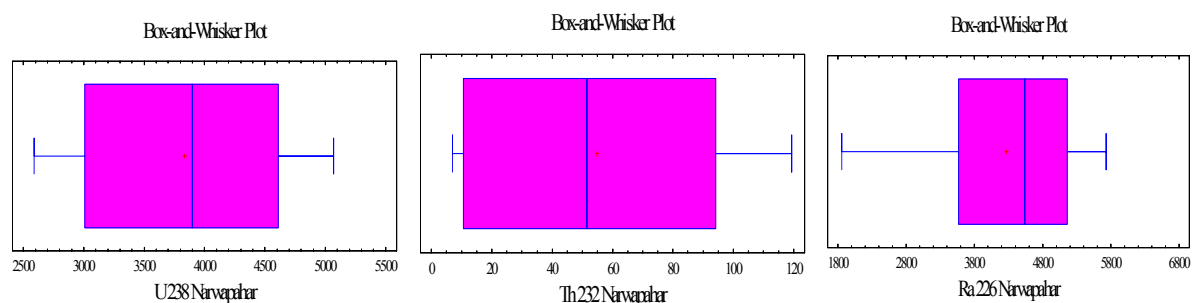
Fig. 36. Distribution of (a) ^{238}U and ^{226}Ra and (b) ^{232}Th in uranium bearing rocks

From the box-whisker plots of radionuclide concentrations, fig. 37 (a), (b), (c) and (d) it is observed that for ^{238}U and ^{226}Ra concentrations in Bhatin deposit and ^{238}U and ^{232}Th concentrations in Narwapahar deposit are nearly normally distributed and nearly

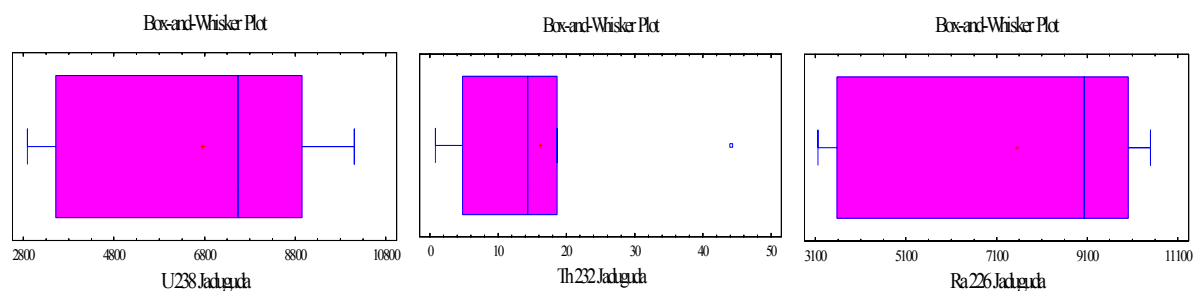
symmetrical. The ^{232}Th values from Bhatin deposit have two outlier values, one each on the lower and higher side of the data set. The ^{232}Th data values have one suspect outlier each, on the higher side of the distribution from the Jaduguda and Turamdih deposit. The ^{238}U and ^{226}Ra activity concentrations from Jaduguda and Turamdih are skewed.



(a)



(b)



(c)

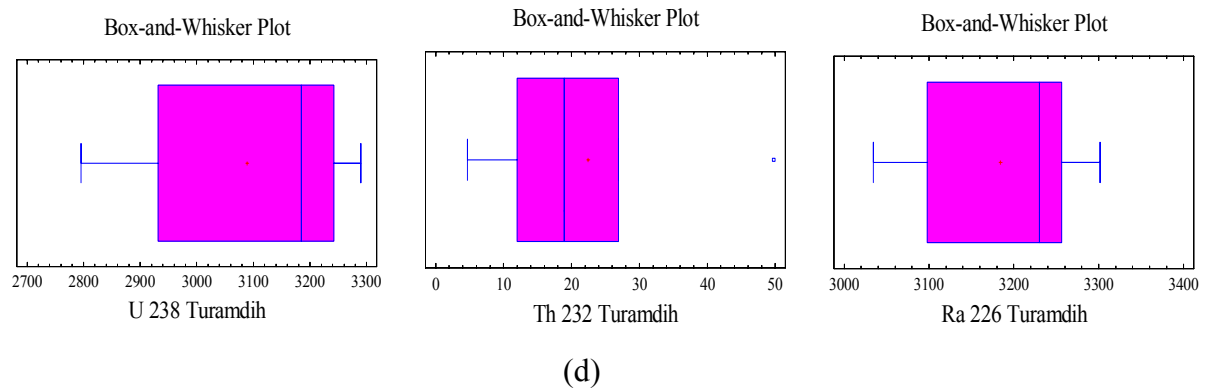
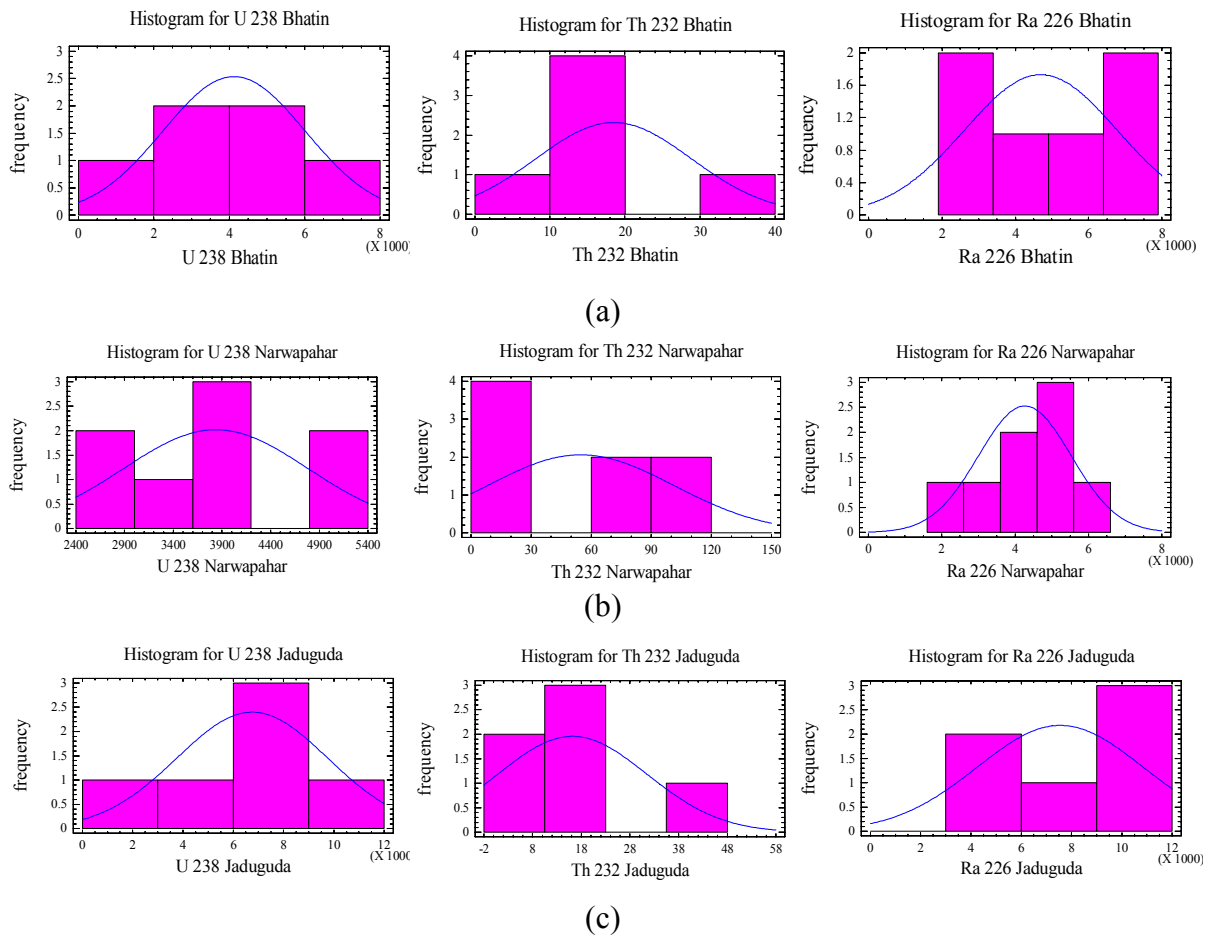
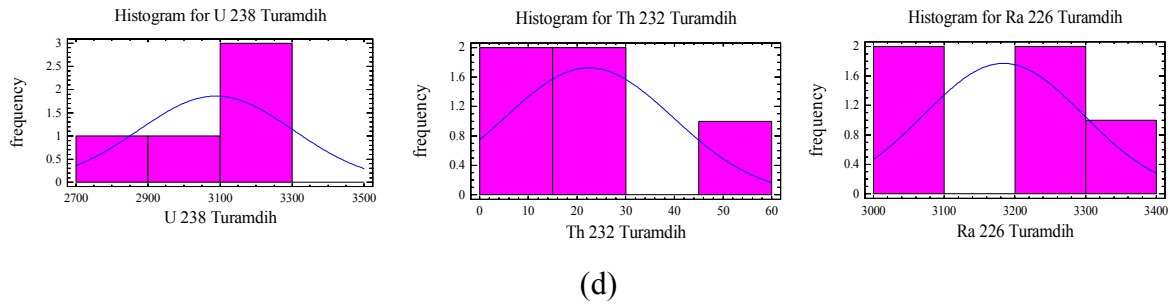


Fig. 37. Box-Whisker plots of radionuclide concentrations in (a) Bhatin, (b) Narwapahar, (c) Jaduguda and (d) Turamdih deposit

The distribution fitting for the data of radionuclide concentrations are shown in fig. 38 (a), (b), (c) and (d). Kolmogorov-Smirnov test, Chi-square test and Shapiro Wilks test were used to identify the underlying distribution of the radionuclide data.





(d)

Fig. 38. Distribution fits for radionuclide concentrations in (a) Bhatin, (b) Narwapahar, (c) Jaduguda and (d) Turamdih deposit

These tests could not reject the hypothesis that the data sets for ^{238}U , ^{226}Ra and ^{232}Th come from a normal distribution with 90% confidence for most of the deposits, except ^{232}Th in Bhatin deposit and ^{226}Ra in Jaduguda deposit, where this hypothesis was rejected with 90% confidence. It has to be borne in mind that the sample number from each mine was less than ten; hence the underlying distributions as identified from the above tests may suffer from this shortcoming.

3.2.4. Distribution of radionuclides in wastes

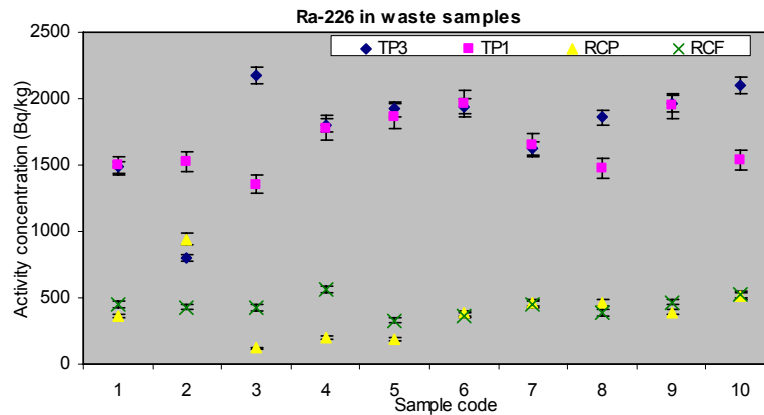
The average activity concentrations, in Bq/kg, of the radionuclides of the ^{238}U series and ^{232}Th measured in the various waste samples are given in table 30. These statistical parameters are based on forty samples collected from the mineralised region. From the table it can be seen that the ^{232}Th concentrations are at least an order of magnitude lower than the ^{238}U and ^{226}Ra concentrations. Since these wastes are generated from rocks that are rich in uranium or copper (with associated uranium present), the values of uranium and its daughter products are expected to be higher than thorium. Again, the uranium concentrations are lower than the radium concentrations in case of uranium tailings; this is due to the chemical processing of the ore to selectively remove uranium. But in the

copper wastes both uranium and radium have similar concentrations, due to no selective removal of any radionuclide.

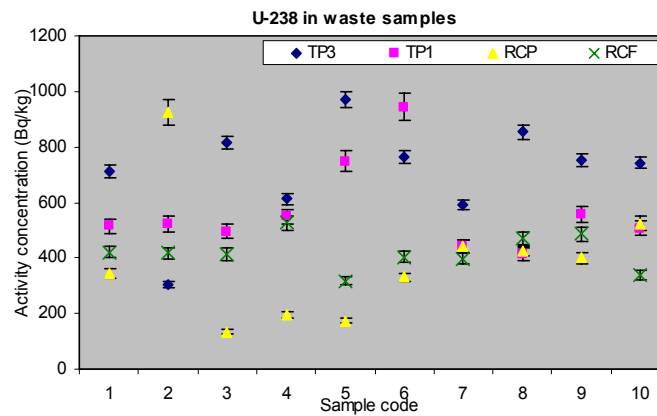
Table 30. Activity concentrations of ^{238}U series and ^{232}Th in waste samples

Sample	Activity concentration (Bq/kg)	^{238}U	^{226}Ra	^{232}Th
U tailings TP3	Max	972.2	2174.7	57.5
	Min	304.4	795.0	7.6
	Mean	712.3	1766.9	41.3
	Standard Deviation	181.1	398.4	14.5
	Skewness	-1.8	-1.1	-1.4
	Kurtosis	3.8	2.4	2.7
U tailings TP1	Max	943.6	1962.0	51.7
	Min	414.0	1354.9	27.9
	Mean	569.4	1659.9	35.2
	Standard Deviation	158.7	215.5	6.6
	Skewness	0.3	1.8	1.9
	Kurtosis	-1.5	3.1	4.7
Cu tailings	Max	925.1	943.2	50.8
	Min	134.6	124.1	7.4
	Mean	389.4	403.7	16.2
	Standard Deviation	227.3	230.4	13.3
	Skewness	1.3	1.4	2.8
	Kurtosis	3.0	3.1	7.9
Cu clinker ash	Max	526.2	561.4	42.5
	Min	318.5	330.2	28.1
	Mean	419.2	439.2	34.0
	Standard Deviation	62.8	69.0	4.6
	Skewness	0.3	0.1	0.7
	Kurtosis	-0.1	-0.1	-0.1

Most of the data sets on radionuclide concentration are deviant from an ideal normal distribution as observed from their skewness values. The deviation from normality is slight for ^{238}U and ^{226}Ra concentrations in copper clinker ash samples. The kurtosis values indicate that most of the datasets are peaked with respect to the ideal normal distribution to a high degree. Copper clinker ash samples are seen to be nearer to a normal distribution considering the kurtosis values.



(a)



(b)

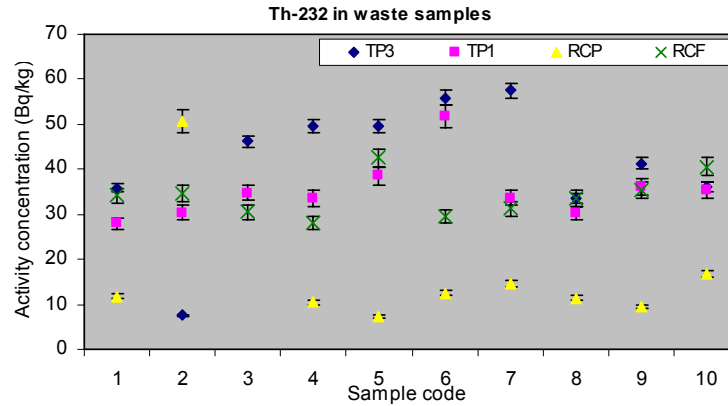
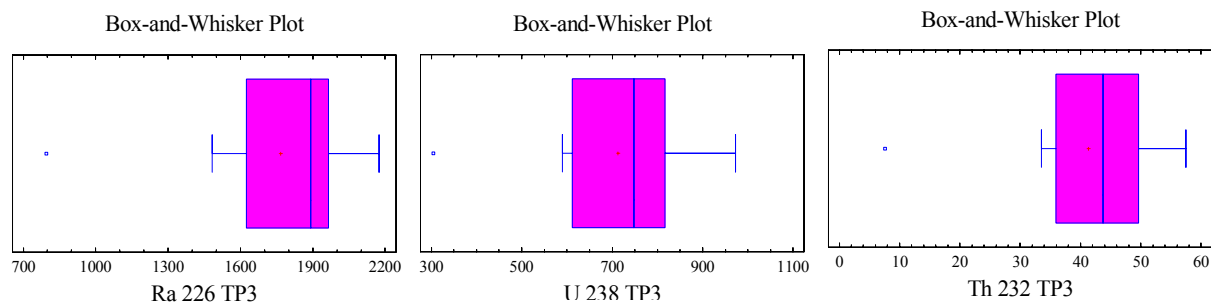


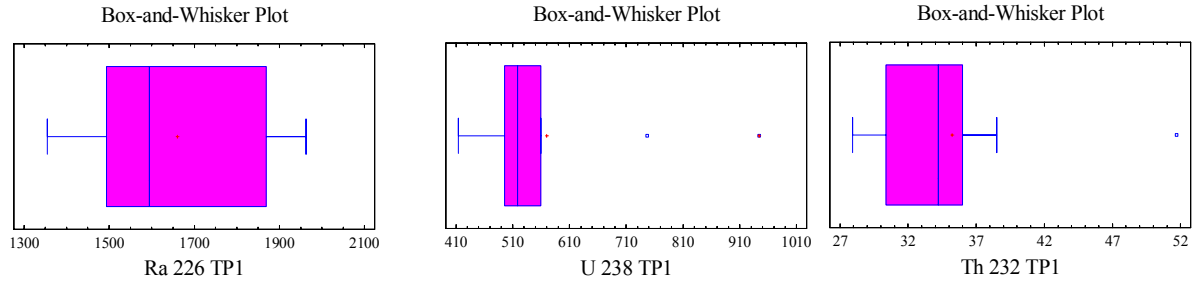
Fig 39. Distribution of (a) ^{226}Ra , (b) ^{238}U and (c) ^{232}Th in waste samples

The distribution of the activity concentrations of the radionuclides are plotted in fig. 39. It can be observed that ^{226}Ra concentrations are higher in uranium tailings compared to copper wastes, but ^{238}U and ^{232}Th are comparable. This is because the uranium tailings are obtained from uranium rich rocks, from which ^{238}U is selectively removed, thus making the tailings rich in ^{226}Ra as compared to ^{238}U .

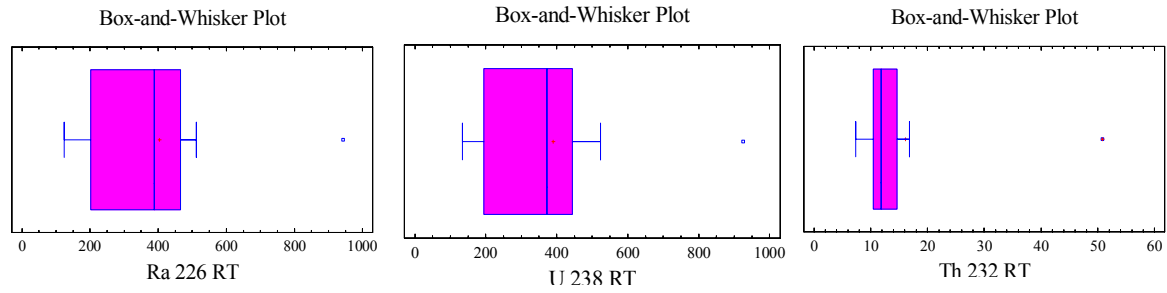
From the box-whisker plots of radionuclide concentrations, fig. 40 (a), (b) and (c), it is observed that each of the radionuclide concentrations in uranium tailings, TP3 have one suspect outlier on the lower side. The ^{238}U values for uranium tailings, TP1 and ^{232}Th values for copper tailings have one outlier on the higher side of the data set. The radionuclide activity concentrations for copper klinker ash samples are slightly skewed.



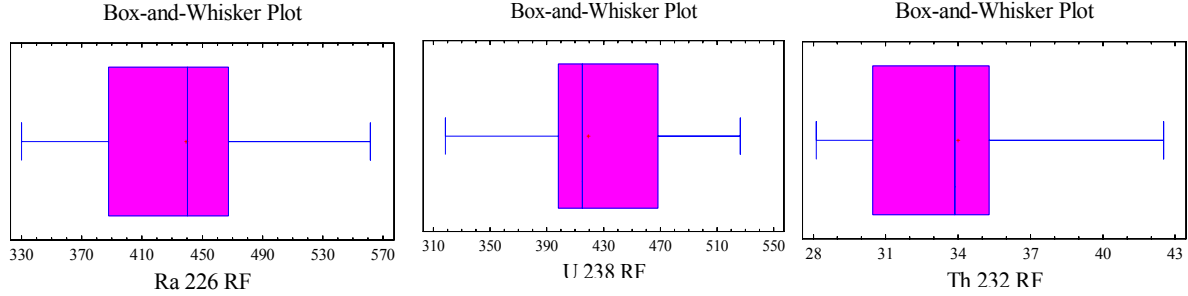
(a)



(b)



(c)



(d)

Fig. 40 . Box-Whisker plots of radionuclide concentrations in (a) TP3, (b) TP1 and (c) copper tailings and (d) copper clinker ash

The distribution fitting for the data of radionuclide concentrations are shown in fig. 41 (a), (b) and (c). Kolmogorov-Smirnov test, Chi-square test and Shapiro Wilks test were used to identify the underlying distribution of the radionuclide data.

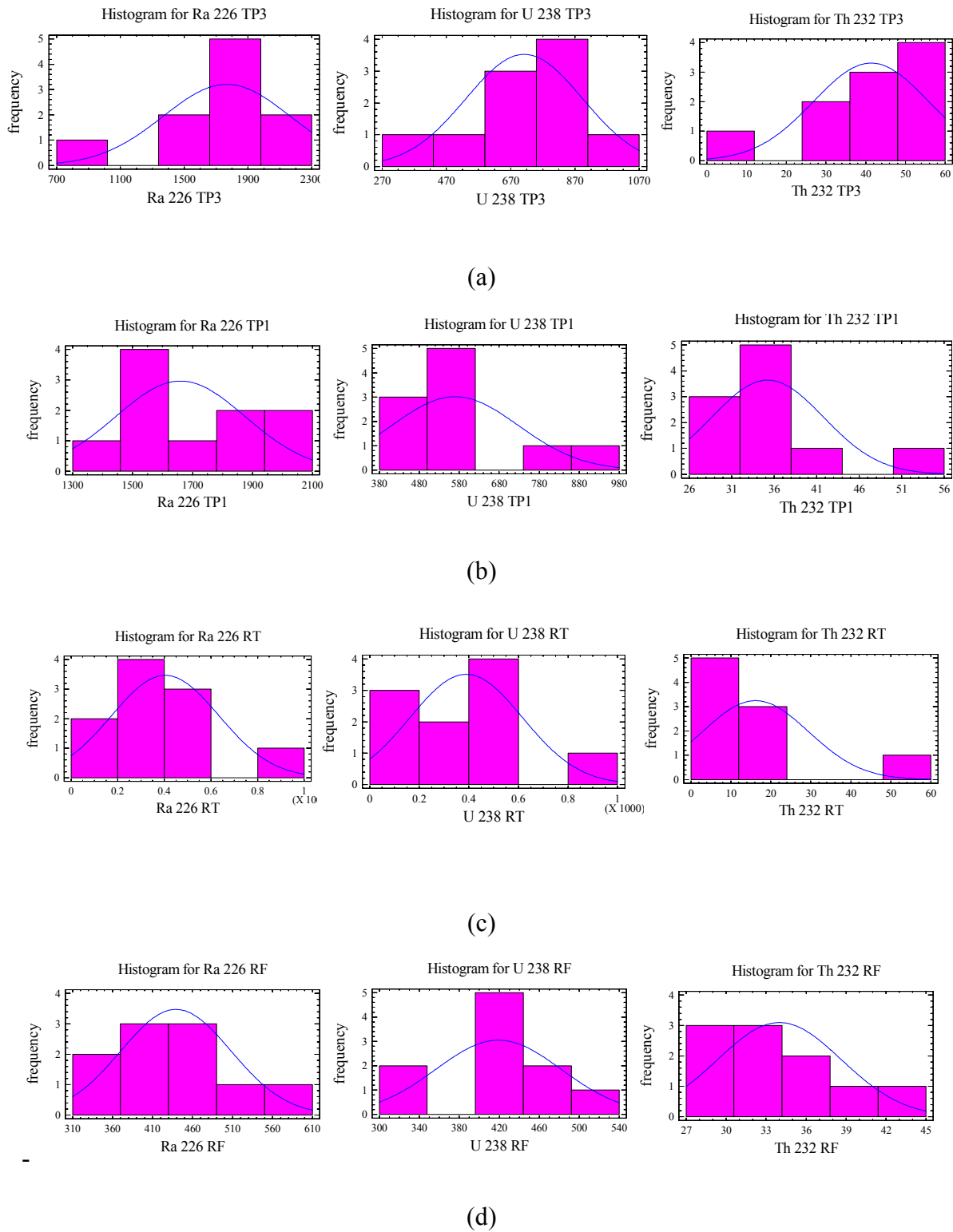


Fig. 41. Distribution fits for radionuclide concentrations for (a) TP3, (b) TP1 and (c) copper tailings and (d) copper clinker ash

These tests could not reject the hypothesis that the data sets for ^{238}U and ^{232}Th come from a normal distribution with 90% confidence, for TP3 and copper klinker ash samples. The underlying distribution for ^{226}Ra distribution in TP1 and copper flyash samples was also identified as normal. In the rest of the samples this hypothesis was rejected with 90% confidence or more.

3.3. Measurements through Instrumental Neutron Activation Analysis

In this thesis Instrumental neutron activation analysis (INAA), involving delayed gamma, was employed to measure elemental concentrations in samples. The APSARA reactor, BARC, Mumbai, with a thermal neutron flux of $10^{12} \text{ neutrons.cm}^{-2}.\text{s}^{-1}$ was used for 7 hr sample irradiations. Comparator technique of INAA was used. The samples were allowed a cooling time of 3 days for decay of short-lived radioactivity. Subsequently, 3 sequential measurements were carried out on a 50% p-type HPGe after a time period of 3 days, 14 days and 30 days for each sample along with the standard and blank. Counting time was 1000 seconds, 10000 seconds and 24 hours, respectively in the three measurements. The gamma energies and the half lives of the radioactive isotopes formed corresponding to the stable elements are given in table 31.

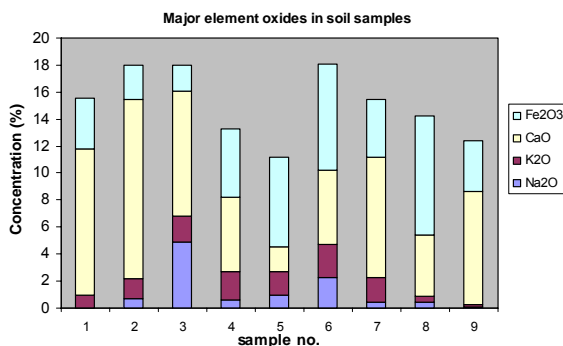
Table 31. Stable elements and the gamma energies and half lives of their corresponding radioisotopes formed

Element	Energy,keV	Half life
Sm	103.2	46.8h
U	116, 228, 277	14.1h
La	328, 487, 815.74, 1596.5	40.3h
Cd	336, 527.8	2.2d

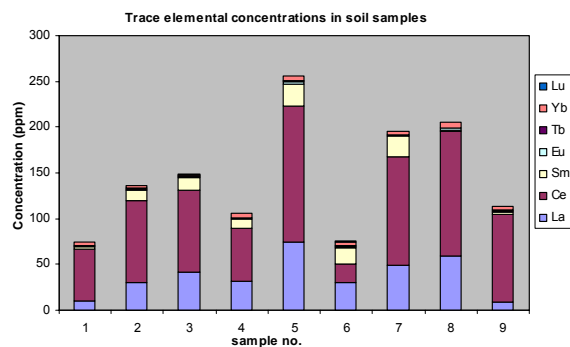
Cu	511	12.7h
Br	554.4, 619.1, 776.5	35.3h
As	559, 1215.8	26.3h
Sb	564.1	2.7d
Ga	630.02	14.1h
Ca	1297.1	4.5d
Na	1368.6	15h
K	1524.7	12.4h
Ta	67.7, 1221.4	42.4d
Eu	121.8, 344.28	13y
Hf	133.2, 482.2	42.4d
Ce	145.4	32.5d
Yb	198	32.0d
Lu	201.8	3.6+E10y
Ba	216.1	12.0d
Se	264.6	118d
Hg	279.2	46.8d
Lu	306.9	3.6+E10y
Th	311.9	27.0d
Cr	320.1	27.7d
Ba	496.3	12.0d
Cs	604, 795.8	2.1y
Ni	810.7	71.3d
Tb	879.4, 1177.9	72.1d
Sc	889.2, 1120.5	83.8d
Rb	1076.8	18.7d
Fe	1099.2, 121.6	45.1d
Zn	1115.5	144d
Co	1173.2, 1332.5	5.2y

3.3.1. Distribution of elements in soils

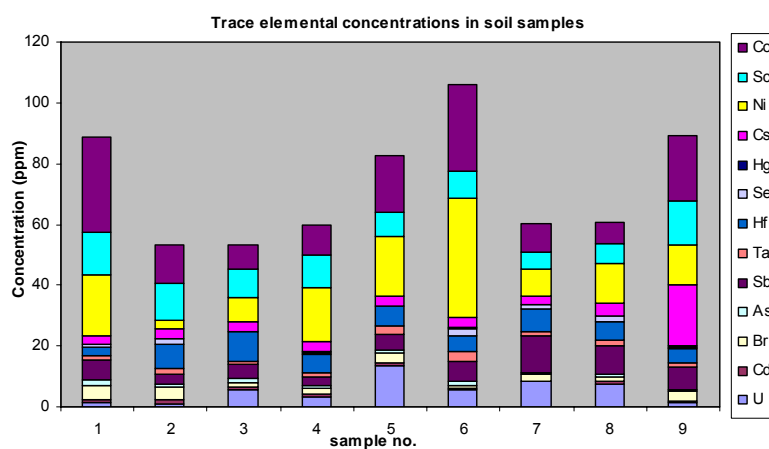
The fig. 42 (a), (b), (c) and (d) show the elemental concentrations in some of the surface soils. The major elements and their oxides, present in soils followed the order $\text{Ca} > \text{Fe} > \text{K}$, Na in general, their concentrations being in percentage levels. The Ca concentrations ranged from 1-9%, Fe concentrations from 1-6%, Na concentrations from 0.02-4% and K concentrations from 0.3-2%. The elemental concentrations indicate the presence of calcite in these soils. Co, Sc, Ni, Th and Rb concentrations were in tens of ppm. Average concentrations of U, Cd, As, Sb, Se, Hg, Cs, Ni, Sc and Co were 5.3 ± 4.1 ppm, 0.7 ± 0.3 ppm, 2.6 ± 1.3 ppm, 1.1 ± 0.4 ppm, 6.4 ± 2.9 ppm, 0.1 ± 0.06 ppm, 2 ± 5.7 ppm, 15.8 ± 10.5 ppm, 9.9 ± 3.2 ppm and 16.3 ± 9.1 ppm, respectively. Average concentrations of Th, Cr, Ba, Cu and Rb were 16.5 ± 3.9 ppm, 242.3 ± 167.2 ppm, 311.1 ± 90.5 ppm, 73.9 ± 44.3 ppm and 88.5 ± 29.8 ppm, respectively. Ce and La ranged from tens to hundreds of ppm. Other REE, except Ce and La had concentrations from sub-ppm to tens of ppm. Average concentrations of La, Ce, Sm, Eu, Tb, Yb and Lu were 37.1 ± 21.5 ppm, 90.6 ± 40.9 ppm, 11.6 ± 8.6 ppm, 1.6 ± 0.5 ppm, 0.7 ± 0.5 ppm, 3.6 ± 1.4 ppm and 0.2 ± 0.2 ppm, respectively.



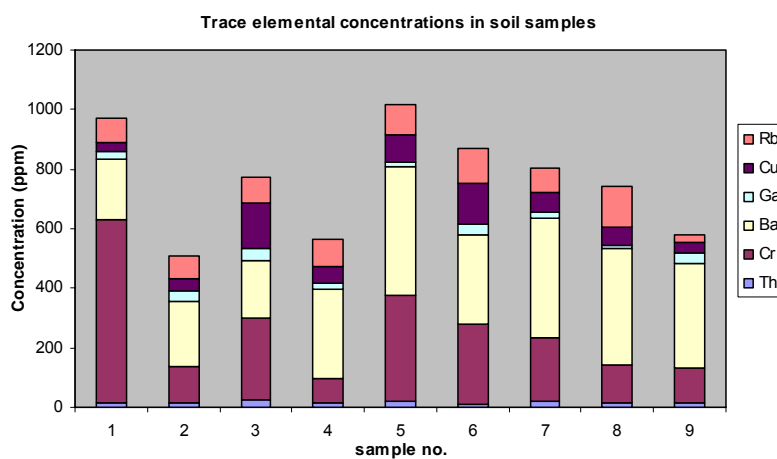
(a)



(b)



(c)



(d)

Fig. 42. Concentrations of (a) Major element oxides and (b) to (d) Trace element in soils

Mass balance calculations

All samples were subdivided and analysed in 12 particle size classes, namely $<36\ \mu\text{m}$, $36\text{--}53\ \mu\text{m}$, $53\text{--}63\ \mu\text{m}$, $63\text{--}75\ \mu\text{m}$, $75\text{--}125\ \mu\text{m}$, $125\text{--}212\ \mu\text{m}$, $212\text{--}300\ \mu\text{m}$, $300\text{--}500\ \mu\text{m}$, $500\text{--}1000\ \mu\text{m}$ and $1000\text{--}2000\ \mu\text{m}$. The mass balance, involving the sum of the weighted concentrations of each element in the various particle size (PS) fractions and the elemental concentration in the whole sample showed a good match, as shown in fig. 43 for soil 4 and fig. 44 for soil 7.

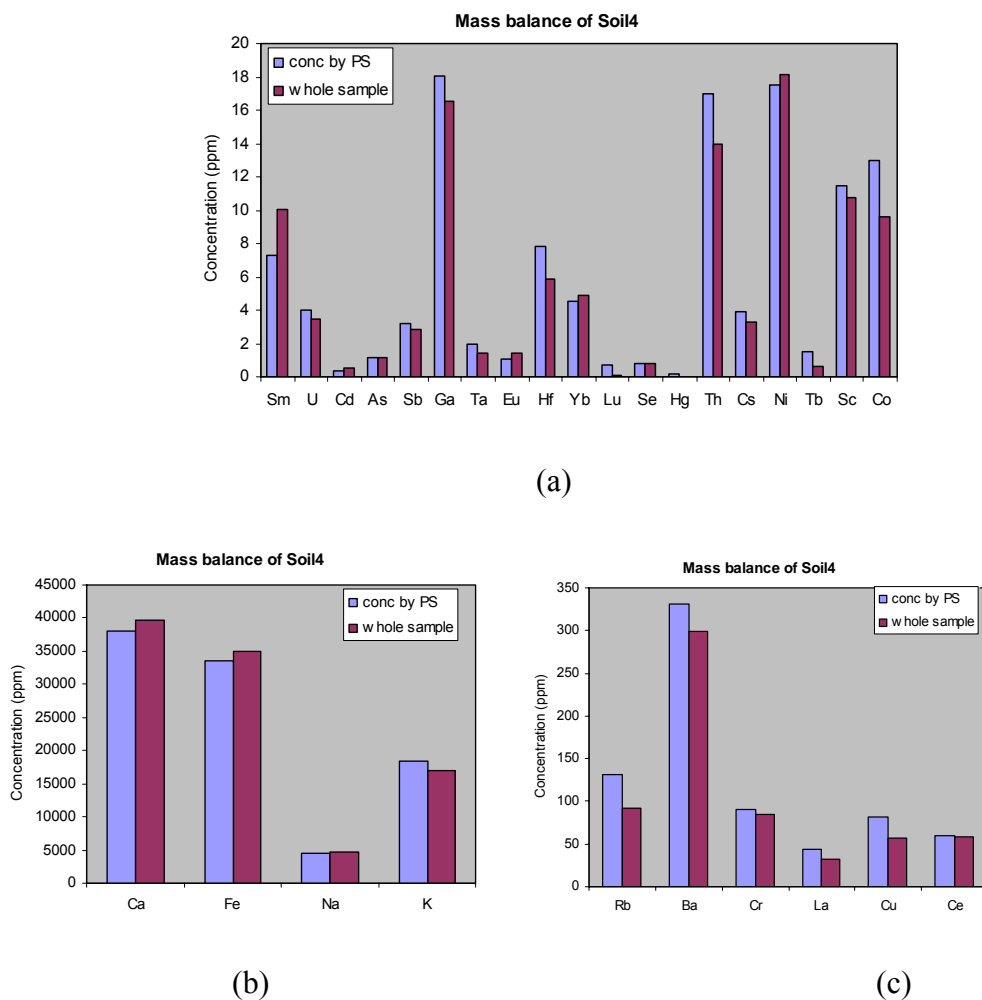


Fig. 43. Mass balance of major and trace elements – soil 4

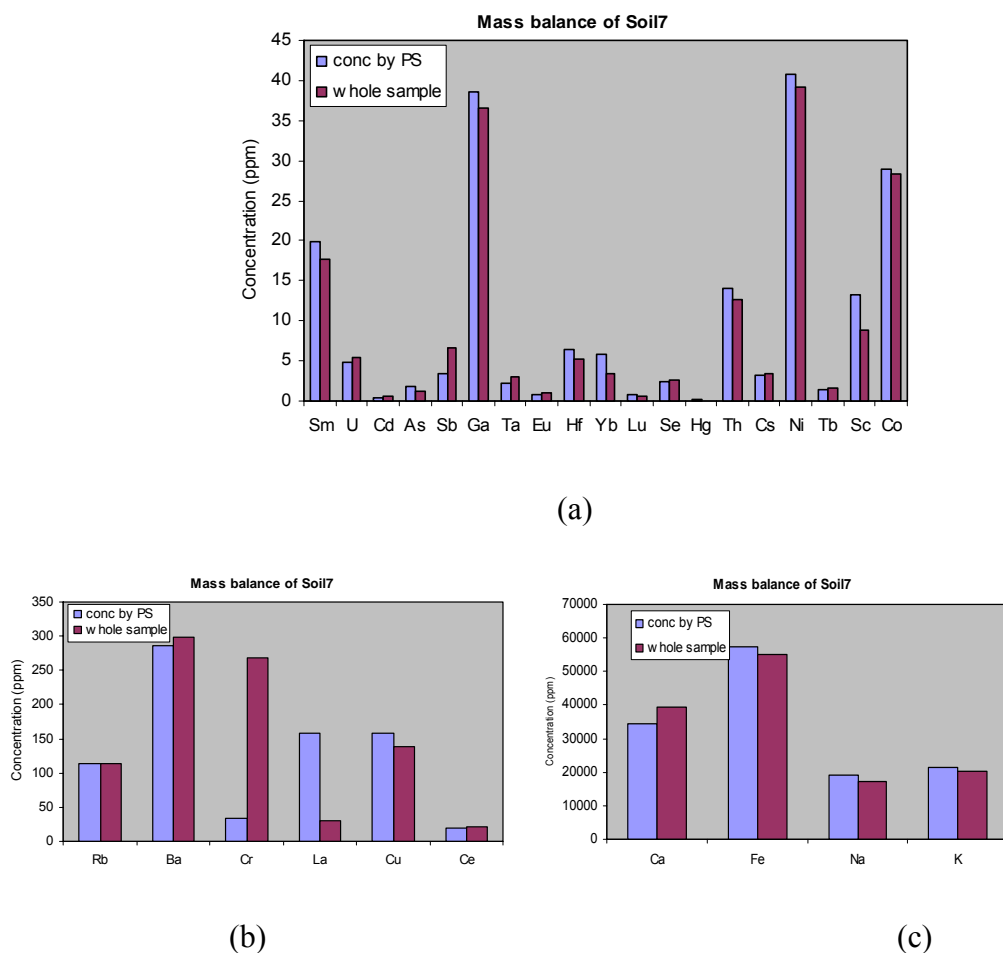


Fig. 44. Mass balance of major and trace elements – soil 7

The contribution of different particle size classes to total element concentrations are shown in fig. 45 for soil 4 and fig. 46 for soil 7 and tables 32 and 33. For soil 4 and soil 7, the contribution from the $<63 \mu\text{m}$ fraction to the total concentration of different elements ranged from 33-90% and 32-80%, respectively. Concentration of most elements were higher in the finer particle sizes ($<75 \mu\text{m}$) for soil 4. Concentration of most elements were higher in the finer particle sizes ($<75 \mu\text{m}$) and 125-150 μm particle size fraction for soil 7.

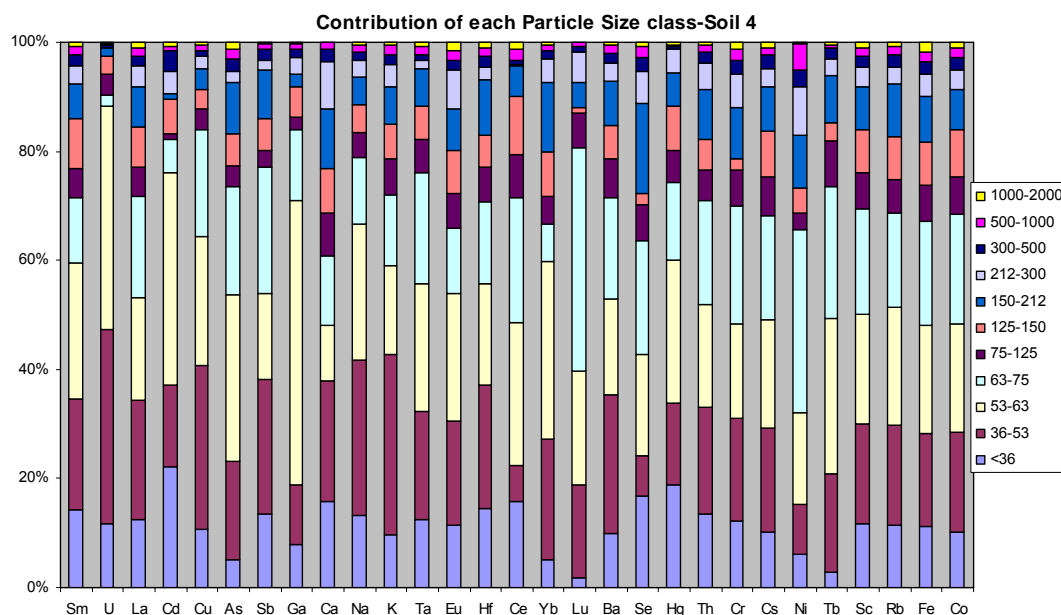


Fig. 45. Contribution of particle sizes towards total elemental concentrations, soil 4

Table 32. Average elemental contribution (%) of particle size fractions, soil 4

Fraction	Average	SD
<36 μm	11.52	4.48
36-53 μm	19.87	6.66
53-63 μm	24.13	10.38
63-75 μm	17.97	7.56
75-125 μm	5.61	1.73
125-150 μm	6.21	2.35
150-212 μm	7.62	3.22
212-300 μm	3.86	2.06
300-500 μm	1.92	0.75
500-1000 μm	1.45	0.81
1000-2000 μm	0.72	0.44

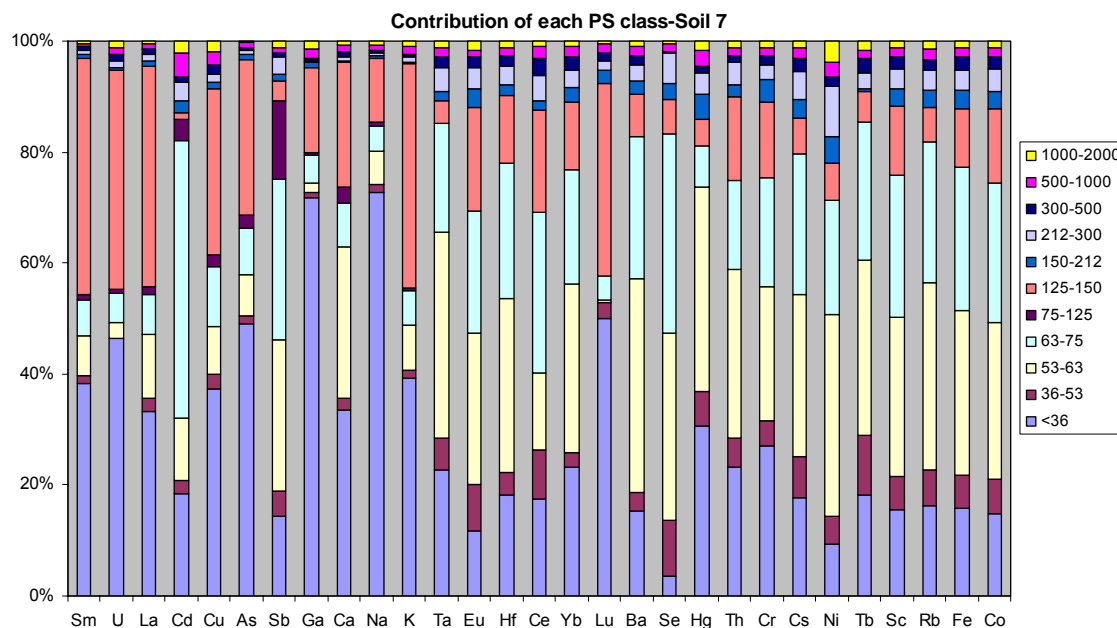


Fig. 46. Contribution of particle sizes towards total elemental concentrations, soil 7

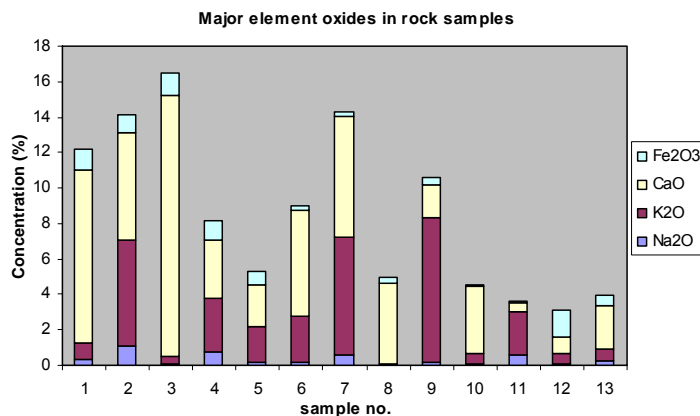
Table 33. Average elemental contribution (%) of particle size fractions, soil 7

Fraction	Average	SD
<36 μm	27.84	17.47
36-53 μm	4.52	2.92
53-63 μm	22.07	12.40
63-75 μm	18.57	9.70
75-125 μm	1.03	2.65
125-150 μm	16.68	12.59
150-212 μm	2.05	1.30
212-300 μm	2.99	1.92
300-500 μm	1.49	0.74
500-1000 μm	1.66	0.53
1000-2000 μm	1.21	0.65

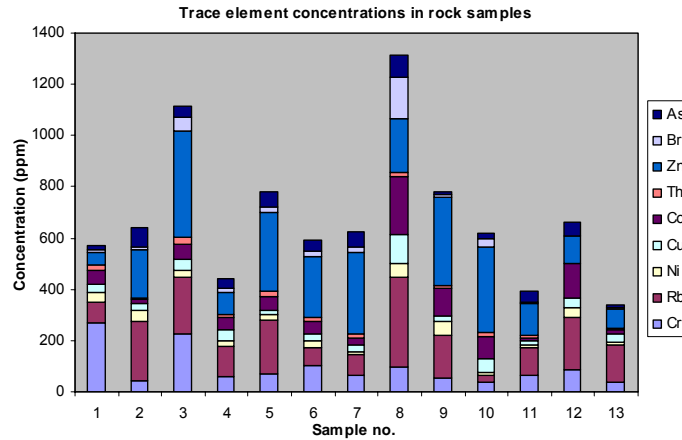
3.3.2. Distribution of elements in host rocks

The fig. 47 shows the elemental concentrations in the metamorphic host rocks.

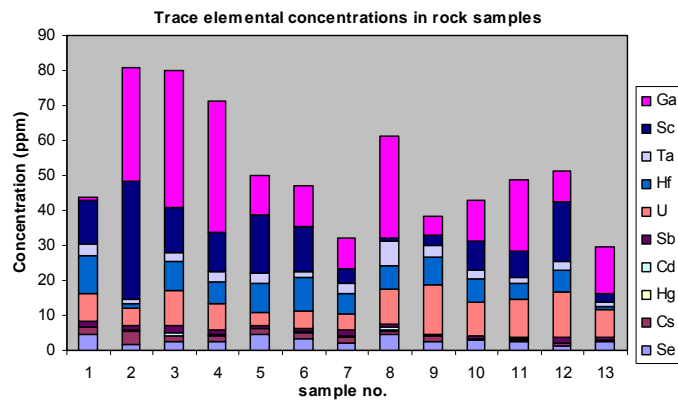
The major elements and their oxides followed the order $\text{Ca} > \text{K} > \text{Fe} > \text{Na}$ in general, their concentrations being in percentage levels. The Ca concentrations ranged from 1-10%, Fe concentrations from 0.2-1.1%, Na concentrations from 0.1-1% and K concentrations from 0.1-7%. Average concentrations of Cr, Rb, Ni, Cu, Co, Th, Zn and As were 93.3 ± 72.2 ppm, 154.7 ± 88.5 ppm, 28.3 ± 14.3 ppm, 37.2 ± 25.9 ppm, 68.9 ± 59.5 ppm, 14.0 ± 8.1 ppm, 215.1 ± 121.1 ppm and 42.0 ± 22.4 ppm, respectively. Average concentrations of Se, Cs, Hg, Cd, Sb, U and Sc were 2.8 ± 1.1 ppm, 1.5 ± 0.9 ppm, 0.1 ± 0.04 ppm, 0.3 ± 0.2 ppm, 1.1 ± 0.6 ppm, 8.4 ± 3.3 ppm and 11.1 ± 8.7 ppm, respectively. Average concentrations of La, Ce, Sm, Eu, Tb, Yb and Lu were 287.6 ± 402.2 ppm, 64.9 ± 55.2 ppm, 5.8 ± 5.2 ppm, 0.7 ± 0.3 ppm, 0.5 ± 0.2 ppm, 2.1 ± 1.6 ppm and 0.8 ± 0.4 ppm, respectively.



(a)



(b)



(c)

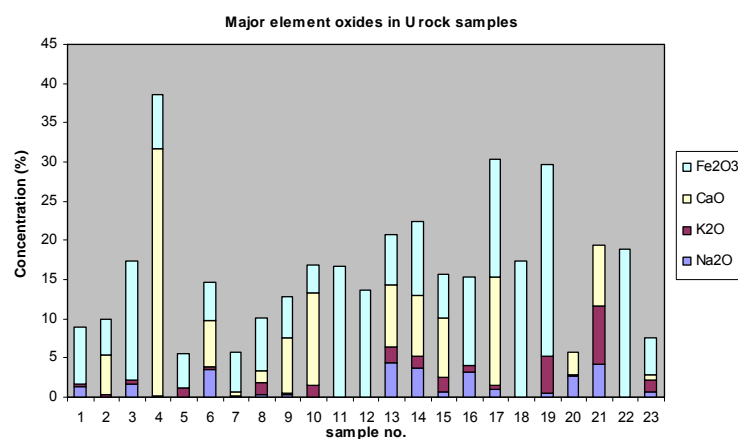
Fig 47. Concentrations of (a) major oxides and (b) and (c) trace elements in host rocks

3.3.3. Distribution of elements in uranium bearing rocks

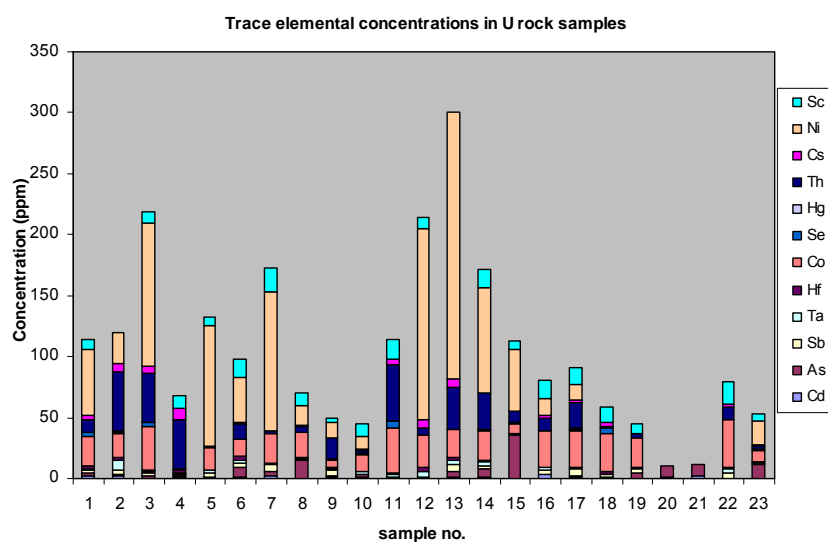
The fig. 48 shows the elemental concentrations in the uranium bearing rocks collected from five underground uranium deposits in the mineralised Singhbhum Thrust Belt.

The major elements and their oxides followed the order $\text{Fe} > \text{Ca} > \text{Na} > \text{K}$ in general, their concentrations being in percentage levels. The Ca concentrations ranged from 0.3-22%, Fe concentrations from 3-18%, Na concentrations from 0.1-3% and K concentrations from 0.1-6%. Average concentrations of Cd, As, Sb, Co, Se, Hg, Cs, Ni and Sc were 1.2

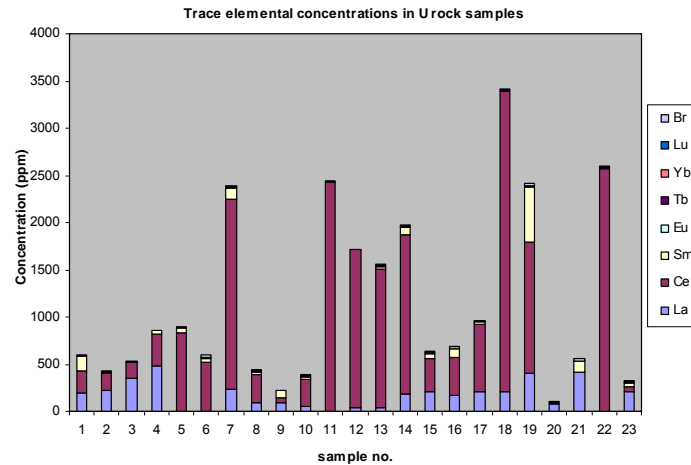
± 0.8 ppm, 6.3 ± 5.1 ppm, 2.9 ± 1.7 ppm,, 23.1 ± 9.6 ppm, 1.9 ± 1.8 ppm, 0.4 ± 0.4 ppm, 3.2 ± 2.6 ppm, 65.1 ± 61.9 ppm and 11.2 ± 4.3 ppm, respectively. Average concentrations of Cr, Ba, Cu and Rb were 260.4 ± 256.9 ppm, 1118.9 ± 987.5 ppm, 263.7 ± 300.9 ppm and 160.6 ± 109.4 ppm, respectively. Average concentrations of La, Ce, Sm, Eu, Tb, Yb and Lu were 203.1 ± 130.9 ppm, 992.9 ± 944.9 ppm, 76.3 ± 66.2 ppm, 1.9 ± 0.7 ppm, 2.7 ± 2.6 ppm, 0.7 ± 0.6 ppm and 7.8 ± 8.7 ppm, respectively.



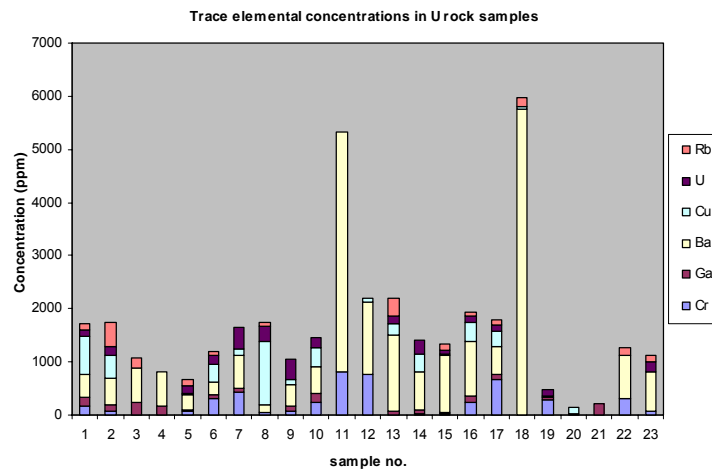
(a)



(b)



(c)



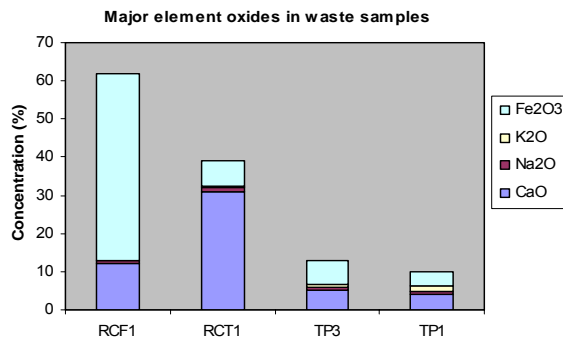
(d)

Fig 48. Concentrations of (a) major oxides and (b), (c) and (d) trace elements in uranium bearing rocks

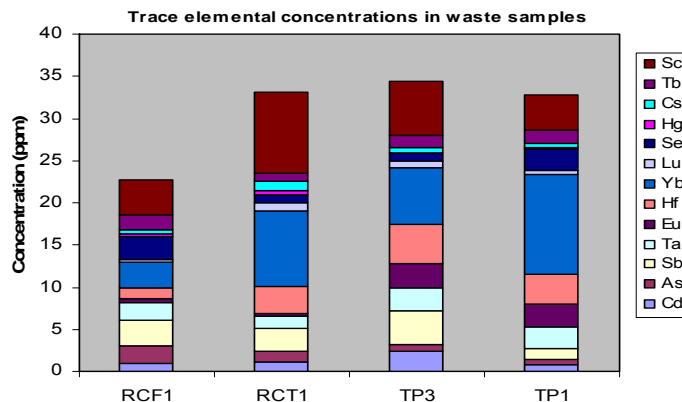
3.3.4. Distribution of elements in wastes

The fig. 49 show the elemental concentrations in the tailings collected from Jaduguda tailings pond and tailings ponds of the Rakha copper mines and clinker ash from the Moubhandar copper smelter.

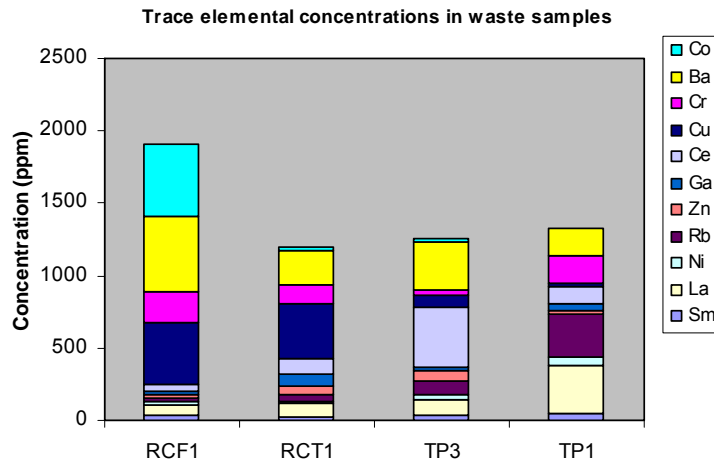
The major elements and their oxides, present in tailings followed the order $\text{Fe} > \text{Ca} > \text{Na} > \text{K}$ in general, their concentrations being in percentage levels. This indicates the pyrite nature of the tailings. The Ca concentrations ranged from 3-22%, Fe concentrations from 3-34%, Na concentrations from 0.6-1% and K concentrations from 0.1-1%. Average concentrations of Cd, As, Sb, Se, Hg, Cs and Sc were 1.3 ± 0.7 ppm, 1.2 ± 0.7 ppm, 2.8 ± 1.2 ppm, 1.8 ± 1.0 ppm, 0.2 ± 0.2 ppm, 0.6 ± 0.2 ppm and 6.1 ± 2.6 ppm, respectively.



(a)



(b)



(c)

Fig 49. Concentrations of (a) major oxides and (b) and (c) trace elements in waste samples

Average concentrations of Ni, Rb, Zn, Cu, Cr, Ba and Co were 32.7 ± 19.1 ppm, 113.2 ± 102.6 ppm, 47.3 ± 27.6 ppm, 170.0 ± 167.4 ppm, 143.3 ± 76.6 ppm, 318.9 ± 143.7 ppm and 136.9 ± 124.2 ppm, respectively. Average concentrations of La, Ce, Sm, Eu, Tb, Yb and Lu were 148.6 ± 121.9 ppm, 170.0 ± 167.4 ppm, 38.7 ± 9.9 ppm, 1.6 ± 1.4 ppm, 1.4 ± 0.3 ppm, 7.7 ± 3.8 ppm and 0.7 ± 0.3 ppm, respectively.

Mass balance calculations

All samples were subdivided and analysed in 5 particle size classes, namely $<36 \mu\text{m}$, $36-53 \mu\text{m}$, $53-63 \mu\text{m}$, $63-75 \mu\text{m}$ and $75-125 \mu\text{m}$. The mass balance, involving the sum of the weighted concentrations of each element in the various particle size (PS) fractions and the elemental concentration in the whole sample showed a good match, as shown in fig. 50 for uranium tailings.

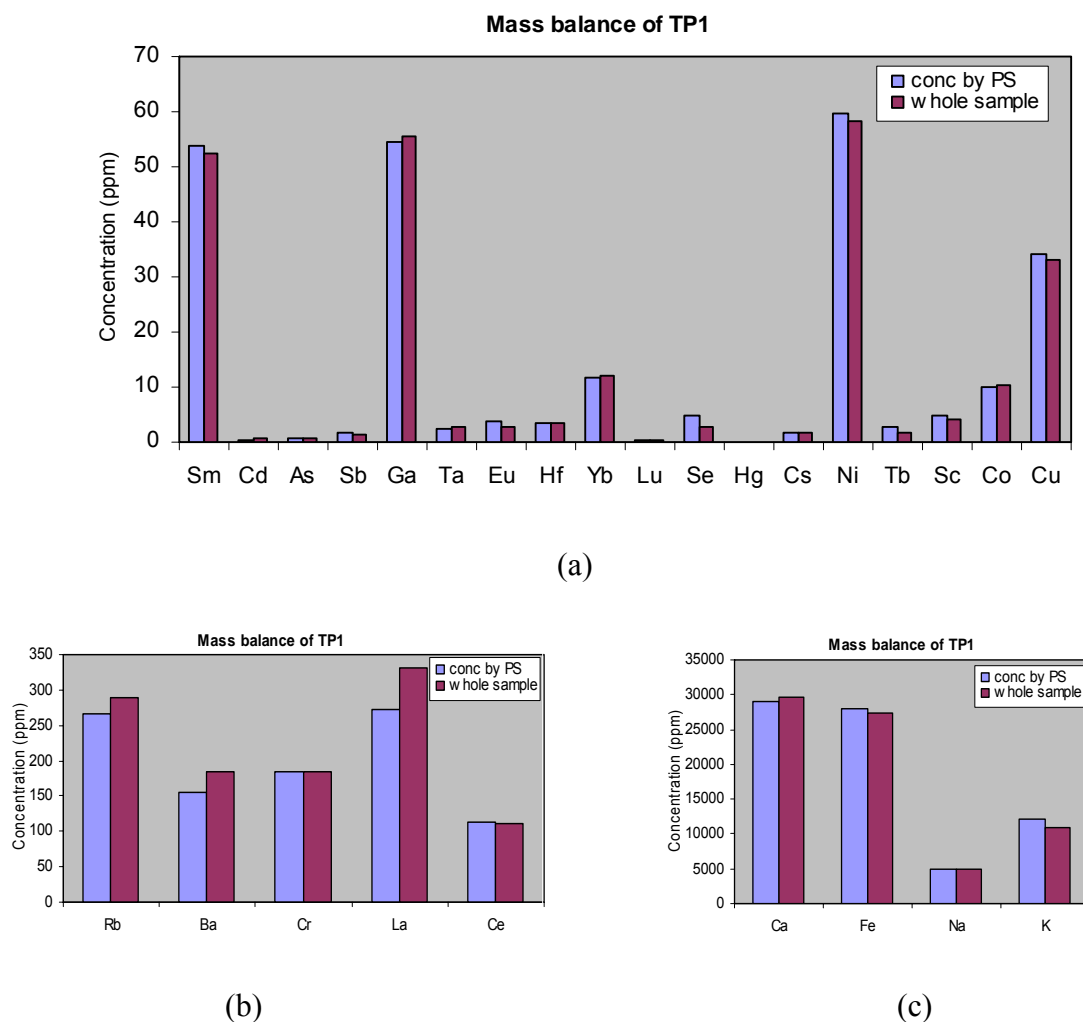


Fig. 50. Mass balance of major and trace elements – uranium tailings

The contribution of different particle size classes are shown in fig. 51 and table 34. The contribution from the $<63 \mu\text{m}$ fraction to the total concentration of different elements ranged from 20-90%. Concentration of most elements were higher in the finer particle sizes for TP.

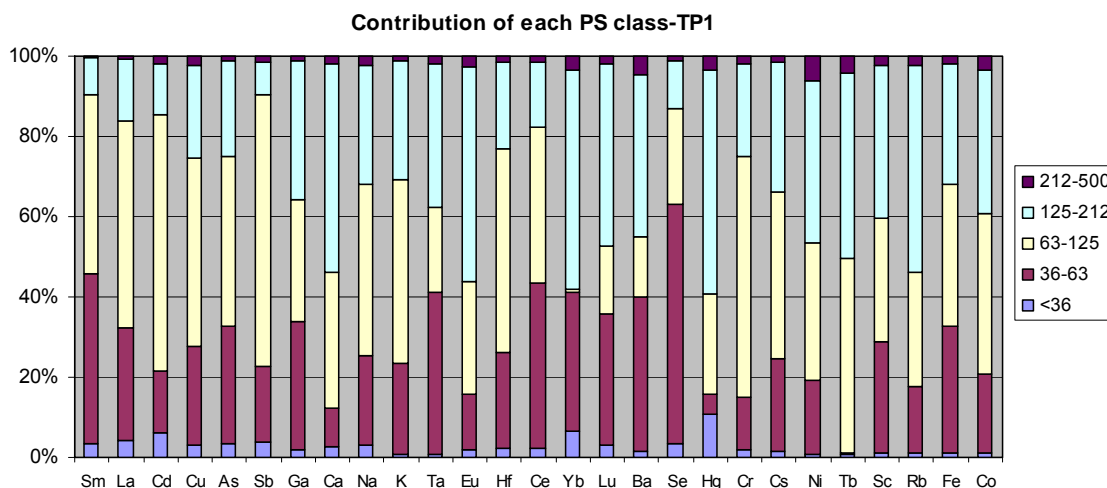


Fig. 51. Contribution of particle size fractions towards total elemental concentrations, TP

Table 34. Average weighted elemental contribution (%) of particle size fractions, TP

Fraction	Average	SD
<36 μm	2.75	2.21
36-53 μm	23.99	12.88
53-63 μm	37.37	15.85
63-75 μm	30.95	14.91
75-125 μm	2.37	1.28

3.4. Leaching experiments

It is important to devise robust chemical methods to predict the persistence and potential mobility of radionuclide and heavy metal contamination and also to quantify the fraction of soil contamination available for plant uptake. Such information is important for predictive models and environmental assessments where the soil–plant pathway is a key contributor to potentially harmful effects to plants and animals. Because the leaching process is very complex, no one single leaching test or single set of leaching conditions is appropriate for a wide variety of leach testing objectives and applications [86]. For this

reason, several leaching tests have been developed in order to try to evaluate the different leaching parameters and conditions being tested.

Kinetic aspects of leaching processes

Any leaching (dissolution) process comprises of three main stages [84, 103]. The first stage is approach of the leachant to the solid surface through either molecular diffusion or convection. In the second stage, chemical reactions at the solid-liquid interface take place, and at the third stage, the ions or molecules of the sample being dissolved are withdrawn to the solution bulk. If the whole process rate is limited by the rate of the first or third stage, the course of the process is governed by the laws of diffusion kinetics. If the second stage is the rate-limiting stage, the process follows the laws of chemical kinetics. Some processes obey mixed kinetics [84].

In external diffusion (external mass transfer) the mass transfer is limited by the rate of diffusion through a liquid layer: a mobile solution layer with a concentration nearly equal to the saturation concentration is formed near the surface of the sample, and the reagent and the solutes diffuse through this solution, the diffusion determining the rate of the whole process. The internal diffusion (internal mass transfer) controls the process rate if either leaching from cracks (pores) or transport of the dissolved substance and the reagent through the formed shell of the solid reaction product is the slowest stage. When the process is governed by internal diffusion, the rate of leaching does not depend on the flow rate of the liquid with respect to the dissolved sample but depends appreciably on the sample porosity; the rate is directly proportional to the reagent concentration. The rate of dissolution and leaching of minerals and other solids is determined, in most cases, by the rate of diffusion [105]. The dissolution (and leaching) rate decreases according to a

logarithmic law following an increase in the solute concentration (c) in the liquid phase [105] and, taking into account the heterogeneous mass transfer, it is expressed by the kinetic equation [185]:

$$dc/dt = k_0 * D * S (c_{eq} - c) / (V * d) \quad (13)$$

where, dc/dt is the rate of variation of the solute concentration in the solution bulk, k_0 is the rate constant for leaching, D is the diffusion coefficient of the compound being dissolved, S is the surface area being dissolved, c_{eq} is the saturation concentration, V is the solution volume, d is the diffusion layer thickness. In the general case, k_0 depends on the physical and chemical properties of reacting species, the design of the leaching device and the reaction mass flow rates. Under stationary experimental conditions,

$$dc/dt = k (c_{eq} - c) \quad (14)$$

the kinetic constant k is directly proportional to the diffusion coefficient and inversely proportional to the thickness of the diffusion layer. In the dissolution of powders (ground solids), the observed reaction rate differs from the true rate at the interface [103]. In this case, the rate of dissolution is affected by a change in the reaction surface, which is either decreased or increased during leaching. The results will be correct only provided that the surface is equally accessible, which is possible only in rare cases. Thus, the results of studies of leaching kinetics of elements from soils and sediments under usual batch extraction conditions are somewhat arbitrary. Nevertheless, the obtained data are important for the understanding of processes of possible mobilisation of elements upon changes in the environmental conditions. In some cases, kinetic curves also provide knowledge about the mobilities of the recovered elemental forms [84].

3.4.1. Methodology of semi-dynamic and dynamic leaching experiments

Extremely important elements of leaching can be determined by a laboratory leaching method. A short term (short equilibration time) leaching test, dynamic in nature, can help in determining the mass of element easily mobilised. Comparisons of the bulk concentrations of elements in the leached solid, with the leachate concentrations are useful in estimating the mobilisation of various elements with respect to time. The evolution of leachate concentrations can be determined with multi-equilibration time long-term leaching experiments, both dynamic and semi-dynamic in nature. Semi-dynamic tests simulate the slow and long-term environmental processes.

Semi-dynamic leaching experiments are called so because the leachant is replaced after different intervals of static leaching. The method followed in this thesis is similar to the ANS16.1 leaching experiment used to study the release of contaminants/elements from samples [99]. Such methods are actually equilibrium experiments that are good simulations of the environmental conditions. Samples were kept in semi-dynamic condition in contact with two different solvents (distilled water and 0.1N NaNO₃) over a time period of 142 days. The experiments were carried out at room temperature (22-25°C). A solid:liquid ratio of 1:20 was maintained throughout the experiment to minimize any change in the composition of leachant and also to provide adequate concentration of extracted species for analysis. If the solid mass to extractant volume ratio is kept very low, for example 1:5, there is a possibility of radionuclide and heavy metal re-adsorption and in such cases the solid-extractant equilibrium condition may not be attained [85]. Water and NaNO₃ are weak extractants that leach out the soluble and exchangeable/weakly bound fraction of uranium respectively, present in the samples

[107, 110]. The soluble and weakly bound phases are the elemental fractions that are most easily leached from a matrix by the slow leaching processes. Leachant was sampled out at time intervals of 2, 4, 8, 16, 33, 36, 54, 68, 102 and 142 days of static leaching and replaced with fresh solvent. The extractant was separated from the solid matrix by filtration through 0.22 μ m membrane filter. The use of water as a leachant is to let the waste matrix be a dominant factor in determining the pH of the leachate, a scenario similar to the ambient environmental conditions. This is similar to the ASTM test, DIN 38414 S4 batch test of Germany and the AFNOR X 31-210 batch test of France generally employed for waste matrices [113].

The dynamic leaching/extraction method involved shaking a known mass of soil (a few grams) with an extractant for a predefined period of time on a horizontal shaker at a speed of 80-100 rpm. All experiments were conducted at ambient temperature (22-25°C), except where the temperature was the variable parameter to study the effect on leaching. Such procedures are essentially equilibrium processes. Different solid: liquid ratios have been used in leaching experiments conducted worldwide. A ratio of 1: 25 has been proposed for nutrients, 1:10 for radionuclides and 1:8 for heavy metals [116-119]. However, a solid: liquid ratio of 1: 20 was maintained throughout the experiments conducted in this thesis. Water was used for the experiments as the leachant, for reasons as discussed earlier. Contact time of the dynamic experiments varied from 50 to nearly 100 h, depending on the time required to reach equilibrium. Leachant was sampled out at regular time intervals and replaced with fresh solvent.

3.4.2. Variation of different physical conditions

The goal of equilibrium batch testing was to represent constituent solubility and release of uranium over a range of conditions by varying a physical parameter/condition of leaching (e.g., pH, particle size). The sampled matrices, like soils, tailings etc. were in contact with the leaching solution and the physical variables included: contact time, pH of the leachant solution, temperature and particle size of the material.

- Contact time was varied from 2 days to 142 days in the case of semi-dynamic leaching tests and from 2h to nearly 100 h for the dynamic leaching tests.
- The samples were subjected to dynamic batch leaching with water as solvent under acidic (pH3), neutral (pH 7) and basic pH (pH10) conditions.
- Particle sizes of the samples subjected to dynamic leaching were 36-63 μm , 63-125 μm , 125-212 μm , 212-500 μm , 500-1000 μm and 1000-2000 μm for soils and <36 μm , 36-63 μm , 63-125 μm , 125-212 μm and 212-500 μm for uranium tailings.
- The dynamic leaching tests were carried out under ambient temperature (25°C) and at an elevated temperature of 60°C.

The effect of variation of these parameters on uranium leaching from different matrices was observed.

3.4.3. Variations in uranium concentrations

Uranium concentrations in the leachant solution were measured through Laser Fluorimetry technique.

Semi-dynamic leaching tests

In semi-dynamic leaching experiments, the concentrations of uranium being leached out, using water as leachant, varied from 0.5-1.6ppb, 0.2-0.9ppb and 0.3-2.7ppb for uranium

tailings, copper klinker ash and copper tailings samples, respectively, as shown in fig. 52. below.

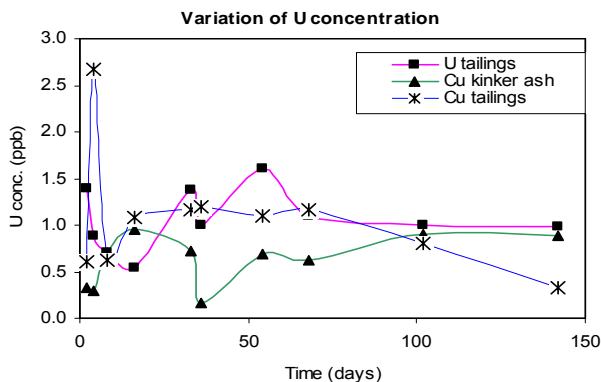


Fig. 52. Evolution of uranium concentrations in semi-dynamic leaching, using water

The concentrations of uranium being leached out, using 0.1N NaNO_3 as leachant, was slightly higher and varied from 0.2-2.9ppb, 0.1-2.2ppb and 0.5-4.7ppb for uranium tailings, copper clinker ash and copper tailings samples, respectively as shown in fig 53. These higher concentrations of uranium leached out using 0.1N NaNO_3 are due to leaching of the exchangeable fraction of apart from the water-soluble fraction by this solvent.

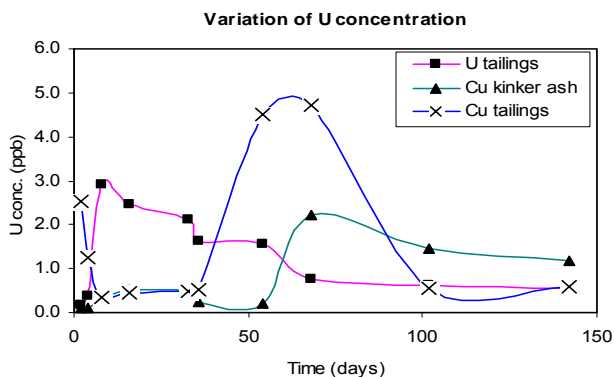


Fig. 53. Evolution of uranium concentrations in semi-dynamic leaching, 0.1N NaNO_3

The concentrations of uranium being leached out from uranium bearing rocks were substantially higher than for all other samples. The concentrations ranged from 2.24-

29.67ppb using water and 4.2-90.8ppb using 0.1N NaNO_3 as leachant as shown in Fig.

54.

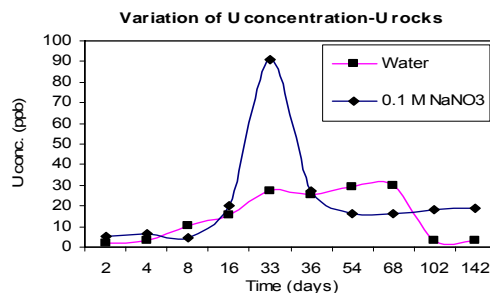


Fig. 54. Evolution of uranium concentrations in semi-dynamic leaching tests

From the figures it can be observed that for most of the samples, uranium concentrations were either constant or showed a reduction towards the end of the leaching period.

Dynamic leaching tests

In dynamic leaching tests different physical conditions of dynamic leaching were varied and the effect on leaching of uranium was observed.

Effect of pH of leachant

The variation in pH from neutral-acidic-basic showed pronounced effects on the uranium concentrations leached out from different matrices. Under neutral pH conditions the uranium concentrations in the leachant (water) ranged from 0.96-9.35ppb, 0.1-9.57ppb, 1.12-15.65ppb and 3.26-23.69ppb for Soil 1, 4, 7 and 11, respectively, as shown in fig. 55.

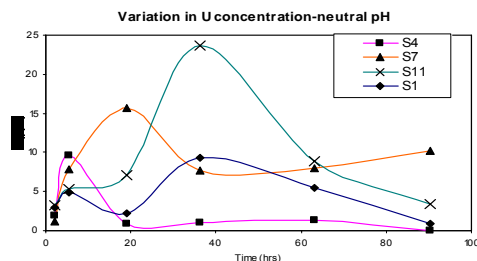


Fig. 55. Evolution of uranium concentrations in dynamic leaching tests-neutral pH

Under acidic pH conditions the uranium concentrations in the leachant (water) ranged from 1.05-87.9ppb, 1.05-8.73ppb, 2.29-64.81ppb and 1.95-24.72ppb for Soil 1, 4, 7 and 11, respectively, as shown in fig. 56.

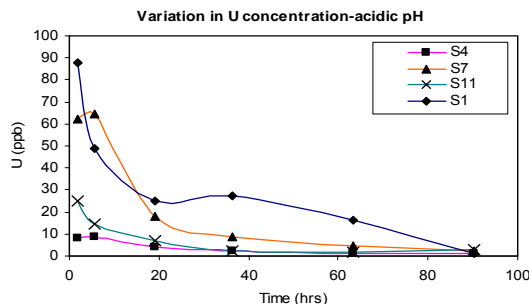


Fig. 56. Evolution of uranium concentrations in dynamic leaching tests-acidic pH

Under basic pH conditions the uranium concentrations in the leachant (water) were highest for most samples and ranged from 4.68-148.28ppb, 6.24-65.78ppb, 32.91-58.49ppb and 4.09-197.25ppb for Soil 1, 4, 7 and 11, respectively, as shown in fig. 57.

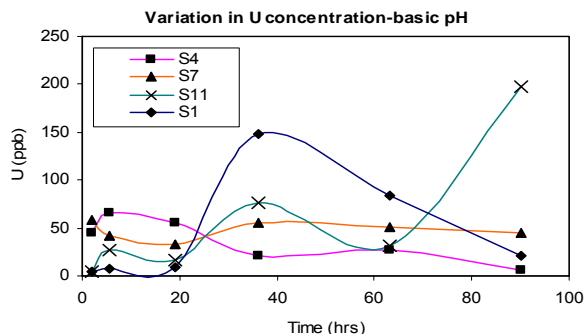


Fig. 57. Evolution of uranium concentrations in dynamic leaching tests-basic pH

The variation in pH from neutral-acidic-basic showed pronounced effects on the uranium concentrations leached out from waste matrices as well. Fig. 58 shows the evolution of uranium concentration for uranium tailings. For TP1 (Fig. 58 a) the uranium concentrations in the leachant (water) ranged from 0.42-6.58ppb, 15.80-195.04ppb and 0.22-2.44ppb under neutral, acidic and basic pH conditions, respectively. For TP3 (Fig.

58 b) the uranium concentrations in the leachant (water) ranged from 0.12-82.58ppb, 0.55-207.67ppb and 0.17-24.62ppb under neutral, acidic and basic pH conditions, respectively.

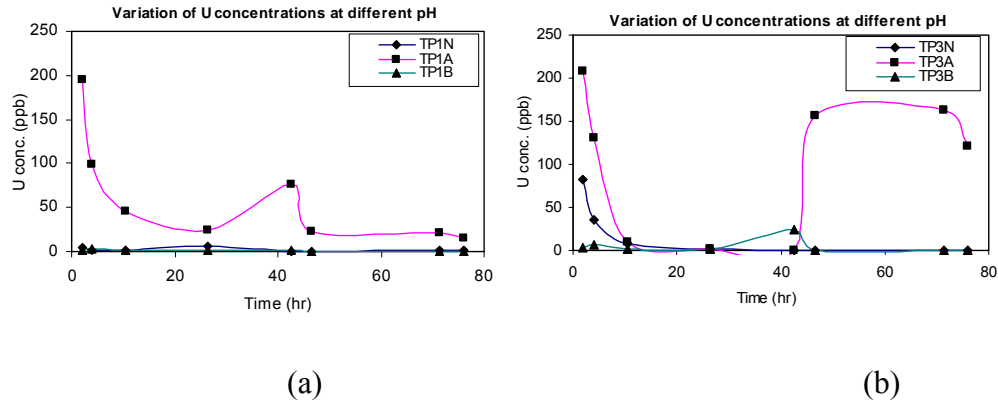


Fig. 58. Evolution of uranium concentrations at different pH (a) TP1 and (b)TP3

Fig. 59 shows the evolution of uranium concentration for wastes from the copper industry. For copper tailings (Fig. 59 a) the uranium concentrations in the leachant (water) ranged from 0.62-71.30ppb, 0.51-672.65ppb and 1.06-181.22ppb under neutral, acidic and basic pH conditions, respectively. For copper clinker ash (Fig. 59 b) the uranium concentrations in the leachant (water) ranged from 0.31-7.99ppb, 4.17-33.84ppb and 0.1-5.63ppb under neutral, acidic and basic pH conditions, respectively.

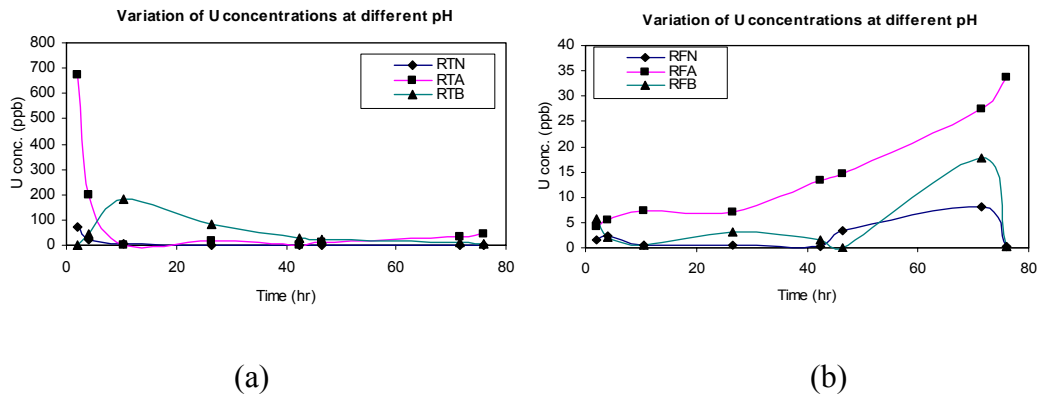


Fig. 59. Evolution of uranium concentrations at different pH (a) copper tailings and (b) copper clinker ash

In all the cases it was observed that highest uranium concentrations were leached from the waste matrices under acidic conditions. This is due to the pyrite nature of the waste forms.

Effect of particle size of sample

Particle sizes of the samples subjected to dynamic leaching were 36-63 μm , 63-125 μm , 125-212 μm , 212-500 μm , 500-1000 μm and 1000-2000 μm for soils. Fig. 60 shows the evolution of uranium concentrations with time for different particle sizes of soil 1, 4, 7 and 11. The uranium concentrations in soil 1 varied from 0.27-9.62ppb, 0.08-5.34ppb, 0.07-5.06ppb, 0.01-3.00ppb, and 0.17-3.53 and 0.12-7.23 ppb for 36-63 μm , 63-125 μm , 125-212 μm , 212-500 μm , 500-1000 μm and 1000-2000 μm , respectively. For soil 4 uranium concentrations varied from 0.54-0.77ppb, 0.33-1.88ppb, 0.29-1.19ppb, 0.23-1.01ppb, 0.28-0.87ppb and 0.27-1.88ppb for 36-63 μm , 63-125 μm , 125-212 μm , 212-500 μm , 500-1000 μm and 1000-2000 μm , respectively. For soil 7 uranium concentrations varied from 0.26-10.55ppb, 0.13-6.20ppb, 0.27-8.30ppb, 0.05-4.14ppb, 0.12-5.63ppb and 0.11-3.42ppb for 36-63 μm , 63-125 μm , 125-212 μm , 212-500 μm , 500-1000 μm and 1000-2000 μm , respectively. For soil 11 uranium concentrations varied from 0.08-2.98ppb, 0.20-1.12ppb, 0.12-0.80ppb, 0.27-0.68ppb, 0.33-2.10ppb and 0.13-1.75ppb for 36-63 μm , 63-125 μm , 125-212 μm , 212-500 μm , 500-1000 μm and 1000-2000 μm , respectively. It can be observed from the figures that the evolution of uranium concentrations follow nearly the same trend in all particle size fractions of a given sample. From the figures it can be observed that for most of the samples, uranium concentrations were either constant or showed a reduction towards the end of the leaching period. Uranium concentrations were generally observed to be higher in the smaller particle size classes.

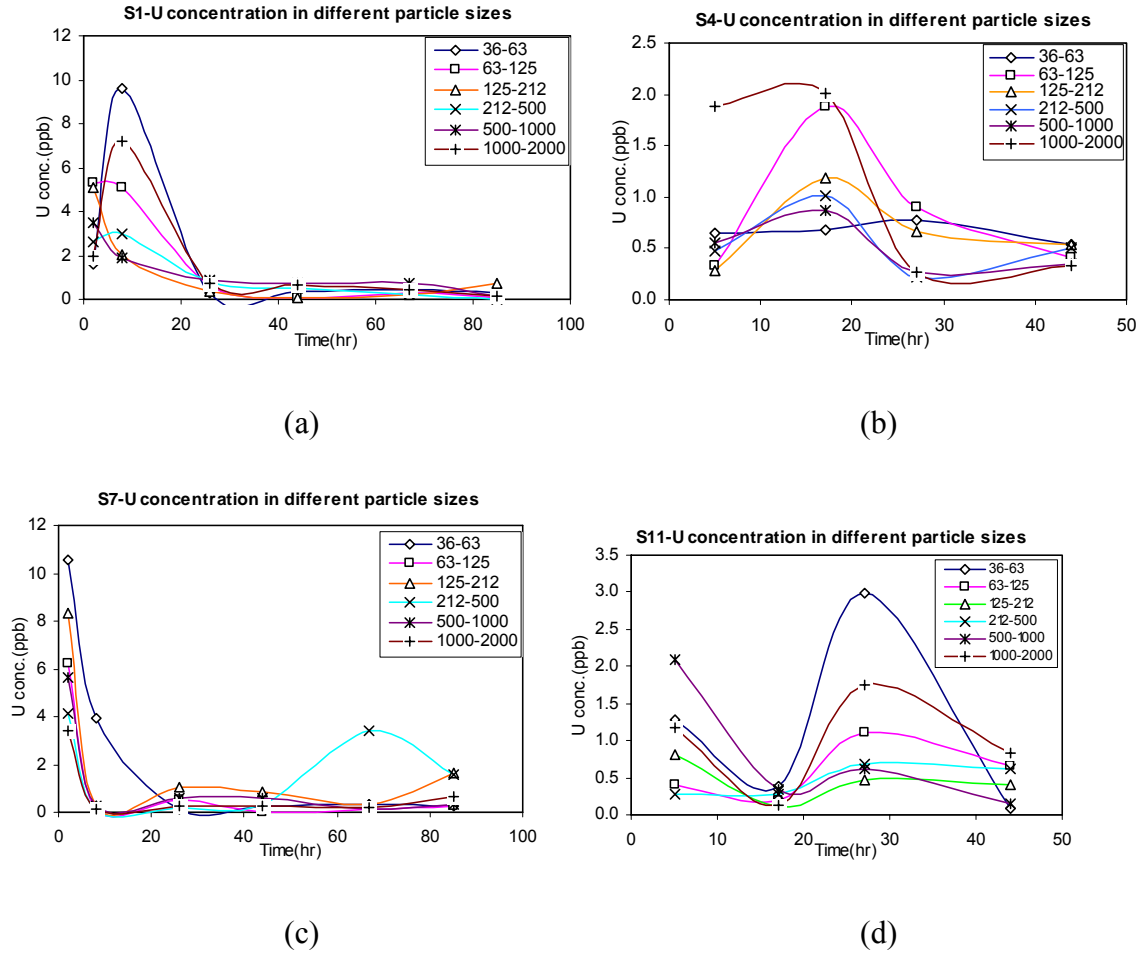


Fig. 60. Evolution of uranium concentrations for different particle sizes (a) soil 1, (b) soil 4, (c) soil 7 and (d) soil 11

Particle sizes of the uranium tailings subjected to dynamic leaching were $<36\ \mu\text{m}$, $36\text{--}63\ \mu\text{m}$, $63\text{--}125\ \mu\text{m}$, $125\text{--}212\ \mu\text{m}$ and $212\text{--}500\ \mu\text{m}$. For tailings, uranium concentrations in leachate varied from 0.88–3.42 ppb, 0.38–6.74 ppb, 0.76–2.87 ppb, 0.53–6.47 ppb, 0.40–4.72 ppb and $<36\ \mu\text{m}$, $36\text{--}63\ \mu\text{m}$, $63\text{--}125\ \mu\text{m}$, $125\text{--}212\ \mu\text{m}$ and $212\text{--}500\ \mu\text{m}$. From Fig. 61 below it can be observed that uranium concentrations in leachate showed a reduction towards the end of the leaching period.

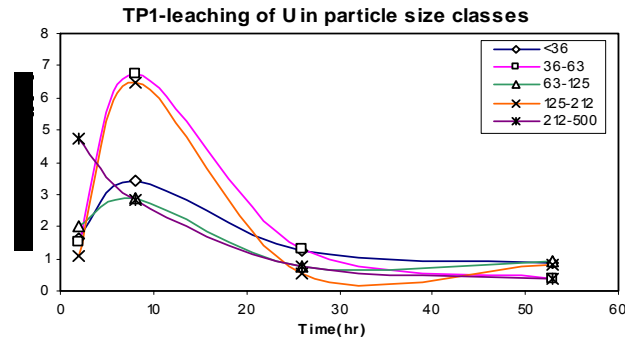


Fig. 61. Evolution of uranium concentrations for different particle sizes in uranium tailings

Effect of temperature

The variation of temperature showed an increase in the uranium concentrations leached out from different matrices. Fig. 62 (a) and (b) depict the same for soil samples. For soil 1 the uranium concentrations in leachate varied from 0.16-17.49 ppb and 0.7-39.55ppb for 25°C and 60°C, respectively. For soil 11 the uranium concentrations in leachate varied from 0.34-3.80 ppb and 0.12-8.99ppb for 25°C and 60°C, respectively.

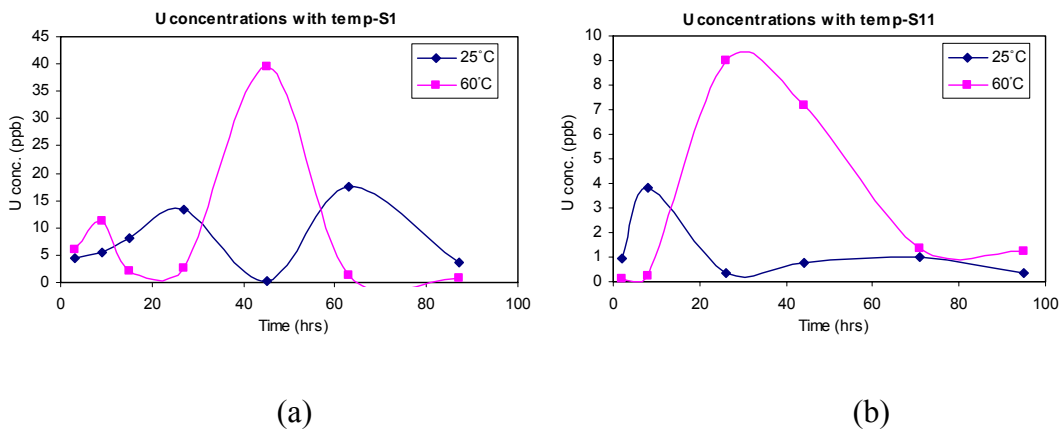


Fig. 62. Evolution of uranium concentrations at different temperatures in (a) soil 1 and (b) soil 11

Fig. 63 (a), (b), (c) and (d) depict the effect of temperature on uranium leaching from TP1, TP3, copper tailings and copper clinker ash, respectively. For TP 1 the uranium

concentrations in leachate varied from 0.27-4.90 ppb and 0.53-11.21ppb for 25°C and 60°C, respectively. For TP 3 the uranium concentrations in leachate varied from 0.46-6.22 ppb and 0.85-20.26ppb for 25°C and 60°C, respectively. For copper tailings the uranium concentrations in leachate varied from 0.38-18.15ppb and 0.14-24.64ppb for 25°C and 60°C, respectively. For copper clinker ash the uranium concentrations in leachate varied from 0.46-2.36 ppb and 0.99-24.84ppb for 25°C and 60°C, respectively.

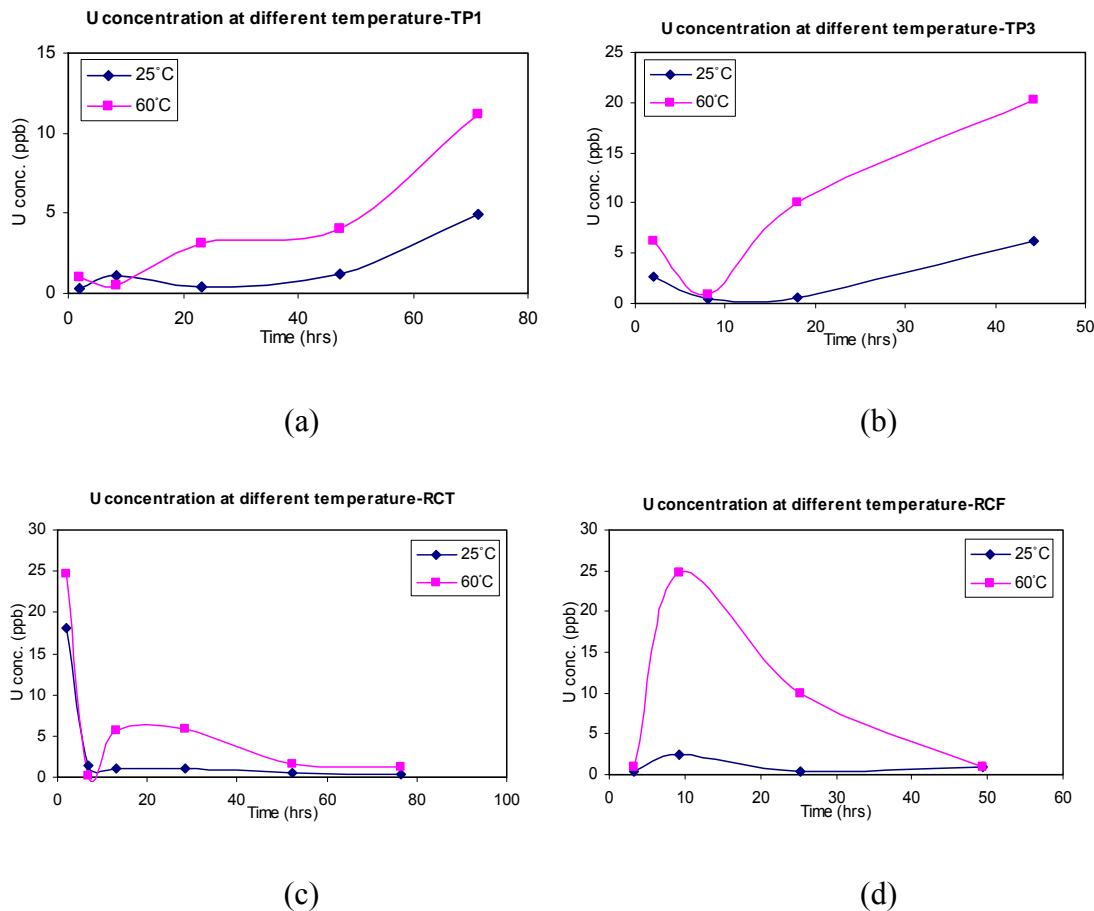


Fig. 63. Evolution of uranium concentrations at different temperatures in (a) TP 1, (b) TP3, (c) copper tailings and (d) copper clinker ash

In general, the leached uranium concentrations were observed to first increase and then gradually decrease with time, apart from the uranium tailings samples, which showed an

increase in leached uranium concentrations with time. The enhancement of leached uranium concentrations with increasing temperature is due to increase in the rate of leaching.

CHAPTER 4

RESULTS AND DISCUSSIONS

Scope

Distribution of elemental concentrations gives us an idea of elemental mobility in a region. It is more clearly understood with the help of activity ratios of radionuclide daughter-parent pairs. In case of secular radioactive equilibrium of daughter-parent, the activity ratio is equal to one. This secular equilibrium condition may be disturbed due to a number of geochemical processes. Elemental mobility can also be studied by laboratory based leaching experiments. Effect of different physical parameters governing leaching and the associated leaching rate gives an idea of leachability of an element. Again, the physicochemical properties of the matrix and other elemental concentrations are important factors governing the concentrations of an element in a matrix.

Activity ratios, elemental correlations and leaching rates have been discussed in this chapter. The elemental concentrations observed in this study have also been compared with other studies carried out worldwide.

4.1. Activity and activity ratios of uranium and thorium series radionuclides

Naturally occurring radioactive elements are present in every compartment of the environment in widely varying concentrations. The radioactivity in an environmental matrix like soil, rock etc. is mainly dependent on the geology of the area. The parent rocks are responsible for the radioactivity in soils originating from them. Different regions are characterised by varying levels of natural radioactivity due to their geological setting.

When the activity ratios (ARs) of geochemically important daughter/ parent are equal to unity, it indicates that the system has achieved equilibrium [47]. It has been observed since a long time that many geological settings do not behave as closed systems for the

radionuclides of the natural radioactive series and are amenable to certain geological processes that can induce radioactive disequilibrium [40]. Radioactive disequilibrium arises in the natural radioactive series due to recent fractionation events (continuous or instantaneous processes) which lead to the loss or gain of radionuclides that are mobile in the ambient environmental conditions. Certain isotopic ratios, mainly of the long-lived radionuclides in the natural radioactive series, are generally used to assess the state of radioactive disequilibrium [47, 186-188]. In closed geological formations, radioactive disequilibria can persist only up to 5 half-lives of the daughter where the parent, of the parent–daughter pair, has a much longer half life than the daughter. For example, ^{238}U - ^{234}U - ^{230}Th radionuclides attain radioactive equilibrium in 1.7 Ma [189]. The observation of a $^{234}\text{U}/^{238}\text{U}$ AR that is less than or greater than 1 indicates that an isotope of uranium has migrated within the rock in the last 1-2 million years; the time required for ^{234}U to reach its equilibrium activity with ^{238}U [48]. Other daughter/parent ARs can be used to detect radionuclide migration over shorter time-scales, such as $^{230}\text{Th}/^{238}\text{U}$ (300,000 years; the time required for ^{230}Th to reach its equilibrium activity if $^{234}\text{U}/^{238}\text{U}$ activity ratio is 1) and $^{226}\text{Ra}/^{230}\text{Th}$ (8,000 years; the time required for ^{226}Ra to reach its equilibrium activity with ^{230}Th). The $^{231}\text{Pa}/^{235}\text{U}$, $^{227}\text{Ac}/^{231}\text{Pa}$ ARs of the ^{235}U series radionuclides can also be used to study the migration and retention of radionuclides in groundwaters [49].

4.1.1. Soils

Any soil will have concentration of natural radionuclides determined by their concentration in the parent material from which the soils originate and also by the physico-chemical phenomena associated with its weathering.

The average activity concentrations of 72.8 ± 48.0 Bq/kg, 65.1 ± 22.7 Bq/kg and 522 ± 201.8 Bq/kg for ^{238}U , ^{232}Th and ^{226}Ra , respectively, in soils from this region are in general higher than the worldwide average activity concentrations [4] of 35, 30 and 400 Bq/kg for ^{238}U , ^{232}Th and ^{226}Ra respectively. The presence of vein/disseminated type uranium mineralisation in this region is the main factor for marginally elevated levels of natural radioactivity in the soils. The ^{238}U and ^{232}Th activities in soils from the present study were compared with studies carried out worldwide in Table 35. The radionuclide activities from the present study are comparable with those from granite environments in Botswana and near a uranium mineralisation zone in China and also with soils in varied geological settings (granites, gneisses, biotite-chlorite schist etc.) in Poland. Some of the other studies by Kam et al. [190], Colmenero Sujo et al. [191], Al-Jundi [192] and Fernandes et al. [193] reveal similar radionuclide concentrations as observed in the soil of Singhbhum Thrust belt, in this thesis. Soils from shear zones in Anatolian fault systems, as reported by Baykara and Doğru [194], were found to have higher ^{232}Th concentrations than the present study. The tin mining area near Jos Plateau in Nigeria has much higher radionuclide concentrations than the present study as reported by Arogunjo et al. [195]. Higher radionuclide activity concentrations have also been reported by Oyedele et al. [196] in soils from Western Namibia. Colmenero Sujo et al. [191] reported ^{238}U values slightly higher than the present study in areas near uranium mining locations in Aldama, Mexico. The radionuclide concentrations reported in Gudalore, Punjab, Lambapur (hosting uranium deposits) and Rajasthan, in India, are similar to those found in this thesis. The radionuclide concentrations reported in Orissa and Meghalaya are higher due to the former being a high background radiation area and the latter hosting surface

uranium deposits. Such variation in concentrations is mainly due to the regional geology of the area.

Table 35. ^{238}U and ^{232}Th activity concentrations in soil samples from worldwide studies

Region	^{238}U (Bq/kg)	^{232}Th (Bq/kg)	References
Sudetes, Poland	40.7-49.8 (^{226}Ra)	42.9-51.9 (^{228}Ac)	[197]
Xiazhuang, China	112	54.6	[198]
Metsemaswaane- Kanye section, Bostwana	48.7 ± 19.4 (^{226}Ra)	59.1 ± 21.5	[199]
Anatolian Fault System, Turkey	12.4-251.1	3.3-195.5	[194]
Nigeria	66-8700	53-16800	[195]
Aldama, Mexico	44.6-460.5	41.9-77.0	[191]
Amman, Jordan	56.4	28.8	[200]
Karak, Jordan	228.9	27.2	[200]
Istanbul, Turkey	21	37	[201]
Costal area, Aegean Sea, Greece	93 ± 47	71 ± 25	[202]
Taiwan	30	44	[203]
Canary Islands	44	54	[204]
Spain	13-165	7-204	[205]
Italy	57-71	73-87	[206]
Spain	20.3-711	13.2-84.4	[207]
Russaifa, Jordan	48.3-523.2	8.7-27.1	[192]
Brazil	68.7 ± 45.0	87.7 ± 10.8	[193]
Bimurra, Australia	45.1-89.8	-	[209]
Newcastle, Australia	26.6-160.3	-	[209]

Western Namibia, South Africa	54.9-1752	70.5-1866	[196]
Batman, Turkey	35 ± 8	25 ± 10	[209]
Canakkale, Turkey	94.55	110.4	[190]
Belgrade, Serbia	31.1 ± 9.02	38.2 ± 11.6	[210]
Kirklareli, Turkey	28 ± 13	40 ± 18	[211]
Kestanol, Turkey	115	192	[212]
Gudalore, India	37.7 ± 10.1	75.3 ± 44.1	[213]
Rajasthan, India	30-78	43-106	[214]
Orissa, India	350 ± 20	2825 ± 50	[215]
Orissa, India	408	1868	[216]
Punjab, India	18.4-53.1	57.3-148.3	[217]
Meghalaya, India	335.3	283.9	[218]
Lambapur, India	25-291	32-311	[219]
Upper Siwaliks and Punjab, India	28.3 ± 0.5	81.0 ± 1.7	[220]
Singhbhum Shear Zone, India	50.7-109.1	28.7-89.8	Present study

Activity Ratios (AR) computed for the soil samples are shown in fig. 64. An uncertainty value of 10% has been considered due to sampling and counting errors around the equilibrium activity ratio of 1. The $^{226}\text{Ra}/^{238}\text{U}$ ARs are deviant from unity in most of the samples. The AR values greater than one indicate a preferential retention or enrichment of ^{226}Ra as compared to ^{238}U . This can be explained by the contrasting properties of the two radionuclides. Uranium remains in the +6 oxidation state in oxidizing environments

and is soluble. In oxidizing environments ^{226}Ra associates with minerals like Fe hydroxides and becomes immobile. If secondary U minerals are present in oxidised environments Ra may also leach out from these minerals, although some Ra is adsorbed onto Fe-hydroxides [38]. Since top soils can be considered to be open systems, the conditions there may be oxidizing, leading to uranium mobility and/or radium retention. The ARs less than 1 indicate a preferential leaching of Ra with respect to uranium from the surface soils. Hence these soils are acting as open environments from where radium and uranium mobility is observed and hence radioactive equilibrium condition between the isotopes of the ^{238}U series is disturbed. The $^{208}\text{Tl}/^{228}\text{Ac}$ ARs in soil samples are close to 1, indicating near equilibrium condition between these isotopes of the ^{232}Th series.

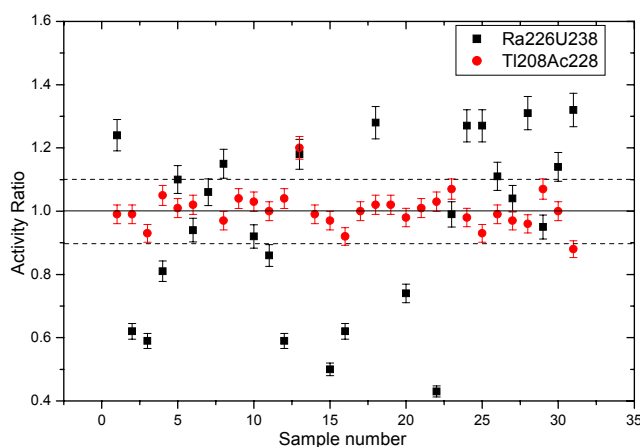
The $^{235}\text{U}/^{238}\text{U}$ activity ratio ideally has the value of 0.04658. In the soils of this mineralised region most $^{235}\text{U}/^{238}\text{U}$ AR values were observed to be close to the ideal value. This data also acts as a quality check for the gamma ray spectrometric system used for the measurements. Due to the low activity concentrations of ^{235}U , its daughter products were below the Minimum Detection Limit in some of the samples.

The $^{234\text{m}}\text{Pa}/^{238}\text{U}$ AR is comparable to 1 in all the soil samples as evident from fig. 64. This shows that $^{234\text{m}}\text{Pa}$ can also be used for ^{238}U estimation in top soils apart from ^{234}Th . But these values are associated with high standard deviations, which is a major limitation associated with the use of 1001.03 keV of $^{234\text{m}}\text{Pa}$ for ^{238}U estimation in soil samples. The $^{227}\text{Th}/^{235}\text{U}$ ARs are greater than 1 in most of the samples. This can be explained by preferential removal of ^{235}U . Due to the long $t_{1/2}$ of ^{231}Pa and ^{227}Ac , of which ^{227}Th is a daughter, it has not moved with ^{235}U , leading to a higher AR value. Again, Th is not

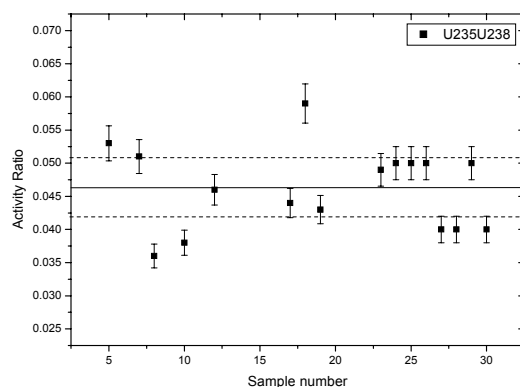
mobile in environmental conditions like U and may have been retained in the soil samples at the point of collection. This may also lead to a higher AR value.

Arogunjo et al. [195] have reported activity concentration values for uranium series radionuclides indicating disequilibrium in soils of the tin mining area near Jos Plateau in Nigeria. $^{226}\text{Ra}/^{238}\text{U}$ values are seen to vary from 0.48 – 0.73. Malczewski et al. [197] have reported activity concentration values in different geological environments in Sudetes, Poland that indicate disequilibrium in thorium series radionuclides. The $^{208}\text{Tl}/^{228}\text{Ac}$ and $^{212}\text{Pb}/^{208}\text{Tl}$ ARs in soil samples varied from 0.32 – 0.39 and 2.20 – 2.64 respectively in areas with granites, gneisses, biotite chlorite schists and schists in contact with gneisses, as reported by them. Rezzoug et al. [221] have suggested uranium as well as thorium mobilisation during the weathering processes by measuring activity and isotopic ratio profiles of ^{230}Th , ^{232}Th , ^{234}U and ^{238}U . Measurements of ^{238}U and ^{226}Ra in 445 soil samples collected from areas throughout Australia show that these soils have a mean activity ratio ($^{238}\text{U}/^{226}\text{Ra}$) of 1.09 ± 0.5 . There is a wide spread in individual values but, overall, more soils are U-rich than Ra-rich [208]. $^{234}\text{U}/^{238}\text{U}$ has been observed to vary from 0.9-1.2 in soil fractions from the vicinity of a former uranium mine in Slovenia [222]. $^{226}\text{Ra}/^{238}\text{U}$ AR of 0.5–9 was exhibited by an upland organic soil in Co. Donegal, Ireland. Radiochemical speciation of ^{226}Ra , ^{238}U and ^{228}Ra indicated that in this organic soil the high $^{226}\text{Ra}/^{238}\text{U}$ ratio was due to loss of ^{238}U relative to ^{226}Ra via oxidation and mobilisation of ^{238}U in the upper layers of the soil and subsequent loss in solution [223]. Fernandes et al. [193] reported equilibrium ($^{238}\text{U}/^{226}\text{Ra}$ ratio of 1.05 ± 0.17) in soils from a uranium mining site in Brazil. ^{228}Ra and ^{232}Th were in close equilibrium with an average $^{228}\text{Ra}/^{232}\text{Th}$ ratio of 0.92 ± 0.14 . Blanco et al. [224] reported $^{226}\text{Ra}/^{238}\text{U}$ activity

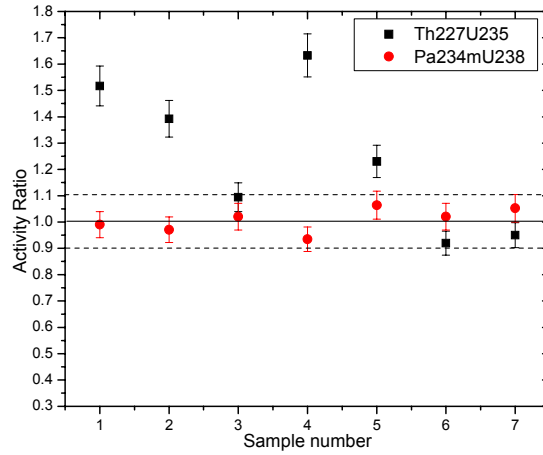
ratio in soil to be equal to 1.20 for the same area. It has been suggested by Ivanovich and Harmon [40] that the disequilibrium between Ra and U isotopes may be due to four factors: (1) precipitation/dissolution reactions; (2) alpha recoil; (3) diffusion; and (4) Szilard-Chalmers effect. Dowdall and O'Dea [223] report that ^{238}U loss in organic soils in Donegal, Ireland, may be primarily due to the oxidation of organic material within the soil.



(a)



(b)



(c)

Fig. 64. The (a) $^{226}\text{Ra}/^{238}\text{U}$ and $^{208}\text{Tl}/^{228}\text{Ac}$, (b) $^{235}\text{U}/^{238}\text{U}$ and (c) $^{234\text{m}}\text{Pa}/^{238}\text{U}$ and $^{227}\text{Th}/^{235}\text{U}$ activity ratios in some soils

4.1.2. Host rocks

Silicic igneous rocks like granites are considered to be important sources of uranium mobilisation as they contain higher uranium and thorium content, are associated with uranium deposits and also contain significant amounts of labile uranium [40]. In the Singhbhum Shear Zone uranium mineralisation has occurred in metamorphic host rocks, which are of Arachean/ Precambrian age. These host rocks have average activity concentrations of ^{238}U , ^{226}Ra and ^{232}Th as 107.8 ± 37.0 Bq/kg, 108.2 ± 38.2 Bq/kg and 59.8 ± 25.7 Bq/kg, respectively. The radionuclide concentrations of host rocks in this thesis have been compared with similar studies carried out worldwide, in Table 36. These values are higher than ^{238}U activity concentrations reported in rock samples from Ghana by Yeboah et al. [225] and sedimentary deposits in Australia [226], but are similar to concentrations in granitic rocks as observed from other studies in Table 36. This was due to the regional geology and moreover due to the fact that sedimentary rocks have lesser

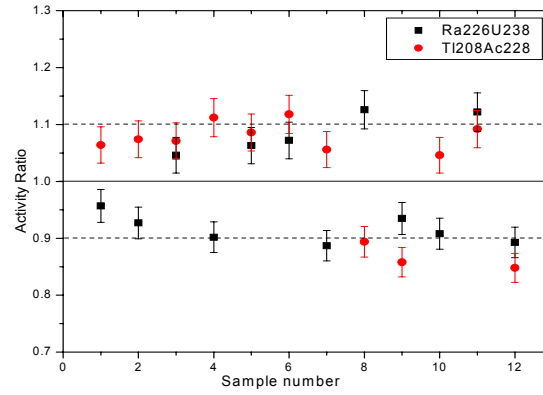
radionuclide concentrations. Granitic rocks from Orissa [216] have much higher radionuclide concentrations due to the samples belonging to a high background radiation area.

Table 36. ^{238}U and ^{232}Th activity concentrations in rock samples from other studies

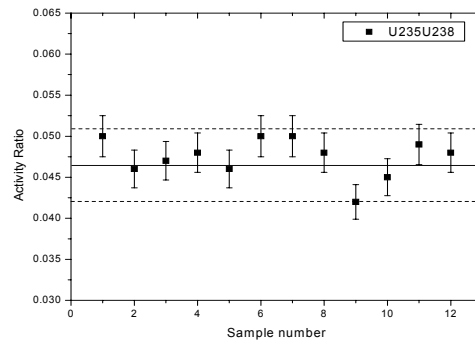
Region, rock type	^{238}U (Bq/kg)	^{232}Th (Bq/kg)	References
Scandenevia, Granites and gneisses	20-130	20-80	[46, 52]
Spain, hydrothermally altered granites	312-538	40.2-41.1	[227]
Spain, hydrothermally weathered granites	166-1305	30.9-52.1	[227]
Ghana, Metamorphic rocks	0.7-15.1	0.5-111.8	[225]
Ghana, Igneous rocks	12.1-40.0	35.7-117.5	[225]
Ghana, Sedimentary rocks	1.0-1.4	2.9-3.7	[225]
Australia, Sedimentary deposits	7.6-18.5	10.8-39.5	[226]
Orissa, Granitic rocks	3865	7012	[216]
Singhbhum, Metamorphic host rocks	107.8 ± 37.0	59.8 ± 25.7	Present study

Activity Ratios (AR) computed for the host rock samples are shown in fig. 65. An uncertainty value of 10% has been considered due to sampling and counting errors around the equilibrium activity ratio of 1. The $^{226}\text{Ra}/^{238}\text{U}$ and $^{208}\text{Tl}/^{232}\text{Th}$ ARs are in near equilibrium condition for most of the samples. The $^{235}\text{U}/^{238}\text{U}$ activity ratio ideally has the value of 0.04658. In the host rocks of this mineralised region most $^{235}\text{U}/^{238}\text{U}$ AR values were observe to be close to the ideal value. These results show that equilibrium condition

prevails in these rock samples and they are not behaving as open systems for elemental exchange.



(a)



(b)

Fig 65. The (a) $^{226}\text{Ra}/^{238}\text{U}$ and $^{208}\text{Tl}/^{228}\text{Ac}$ and (b) $^{235}\text{U}/^{238}\text{U}$ activity ratios in soils Åkerblom et al. [46], Åkerblom [52] have reported radioactive equilibrium between ^{238}U and ^{226}Ra and also within the ^{232}Th series in the Nordic bedrock. Ibraheim [53] has observed disequilibrium between ^{226}Ra and ^{238}U , in favour of ^{238}U , using $^{238}\text{U}/^{226}\text{Ra}$ activity ratio for different rock types in Wadi Wizr desert, Egypt. El-Dine [47] has also observed disequilibrium between the daughters of the ^{238}U series for rock samples from the North Eastern desert, Egypt. In a fissured granitic environment $^{234}\text{U}/^{238}\text{U}$ ratio of 0.96-1.20 and $^{230}\text{Th}/^{234}\text{U}$ ratio of 0.85-1.04 (hydrothermally altered granite) and $^{234}\text{U}/^{238}\text{U}$

ratio of 0.98-1.13 and $^{230}\text{Th}/^{234}\text{U}$ ratio of 0.98-1.24 (hydrothermally altered granite) was observed by Perez Del Villar et al. [227]. Laboratory experiments by Andersen and co-workers support the $^{234}\text{U}/^{238}\text{U}$ disequilibria due to ^{234}U removal by alpha recoil [228]. Studies by Pekala et al. [229] also point to a limited redistribution of U in rock samples.

4.1.3. Uranium bearing rocks

Since the Singhbhum Shear Zone/Singhbhum Thrust Belt is a highly mineralised zone; the mineralised rock samples from this area have high radionuclide concentrations in them. The ^{238}U activity concentrations observed from the samples analysed in this thesis are compared with other studies carried out in the same region, in table 37. It can be observed that the activity concentration values are comparable.

Table 37. ^{238}U activity concentrations in rock samples compared with other studies

Region, rock type	^{238}U (Bq/kg)	References
Singhbhum, India	265-35528	[139]
Mosabani, Narwapahar and Jaduguda, Singhbhum, India	37-52064	[140]
Mosabani and Jaduguda, Singhbhum, India	1737-168510	[141]
Surda- Rakha mines, Singhbhum, India	135-4573	[142]
Jaduguda, Singhbhum, India	122-40559	[127]
Bhatin, Singhbhum, India	4126 ± 1887	Present study
Narwapahar, Singhbhum, India	3837 ± 949	Present study
Jaduguda, Singhbhum, India	6756 ± 2996	Present study
Turamdih, Singhbhum, India	3089 ± 215	Present study

The activity concentrations of radionuclides when plotted with respect to the depth in the deposits showed some variation, as evident in fig. 66, but no clear trend was observed. This variation in concentration can be attributed to the inherent heterogeneity in the distribution of radioactivity in the rocks of the uranium deposits.

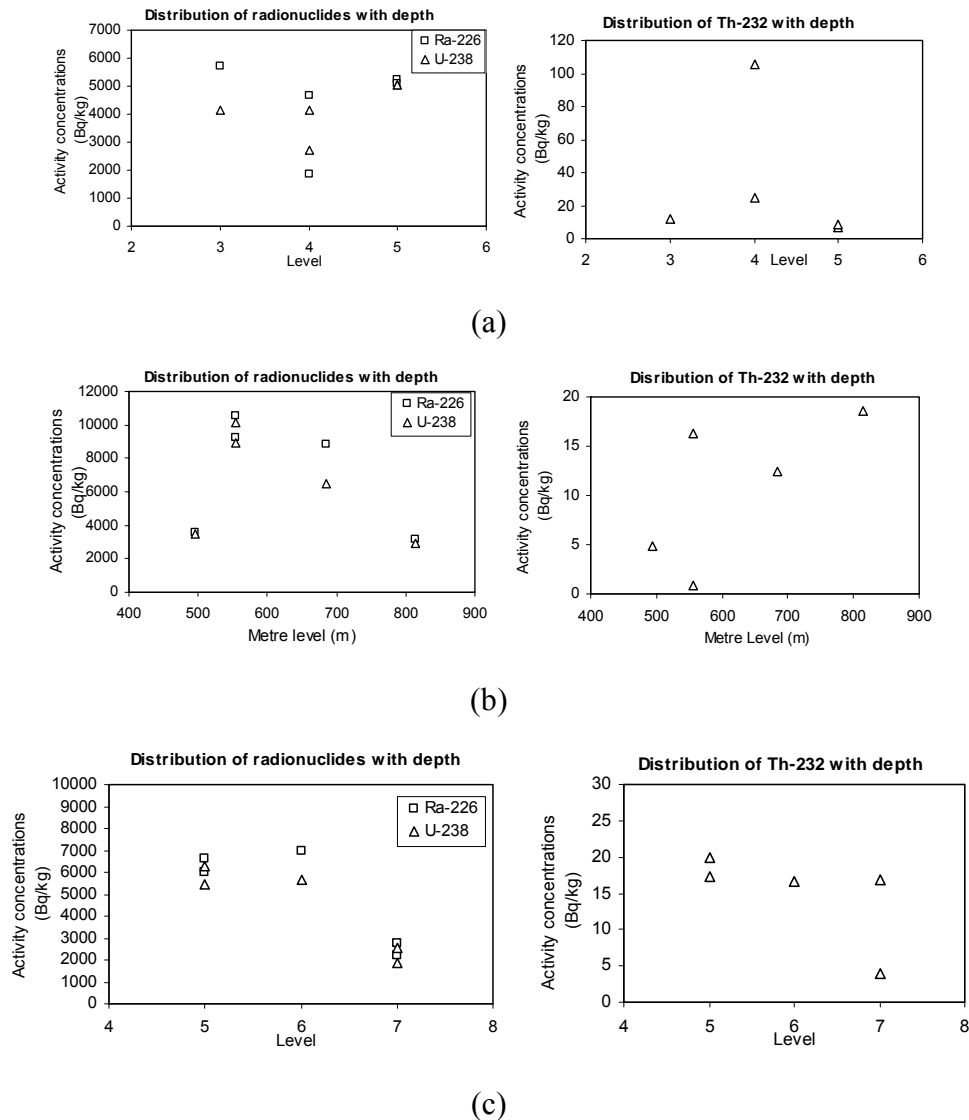


Fig. 66. Distribution of radionuclides with mine depth in (a) Narwapahar, (b) Jaduguda and (c) Bhatin deposits

Since the uranium deposits in the Singhbhum Shear Zone are of the Arachean/Precambrian age they are considerably older than 1.7 Ma and hence they can be considered to be in secular equilibrium. The measurement of $^{226}\text{Ra}/^{238}\text{U}$, $^{226}\text{Ra}/^{210}\text{Pb}$,

$^{230}\text{Th}/^{238}\text{U}$, $^{234}\text{U}/^{238}\text{U}$, $^{226}\text{Ra}/^{230}\text{Th}$, $^{228}\text{Th}/^{228}\text{Ra}$, $^{231}\text{Pa}/^{235}\text{U}$ and $^{227}\text{Ac}/^{235}\text{U}$ ARs were used to understand the migration of different radionuclides in the deposits.

^{238}U series

The $^{226}\text{Ra}/^{238}\text{U}$ ARs, as reported in table 38, for most of the samples from Turamdih uranium deposit are close to unity, varying from 0.98-1.03. This indicates a near secular equilibrium condition for this daughter-parent pair for this deposit. But for the Bhatin, Narwapahar and Jaduguda deposits samples B3, B4 (Bhatin), N1, N2, N4 (Narwapahar) and J2 (Jaduguda) have ARs significantly different from unity. These samples (except N4) indicate uranium mobilisation in the deposits. The other samples from these deposits indicate secular equilibrium condition being maintained.

The $^{226}\text{Ra}/^{230}\text{Th}$, $^{226}\text{Ra}/^{210}\text{Pb}$, $^{230}\text{Th}/^{238}\text{U}$, $^{234}\text{U}/^{238}\text{U}$ and $^{230}\text{Th}/^{234}\text{U}$ ARs, reported in table 40, were determined in few samples from three uranium deposits, namely Narwapahar (N6-N8), Bhatin (B6) and Jaduguda (J6). The $^{226}\text{Ra}/^{230}\text{Th}$ ARs are significantly different from unity in N7, N8 and B6, indicating the system was not closed to groundwater movement for a maximum time period of 8ky. The sample B6 indicates ^{226}Ra mobility from the place of sample collection in Bhatin deposit. On the other hand, samples N7 and N8 from Narwapahar indicate ^{226}Ra accumulation at the place of sample collection. The $^{226}\text{Ra}/^{210}\text{Pb}$ ARs are greater than unity for three (N6, N8 and J6) out of five samples, indicating loss of radon from these samples or a preferential enrichment of ^{226}Ra in these samples. The former of these processes may occur if radon gets dissolved in the groundwater. $^{230}\text{Th}/^{238}\text{U}$ ARs indicate that in samples N8 preferential ^{238}U accumulation has occurred. It has to be mentioned here that the ^{210}Pb , ^{230}Th and ^{234}U activity concentrations are associated with high errors, as reported in table 39. The $^{234}\text{U}/^{238}\text{U}$ ARs

calculated for all the samples are close to unity indicating a secular equilibrium being maintained for ^{234}U - ^{238}U . The $^{230}\text{Th}/^{234}\text{U}$ ARs for N7 and N8 are less than unity, which indicates preferential ^{234}U accumulation in the samples. It can be observed that in sample N8 the $^{230}\text{Th}/^{238}\text{U}$ and $^{230}\text{Th}/^{234}\text{U}$ ARs are both less than unity, indicating the selective accumulation of uranium at this location.

The Thiel diagram [51, 48] in fig. 67, points to the fact that in Jaduguda and Bhatin deposit secular equilibrium condition is maintained. Samples with ARs from 0.9-1.1 (due to the analytical error of 10%) are considered to be in secular equilibrium. One sample lies on the verge of the uranium accumulation region (region II in fig. 67) and another lies in the forbidden region for any single process (region III in fig. 67) from Narwapahar deposit. For the latter sample an initial uranium accumulation phase may have been followed by relatively recent uranium leaching. It can be concluded that the Thiel plot of $^{234}\text{U}/^{238}\text{U}$ vs. $^{230}\text{Th}/^{238}\text{U}$ activity ratios indicates uranium accumulation and complex processes of uranium redistribution, but an overall slight shift from secular equilibrium condition in the uranium deposits.

^{235}U series

The $^{231}\text{Pa}/^{235}\text{U}$ ARs, given in Table 2, indicate that in half of the samples this daughter-parent pair is in a state of secular equilibrium. In the samples B2, B4, N1, N3, J5 and T3 uranium may have migrated from the point of sample collection. Due to the long half life of ^{231}Pa , it has remained at the point of sample collection and has not moved with ^{235}U . On the other hand in samples B6, N6 and J4 uranium has been preferentially accumulated. The $^{227}\text{Ac}/^{235}\text{U}$ ARs show that in 11 samples out of 25 the secular equilibrium condition has been maintained between this daughter-parent pair. In samples

B2, B4, N1, N2, N3, J5, T1, T2, T3 and T5 uranium has migrated from the point of sample collection and in samples B5, B6 and N5 uranium has been preferentially accumulated. The ^{227}Ac activities have been determined from ^{227}Th , which is also mobile under acidic pH conditions and proximity to groundwater.

^{232}Th series

The $^{228}\text{Th}/^{228}\text{Ra}$ ARs in fifteen of the samples had values close to unity, 0.91-1.09. Nine of the samples have AR values significantly different from unity. This indicates that ^{228}Th and ^{228}Ra are not in equilibrium in these samples and the deposit may be open for geochemical changes. Similar results have also been reported by Ribeiro et al. [50], in quaternary carbonate deposits. But more samples need to be analysed to confirm a hypothesis in this case.

Variation of ARs with U concentration

The ARs of $^{226}\text{Ra}/^{238}\text{U}$, $^{227}\text{Ac}/^{235}\text{U}$, $^{231}\text{Pa}/^{235}\text{U}$, $^{230}\text{Th}/^{238}\text{U}$, $^{226}\text{Ra}/^{230}\text{Th}$ and $^{226}\text{Ra}/^{210}\text{Pb}$ have been plotted with uranium concentrations in the samples in fig. 68. The $^{226}\text{Ra}/^{238}\text{U}$ AR is seen to have values closer to unity in the samples with uranium concentrations in the 700-800ppm range rather than at lower uranium concentrations. This can be explained by the fact that the greater the original amount of uranium in the sample, the greater is the amount of uranium or daughter products that have to be added or removed to change the equilibrium ratio significantly [38].

The ARs of $^{227}\text{Ac}/^{235}\text{U}$ and $^{231}\text{Pa}/^{235}\text{U}$ when plotted as a function of uranium concentrations show that the ARs are in general slightly more close to unity in the samples with uranium concentrations in the 700-800 ppm range. It can also be concluded that in case of $^{227}\text{Ac}/^{235}\text{U}$ ARs more number of samples are deviant from unity by a

greater extent than the $^{231}\text{Pa}/^{235}\text{U}$ ARs. This may be due to the fact that ^{227}Th is more mobile than ^{231}Pa under acidic pH conditions of the groundwater. This was also observed by Rekha et al. [49].

The plot of $^{230}\text{Th}/^{238}\text{U}$ and $^{226}\text{Ra}/^{230}\text{Th}$ ARs as a function of U concentration shows that the deviation of the AR from unity decreases with increasing U concentration.

Table 38. U and Th contents in the samples and the corresponding activity ratios. Reported errors are the errors associated with counting for Gamma spectrometry of the samples.

Sample code	^{238}U Bq/kg	^{226}Ra Bq/kg	^{232}Th Bq/kg	U ppm	Th ppm	$^{226}\text{Ra}/^{238}\text{U}$	$^{231}\text{Pa}/^{235}\text{U}$	$^{227}\text{Ac}/^{235}\text{U}$	$^{228}\text{Th}/^{228}\text{Ra}$
B1	2 573 ± 98	2 761 ± 11	4.0 ± 0.6	208.2 ± 7.9	0.98 ± 0.15	1.07 ± 0.04	1.04 ± 0.04	0.94 ± 0.05	1.41 ± 0.51
B2	6 294 ± 145	6 592 ± 26	19.9 ± 2.3	509.2 ± 11.7	4.88 ± 0.56	1.05 ± 0.02	1.20 ± 0.08	1.25 ± 0.07	1.04 ± 0.17
B3	1 880 ± 295	2 179 ± 27	16.8 ± 0.1	152.1 ± 23.9	4.12 ± 0.01	1.16 ± 0.18	0.94 ± 0.09	0.98 ± 0.10	1.07 ± 0.06
B4	5 673 ± 13	6 970 ± 21	16.7 ± 0.5	459.0 ± 1.1	4.10 ± 0.12	1.23 ± 0.003	1.16 ± 0.09	1.29 ± 0.10	1.07 ± 0.11
B5	5 443 ± 144	5 989 ± 24	17.3 ± 1.6	440.3 ± 11.7	4.25 ± 0.39	1.10 ± 0.02	0.91 ± 0.03	0.89 ± 0.03	0.94 ± 0.14
B6	3 978 ± 72	3 677 ± 11	36.2 ± 1.0	321.9 ± 5.8	8.90 ± 0.24	0.92 ± 0.02	0.69 ± 0.15	0.81 ± 0.10	0.92 ± 0.07
N1	4 123 ± 181	5 730 ± 17	12.3 ± 1.4	333.6 ± 14.7	3.02 ± 0.34	1.39 ± 0.06	1.17 ± 0.20	1.27 ± 0.41	1.04 ± 0.14
N2	4 165 ± 171	4 664 ± 19	105.5 ± 10.8	337.0 ± 13.8	25.90 ± 2.65	1.12 ± 0.05	1.00 ± 0.05	1.20 ± 0.06	1.15 ± 0.12
N3	5 055 ± 111	5 216 ± 21	6.9 ± 1.7	408.9 ± 9.0	1.69 ± 0.42	1.03 ± 0.02	1.26 ± 0.24	1.13 ± 0.48	1.01 ± 0.26
N4	2 722 ± 215	1 856 ± 02	25.1 ± 2.1	220.2 ± 17.4	6.16 ± 0.52	0.68 ± 0.12	0.97 ± 0.06	0.91 ± 0.04	1.18 ± 0.07
N5	5 067 ± 198	5 111 ± 15	8.9 ± 1.3	409.9 ± 16.0	2.18 ± 0.32	1.01 ± 0.04	0.94 ± 0.03	0.78 ± 0.02	1.09 ± 0.16
N6	4 399 ± 75	4 410 ± 31	78.0 ± 1.1	355.9 ± 6.1	19.16 ± 0.28	1.00 ± 0.02	0.76 ± 0.16	1.02 ± 0.17	1.05 ± 0.04
N7	3 038 ± 377	3 090 ± 62	82.9 ± 7.8	245.8 ± 30.5	20.37 ± 1.92	1.02 ± 0.13	n.d.	1.07 ± 0.17	1.24 ± 0.21
N8	3 814 ± 614	4 043 ± 97	119.3 ± 13.2	308.6 ± 49.7	29.31 ± 3.24	1.06 ± 0.17	n.d.	1.05 ± 0.22	1.13 ± 0.25
J1	3 516 ± 56	3 573 ± 14	4.8 ± 0.3	284.5 ± 4.6	1.18 ± 0.07	1.02 ± 0.02	0.99 ± 0.03	0.93 ± 0.02	0.88 ± 0.26
J2	6 499 ± 253	8 836 ± 27	12.4 ± 1.7	525.8 ± 20.5	3.04 ± 0.42	1.36 ± 0.05	n.d.	n.d.	0.88 ± 0.16
J3	8 949 ± 215	9 227 ± 37	0.8 ± 0.7	724.1 ± 17.4	0.20 ± 0.17	1.03 ± 0.03	0.99 ± 0.06	0.93 ± 0.03	n.d.
J4	2 888 ± 78	3 158 ± 9	18.6 ± 4.2	233.7 ± 6.3	4.57 ± 1.03	1.09 ± 0.03	0.81 ± 0.05	0.98 ± 0.05	0.95 ± 0.23
J5	10 107 ± 273	10 502 ± 32	16.3 ± 2.0	817.7 ± 22.1	4.00 ± 1.49	1.04 ± 0.03	1.17 ± 0.14	1.29 ± 0.15	0.99 ± 0.66
J6	9 488 ± 342	10 007 ± 50	44.2 ± 2.9	767.7 ± 27.6	10.85 ± 0.72	1.05 ± 0.04	0.90 ± 0.15	1.08 ± 0.12	0.92 ± 0.17
T1	3 185 ± 96	3 256 ± 13	12 ± 2.4	257.7 ± 7.7	2.95 ± 0.59	1.02 ± 0.03	1.02 ± 0.08	1.39 ± 0.11	0.91 ± 0.19
T2	3 242 ± 101	3 301 ± 13	49.8 ± 2.1	262.3 ± 8.1	12.22 ± 0.52	1.02 ± 0.03	1.09 ± 0.37	1.20 ± 0.26	1.20 ± 0.07
T3	2 795 ± 75	3 098 ± 12	4.7 ± 0.2	226.2 ± 6.1	1.15 ± 0.05	1.11 ± 0.03	1.16 ± 0.12	1.26 ± 0.13	0.94 ± 0.06
T4	3 290 ± 128	3 230 ± 13	18.9 ± 4.6	266.2 ± 10.4	4.64 ± 1.13	0.98 ± 0.04	1.09 ± 0.07	0.91 ± 0.03	1.03 ± 0.26
T5	2 932 ± 70	3 034 ± 12	26.90 ± 1.7	237.20 ± 5.7	6.60 ± 0.42	1.03 ± 0.03	0.94 ± 0.05	1.21 ± 0.07	1.19 ± 0.09

B1 to B6- Bhatin uranium deposit; N1 to N8- Narwapahar uranium deposit; J1 to J6- Jaduguda uranium deposit; T1-T5- Turamdih uranium deposit.

Table 39. Activity concentrations of uranium series radionuclides measured in some of the samples. Reported errors are the errors associated with counting for Gamma spectrometry of the samples.

Sample code	^{210}Pb	^{230}Th	^{234}U
N6	3771 ± 213	4012 ± 1882	4201 ± 350
N7	2980 ± 77	2732 ± 1156	$3\ 283 \pm 420$
N8	3105 ± 118	2579 ± 1271	$3\ 461 \pm 751$
B6	3395 ± 113	4167 ± 421	3783 ± 274
J6	9160 ± 751	9463 ± 1858	9247 ± 892

Table 40. Activity ratios of the uranium series daughters. Reported errors are the errors associated with counting for Gamma spectrometry of the samples.

Sample code	$^{226}\text{Ra}/^{230}\text{Th}$	$^{226}\text{Ra}/^{210}\text{Pb}$	$^{230}\text{Th}/^{238}\text{U}$	$^{234}\text{U}/^{238}\text{U}$	$^{230}\text{Th}/^{234}\text{U}$
N6	1.10 ± 0.52	1.17 ± 0.07	0.91 ± 0.39	0.96 ± 0.08	0.96 ± 0.45
N7	1.13 ± 0.48	1.04 ± 0.03	0.90 ± 0.36	1.08 ± 0.19	0.83 ± 0.37
N8	1.57 ± 0.77	1.30 ± 0.06	0.68 ± 0.28	0.91 ± 0.25	0.75 ± 0.4
B6	0.88 ± 0.09	1.08 ± 0.04	1.05 ± 0.11	0.95 ± 0.07	1.10 ± 0.14
J6	1.08 ± 0.22	1.23 ± 0.11	0.98 ± 0.19	0.97 ± 0.10	1.00 ± 0.22

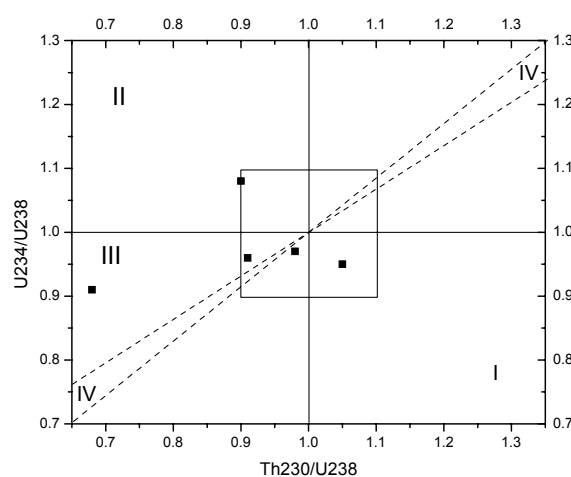


Fig. 67. Thiel diagram of uranium decay series of the ore samples from the deposits of Bhatin, Narwapahar and Jaduguda, drawn from the data presented in table 40. I: U leaching region, II: U accumulation region, III: forbidden region for any single process

and IV: forbidden region for any single continuous process. The boxed-in area indicates secular equilibrium condition.

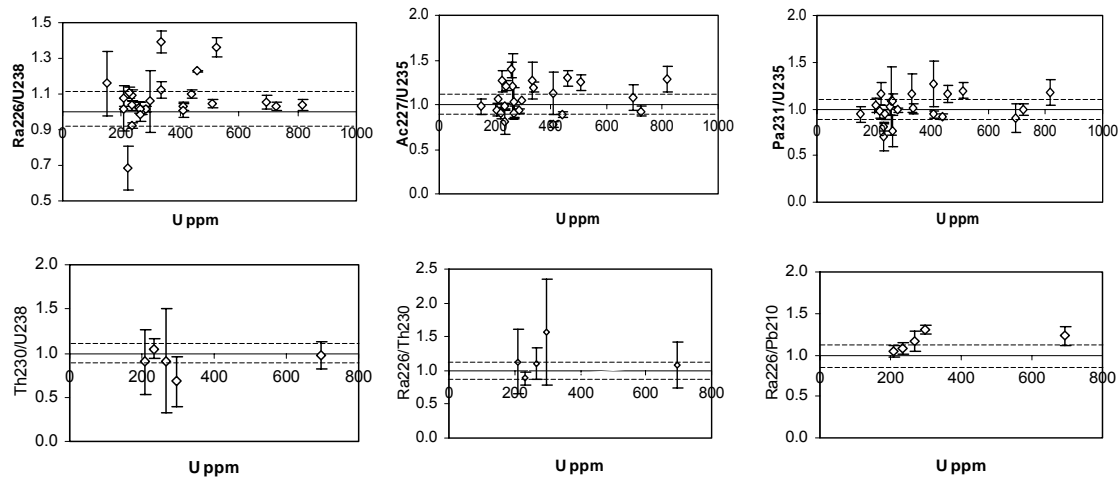


Fig 68. Activity ratios of various daughter-parent pairs, plotted with U concentration.

Error bars correspond to 10% error.

Dawood [230] has reported $^{234}\text{U}/^{238}\text{U}$ and $^{230}\text{Th}/^{234}\text{U}$ equilibrium for both secondary ore and whole-rock samples. Airey [231] observed substantial $^{234}\text{U}/^{238}\text{U}$ and $^{230}\text{Th}/^{234}\text{U}$ fractionation attributed to α -recoil. Condomines et al. [38] have employed $^{230}\text{Th}/^{238}\text{U}$, $^{234}\text{U}/^{238}\text{U}$, $^{226}\text{Ra}/^{238}\text{U}$, $^{210}\text{Pb}/^{226}\text{Ra}$ and $^{231}\text{Pa}/^{235}\text{U}$ to study elemental mobility in the Bernardan uranium deposit of French Massif Central. Their results suggest that Ra distribution has occurred but uranium has been little affected by remobilisation. Min et al. [48] have ascertained near secular equilibrium conditions in the ores and host sandstones from a uranium deposit in Northwest China, by employing $^{230}\text{Th}/^{238}\text{U}$, $^{234}\text{U}/^{238}\text{U}$ and $^{230}\text{Th}/^{234}\text{U}$ activity ratios.

Variation of AR with Depth

The ARs of $^{226}\text{Ra}/^{238}\text{U}$, $^{231}\text{Pa}/^{235}\text{U}$ and $^{227}\text{Ac}/^{235}\text{U}$ have been plotted against their depths for three operational U-deposits in fig. 69. Although a very clear trend is not evident in the figures, it can be observed that there is a reduction in the ARs at greater depths. This may

be due to the reduction in the mobility of uranium and increase in that of ^{226}Ra at greater depths. This can be explained by the fact that less oxidizing conditions prevail at greater depths in the deposits, thereby reducing the mobility of U and enhancing the same for Ra. But more samples need to be analysed for a better understanding of the depth profile in these deposits.

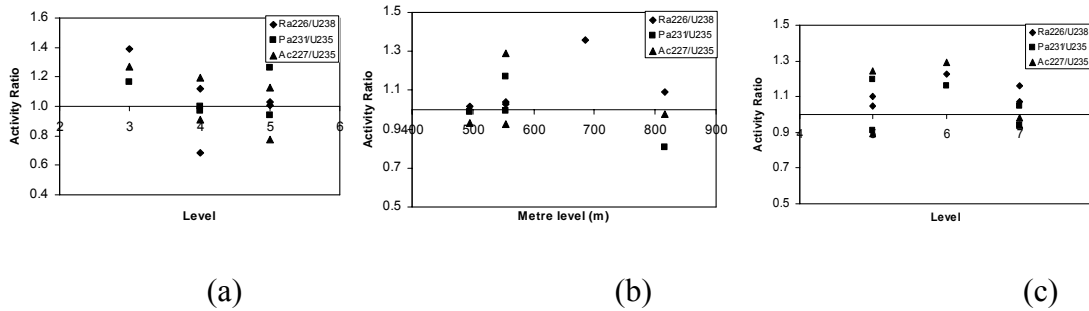


Fig. 69. Variation of $^{226}\text{Ra}/^{238}\text{U}$, $^{231}\text{Pa}/^{235}\text{U}$ and $^{227}\text{Ac}/^{235}\text{U}$ Activity Ratios with mine depth levels for (a) Narwapahar, (b) Jaduguda and (c) Bhatin mines

4.1.4. Wastes

The radioactivity in uranium tailings depends on the grade of ore mined and is generally found to vary from less than 1000Bq/kg to 100000Bq/kg [232]. In this thesis, the uranium tailings collected from the two tailings ponds had ^{238}U concentrations as, 712.3 ± 181.1 and 569.4 ± 158.7 Bq/kg. The activities of ^{226}Ra were higher, being 1766.9 ± 398.4 and 1659.9 ± 215.5 Bq/kg for the two tailings ponds. Scimmanck et al. [233] have reported ^{238}U activity concentration of 1630 Bq/kg in the Crossen Tailings [233].

The activity ratios of $^{226}\text{Ra}/^{238}\text{U}$ were observed to be greater than one in all the uranium tailings samples, due to the preferential removal of uranium by chemical processes. The other activity ratios were mostly near unity, as seen in fig. 70. It can be observed that the $^{226}\text{Ra}/^{238}\text{U}$ activity ratios for the copper tailings and clinker ash samples were near unity, due to no selective removal of uranium from the copper ore.

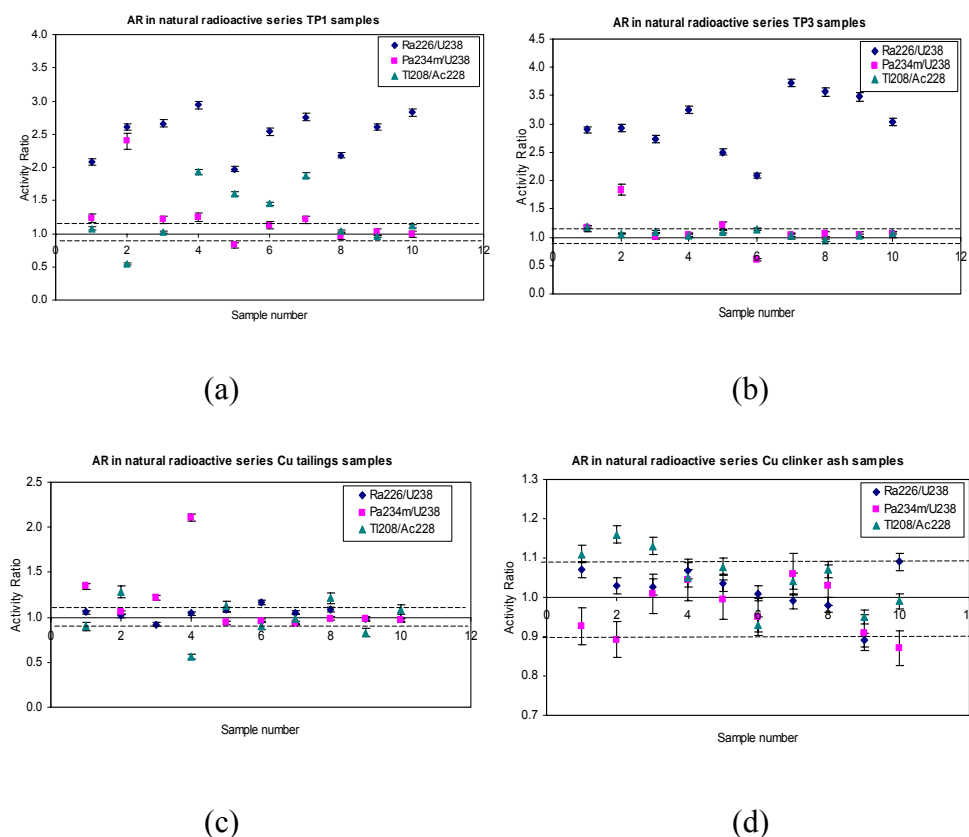


Fig. 70. Activity ratios of various daughter-parent pairs for (a) uranium tailings, TP1, (b) uranium tailings, TP3, (c) copper tailings and (d) copper clinker ash.

4.2. Trace elemental concentrations and distributions

The elemental concentrations in soils, in this thesis, are comparable with the mean concentrations of Cd, Cu, Cr, Zn and Fe as reported by Maas et al. [234] for different types of soils in Algeria, with Fe, Co, Cr, Cu and Ni concentrations in forest soils reported by Nael et al. [235], with elemental concentrations from a geochemical survey in North America as reported by Reeves and Smith [236] with concentrations reported in agricultural and non-agricultural soils of Dexing, China [237] and also with elemental concentrations reported in French soils [238]. Soils developed over granite-gneiss and schist-quartzite basement rocks in Nigeria have similar concentrations as reported in this

thesis [239]. The Rare Earth Element (REE) concentrations for soils in this thesis are comparable with REE concentrations reported by Mao et al. [77]. Oswal et al. [30] have reported similar concentrations in soils from a mining area in Hamadan province, Iran.

The elemental concentrations in metamorphic host rocks and uranium bearing rocks, in this thesis, are comparable with the concentrations reported by El-Taher [240] and Middelburg et al. [241] for granitic rocks except some of the REE having higher concentrations in uranium bearing rocks reported in this thesis. This is due to the association of REE with apatite mineral. The presence of higher concentrations of U and Ce, as observed in this thesis, signify granitic and metamorphic rocks [78, 79].

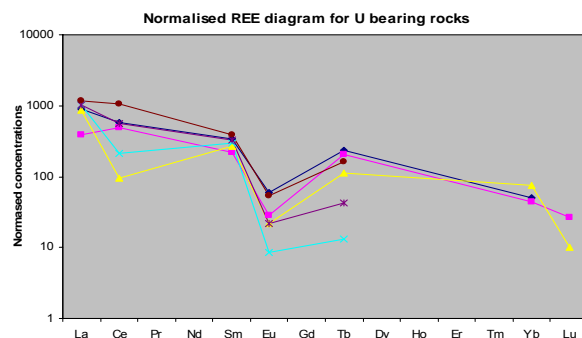
The elemental concentrations in uranium tailings, in this thesis, are comparable with concentrations reported by Donahue [242] for Rabbit Lake uranium mill tailings.

The study of REE concentrations has long been appreciated as an important source of scientific information, which helps in predicting the source and evolutionary history of rocks [80]. From the geochemical point of view, the REE are dispersed elements, i.e., they are spread among many common materials, rather than concentrated into a select few. They are lithophilic in nature i.e., when allowed to distribute themselves overwhelmingly, enter the silicate. The minerals that do take up REE in their structures will generally show a preference for either light or heavy REE depending on the nature of the ionic positions available for substitution. When comparing the REE contents of different rocks or minerals, one generally normalizes the concentrations of the individual REE to their abundance in chondrites (the meteorites that best represent the composition of the nonvolatile fraction of solar system material). This is done to take into account the fact that the elements with even atomic numbers are more abundant than their neighbours

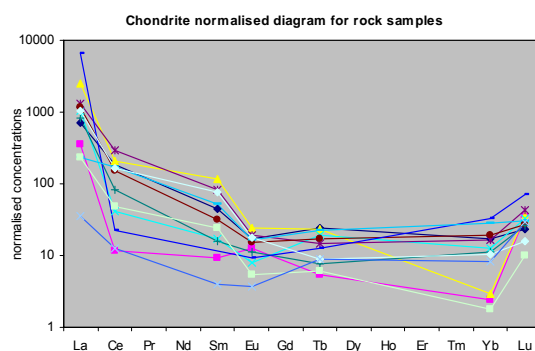
with odd atomic numbers (Oddo-Harkins effect), a consequence of nuclear stability. The normalisation results in REE patterns (normalised concentration versus atomic number) that are smooth, except for occasional anomalies for Eu and Ce (because of their sometimes differing oxidation states) and for Eu and Yb (the two most volatile REE that are sometimes depleted in the refractory Ca–Al-rich form) inclusions present in carbonaceous chondrites [240].

Rare earth element (REE) concentrations, as mentioned in the earlier chapter, were normalised using chondrite values given by Anders and Grevesse [243]. The normalised REE values are shown in fig. 71 below for uranium bearing rocks and host rocks, respectively. Negative Ce and Eu anomaly is evident for both types of rocks, being greater in the uranium bearing ones [244]. The light REE (LREE) are enriched as compared to the heavy REE (HREE) in the uranium bearing rocks (La/Yb ranges from 8.64 – 17.94) and La/Sm ratio ranges from 1.76 – 3.48 indicating LREE fractionation [245]. LREE enrichment and REE fractionation are evident in the host rocks as well.

REE are incompatible in all minerals crystallising, so their concentration increases in the residual melts, with the exception of Eu^{2+} in plagioclase, which replaces Sr and Ca and is removed by plagioclase. The result is a negative Europium anomaly, which suggests that these samples are plagioclase depleted [244]. A negative Ce anomaly suggests the reducing conditions and hence the change of Ce^{4+} to soluble Ce^{3+} and therefore depletion of Ce [246]. Hence the samples showing negative Eu and Ce anomaly are plagioclase depleted and present in a reducing environment.



(a)



(b)

Fig. 71. Chondrite normalised REE diagram for (a) uranium bearing rocks and (b) host rocks

4.2.1. Variation with particle size

Distribution of elements in different particle sizes is due to their association with the minerals in these fractions. Minerals like quartz, calcite, feldspar, etc. are associated with coarser particle sizes. Clayey minerals like montmorillonite, chlorite, muscovite etc. are associated with finer particle sizes, as shown in fig. 72 below. Since quartz does not bind with trace elements, in the coarser particle sizes feldspars are more important with regard to binding with trace elements. The primary reason for association of trace elements with clayey minerals is the fact that they have smaller particle size and higher reactive surface area [247].

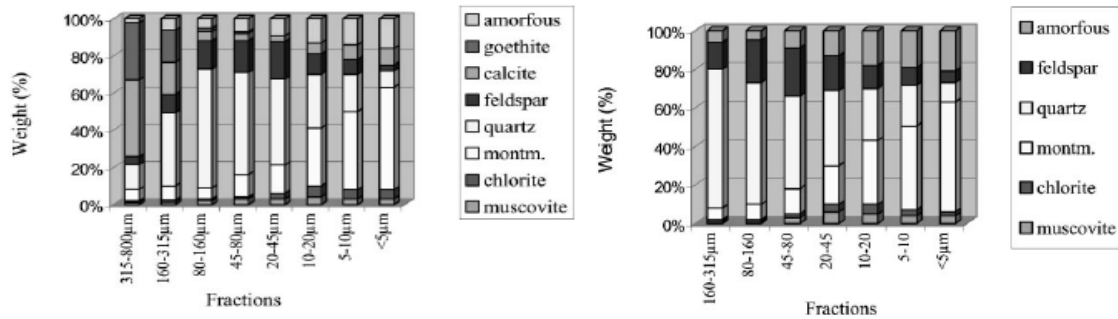
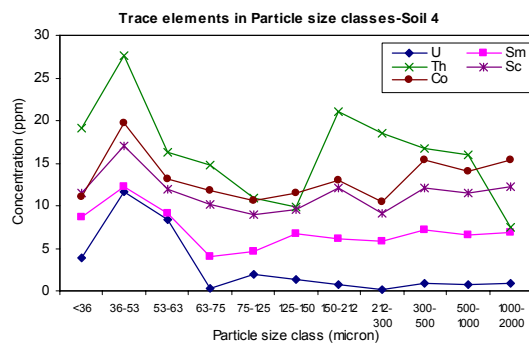


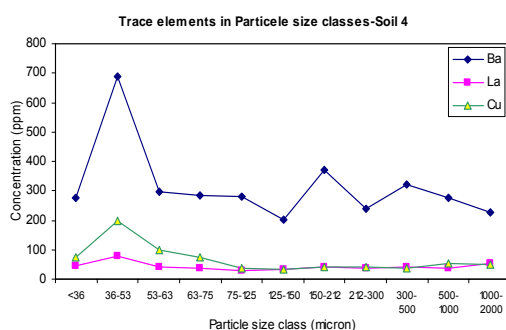
Fig. 72. Minerals in different particle sizes (Hartýani et. al, 2000)

As mentioned in the earlier chapter, the samples collected in this work were divided into particle size classes and trace elements were measured in each particle size class separately. It can be observed from fig. 73 below that the concentrations of elements were highest in the smaller particle sizes and gradually reduced for the larger particle sizes for soil 4. In soil 7 (fig. 73) the 75-150µm had higher concentration of elements apart from the <36µm fraction. This may be due to the presence of a mineral in this size class that also has greater association with elements apart from the clayey minerals. The same trend was observed for uranium tailings samples as well, as shown in fig. 74.

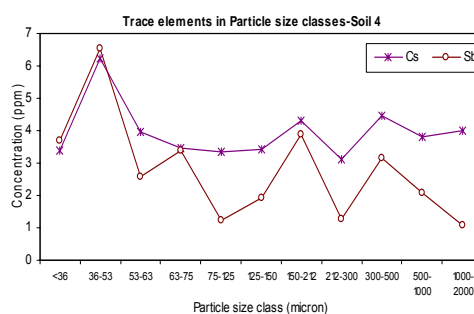
Horváth et al. [248] have reported similar studies on different size fractions of soils. Donahue et al. [242] have reported similar results for uranium tailings from Rabbit Lake, Canada. Peppas et al. [249] have reported similar results for size-fractionated fly-ash samples. Giuliano et al. [250] have carried out size fractionation studies on sediments and pyrite tailings and observed higher concentration in the lower particle sizes.



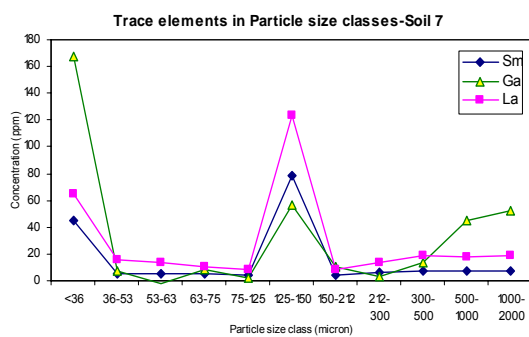
(a)



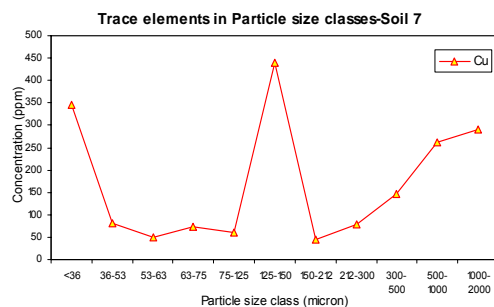
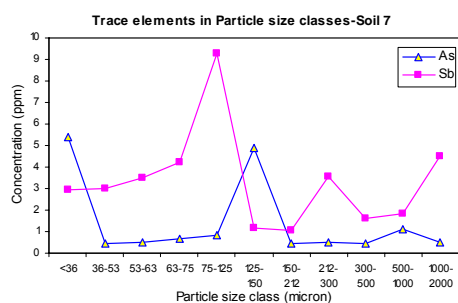
(b)



(c)



(d)



(e)

(f)

Fig. 73. Trace element concentration sin different particle size classes: (a) to (c) Soil 4 and (d) to (f) Soil 7.

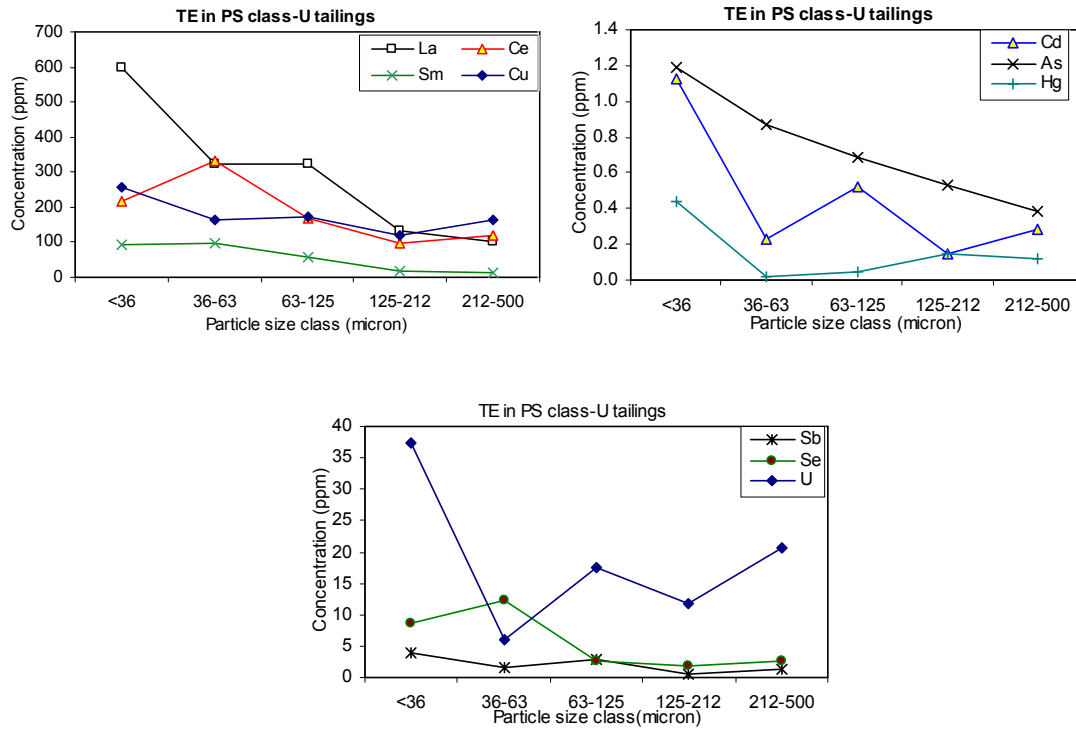


Fig. 74 . Trace element concentrations in different particle size classes: uranium tailings

The trace element concentrations were fitted with the help of power law to find out whether there exists a relation of elemental concentration with the size of a particle.

Power law has the simple form of:

$$f(x) = a * x^k \quad (15)$$

where, x is the particle size (μm), $f(x)$ is the elemental concentration in the particular particle size fraction (ppm), a is a constant and k is the scaling constant or power of the particle size in μm .

From the Fig. 75, 76 and 77 it can be seen that the decrease of elemental concentration with increase in particle size is substantial in case of the soils and uranium tailings for

some elements. Although the elements concentrate in the lower particle sizes their concentrations are not surface or volume distributed with respect to particle sizes in the soils and tailings, except Sm and Ga being surface distributed in soil 7.

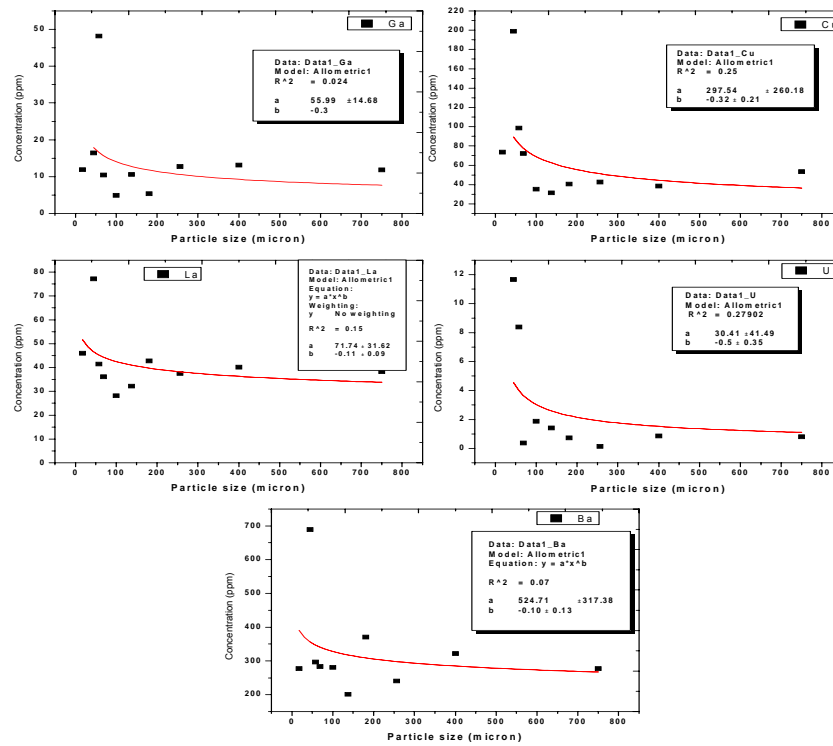


Fig. 75. Power law fitting of trace elements for soil 4

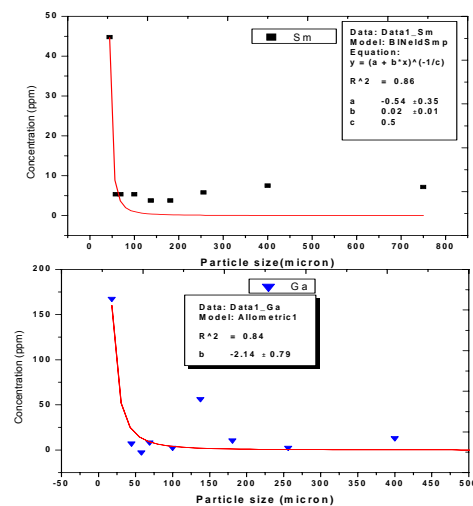


Fig. 76. Power law fitting of trace elements for soil 7

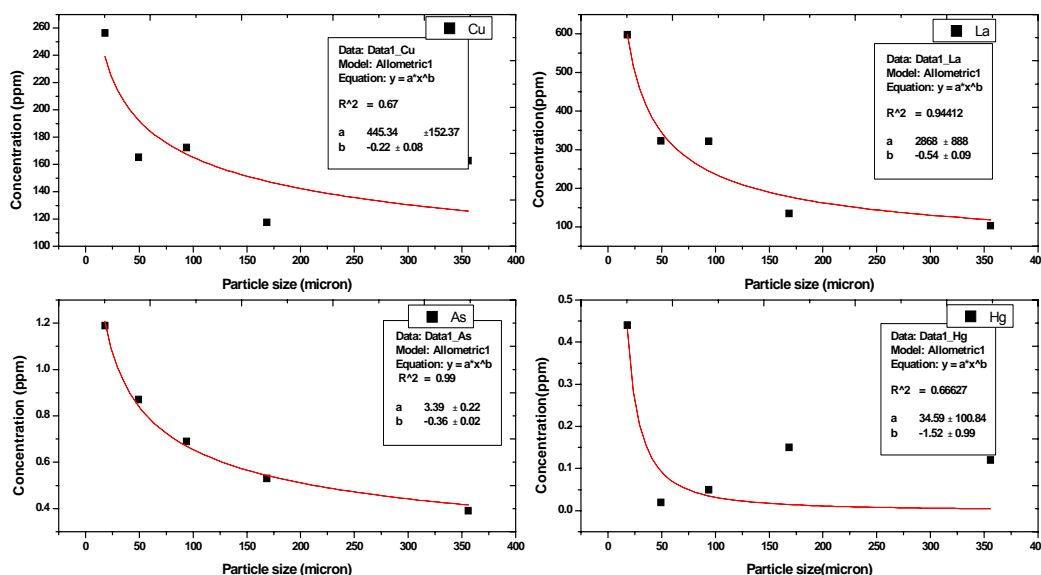


Fig. 77. Power law fitting of trace elements for uranium tailings

4.2.2. Correlation with elements and physico-chemical properties

The presence of different concentrations of elements in a matrix is influenced by the physical properties and chemical composition of the matrix. Elements that are similar in nature have similar behaviour in the environment and hence can show similar environmental distribution.

The trace and major elements measured in the host rock samples were hence checked for any correlation between the elemental concentrations, as shown in table 41 and 42. It was observed that the major oxides were generally negatively correlated with trace elements. Ca-oxide was positively correlated with Cr and Fe-oxide with Sb. Siderophile elements Ni and Co were well-correlated. The chalcophile elements, Se and Hg and Cd and Hg were also observed to be well correlated.

Table 41. Correlation matrix for trace elements in host rock samples

	Cr	Rb	Ni	Cu	Co	Th	Se	Cs	Hg	Cd	Na ₂ O	K ₂ O	CaO	Fe ₂ O ₃
Cr	1.0													
Rb	0.1	1.0												
Ni	0.2	0.7	1.0											
Cu	0.1	0.5	0.4	1.0										
Co	0.1	0.6	0.7	0.8	1.0									
Th	0.6	-0.2	-0.2	0.1	-0.1	1.0								
Se	0.5	0.1	0.2	0.4	0.3	0.6	1.0							
Cs	0.1	0.2	0.3	-0.2	-0.3	0.1	0.1	1.0						
Hg	0.5	0.5	0.3	0.5	0.5	0.7	0.6	0.1	1.0					
Cd	0.3	0.5	0.3	0.7	0.3	0.2	0.4	0.2	0.6	1.0				
Na ₂ O	-0.3	-0.1	-0.1	-0.3	-0.6	-0.4	-0.4	0.6	-0.6	0.1	1.0			
K ₂ O	-0.4	-0.1	0.2	-0.4	-0.3	-0.2	-0.4	0.6	-0.3	-0.3	0.5	1.0		
CaO	0.8	0.1	0.1	0.1	-0.1	0.7	0.2	0.4	0.6	0.5	-0.1	-0.1	1.0	
Fe ₂ O ₃	0.4	0.3	0.3	-0.1	0.1	-0.1	-0.2	0.2	0.1	-0.1	0.1	-0.2	0.3	1.0

Table 42. Correlation matrix for trace elements in host rock samples

	Sb	U	Hf	Ta	Sc	Zn	Br	As	Ga	Na ₂ O	K ₂ O	CaO	Fe ₂ O ₃
Sb	1.0												
U	-0.1	1.0											
Hf	0.3	0.1	1.0										
Ta	0.2	0.2	0.4	1.0									
Sc	0.2	-0.4	-0.1	-0.4	1.0								
Zn	0.1	0.1	0.3	0.1	-0.1	1.0							
Br	0.1	0.1	0.2	0.8	-0.3	0.2	1.0						
As	0.2	-0.3	-0.1	0.4	0.4	0.1	0.6	1.0					
Ga	0.3	-0.1	-0.3	0.1	0.3	0.1	0.4	0.4	1.0				
Na ₂ O	0.1	-0.4	-0.5	-0.4	0.5	-0.3	-0.3	0.2	0.4	1.0			
K ₂ O	-0.2	-0.1	-0.2	-0.2	0.1	0.3	-0.3	0.1	-0.1	0.5	1.0		
CaO	0.7	-0.2	0.4	0.0	0.2	0.3	0.2	0.1	0.3	-0.1	-0.1	1.0	
Fe ₂ O ₃	0.6	0.1	0.1	-0.1	0.5	-0.3	-0.2	0.1	0.2	0.1	-0.2	0.3	1.0

In soil samples the elemental concentrations were checked for any correlation among them and also with the physico-chemical properties of the samples, as shown in table 43 and 44. It was observed that U was negatively correlated with Ca-oxide and positively with Fe-oxide and pH. Hg was positively correlate with Ba; Cr and As were positively correlated; Siderophile elements Ni and Co were well-correlated; Sc was negatively correlated with Ba and Ba and CaO were negatively correlated. Cation exchange capacity (CEC) was positively correlated with moisture content (MC%), pH, clay% and Humic acid (HA%). The increase in Humic acid content (HA%) and clay content leads to an increase in the CEC due to the increase in the number of charge binding sites [251, 252]. HA% was positively correlated with As, Se, Hg, Cr, Ni, Co, clay% and MC%; No correlation was observed between trace elements and sand% since trace elements do not associate with sand. REE were generally correlated, this was chiefly due to their similar behaviour. The REE had generally no correlation with sand%, silt% and clay%.

Table 43. Correlation matrix for trace elements in soil samples

	U	Cd	Cu	Br	As	Sb	Ga	Ta	Hf	Na ₂ O	K ₂ O	CaO	Fe ₂ O ₃	sand%	silt%	LOI%	MC%	pH	clay%	HA%	CEC
U	1.0																				
Cd	-0.4	1.0																			
Cu	0.4	-0.1	1.0																		
Br	-0.3	0.3	-0.6	1.0																	
As	-0.1	0.1	0.1	0.4	1.0																
Sb	0.3	-0.6	-0.1	-0.3	-0.3	1.0															
Ga	-0.5	0.3	0.3	0.1	-0.1	-0.3	1.0														
Ta	0.6	0.0	0.4	-0.2	0.1	0.1	-0.2	1.0													
Hf	0.2	0.2	0.5	-0.4	-0.4	-0.1	0.3	-0.2	1.0												
Na ₂ O	0.1	0.2	0.9	-0.5	0.2	-0.3	0.5	0.1	0.6	1.0											
K ₂ O	0.3	-0.3	0.6	-0.3	0.2	-0.3	0.1	0.3	0.4	0.5	1.0										
CaO	-0.7	0.3	-0.3	0.5	0.1	-0.1	0.6	-0.7	0.2	0.1	-0.1	1.0									
Fe ₂ O ₃	0.5	-0.2	0.1	-0.4	-0.1	0.3	-0.6	0.7	-0.4	-0.2	0.1	-0.8	1.0								
sand%	0.1	-0.5	-0.1	0.1	0.2	0.5	-0.1	-0.2	-0.4	-0.1	-0.4	-0.1	0.1	1.0							
silt%	-0.1	0.5	0.1	0.1	-0.2	-0.5	0.1	0.2	0.4	0.1	0.4	0.1	0.1	-1.0	1.0						
LOI%	-0.3	0.6	0.3	-0.2	-0.1	-0.2	0.5	-0.4	0.4	0.6	-0.3	0.3	-0.4	0.1	0.1	1.0					
MC%	0.4	0.3	0.5	0.2	0.3	-0.5	0.2	0.6	0.1	0.4	0.4	-0.3	0.1	-0.4	0.4	-0.1	1.0				
pH	0.8	-0.2	0.1	0.1	0.0	0.3	-0.6	0.3	0.2	-0.2	0.1	-0.4	0.3	0.2	-0.2	-0.4	0.3	1.0			
clay%	-0.2	0.5	-0.2	0.6	0.7	0.6	0.3	0.1	-0.8	-0.2	-0.5	0.7	-0.1	0.9	-0.9	0.1	0.4	0.4	1.0		
HA%	0.3	0.2	0.5	0.2	0.7	0.4	0.2	0.6	-0.6	0.4	0.3	0.3	0.4	0.1	-0.1	-0.7	0.9	0.5	0.9	1.0	
CEC	0.1	0.5	0.3	0.2	0.4	0.5	0.7	0.2	0.1	0.4	-0.1	0.5	-0.2	0.2	-0.2	0.3	0.8	0.6	0.9	0.9	1.0

Table 44. Correlation matrix for trace elements in soil samples

	Ba	Se	Hg	Th	Cr	Cs	Ni	Sc	Rb	Co	Na ₂ O	K ₂ O	CaO	Fe ₂ O ₃	sand%	silt%	LOI%	MC%	pH	clay%	HA%	CEC
Ba	1.0																					
Se	0.1	1.0																				
Hg	0.5	-0.2	1.0																			
Th	0.1	-0.6	0.3	1.0																		
Cr	-0.3	-0.2	0.2	0.1	1.0																	
Cs	0.2	-0.2	-0.1	-0.2	-0.3	1.0																
Ni	0.1	0.4	0.2	-0.4	0.3	-0.1	1.0															
Sc	-0.6	-0.2	-0.3	-0.4	0.2	0.5	-0.1	1.0														
Rb	0.2	0.4	0.2	0.1	0.1	-0.7	0.4	-0.7	1.0													
Co	-0.2	0.1	0.2	-0.5	0.7	0.2	0.7	0.5	-0.2	1.0												
Na ₂ O	-0.4	-0.2	-0.1	0.6	0.1	-0.3	0.1	-0.2	0.1	-0.2	1.0											
K ₂ O	-0.2	0.2	0.2	0.2	0.1	-0.6	0.3	-0.4	0.3	-0.1	0.5	1.0										
CaO	-0.7	0.1	-0.6	-0.1	0.1	0.1	-0.5	0.5	-0.5	0.1	0.1	-0.1	1.0									
Fe ₂ O ₃	0.6	0.4	0.4	-0.3	-0.1	-0.1	0.6	-0.5	0.7	0.1	-0.2	0.1	-0.8	1.0								
sand%	0.3	-0.5	-0.3	0.2	0.5	0.4	0.1	0.1	-0.4	0.4	-0.1	-0.4	-0.1	0.1	1.0							
silt%	-0.3	0.5	0.3	-0.2	-0.5	-0.4	-0.1	-0.1	0.4	-0.4	0.1	0.4	0.1	0.1	-1.0	1.0						
LOI%	-0.5	-0.3	-0.4	0.4	-0.2	0.3	-0.4	0.2	-0.2	-0.3	0.6	-0.3	0.3	-0.4	0.1	0.1	1.0					
MC%	-0.1	-0.2	0.8	0.3	0.4	-0.2	0.3	0.1	0.1	0.3	0.4	0.4	-0.3	0.1	-0.4	0.4	-0.1	1.0				
pH	0.6	-0.3	0.7	0.5	0.2	-0.3	-0.2	-0.6	0.3	-0.2	-0.2	0.1	-0.4	0.3	0.2	-0.2	-0.4	0.3	1.0			
clay%	-0.4	0.0	0.3	-0.1	0.9	-0.2	0.1	0.3	-0.1	0.7	-0.2	-0.5	0.7	-0.1	0.9	-0.9	0.1	0.4	0.4	1.0		
HA%	-0.7	0.6	0.6	-0.7	0.8	-0.6	0.7	-0.3	0.6	0.9	0.4	0.3	0.3	0.4	0.1	-0.1	-0.7	0.9	0.5	0.9	1.0	
CEC	-0.6	0.1	0.4	0.4	0.6	-0.2	0.1	-0.1	0.1	0.4	0.4	-0.1	0.5	-0.2	0.2	-0.2	0.3	0.8	0.6	0.9	0.9	1.0

The elemental correlation for uranium bearing rocks was checked as shown in table 45. The trace metals showed positive correlation with major oxides, indicating their association with Na₂O and K₂O bearing minerals. Positive correlation between trace metals indicated similarity in their mineralogical and chemical association. This can be explained by their similar behaviour. REE were generally positively correlated with the major oxides, showing co-existence of the minerals.

Table 45. Correlation matrix for trace elements in uranium bearing rock samples

	Th	As	Cd	Sb	Hg	Zn	Na ₂ O	K ₂ O	CaO	Fe ₂ O ₃
Th	1.0									
As	0.9	1.0								
Cd	0.9	0.9	1.0							
Sb	0.5	0.7	0.3	1.0						
Hg	-0.7	-0.4	-0.8	0.4	1.0					
Zn	0.9	0.7	0.9	-0.01	-0.9	1.0				
Na ₂ O	0.3	0.6	0.2	0.9	0.5	-0.2	1.0			
K ₂ O	0.9	1.0	0.9	0.7	-0.5	0.8	0.5	1.0		
CaO	0.9	1.0	0.9	0.7	-0.4	0.7	0.6	1.0	1.0	
Fe ₂ O ₃	0.3	0.0	0.5	-0.7	-0.9	0.7	-0.8	0.1	0.01	1.0

4.3. Uranium leaching

4.3.1. Semi-dynamic leaching experiments

Several parameters associated with semi-dynamic leaching of uranium from different matrices have been covered in the following sections.

4.3.1.1. Cumulative leach fraction

The cumulative fraction of mobile U leached from the samples are shown as a function of square root of time in fig. 78 using a semi log graph. From the figure it is seen that the release of U was faster in the initial stage for all samples and then went on to attain a near

steady state condition. This was true for both the solvents used. The maximum cumulative fraction of U leached out was 0.22, 0.22, 0.07 and 0.39% for rock, uranium tailings, copper clinker ash samples and copper tailings respectively using water as solvent. The maximum cumulative fraction of U leached out was 0.31, 0.27, 0.05 and 0.59% for rock, uranium tailings, copper clinker ash samples and copper tailings respectively using 0.1N NaNO_3 . As 0.1N NaNO_3 is capable of extracting the weakly bound/exchangeable fraction of U, the cumulative fraction in its case is slightly higher in most cases when using 0.1N NaNO_3 , than when using distilled water. The lowest cumulative fraction of mobile U leached out was from the clinker ash samples.

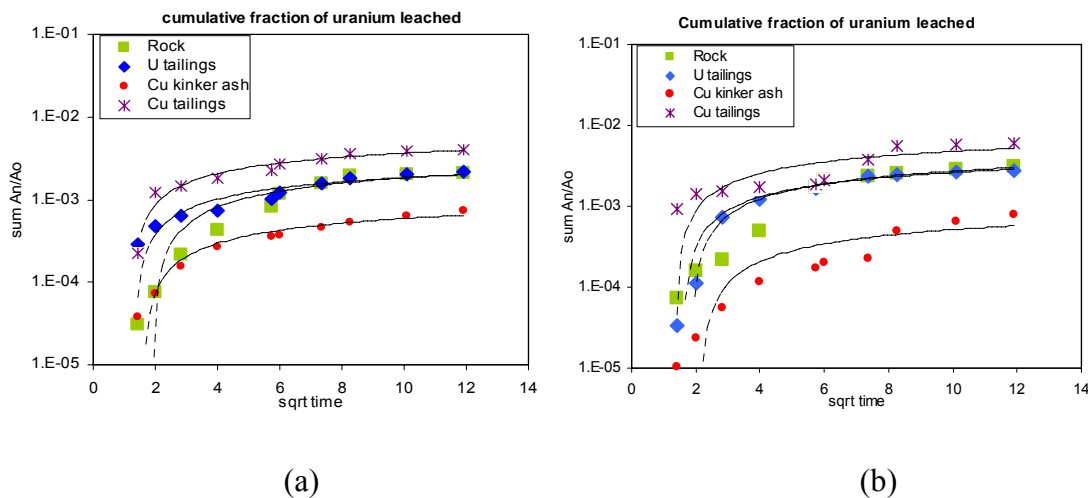


Fig. 78. Cumulative fraction of uranium leached with (a) water and (b) 0.1N NaNO_3

It may be noted here that the particle size distribution of these samples showed that clinker ash was of coarser grain size as compared to the other samples. Hence the reactive surface area of the clinker ash samples was less than other samples. This can be a cause of lesser leaching of U from clinker ash samples.

The cumulative leach fraction (CLF), in cm, is a measure of the elemental mobility, which is the leaching rate, from a sample. It is calculated by the following equation, as applied in Abdel Rahman et al. [253]:

$$CLF = (\sum A_n / A_0) / (V/S) \quad (16)$$

where, $\sum A_n$ is the cumulative radioactivity leached during the cumulative experimental time period t_n , A_0 the initial radioactivity present in the specimen, V the volume of specimen (cm^3), and S is the exposed surface area of specimen (cm^2).

The CLF of all the samples have been plotted with time in fig. 79. These plots show the same trend as the plots in fig. 79. The CLF values were highest for copper tailings, whereas rock samples and uranium tailings samples had the same values of CLF.

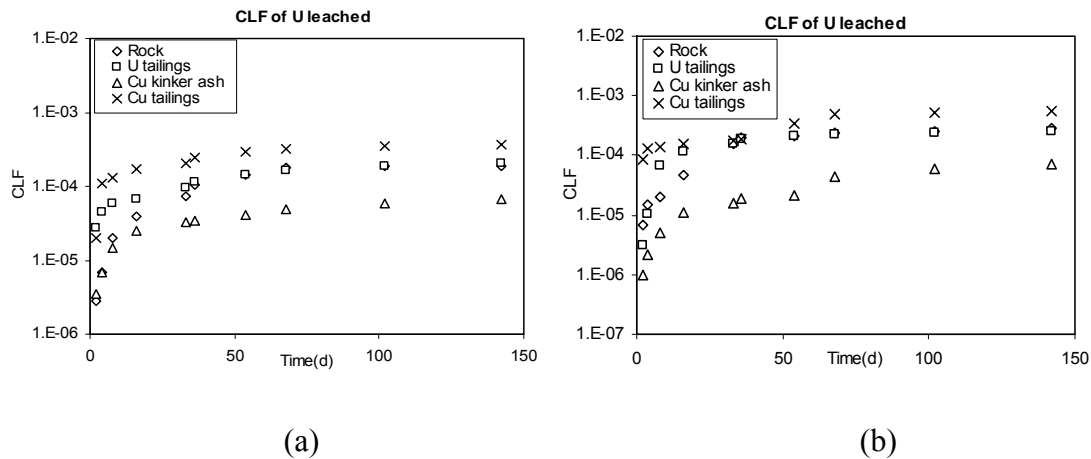


Fig. 79. CLF of uranium leached with (a) water and (b) 0.1N NaNO₃

4.3.1.2. Controlling leaching mechanism

In general, any leaching phenomena under static/ semi-dynamic conditions can be explained as a combination of the diffusion and dissolution mechanisms. The leaching phenomenon is divided into three regions according to studies reported in the literature [254]. The first is controlled by the rapid release of dissolved soluble material existing on the surface of the solid matrix, which is known as surface wash-off. After this, material

release is controlled by diffusion through the pore space of the solid matrix. In the last region, the slow portion of dissolution controls the leaching phenomena. In this case, dissolution of materials from the surface of the solid proceeds faster than diffusion through the pores. The rapid and slow portion of dissolution will actually result in the release of highly soluble materials but will not cause depletion of material.

The examination of the plot of incremental leach fractions (IF) of uranium from the studied matrices expressed as cm/day on log scale versus time (Fig. 80), indicate that the leaching pattern can be divided into two regions.

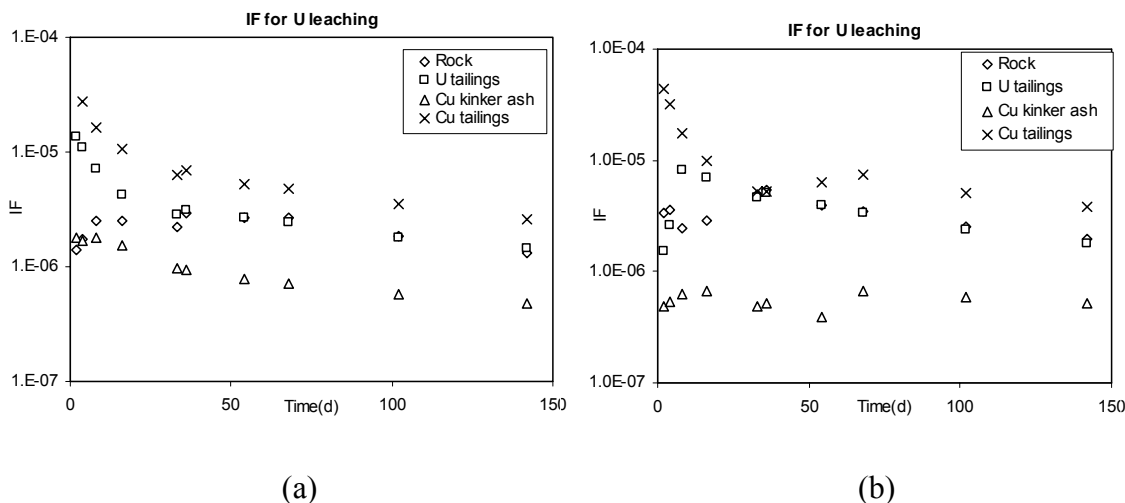


Fig. 80. IF of uranium leached with (a) water and (b) 0.1N NaNO₃

The first region (first 16 days) shows initial rapid release of radionuclides, then a reduction in the release takes place over a longer period of time. This is true for the samples in fig. 80a and the uranium and copper tailings samples in fig. 80b. Thereby it can be said that the leaching of uranium is mainly due to surface wash-off and diffusion and the slow portion of dissolution did not set-in in these samples. But in fig. 80b, the copper clinker ash samples show a very uniform trend of leaching, which indicates diffusion being the controlling step for these samples when using 0.1N NaNO₃ solvent.

The determination of the controlling leaching mechanism was based on the slope of the linear regression of the logarithm of CLF versus the logarithm of time as shown in fig. 81. If the slope is less than 0.35 the controlling leaching mechanism will be surface wash-off; for slope values in between 0.35 to 0.65, the controlling mechanism will be diffusion and higher slope values represent dissolution mechanism [253]. To eliminate any errors in interpretation due to the surface wash off mechanism (the initial period, first 16 days), the initial leached fractions have been excluded. The result of the linear regression in the second region (16-142 days) is shown in fig. 81. From the figure it is evident that the slope values lie between 0.35 and 0.65 for the rock sample and clinker ash sample with water as solvent, which indicate that diffusion is the controlling leaching mechanism for these studied cases. But for uranium and copper tailings the slope lies below 0.35, indicating surface wash off to be the mechanism in the initial phase of leaching when water is used as the solvent. When using 0.1N NaNO_3 , the controlling mechanism was observed to be diffusion for all the samples except uranium tailings, for which surface wash-off was still the controlling mechanism. This indicates that when a stronger solvent was used, the initial phase of surface wash off was over and the controlling mechanism for U release changed to diffusion for the copper tailings sample.

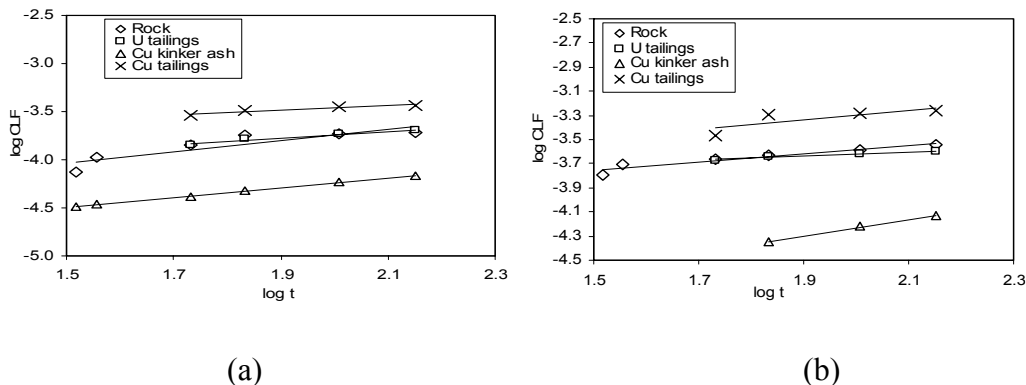


Fig 81. Linear regression for $\log \text{CLF}$ vs. $\log t$ for (a) water and (b) 0.1N NaNO_3

4.3.1.3. Apparent Diffusion coefficient

The mobile uranium leaching behavior can be evaluated by using a diffusion model. The diffusion coefficient used to assess the long-term behaviour of uranium can be determined by Fick's diffusion theory for semi infinite medium. This theory can be simplified to the form:

$$\sum A_n/A_0 = 2 * (S/V) * \sqrt{(Dt/\pi)} \quad (17)$$

where, A_n is the activity or concentration leached out after time t_n (Bq or ppm), A_0 the initial activity or concentration in the solid (Bq or ppm), and D is the diffusion coefficient (cm^2/s). Here $\sum A_n/A_0$ signifies the CLF of the solid matrix [253].

The value of the apparent diffusion coefficient (D) can be calculated from the slope (m) of the straight line of the plot of $[\sum A_n/A_0]$ versus $(t_n)^{1/2}$, as given in Abdel Rahman et al. [253]:

$$D = \pi * [(m*V)/(2S)]^2 \quad (18)$$

In fig. 78 above, the fraction of mobile uranium leached from studied matrices has been plotted versus the square root of leaching time. As can be seen from these plots, for all studied cases, the results indicate an initial fast leaching followed by slow leaching. This behavior suggests the presence of two different values of diffusion coefficients for the fast and slow components. This approach of determining the apparent diffusion coefficient is valid when the leached fraction less than 20% [253].

The diffusion coefficient (D) was calculated using Eq. (18) for the slow component of leaching in the time period of 16-142 days. It was obtained by conducting a linear regression analysis between $(\sum A_n/A_0)$ and the square root of time in the above mentioned period, as shown in fig. 81 above. The obtained values of D are listed in table 46. The

diffusion coefficient values generally range from 10^{-5} cm²/s for very mobile species to 10^{-15} cm²/s for immobile species [255, 256]. The D values ranged from 6.6 E-11 to 1.1 E-09 cm²/s in all the studied samples, indicating that the uranium in these samples is not very mobile. These D values are comparable with those of 10^{-8} to 10^{-11} cm²/s reported by Moon and Dermatas for untreated soils [255]; 10^{-9} to 10^{-11} cm²/s reported by Abdel Rahman et al. [253]; 10^{-8} cm²/s reported by El-Kamash et al. [254]; 10^{-7} to 10^{-8} cm²/s reported by Papadokostaki and Savidou [257] and 10^{-6} to 10^{-10} cm²/s reported by Ogunro and Inyang [258]. The change in solvent did not affect the D values much in most of the cases.

Table 46. Mean apparent diffusion coefficients (D in cm²/s) for U release from the studied matrices using different solvents

Sample	D, water	D, 0.1N NaNO ₃
Rock	2.6E-10	6.0E-10
U tailings	6.6E-11	4.2E-11
Cu clinker ash	2.4E-11	6.6E-11
Cu tailings	2.6E-10	1.1E-09

4.3.1.4. Bulk release

The Bulk release of mobile uranium from the samples can be defined as the amount of element released with respect to the surface area of the solid [102, 120] and is expressed as:

$$R_i = [c_i * (V/m)]/S \quad (19)$$

where, R_i is the bulk release of uranium ($\mu\text{g}/\text{m}^2$), c_i is the concentration of U in leachate ($\mu\text{g}/\text{L}$), V is the total volume of leachate (L), m is the mass of leached solid (g) and S is the surface area of solid sample (m^2).

The bulk release of mobile uranium has been calculated from Eq. (19) for all the studied matrices. The $R_i(\mu\text{g}/\text{m}^2)$ values show that the bulk release is mainly governed by the initial phase of leaching. The average R_i values for the studied matrices are given in table 47. It is observed that for the rock samples the bulk release values were much higher compared to those for the other matrices. This can be attributed to the fact that the uranium concentration is much higher in the rock sample than the matrices studied and also the fact that the rock samples were available in fine powder form. Again, these values, for the rock sample, were higher when using NaNO_3 as solvent as compared to distilled water. This is because the former is a stronger solvent than the latter. The average bulk release values were highly comparable for the waste matrices studied.

Table 47. The bulk release values, $R_i(\mu\text{g}/\text{m}^2)$, for U release from the studied matrices using different solvents

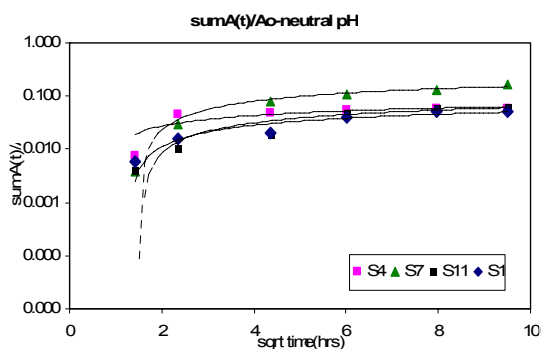
Sample matrix	Using distilled water			Using 0.1N NaNO_3		
	average	min	max	average	min	max
Rock	0.18	0.03	0.35	0.26	0.05	1.05
U tailings	0.01	0.01	0.02	0.02	0.002	0.03
Cu clinker ash	0.01	0.002	0.01	0.01	0.001	0.03
Cu tailings	0.01	0.004	0.03	0.02	0.004	0.05

4.3.2. Dynamic leaching: cumulative fraction leached and associated leaching rate

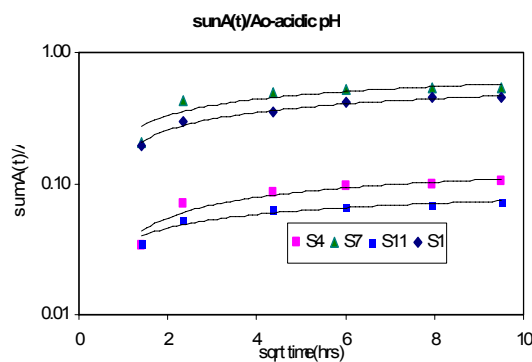
The cumulative fraction of uranium leached out and the rate of leaching was determined for dynamic leaching of uranium from different matrices. The change in this parameter value with the variation of the physical conditions of leaching have been covered in the following sections.

4.3.2.1. Effect of pH of leachant

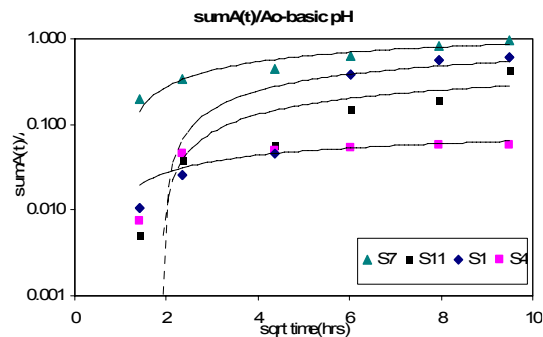
The variation in pH from neutral-acidic-basic showed marked effects on the cumulative fraction of uranium leached out from different matrices and also the associated leaching rate. The cumulative fraction of mobile U leached from soil samples are shown as a function of square root of time using a semi log graph in fig. 82 (a), (b) and (c) below. From the figures it is seen that the maximum cumulative fraction of U leached out followed the order, basic>acidic>neutral. The maximum cumulative fraction of U leached out under neutral conditions was 5.19, 5.86, 16.68 and 6.35% for soil 1, soil 4, soil 7 and soil 11, respectively. Under acidic conditions it was 45.19, 10.44, 53.90 and 6.92% for soil 1, soil 4, soil 7 and soil 11, respectively.



(a)



(b)



(c)

Fig. 82. Cumulative fraction of U leached from soils under different pH conditions (a) neutral, (b) acidic and (c) basic pH

Under basic conditions it was 61.35, 93.07, 96.36 and 42.87% for soil 1, soil 4, soil 7 and soil 11, respectively.

The leaching rate was calculated according to the formula,

$$\text{Leaching Rate (h}^{-1}\text{)} = \frac{\text{Conc. in leachate} * \text{leachate volume}}{\text{Conc. in sample} * \text{sample weight} * \text{time}} \quad (20)$$

The leaching rate followed the order, basic>acidic>neutral; values of it under different pH conditions are given in table 48.

Table 48. Leaching rate of uranium from soils under different pH conditions

Leaching Rate (h ⁻¹)	S1	S4	S7	S11
Neutral	0.0006	0.0006	0.0018	0.0007
Acidic	0.0050	0.0012	0.0060	0.0008
Basic	0.0068	0.0103	0.0107	0.0048

The cumulative fraction of mobile U leached from waste samples are shown as a function of square root of time using a semi log graph in fig. 83 (a), (b), (c) and (d) below. The maximum cumulative fraction of U leached out for uranium tailings, TP1 was 0.75, 1.94

and 0.40% under neutral, acidic and basic pH, respectively. The same for uranium tailings, TP3 was 2.80, 17.17 and 0.84% under neutral, acidic and basic pH, respectively. The maximum cumulative fraction of U leached out from copper tailings was 4.78, 45.28 and 16.91% under neutral, acidic and basic pH, respectively. The same for copper clinker ash was 1.69, 10.50 and 2.91% under neutral, acidic and basic pH, respectively. From the figures it is seen that the maximum cumulative fraction of U leached out followed the order, acidic>neutral>basic for uranium tailings and acidic>basic>neutral for copper wastes. The pyrite nature of the tailings are responsible for greater leaching under acidic conditions.

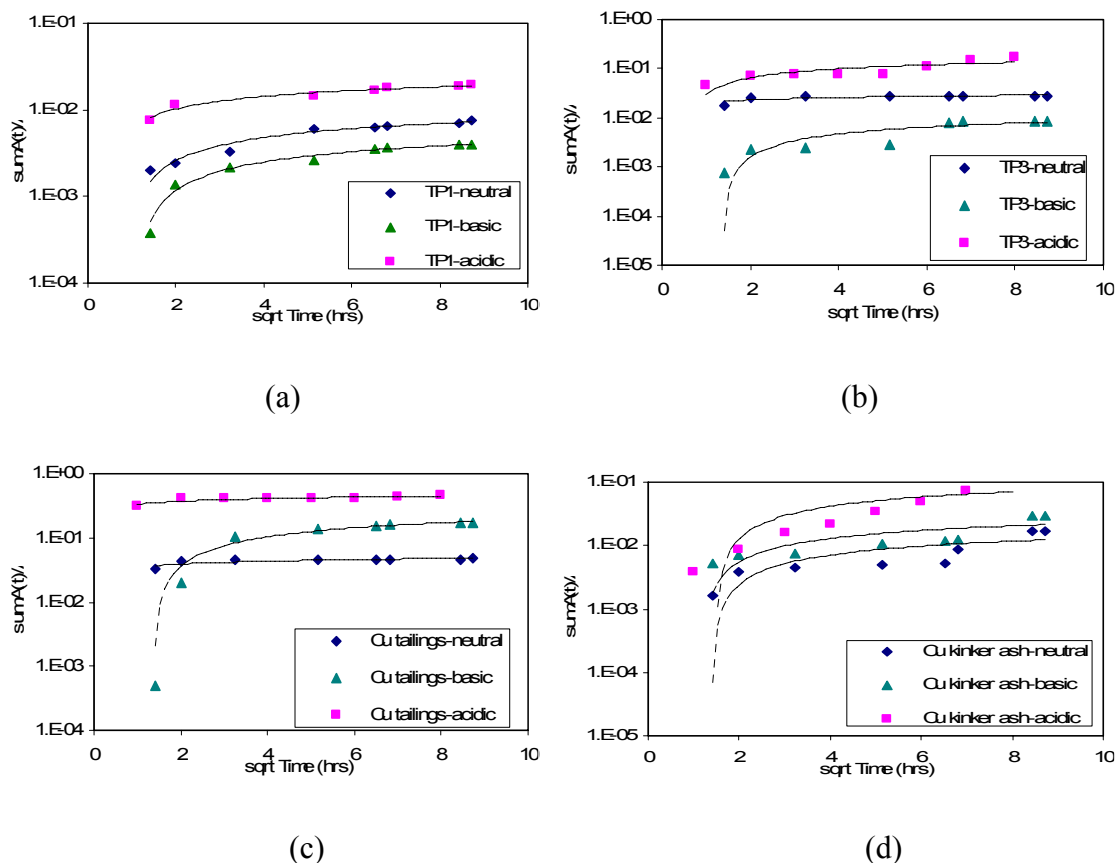


Fig. 83 . Cumulative fraction of U leached from wastes under different pH conditions (a) neutral, (b) acidic and (c) basic pH

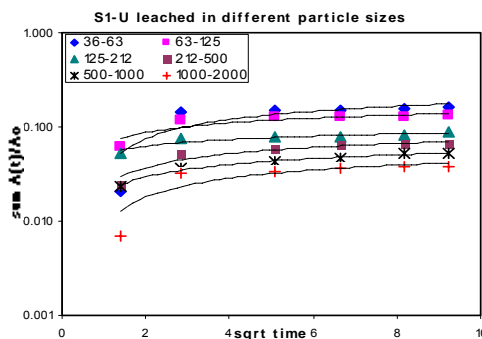
The leaching rate followed the order, acidic > basic > neutral in most cases; values of it under different pH conditions are given in table 49.

Table 49. Leaching rate of uranium from wastes under different pH conditions

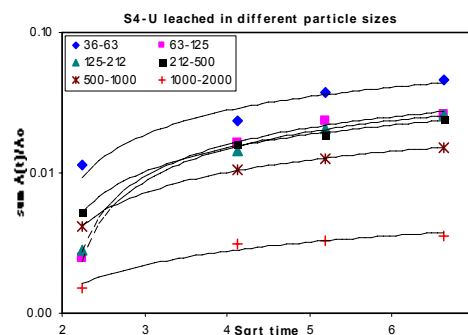
Leaching Rate (h^{-1})	TP3	TP1	RF	RT
Neutral	0.0004	0.0002	0.0001	0.0006
Acidic	0.0023	0.0014	0.0003	0.0060
Basic	0.0001	0.0004	0.0001	0.0022

4.3.2.2. Effect of particle size of sample

Different particle sizes of a sample subjected to dynamic leaching experiments exhibited differences in the parameters associated with leaching. The maximum cumulative fraction of U leached out from different particle sizes of soils are shown in fig. 84 (a), (b), (c) and (d) below. The maximum cumulative fraction of U leached out from soil 1 was 16.11, 13.07, 8.90, 6.62, 5.30 and 3.85% for 36-63 μm , 63-125 μm , 125-212 μm , 212-500 μm , 500-1000 μm and 1000-2000 μm , respectively. The maximum cumulative fraction of U leached out from soil 4 was 4.64, 2.64, 2.60, 2.40, 1.53 and 0.36% for 36-63 μm , 63-125 μm , 125-212 μm , 212-500 μm , 500-1000 μm and 1000-2000 μm , respectively.



(a)



(b)

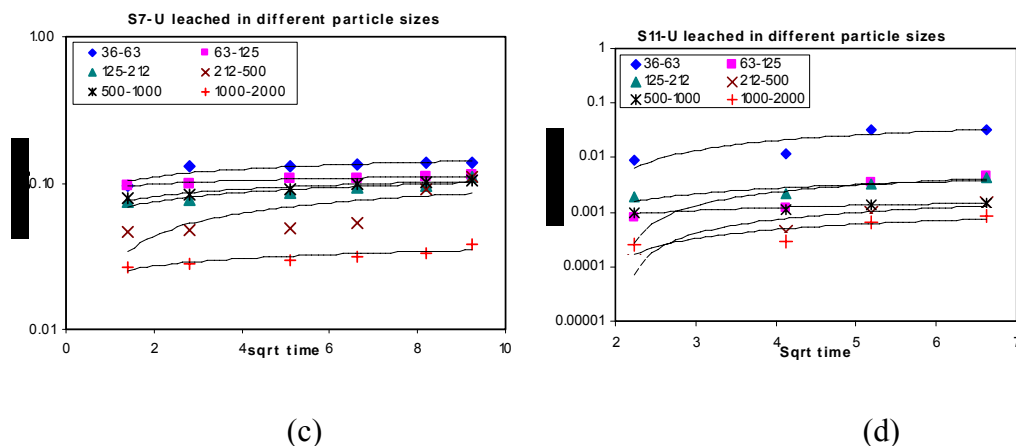


Fig. 84 . Cumulative fraction of U leached from wastes under different particle sizes

(a) soil 1, (b) soil 4 (c) soil 7 and (d) soil 11

The maximum cumulative fraction of U leached out from soil 7 was 13.90, 11.35, 11.01, 10.95, 10.57 and 3.84% for 36-63 μm , 63-125 μm , 125-212 μm , 212-500 μm , 500-1000 μm and 1000-2000 μm , respectively. The maximum cumulative fraction of U leached out from soil 11 was 3.33, 0.47, 0.42, 0.15, 0.15 and 0.08% for 36-63 μm , 63-125 μm , 125-212 μm , 212-500 μm , 500-1000 μm and 1000-2000 μm , respectively.

The leaching rate was highest for the smaller particle size fraction of soils and reduced with increasing particle size; values of it are given in table 50.

Table 50. Leaching rate of uranium from different particle sizes of soil

Leaching Rate (h^{-1})	36-63 μm	63-125 μm	125-212 μm	212-500 μm	0.5-1mm	1- 2mm
S1	0.00190	0.00154	0.00105	0.00078	0.00062	0.00045
S4	0.00106	0.00060	0.00059	0.00055	0.00035	0.00008
S7	0.00164	0.00133	0.00130	0.00129	0.00124	0.00045
S11	0.00076	0.00011	0.00009	0.00003	0.00003	0.00002

Like soils, different particle size fractions of uranium tailings were also subjected to batch leaching. The maximum cumulative fraction of U leached out from TP was 2.42, 1.17, 1.14, 0.89 and 0.48% for <36 μm , 36-63 μm , 63-125 μm , 125-212 μm and 212-500 μm , respectively, as evident from fig. 85.

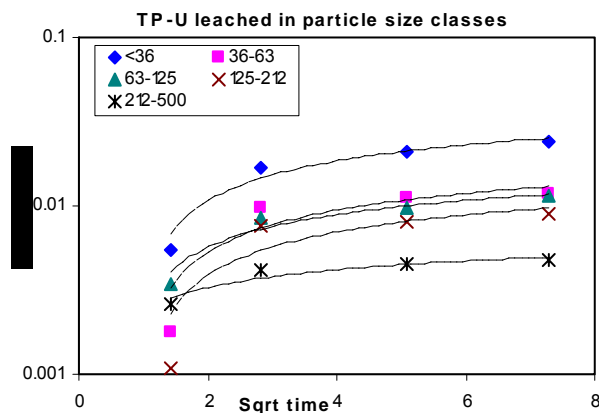


Fig. 85. Cumulative fraction of U leached from wastes under different particle sizes of uranium tailings

The leaching rate was highest for the smaller particle size fraction of uranium tailings and reduced with increasing particle size; values of it are given in table 51.

Table 51. Leaching rate of uranium from different particle sizes of uranium tailings

Leaching Rate (h^{-1})	<36 μm	36-63 μm	63-125 μm	125-212 μm	212-500 μm
TP	0.00046	0.00022	0.00021	0.00017	0.00009

4.3.2.3. Effect of temperature

The variation of temperature caused a change in the parameters of leaching for soils and waste samples as shown in fig. 86 (a) and (b) and fig. 86 (a), (b), (c) and (d). The maximum cumulative fraction of U leached out from soil 1 was 11.93 and 14.23% for

25°C and 60°C, respectively. The same for soil 11 was 0.97 and 2.49% for 25°C and 60 °C, respectively.

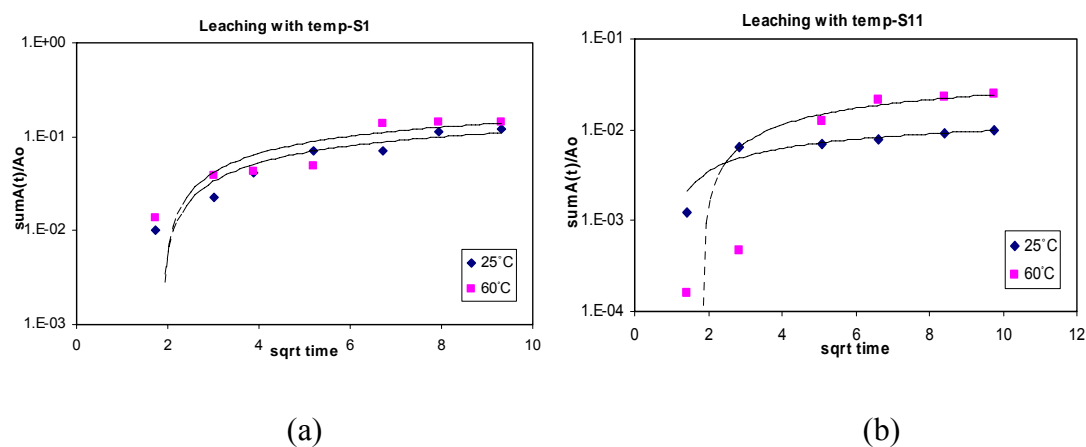


Fig. 86 . Cumulative fraction of U leached from (a) soil 1 and (b) soil 11 at different temperatures

The leaching rate was higher at elevated temperatures; values of it are given in table 52.

Table 52. Leaching rate of uranium from soils at different temperatures

Leaching Rate (h^{-1})	25°C	60°C
Soil 1	0.0014	0.0016
Soil 11	0.0001	0.0003

The maximum cumulative fraction of U leached out from TP1 was 0.34 and 0.87% for 25°C and 60°C, respectively. The same for TP3 was 0.33 and 1.24% for 25°C and 60 °C, respectively, as evident from fig. 87.

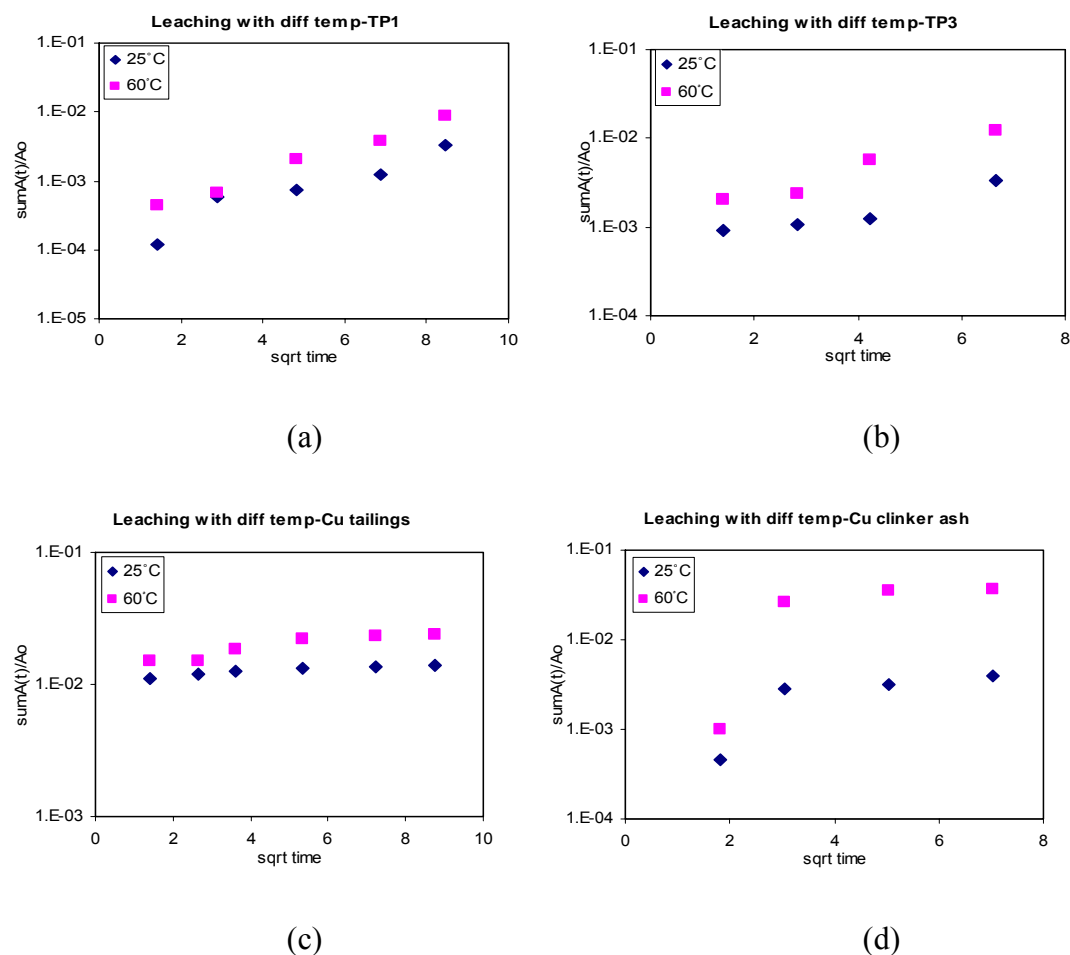


Fig. 87. Cumulative fraction of U leached from (a) U tailings TP1, (b) U tailings TP3, (c) Cu tailings and (d) Cu clinker ash at different temperatures

The maximum cumulative fraction of U leached out from copper tailings was 1.39 and 2.40% for 25°C and 60°C, respectively. The same for copper clinker ash was 0.40 and 3.69% for 25°C and 60 °C, respectively, as evident from fig. 87.

The leaching rate increased at elevated temperatures; values of it are given in table 53.

Table 53. Leaching rate of uranium from wastes at different temperatures

Leaching Rate (h^{-1})	25°C	60°C
TP1	0.00007	0.00008
RCF	0.00008	0.00075

TP3	0.00008	0.00028
RCT	0.00018	0.00031

Similar studies have been carried out to observe the effects of physical parameters on chalcopyrite leaching by Sokić et al. [259] and on leaching from coal fly ash by Otero-Rey et al. [260]. Brunori et al. [261] have carried out kinetic studies from treated abandoned mine-polluted soil, which attained equilibrium in a time period of 1000 minutes.

All the leaching rates obtained from semi-dynamic and dynamic leaching experiments were small. This indicates that the mobility of uranium from the matrices in this region is low and so there is a substantially low chance of uranium to reach the groundwater from these matrices and get transported in the environment.

CHAPTER 5

CONCLUSIONS AND FUTURE PROSPECTS

5.1. Conclusions

Radiological and chemical investigations coupled with laboratory based experiments have been employed in this thesis to gain knowledge on the transport and behaviour of elements in the highly mineralised Singhbhum Shear Zone in East Singhbhum district of Jharkhand state in Eastern India. The important findings from this thesis are summarised below:

1. Heterogeneous distribution of radionuclide activity in matrices like soils and rocks was observed due to their crustal nature of origin.
2. Radionuclide activity concentrations were found to be nearly constant and the lowest in Turamdih among the uranium deposits. Radionuclide activity concentrations in soils were observed to be of disseminated type and are not solely dependent on proximity to uranium deposits but mainly dependent on the regional geology and elemental geochemistry.
3. Average ^{238}U , ^{226}Ra and ^{232}Th activity concentrations were observed to be 4457 ± 2179 Bq/kg, 4940 ± 2478 Bq/kg and 30.4 ± 20.2 Bq/kg in ore samples from the uranium deposits of Jaduguda, Bhatin, Narwapahar and Turamdih; 107.8 ± 37.1 Bq/kg, 107.1 ± 37.6 Bq/kg and 59.8 ± 25.7 Bq/kg in non-uranium bearing rocks; 76.1 ± 59.6 Bq/kg, 81.5 ± 53.3 Bq/kg and 65.1 ± 22.7 Bq/kg in surface soils and 640.9 ± 101.1 Bq/kg, 1713.4 ± 75.7 Bq/kg and 38.3 ± 4.3 Bq/kg in uranium tailings.
4. The activity and activity ratios do not show a very clear trend with depth, in the deposits.
5. The $^{226}\text{Ra}/^{238}\text{U}$ daughter–parent pair was observed to be in secular equilibrium condition in the uranium deposits, especially Turamdih, while $^{231}\text{Pa}/^{235}\text{U}$, $^{227}\text{Ac}/^{235}\text{U}$

and $^{228}\text{Th}/^{228}\text{Ra}$ daughter–parent pairs are not in secular equilibrium in most samples from the deposits. The activity ratios of $^{226}\text{Ra}/^{230}\text{Th}$ suggest that the deposits were not closed to groundwater movement for a maximum time period of 8ky.

6. The Thiel plot of $^{234}\text{U}/^{238}\text{U}$ vs. $^{230}\text{Th}/^{238}\text{U}$ activity ratios indicates uranium accumulation and complex processes of uranium redistribution, but an overall slight shift from secular equilibrium condition in the uranium deposits.
7. The analysis of uranium and its daughter products in soils show deviation from secular equilibrium. Elemental mobility in soils is indicated and it is attributed to the system being open.

On the other hand, deviation from secular equilibrium (^{226}Ra - ^{238}U daughter-parent pair) in the case of uranium bearing tailings is attributed to the fact that the tailings are chemically treated for selective uranium extraction. Equilibrium was observed for copper tailings and copper clinker ash samples since they are not chemically treated for selective removal of an element.

Non-uranium bearing host rocks are in secular equilibrium, indicating that these are unfractured rocks which have not been affected by groundwater movements.

8. The analyses of various samples of uranium bearing rocks indicate that the Cu and Ba concentrations ranged from hundreds to thousands of ppm; Ni, Cu, Cr, U, La and Sm ranged from tens to hundreds of ppm and Sc, Co, Th and As concentrations were in tens of ppm. The Co, Sc, Ni, Cs, Sb, Th and Rb concentrations were in tens of ppm; Ce, La and Cu ranged from tens to hundreds of ppm in surface soils. The Co, Ba, Cr, Cu, U, Ni range from tens to hundreds of ppm; As, Hg, Th, Cd, Sb, Se, Sc range from sub ppm to ppm concentrations in tailings. The Zn, Rb, Cr and Co concentrations

range from tens to hundreds of ppm; Ni, Cu, Th and As concentrations were in tens of ppm; Se, U in ppm; Hg, Cs, Cd, Sb and Sc in sub-ppm to ppm range in non-uranium bearing rocks. Major elements, like Fe, Ca etc. indicate the presence of calcite in soils and pyrite nature of uranium tailings.

9. Different extents of negative Ce and Eu anomaly in uranium and non-uranium bearing host rocks reflected reducing conditions and hence uranium mineralisation in the uranium bearing rocks. The La/Sm ratio indicates light rare earth element fractionation and fractional condensation at the time of solidification of magma
10. Trace elements in soils and uranium tailings concentrate in smaller particle sizes due to their association with minerals like kaolinite, chlorite, montmorillonite, vermiculite etc. in the smaller particles. Mass balance of total elemental concentrations and sum of elemental concentrations in particle size fractionated samples showed a good match.
11. The siderophile elements Ni-Co were well-correlated; the chalcophile elements Se-Hg and Cd-Hg were found to be well correlated in non-uranium bearing rocks. This is due to the elemental properties and subsequent association with minerals in the environment. The Na and K concentrations are positively correlated with trace elements, indicating the mineralogical association of the elements with primary minerals of Na and K.
12. The cation exchange capacity (CEC) is positively correlated with moisture content, pH, clay content and Humic acid content in soils, showing the interrelation of these properties.

13. The leaching of uranium from soils, ores and wastes was very slow, being faster in the initial stage and then attaining a near steady state condition in laboratory experiments under semi-dynamic conditions carried over a long time. The apparent diffusion coefficient (cm^2/s) ranged from 10^{-10} to 10^{-11} .
14. In dynamic conditions of leaching, cumulative percent of U leached from soils was highest under basic pH conditions. For U tailings cumulative percent of U leached varied from 0.8-2.8%, 1.9-17.2% and 0.4-0.8% in the neutral, acidic and basic pH, respectively. Leaching rate ranged from $6 \times 10^{-4} \text{ h}^{-1}$ to $1.8 \times 10^{-3} \text{ h}^{-1}$, $8 \times 10^{-4} \text{ h}^{-1}$ to $6 \times 10^{-3} \text{ h}^{-1}$ and $5 \times 10^{-3} \text{ h}^{-1}$ to $1 \times 10^{-2} \text{ h}^{-1}$ from soils and $2 \times 10^{-4} \text{ h}^{-1}$ to $4 \times 10^{-4} \text{ h}^{-1}$, $1.4 \times 10^{-3} \text{ h}^{-1}$ to $2.3 \times 10^{-3} \text{ h}^{-1}$ and $1 \times 10^{-4} \text{ h}^{-1}$ to $4 \times 10^{-4} \text{ h}^{-1}$ from uranium tailings in the neutral, acidic and basic pH, respectively.
15. The leaching rate was observed to be variable for the different particle sizes, being higher in the lower particle sizes. This is due to the different reactive surface area of the different particle sizes.
16. With the increase in temperature the cumulative fraction of U leached increases; equilibrium condition is reached in the case of soil samples but not for U tailings samples in the time period of nearly 100hrs. The cumulative percent of U leached was higher at 60°C than at 25°C . The leach rate varies in same order of magnitude at 25°C and 60°C .
17. The leach rate under all the experimental conditions is observed to be low, indicating less mobility of uranium in the studied environment.

5.2. Future prospects

In future, studies will be carried out on the depth profile of radionuclides and trace element distributions in soils, uranium tailings etc. from the Singhbhum area. The equilibrium status of the natural radioactive series radionuclides in soils and uranium tailings ponds will also be examined to get a better idea of interaction of the same with groundwater and the possibility of elemental mobility. Disequilibrium studies will also be applied to ground water and soil pore water in this area to study the equilibrium/disequilibrium of $^{234}\text{U}/^{238}\text{U}$ and other radionuclides.

Since the environmental behaviour of an element is dependent on parameters like its oxidation state, chemical environment/ chemical association in the matrix, such information will be of aid in assessing its mobility, toxicity and geochemical behaviour. These properties will be probed by X-ray based techniques like EXAFS, XPS and XANES.

The chemical form of an element present in a matrix influences its mobility, transport and bioavailability. Studies on the chemical forms of uranium in different matrices can be ascertained by the use of single extractions (using specific solvents) and sequential batch extractions. These experiments have already been carried out in our lab. Preliminary investigations have yielded interesting results, making this an important avenue for further exploration in future.

REFERENCES

1. Gupta, R. and Siddique, S, 2003. Management of the tailings and liquid effluents in uranium mining and milling operations. *Radiation Protection and Environment*, 26(3 & 4), 506 -515.
2. NCRP Report No. 93, 1987. Ionising Radiation Exposure of the Population of the United States National Council on Radiation Protection and Measurements. Bethesda, MD.
3. Pearson, E. A. and Fraja Frangipane, E. D. Marine pollution and marine waste disposal: supplement to progress in water technology. In: *Proceedings of the Second International Congress on Marine Pollution and Marine Waste Disposal*, San Remo, 17–21 December 1973 (Library of Congress Catalog No. 75-16916).
4. UNSCEAR, 2000. Sources and Effects of Ionising Radiation, United Nations. Report to General Assembly with Scientific Annexes. United Nations, New York.
5. Neher, H. V., 1967. Cosmic ray particles that changed from 1954 to 1958. *Journal of Geophysics research*, 72.
6. UNSCEAR, 1988. Exposures from natural sources of radiation , United Nations. Report to General Assembly with Scientific Annexes. United Nations, New York.
7. Adams John A.S., 1977. The Geological origins of radioactive anomalies. *International symposium on areas of High Natural Radioactivity*, 6-11.
8. Taylor, S.R., 1964. Abundance of chemical elements in the Continental Crust: A new table, *Geochim. Cosmochim. Acta*, 28, 1273-1284.
9. Eisenbud Merrill, 1977. Summary report, *Proceedings of International symposium on High Natural Radioactivity*, Pocos de Caldas, Brazil June 16-20, 1975, eds. Cullen, T.L. and Penna Franca, E., 168-172.

10. Eisenbud, Merrill 1987. Environmental Radioactivity. Third Edition, 125-179.
11. Kamath, R.R., Menon, M.R., Shukla, V.K., Sadasivan, S., Nambi, K.S.V., 1996. Natural and fallout radioactivity measurement of Indian soils by Gamma spectrometric technique. Proceedings of the fifth National symposium on Environment, 56-60.
12. Mason, B., and Moore, C. B., 1984. Principles of Geochemistry. Fourth edition. John Wiley & Sons, Inc., New York., 344.
13. Hamaguchi, H., 1962. Study of radionuclides sorbed on marine sediments. Progress report. Contract No. 88/RI/Rb IV. IAEA, Vienna.
14. Sankaran, A.V., Jayaswal, B., Nambi K. S. V., Sunta, C. M., 1986. U, Th, and K Distributions Inferred from Regional Geology and Terrestrial Radiation Profiles in India. BARC Report.
15. The radiation protection authorities in Denmark, Finland, Iceland, Norway and Sweden, 2000. Naturally occurring radioactivity in the Nordic countries – Recommendations. ISBN 91-89230-00-0.
16. Lundström, U. S., van Breemen, N., Bain, D., 2000. The podzolisation process. A review. Geoderma, 94, 91-107.
17. Washington, J. W., Rose, A. W., 1992. Temporal variability of radon concentration in the interstitial gas of soils in Pennsylvania. Journal of Geophysical Research, 97(B6), 9145-9159.
18. Greeman, D. J., Rose, A. W., Jester, W. A., 1990. Form and behaviour of radium, uranium and thorium in Central Pennsylvania soils derived from dolomite. Geophysical Research Letters, 17(6), 833-836.

19. Wanty, R. B., Johnson, S. L., Briggs, P. H., 1991. Radon-222 and its parent nuclides in groundwater from two study areas in New Jersey and Maryland, U.S.A. *Applied Geochemistry*, 6, 305-318.
20. Ek, J., and Ek, B. M., 1996. Radium and Uranium Concentrations in two eskers with Enhanced Radon Emission. *Environment International*, 22 (Suppl. 1, 1996), S 495-S 498.
21. The Royal Society, 2001. The Health Hazards of Depleted Uranium Munitions, Part I. The Royal Society London.
22. Hopkins, B.S., 1923. *Chemistry of the Rarer Elements*, D.C. Heath and Company, Boston/NewYork/Chicago/London, Online at: http://www.sciencemadness.org/library/books/chemistry_of_the_rarer_elements.pdf.
23. Stegnar, P., Benedik, L., 2001. Depleted uranium in the environment—an issue of concern? *Arch. Oncol.*, 9, 251–255.
24. Rogers, J. J. W, and Adams, J. A. S., 1969. Uranium. In: *Handbook of Geochemistry*. Edited by Wedepohl, K. H. Springer-Verlag Heidelberg., 92 B-O.
25. Tieh, T. T., Ledger, E. B., Rowe, M. W., 1980. Release of uranium from granitic rocks during in situ weathering and initial erosion (central Texas). *Chemical Geology*, 29, 227-248.
26. Michel, J., 1984. Redistribution of uranium and thorium series isotopes during isovolumetric weathering of granite. *Geochimica et Cosmochimica Acta*, 48(6), 1249-1255.
27. Morawska, L., and Phillips, C. R., 1993. Dependence of the radon emanation on radium distribution and internal structure of the material. *Geochimica et Cosmochimica Acta*, 57, 1783-1797.

28. Wathen, J. B. (1987). The effect of uranium siting in two- mica granites on uranium concentrations and radon activity in ground water. In: Radon, Radium, and Other Radioactivity in Ground Water, (ed. B. Graves), Lewis Publishers. Pp. 31-46.
29. Berzina, I. G., Yeliseva, O. P., and Popenko, D. P. (1975). Distribution of uranium in intrusive rocks of Northern Kazakhstan. *International Geology Review*, 16(11), 1191-1204.
30. Gabelman, J. W. (1977). Migration of uranium and thorium - exploration significance. AAPG Studies in Geology no 3. American Association of Petroleum Geologists. Tulsa, Oklahoma. 168 pp.
31. Guthrie, V. A., and Kleeman, J. D. (1986). Changing uranium distributions during weathering of granite. *Chemical Geology* 54, 113-126.
32. Gundersen, L. C. S., Schumann, R. R., Otton, J. K., Dubiel, R. F., Owen, D. E., Dickinson, K. A., 1992. Geology of radon in the United States. In: Geologic controls on radon. Special Paper 271. Ed. Gates, A., Alexander, E, Gundersen, L. C. S. Geological Society of America, 1-16.
33. Langmuir, D., 1978. Uranium solution- mineral equilibria at low temperatures with applications to sedimentary ore deposits. *Geochimica et Cosmochimica Acta*, 42, 547-569.
34. Molinari, J., and Snodgrass, W. J., 1990. The chemistry and radiochemistry of radium and the other elements of the uranium and thorium natural decay series. In: *The Environmental Behaviour of Radium; Volume 1*. IAEA Technical Reports Series No 310. International Atomic Energy Agency, Vienna, 11-56.

35. Ames, L. L., McGarrah, J. E., and Walker, B. A., 1983. Sorption of trace constituents from aqueous solutions onto secondary minerals. I. Uranium. *Clays and Clay Minerals*, 31, 321-334.
36. Finch R. and Murakami T., 1999. Systematics and Paragenesis of Uranium Minerals. In *Uranium: mineralogy, geochemistry and the environment*, Vol. 38 (ed. P. C. Burns and R. Finch), Mineralogical Society of America, 91-180.
37. Langmuir, D. and Herman, J. S., 1980. The mobility of thorium in natural waters at low temperatures. *Geochimica et Cosmochimica Acta*, 44, 1753-1766.
38. Condomines, M., Loubeau, O., Patrier, P., 2007. Recent mobilisation of U- series radionuclides in the Bernardan U deposit (French Massif Central). *Chem. Geol.* 244, 304–315.
39. IAEA, 2003. Guidelines for radioelement mapping using gamma ray spectrometry data. IAEA-TECDOC-1363. IAEA, Vienna.
40. Ivanovich, M., Harmon, R.S., 1982. Uranium series disequilibrium – applications to environmental problems. Clarendon Press, Oxford.
41. Bourdon, B., Henderson, G.M., Lundstrom, C.C., Turner, S.P., 2003. “Uranium-series geochemistry” *Reviews in Mineralogy and Geochemistry* Vol. 52. Mineralogical Society of America.
42. Waite, T. David, and Payne, T. E., 1993. Uranium transport in the sub-surface environment. Koongarra - a case study. In *Metals in groundwater*. Edited by Allen, Herbert E., Perdue, E. Michael, and Brown, David S. Lewis Publishers, Chelsea, 349-410.
43. Hogue, J. R., Rose, A. W., and Jester, W. A., 1997. Patterns of disequilibrium among ^{238}U , ^{234}U , ^{230}Th and ^{226}Ra in total soil and soil phases in two soil profiles. In: *Generation and*

- mobility of radon in soils. Final Report to U.S. Dept. of Energy, Contract DE-FG02-87ER60577. Edited by A. W. Rose, Pennsylvania State University, Department of Geosciences. Appendix B. 43.
44. Vanden Bygaart, A. J., Protz, R., 1999. Gamma radioactivity in podzolic soils of Northern Ontario, Canada. *Journal Environmental Radioactivity*, 42, 51-64.
 45. Kigoshi, K., 1971. Alpha-Recoil thorium-234: Dissolution into Water and the Uranium-234/Uranium-238 Disequilibrium in Nature. *Science*, 173, 47-48.
 46. Åkerblom, G., Pettersson, B., Rosén, B., 1990. Markradon. Handbok för undersökning av markradonförhållanden. In the Series: Radon i bostäder. The Swedish Council for Building Research. Report R85: 1988, Stockholm.
 47. El-Dine, Nadia Walley, 2008. Study of natural radioactivity and the state of radioactive disequilibrium in U-series for rock samples, North Eastern Desert, Egypt. *Appl. Radiat. Isot.*, 66, 80-85.
 48. Min, Maozhong, Peng, Xinjian, Wang, Jinping, Osmond, J. K., 2005. Uranium-series disequilibria as a means to study recent migration of uranium in a sandstone-hosted uranium deposit, NW China. *Appl. Radiat. Isot.*, 63, 115-125.
 49. Rekha, A. K., Dingankar, M. V., Anilkumar, S., Narayani, K., Sharma, D. N., 2006. Determination of the activity ratios of ^{231}Pa to ^{235}U and ^{227}Th to ^{235}U in ore samples using gamma spectrometry. *J. Radioanal. Nuc. Chem.*, 268, 453-460.
 50. Ribeiro, Fernando Renha, Roque, Arnaldo, Boggiani, Paulo César, Floxor, Jean-Marie, 2001. Uranium and thorium series disequilibrium in quaternary carbonate deposits from the Serra Bodoquena and Pantanal do Miranda, Mato Grosso do Sul State, central Brazil. *Appl. Radiat. Isot.*, 54, 153-173.

51. Thiel, K., Vorwerk, R., Saager, R., Stupp, H. D., 1983. ^{235}U fission tracks and ^{238}U -series disequilibria as a means to study recent mobilisation of uranium in Arachean pyritic conglomerates. *Earth Planet. Sci. Lett.*, 65, 249-262.
52. Åkerblom, G., 1999. Concentrations of Radium-226, Thorium-232 and Potassium-40 in different types of rocks. Results compiled from different publications and from gamma ray spectrometric field measurements made during uranium exploration and geological surveys in the Nordic countries. Personal communication.
53. Ibraheim, N., 2003. Radioactive disequilibrium in the different rock types in Wadi Wizr, the Eastern Desert of Egypt. *Appl. Radiat. Isot.*, 58, 385-392.
54. Kokfelt, T.F., Lundstrom C., Hoernle, K., Hauff, F., Werner R., 2005. Plume-ridge interaction studied at the Galápagos spreading center: Evidence from ^{226}Ra - ^{230}Th - ^{238}U and ^{231}Pa - ^{235}U isotopic disequilibria. *Earth Planet. Sci. Lett.*, 234, 165-187.
55. Zhang, Guo-Liang, Zeng, Zhi-Gang, Beier, C., Yin, Xue-Bo, Turner, S., 2010. Generation and evolution of magma beneath the East Pacific Rise: Constraints from U-series disequilibrium and plagioclase-hosted melt inclusions. *Journal of Volcanology and Geothermal Research*, doi:10.1016/j.jvolgeores.2010.03.002
56. Van Orman, J.A., Saal, A.E., 2009. Influence of crustal cumulates on ^{210}Pb disequilibria in basalts. *Earth Planet. Sci. Lett.*, 284, 55-66.
57. Russo, C.J., Rubin, K.H., W. Graham, D.W., 2009. Mantle melting and magma supply to the Southeast Indian Ridge: The roles of lithology and melting conditions from U-series disequilibria. *Earth Planet. Sci. Lett.*, 278, 284-291.

58. Santos, R.N., Marques, L.S., 2007. Investigation of ^{238}U - ^{230}Th - ^{226}Ra and ^{232}Th - ^{228}Ra - ^{228}Th radioactive disequilibria in volcanic rocks from Trindade and Martin Vaz Islands (Brazil; Southern Atlantic Ocean). *J. Volcanology and Geothermal Research*, 161, 215-233.
59. Chakrabarti, R., Sims, K.W.W., Basu, A.R., Reagan, M., Durieux, J., 2009. Timescales of magmatic processes and eruption ages of the Nyiragongo volcanics from ^{238}U - ^{230}Th - ^{226}Ra - ^{210}Pb disequilibria. *Earth Planet. Sci. Lett.*, 288, 149-157.
60. Dosseto, A., Bourdon, B., Gaillardet, J., Allègre, C. J., Filizola, N., 2006. Timescale and conditions of chemical weathering under tropical climate: Study of the Amazon basin with U-series. *Geochimica et Cosmochimica Acta*, 70 (1), 71-89.
61. Dosseto, A., Turner, S.P., Douglas, G.B., 2006. Uranium-series isotopes in colloids and suspended sediments: Timescale for sediment production and transport in the Murray–Darling River system. *Earth Planet. Sci. Lett.*, 246, 418-431.
62. Dosseto, A., Turner, S.P., Chappell, J., 2008. The evolution of weathering profiles through time: new insights from uranium-series isotopes. *Earth Planet. Sci. Lett.* 274 (3-4) 359-371.
63. Granet, M., Chabaux, F., Stille, P., Dosseto, A., France-Lanord, C., Blaes, E., Galy, V., Pelt, E., 2010. U-series disequilibria in suspended river sediments and implication for their transfer time in alluvial plains: the case of the Himalayan rivers. *Geochimica et Cosmochimica Acta* 74, 2851-2865.
64. Cornu, S., Deschatrettes, V., Salvador-Blanes, S., Clozel, B., Hardy, M., Branchut, S., Le Forestier, L., 2005. Trace element accumulation in Mn-Fe-oxide nodules of a pliozoic horizon. *Geoderma* 125, 11-24.
65. Cousin, I., Cornu, S., Rose, J., Deschatrettes, V., Montagne, D., Clozel, B., Chevallier, P., 2005., Distribution of major and trace elements at the aggregate scale in a soil naturally

- rich in trace elements: A spatial approach using electron microprobe and X-ray microfluorescence analysis. *Soil Sci.* 170, 516-529.
66. Marques, J.J., Schulze, D.J., Curi, N., Martzman, S.A., 2004. Major element geochemistry and geomorphic relationships in Brazilian Cerrado soils. *Geoderma* 119, 179-195.
 67. Cameron, K.C., Di, H.J., McLoren, R.G., 1997. Is soil an appropriate dumping ground for our waste. *Aust. J. Soil Res.*, 33, 995-1035.
 68. Nriagu J.O., 1988. A silent epidemic of environmental poisonins. *Environmental Pollution*, 50, 139-161.
 69. Hendersen, P., 1982. *Inorganic geochemistry*, Pergamon press.
 70. Mason, B., 1966. *Principles of geochemistry*. Third edition, John Wiley and sons.
 71. Brooks, R.R., 2004. Pollution through trace elements, pp. 429-476.
 72. Vinogradov, A., Tugarinov, A., Zhykov, C., Spanikova, N., Bibikova, E., Khorre, K., 1964. Geochronology of Indian Precambrians, Rept. 22nd Intern. Geol. Cong. 10, 553-567.
 73. Alloway, B.J., 1990. *Heavy metals in soils*. John Wiley and sons, New York.
 74. Navratil, T., Minarik, L., 2005. Trace elements and contaminants, www.gli.cas.cz.
 75. Bohn, H.L., McNeal, B.L., O'Connor, G.A., 1979. *Soil chemistry*. John Wiley and sons.
 76. Burt, R., Wilson, M.A., Mays, M.D., Lee, C.W., 2003. Major and trace elements of selected pedons in the USA. *J. of Environ. Qual.* 32, 2109-2121.
 77. Mao, L. J., Mo, D. W., Yang, J. H. and Shi, C. X., 2009. Geochemistry of trace and rare earth elements in red soils from the Dongting Lake area and its environmental significance. *Pedosphere*, 19(5), 615–622.
 78. Kumru, M.N., Bakaç, M., 2003. R-mode factor analysis applied to the distribution of elements in soils from the Aydın basin, Turkey. *J. Geochem. Explor.*, 77, 81-91.

79. Bakaç, M., 2000. Factor analysis applied to geochemical study of suspended sediments from the Gediz River, western Turkey. *Environ. Geochem. Health.*, 22, 93-111.
80. Laveuf, C., Cornu, S., 2009. A review on the potentiality of Rare Earth Elements to trace pedogenetic processes. *Geoderma*, 154, 1-12.
81. Carman Rivas, M., 2005. Interactions Between Soil Uranium Contamination and Fertilisation with N, P and S on the Uranium Content and Uptake of Corn, Sunflower and Beans, and Soil Microbiological Parameters (Special Issue). *Landbauforschung Völkenrode–FAL Agricultural Research*, Braunschweig, Germany.
82. Bibler, J.P., Marson, D.B., 1992. Behavior of mercury, lead, cesium, and uranyl ions on four SRS soils (U). Technical Report, Westinghouse Savannah River Company Savannah River Site, WSR-RP-92-326, Online at: <http://www.osti.gov/energycitations/servlets/purl/7064035-hwmdrD/7064035.PDF>.
83. Allard, B., Olofsson, U., Torstenfelt, B., Kipasti, H., Andersson K., 1982. Sorption of actinides in well-defined oxidation states on geologic media. *Mater. Res. Soc. Symp. Proc.* 11, 775–782.
84. Fedotov, P. S., Spivakov B. Ya, 2008. Fractionation of elements in soils, sludges and sediments: batch and dynamic methods. *Russian Chemical Reviews*, 77 (7) 649 – 660.
85. Kennedy, V.H., Sánchez, A.L., Oughton, D.H., Rowland, A.P., 1997. Use of Single and Sequential Chemical Extractants to Assess Radionuclide and Heavy Metal Availability From Soils for Root Uptake. *Analyst* 122, 89R-100R.
86. Garrabrants, A.C., Kosson, D.S., 2005. Leaching processes and evaluation tests for inorganic constituent release from cement-based matrices. *Stabilisation and solidification*

- of hazardous, radioactive and mixed waste. R. Spence and C. Shi. Boca Raton, CRC Press, 229-280.
87. Oughton, D. H., Salbu, B., 1994. The Transfer of Radionuclides Through Nordic Ecosystems to Man : in Nordic Radioecology, ed. Dahlgaard, H., Elsevier, Oxford, 165–184.
88. Jackson, D.R., Garrett, B.C., Bishop, T.A., 1984. Comparison of batch and column methods for assessing leachability of hazardous waste. *Environ. Sci. Tech.*, 18, 668-673.
89. Caldwell, R., Constable, T.W., Cote, P., McLellan, J., Sawell, S.E., Stegemann, J., 1990. Compendium of Waste Leaching Tests, Environmental Protection Series.
90. Kjeldsen, P., Christensen, T.H., 1990. Leaching tests to evaluate pollution potential of combustion residues from an iron recycling industry. *Waste Management & Research*, 8, 277-192.
91. Förstner, U., Calmano, W., Kienz, W., 1991. Assessment of long-term metal mobility in heat-processing wastes. *Water Air Soil Poll.*, 57-58, 319-328.
92. Sawhney, B. L., Frink, C.R., 1991. Heavy metals and their leachability in incinerator ash. *Water Air Soil Poll.*, 57-58, 289-296.
93. Wasay, S.A., 1992. Leaching study of toxic trace elements from fly ash in batch and column experiment. *Journal of Environmental Science and Health A*, 27(3), 697-712.
94. Van der Sloot, H. A., Heasman, L., Quevauviller, P., 1997. Harmonisation of leaching/extraction tests. *Studies in Environmental Science*. Amsterdam, Elsevier.
95. Jang, A., Choi, Y. S., Kim, I. S., 1998. Batch and column tests for the development of an immobilisation technology for toxic heavy metals in contaminated soils of closed mines. *Water Science and Technology*, 37(8), 81-88.

96. Kosson, D.S., van der Sloot, H.A., Sanchez, F., Garrabrants, A. C., 2002. An integrated framework for evaluating leaching in waste management and utilisation of secondary materials. *Environmental Engineering Science*, 19(3), 159-204.
97. Dutta, B.K., Khanra, S., Mallick, D., 2009. Leaching of elements from coal fly ash: assessment of its potential for use in filling abandoned coal mines. *Fuel*, 88, 1314-1323.
98. Kumar, V., Sharma, P., 1998. Mission mode management of fly ash: Indian experience. *J Coal Ash Inst India* 2, 90-95.
99. ANS, 1986. American national standard measurements of the leachability of solidified low-level radioactive wastes by a short-term test procedure, ANSI/ANS, 16.1, in: *American Nuclear Society (Eds.), La Grange Park, Illinois*.
100. Moon, D.H., Dermatas, D., 2007. Arsenic and lead release from fly ash stabilised/solidified soils under modified semi-dynamic leaching conditions. *J. Hazard.Mater.*, 141, 388-394.
101. Abdel Rahman, R.O., Zaki, A.A., El-Kamash, A.M., 2007. Modeling the long-term leaching behaviour of ^{137}Cs , ^{60}Co and $^{152,154}\text{Eu}$ radionuclides from cement-clay matrices. *J. Hazard.Mater.*, 145, 372-380.
102. Ettler, V., Piantone, P., Touray, J. C., 2003. Mineralogical control on inorganic contaminant mobility in leachate from lead-zinc metallurgical slag: experimental approach and long-term assessment. *Mineral. Mag.*, 67 (6), 1269-1283.
103. Kakovskii, I.A., Potashnikov, Yu.M., 1975. *Kinetika Protsessov Rastvoreniya (Kinetics of Dissolution Processes)*. Moscow: Metallurgiya.

104. Ovchinnikov, A.A., Timashev, S.F., Belyi, A.A., 1986. Kinetika Diffuzionno-kontroliruemykh Khimicheskikh Protsessov (Kinetics of Diffusion-controlled Chemical Processes). Moscow: Khimiya.
105. Chernyak, A.S., 1998. Protsessy Rastvoreniya: Vyshchelachivanie, Ekstraktsiya (Dissolution Processes. Leaching, Extraction). Irkutsk: Irkutsk State University.
106. Van der Sloot, H. A., Comas, R. N. J., Hjelmar, O., 1996. Similarities in the leaching behaviour of trace contaminants from waste, stabilised waste, construction materials and soils. *Sci. Total Environ.* 178, 111-126.
107. Quevauviller, Ph., 2002. Methodologies for soil and sediment Fractionation Studies, RSC, Cornwall, UK.
108. Wilkins, B. T., Green, N., Stewart, S. P., Major, R. O., Dodd, N. J., 1984. Seminar on the Behaviour of Radionuclides in Estuaries. Renesse 17-21 September. Council for the European Community, Luxembourg, 55–70.
109. Nirel, P., Thomas, A. J., and Martin, J. M., 1986. Speciation of Fission Activation Products, ed. Bulman, R. A., and Cooper, J. R., Elsevier Applied Science, London, 19–26.
110. Sahuquillo, A., Rigol, A., Rauret, G., 2003. Overview of the use of leaching/ extraction tests for risk assessment of trace elements in contaminated soils and sediments. *Trends in Anal. Chem.*, 22(3), 152-159.
111. Al-Hashimi, A., Evans, G.J., Cox, B., 1996. Aspects of the permanent storage of uranium tailings. *Water Air Soil Poll.* 88, 83-92.
112. IAEA, 1986. Environmental migration of radium and other contaminants present in liquid and solid wastes from the mining and milling of uranium. IAEA-TECDOC-370. IAEA, Vienna.

113. Townsend, Timothy, Jang, Yong-Chul, Tolaymat, Thabet, 2003. A Guide to the Use of Leaching Tests in Solid Waste Management Decision Making. Report #03-01(A), Gainesville, Florida.
114. Goumans, J., van der Sloot, H., and Aalbers, Th., 1991. Waste Materials in Construction, Elsevier, Amsterdam, The Netherlands.
115. Jang, Y., Townsend, T., Ward, M., and Bitton, G., 2002. Leaching of Arsenic, chromium, and copper in a contaminated soil at a wood preserving site, Bull. Environ. Contam. Toxicol., 69, 808-816.
116. Grimshaw, H. M., 1989. In Chemical Analysis of Ecological Materials, ed. Allen, S. E., Blackwell Scientific Publications, Oxford, 7–45.
117. Oughton, D. H., Salbu, B., Riise, G., Lien, H., Østby, G., Nøren, A., Analyst, 1992, 117, 481.
118. Wilkins, B. T., Green, N., Stewart, S. P., Major, R. O., 1986. In Speciation of Fission and Activation Products in the Environment, ed. Bulman, R. A., and Cooper, J. R., Elsevier, New York, 101–113.
119. Tessier, A., Campbell, P.G.C.; Bisson, M., 1979. Sequential extraction procedure for the speciation of particulate trace metals. Anal. Chem., 51, 844-851.
120. Ettler, V., Komárková, M., Jehlička, J., Coufal, P., Hradil, D., Machovič, V., Delorme, F., 2004. Leaching of lead metallurgical slag in citric solutions-implications for disposal and weathering in soil environments. Chemosphere, 57, 567-577.
121. Moon, D.H., Dermatas, D., 2006. An evaluation of lead leachability from stabilised/solidified soils under modified semi-dynamic leaching conditions. Eng. Geol., 85, 67–74.

122. Sahuquillo, A., Rigol, A., Rauret, G., 2002. Comparison of leaching tests for the study of trace metals remobilisation in soils and sediments. *J. Environmen. Monit.* 4, 1003-1009.
123. Bhola, K.L., 1964. Uranium prospecting and mining in India. Symposium held at Jaduguda, Oct 1964, 79.
124. ISM, 2009. Baseline studies of Bagjata and Banduhurang Sites of UCIL. DAE/187(1)/2007BRNSProject#2005/36/22-BRNS/584.
125. Bhasin J.L., 1997. Mining and milling of uranium ore: Indian scenario; IAEA-TECDOC-1244, 2001, 189-200.
126. Geological survey of India, 1975. Geology and mineral resources of the states of India, Part V – Bihar. Miscellaneous publication no. 30.
127. Mahur, A. K., Kumar, R., Sonkawade, R. G., Sengupta, D., Rajendra Prasad, 2008. Measurement of natural radioactivity and radon exhalation rate from rock samples of Jaduguda uranium mines and its radiological implications, *Nuclear Instruments and Methods in Physics Research B* 266, 1591–1597.
128. IAEA, 2009. World distribution of uranium deposits (UDEPO) with uranium deposit classification. IAEA-TECDOC- 1629. IAEA, Vienna.
129. Dikshitulu, G. R., Dhana Raju, R., Gajapathi Rao, R., 1997. Uranium mineralisation at Mouldih, Singhbhum shear zone, Bihar – An ore petrological study. *Journal of Atomic mineral science* 5, 81-86.
130. Bhola, K.L., 1968. Uranium deposits in Singhbhum and their development for use in the nuclear power programme in India. Symposium on Geology and Mineralogy of Atomic Mineral Deposits and Their Development for use in the Nuclear Power Programme in India, Vol 37, A, No. 4, 277-296.

131. Rao, N.K., 1977. Mineralogy, petrology and geochemistry of uranium prospects from parts of Singhbhum shear zone, Bihar. Ph.D. thesis, Banaras Hindu University.
132. Shankaran, A., V., Bhattacharyya, T.K., Dar K.K., 1970. Rare earth and other trace elements in uraninites. Jour. Geol. Soc. India 11, 205-216.
133. Sarkar, S.C., 1982. Uranium (nickel-cobalt-molybdenum) mineralisation along the Singhbhum copper belt, India and the problem of ore genesis. Mineral Deposita 17, 257-278.
134. Rao, N.K., Aggarwal, S.K., Rao, G.V.U., 1979. Lead isotope ratios of uraninites and the age of uranium mineralisation in Singhbhum shear zone, Bihar. Jour. Geol. Soc. India 20, 124-127.
135. Markose, P.M., 1990. Studies on the Environmental behavior of Radium from uranium mill tailings, Ph.D. Thesis, University of Mumbai, 62.
136. Jha, S., Khan, A.H., Mishra, U.C., 2000. A study of the ^{222}Rn flux from soil in the U mineralised belt at Jaduguda. J. Env. Radioact., 49, 157-169.
137. Jha, S., Khan, A.H., Mishra, U.C., 2000. Environmental Rn levels around an Indian U complex. J. Env. Radioact., 48, 223-234.
138. Jha, S., Khan, A.H., Mishra, U.C., 2001. A study of the technologically modified sources of ^{222}Rn and its environmental impact in an Indian U mineralised belt. J. Env. Radioact., 53, 183-197.
139. Sengupta, D., Kumar, R., Singh, A.K., Prasad, R., 2001. Radon exhalation and radiometric prospecting on rocks associated with Cu-U mineralisations in the Singhbhum shear zone, Bihar. App. Rad. Isot., 55, 889-894.

140. Singh, A.K., Sengupta, D., Prasad, R., 1999. Radon exhalation rate and uranium estimation in rock samples from Bihar uranium and copper mines using the SSNTD technique. *App. Rad. Isot.*, 51, 107-113.
141. Sengupta, D., Mitra, S., Patnaik, S.K., Ghosh, A.R., 1996. Radiometric prospecting and physical assay of rock samples from Singhbhum, Bihar. *Indian J. Geol.*, 68, 20-26.
142. Kumar, R., Sengupta, D., Prasad, R., 2003. Natural radioactivity and radon exhalation studies of rock samples from Surda Copper deposits in Singhbhum shear zone. *Radiat. Measur.*, 36, 551 – 553.
143. Jha, V.N., Sethy, N.K., Sahoo, S.K., Shukla, A.K., Tripathi, R.M., Puranik, V.D., 2009. A comparative study of radiological environment around an operating uranium industry and proposed sites in Singhbhum region of Jharkhand, India. *Radiation protection and environment*, 32 (1-2), 57-61.
144. Jha, V.N., Sethy, N.K., Sahoo, S.K., Shukla, A.K., Tripathi, R.M., Khan, A.H., 2009. A comparison of radioactivity level in discharged waste and natural sources in uranium mineralised areas of Singhbhum, Jharkhand, India. *Proceedings of 27th IARP National conference on occupational and environmental radiation protection*, 28(1-4), 284-286.
145. Mishra, S., Bhalke, S., Manikandan, S.T., Sunny Fabby, Nair, R.N., Pandit, G.G., Puranik, V.D., 2008. Migration of metals into groundwater from U TP. *Proceedings of 16th NSE*, 86-89.
146. IAEA, 2004. Soil sampling for environmental contaminants. AEA-TECDOC-1415, International Atomic Energy Agency, Vienna.
147. Popek, E. M., 2003. Sampling and analysis of environmental chemical pollutants, Academic Press, Elsevier, USA.

148. Scwedt, G., 1997. The Essential Guide to Analytical Chemistry (Translation of the revised and updated German Second Edition. Translated by Brooks Haderlie), John Wiley & Sons, England.
149. Adeloju, S.B., Bond, A.M. and Briggs, M.H., 1985. Multielemental determination in biological materials by differential pulse voltammetry. *Analytical Chemistry*, 57, 1386 - 1390.
150. Milford, J.B. and Davidson, C.I., 1985. The sizes of particulate trace elements in the atmosphere. A review *APCA journal*, 35, 1249-1260.
151. Chan, W.H., Thonassini, F. and Loescher, B., 1983. An evaluation of sorption properties of precipitation constituents on polyethylene surfaces. *Atmos. Environ.*, 17, 1779-1785.
152. Stumpler, A.W., 1973. Adsorption characteristics of Ag, Pb, Cd, Zn and Ni on borosilicate glass, polyethylene and polypropylene container surfaces. *Analytical Chemistry*, 15, 2251.
153. U.S. Environmental Protection Agency (EPA), 1992. Manual for the Certification of Laboratories Analyzing Drinking Water: Criteria and Procedures. Fourth Edition, EPA 814-B-92-002, Office of Ground Water and Drinking Water, Cincinnati, Ohio.
154. Knoll, G. F., 1999. Radiation Detection and measurement, 3rd edition, Wiley, ISBN 978-0471073383.
155. Shukla, V. K., Chinnaesakki, S., Shanbhag, A. A., Sartandel, S. J., Srivastava, G. K., Khan, A. H., Puranik, V. D., 2004. Proceedings of the National Symposium on Environment, 445-448.
156. De Corte, F., 1987. The k₀-standardisation method: A move to the optimisation of NAA. Agrege Thesis. Belgium: University of Gent.

157. Simonits, A., De Corte, F., Hoste, J., 1975. Single-comparator methods in reactor neutron activation analysis. *J. Radioanal. Chem.*, 24, 31 – 46.
158. Kolotov, V. P., De Corte, F., 2004. Compilation of k_0 and related data for neutron-activation analysis (NAA) in the form of an electronic database. IUPAC Technical Report. *Pure Appl. Chem.*, 76(10), 1921–1925.
159. Bode, P., van Dijk, C.P., 1997. Operational management of results in INAA utilizing a versatile system of control charts. *J. Radioanal. Nuc. Chem.*, 215 (1), 87-94.
160. Tosheva, Z., Stoyanova, K., Nikolchev, L., 2004. Comparison of different methods for uranium determination in water. *Journal of Environ. Radioact.*, 72, 47-55.
161. Manuals for fluorimeter, 2001. Raja Ramanna Centre for Advanced Technology, DAE, India.
162. Veselsky, J.C., Kwiecinska, B., Wehrstein, E., Suschny, O., 1988. Determination of uranium in minerals by laser fluorimeter. *Analyst*, 113, 451-455.
163. Sahoo, S. K., Sekhar Singh, Chakrabarty, A., Mohapatra, S., Sumesh, C. G., Tripathi, R. M., Puranik, V. D, 2009. Concentration of uranium in packaged drinking water by laser fluorimetry. In: *Proceedings of the Eighth DAE-BRNS National Laser Symposium*, Cat.11-2-1-2.
164. Sahoo, S. K., Tripathi, R. M., Chakrabarty, A., Mohapatra, S., Sumesh, C. G., Puranik, V. D, 2008. Optimisation of method parameters for estimation of uranium at nanogram level in drinking water samples by laser fluorimeter. In: *Proceedings of the Indian Analytical Science Congress 2008*, 111–112.
165. Rathore, D. P. S., Tarafder, P. K., Kayal, M. , Manjeet Kumar, 2001. Application of a differential technique in laser-induced fluorimeter: simple and a precise method for the

- direct determination of uranium in mineralised rocks at the percentage level. *Anal. Chim. Acta*, 434, 201–208.
166. Rani, A., Singh, S, 2006. Analysis of uranium in drinking water samples using laser induced fluorimetry. *Health Phys.* 91(2), 101–107.
167. Singh, S., Rani, A., Mahajan, R. K., Walia, T. P. S., 2003. Analysis of uranium and its correlation with some physicochemical properties of drinking water samples from Amritsar, Punjab. *J. Environ. Mon.* 5, 917–921.
168. Beauregard, M.R., Mikulak, R.J., Olson, B.A., 1992. *A Practical Guide to Statistical Quality Improvement: Opening Up the Statistical Toolbox*. Van Nostrand Reinhold, New York.
169. Montgomery, D.C., 2001. *Introduction to Statistical Quality Control*, 5th edn. Wiley, New York.
170. Morrison, L. W., 2008. The use of Control Charts to Interpret Environmental Monitoring data. *Natural Areas Journal*, 28 (1), 66-73.
171. Ghosh, A.B., Bajaj, J.C., Hasan, R., Singh, D., 1983. *Soil and water testing methods*. Indian Agricultural Research Institute, New Delhi, India.
172. Gillman, G.P., 1979. A proposed method for the measurement of exchange properties of highly weathered soils. *Aust. J. Soil. Res.*, 17, 129-139.
173. Gillman, G.P., Sumpter, E.A., 1986. Modification to the compulsive exchange method for measuring exchange characteristics of soils. *Aust. J. Soil Res.*, 24:61-66.
174. Rhoades, J.D., 1982. Cation exchange capacity. In: A.L. Page (ed.) *Methods of soil analysis, Part 2 Chemical and microbiological properties*, 2nd edition. *Agronomy*, 9, 149-157.

175. Sumner, M. E., Miller, W. P., 1996. Cation exchange capacity , and exchange coefficients. In: D. L. Sparks (ed.) Methods of soil analysis. Part 2: Chemical properties, (3rd ed.) ASA, SSSA, CSSA, Madison, WI.
176. Kandráč, J., Hutta, M., Foltin, M., 1996. Preparation and characterisation of humic and fulvic acid working standards - practical experience. Journal of Radioanal. and Nuc. Chem., 208 (2), 577-592.
177. Anđelković, T., Anđelković, D., Perović, J., Purenović, M., Polić, P., 2001. Decrease of oxygen interference on humic acid Structure alteration during isolation. Facta universitatis Series: Physics, Chemistry and Technology, 2(3), 163 – 171.
178. García-Talavera, M., 2003. Evaluation of the suitability of various γ lines for the γ spectrometric determination of ^{238}U in environmental samples. Appl. Radiat. Isot., 59, 165-173.
179. Morillon, C., Bé, M.M., Lamé, J., Jean, C., 2000. Nucléide- Lara. ISBN 2-7272-212-1, CEA-LNHB, Saclay.
180. Kim, K. H., Burnett, W. C., 1985. ^{226}Ra in phosphate nodules from the Peru/ Chile seafloor. Geochim. Cosmochim. Acta, 49, 1073-1081.
181. Yucel, H., Cetiner, M.A., Demirel, H., 1998. Use of the 1001 keV peak of $^{234\text{m}}\text{Pa}$, daughter of ^{238}U in measurement of uranium concentration by HPGe gamma-ray spectrometry. Nuc. Inst. Methods, 413, 74-82.
182. EPA, 1996. Guidance for Data Quality Assessment, Practical Methods for Data Analysis, EPA QA/G-9, QA96 Version, EPA/600/R-96/084, U.S. Environmental Protection Agency, Office of Research and Development, Washington, DC.
183. Conover, W.J., 1980. Practical Nonparametric Statistics, 2nd edn. Wiley, New York.

184. Gilbert, R.O., 1987. Statistical Methods for Environmental Pollution Monitoring, Van Nostrand Reinhold, New York (now published by Wiley & Sons, New York, 1997).
185. Gismera, M.J., Lacal, J., Da Silva, P., García, R., Sevilla, M.T., Procopio, J. R., 2004. Study of metal fractionation in river sediments. A comparison between kinetic and sequential extraction procedures. *Environ. Pollut.*, 127, 175-182.
186. Cochram, J.K., 1992. The oceanic chemistry of the uranium and thorium series nuclides. In: Ivanovich, M., Harmon, R.S. (Ed), *Uranium series Disequilibrium: Applications to Earth, Marine and Environmental Sciences*. Clarendon Press, Oxford, 334–395.
187. Sam, A.K., 2000. The state of disequilibrium between U and Th series isotopes in marine sediments from the Sudanese Red Sea Coast. In: *Fifth Arab Conference on the Peaceful uses of Atomic Energy*, Beirut, 13–17/11/2000.
188. Richter, S., Alonso, A., Bolle, W. De, Wellum, R., Taylor, P.D.P., 1999. Isotopic “fingerprints” for natural uranium in ore samples. *Int. Journal of Mass Spec.* 193, 9-14.
189. Gascoyne, M., Millera, N.H., Neymarkb, L.A., 2002. Uranium series disequilibrium in tuffs from Yucca Mountain, Nevada, as evidence of pore-fluid over the last million years. *Appl. Geochem.* 17, 781-795.
190. Kam, E., Bozkurt, A., Ilgar, R., 2010. A study of background radioactivity level for Canakkale, Turkey. *Environ. Monit. Assess.* DOI 10.1007/s10661-009-1143-y.
191. Colmenero Sujo, L., Montero Cabrera, M.E., Villalba, L., Rentería Villalobos, M., Torres Moye, E., García León, M, García-Tenorio, R., Mireles García, F., Herrera Peraza, E.F., Sánchez Aroche, D., 2004. Uranium-238 and thorium-232 series concentrations in soil, radon-222 indoor and drinking water concentrations and dose assessment in the city of Aldama, Chihuahua, Mexico. *J. Environ. Radioact.*, 77, 205-219.

192. Al-Jundi, J., 2002. Population doses from terrestrial gamma exposure in areas near to old phosphate mine, Russaifa, Jordan. *Radiat. Measur.*, 35, 23-28.
193. Fernandes, H. M., Simoes Filho, F.F.L., Perez, V., Franklin, M.R., Gomiero, L.A., 2006. Radioecological characterisation of a uranium mining site located in a semi-arid region in Brazil. *J. Environ. Radioact.*, 88 140-157.
194. Baykara, O., Doğru, M., 2009. Determinations of terrestrial gamma, ^{238}U , ^{232}Th and ^{40}K in soil along fracture zones. *Radiat. Meas.*, 44 (1), 116-121.
195. Arogunjo, A.M., Höllriegl, V., Giussani, A., Leopold, K., Gerstmann, U., Veronese, I., Oeh, U., 2009. Uranium and thorium in soils, mineral sands, water and food samples in a tin mining area in Nigeria with elevated activity. *J. Environ. Radioact.*, 100, 232-240.
196. Oyedele, J.A., Shimboyo, S., Sitoka, S., Gaoseb, F., 2010. Assessment of natural radioactivity in the soils of Rössing Uranium Mine and its satellite town in western Namibia, southern Africa. *Nucl. Instr. And Meth. A*, doi:10.1016/j.nima.2010.01.068.
197. Malczewski, D., Teper, L., Dorda, J. Assessment of natural and anthropogenic radioactivity levels in rocks and soils in the environs of Swieradow Zdroj in Sudetes, Poland, by in situ gamma-ray spectrometry. *J. Environ. Radioact.*, 73, 233-245.
198. Yang, Ya-xin, Wu, Xin-min, Jiang, Zhong-ying, Wang, Wei-xing, Lu, Ji-gen, Lin, Jun, Wang, Lei-Ming, Hsia, Yuan-fu, 2005. Radioactivity concentrations in soils of the Xiazhuang granite area, China. *Appl. Radiat. Isot.*, 63, 255-259.
199. Murty, V.R.K., Karunakara, N., 2008. Natural radioactivity in the soil samples of Bostwana. *Radiat. Meas.*, 43, 1541-1545.
200. Ahmad, N. et al., 1997. Indoor radon levels and natural radioactivity in Jordanian soil. *Radiat. Protect. Dosim.* 71 (3), 231-233.

201. Karahan, G. et al., 2000. Assessment of gamma dose rates around Istanbul. *J. Environ. Radioact.* 47, 213-221.
202. Florou, H. et al., 1992. Gamma radiation measurements and dose rates in the coastal areas of a volcanic island, Aegean Sea, Greece. *Radiat. Protect. Dosim.*, 45 (1/4), 277-279.
203. Yu-Ming, L. et al., 1987. Measurement of terrestrial gamma radiation in Taiwan, Republic of China. *Health Physics*, 52, 805-811.
204. Fernandez, J.C. et al., 1992. Natural radiation in Tenerife (Canary Islands). *Radiat. Protect. Dosim.*, 45 (1/4), 545-548.
205. Baeza, A. et al., 1992. Natural radioactivity in soils in the province of Caceres (Spain). *Radiat. Protect. Dosim.*, 45 (1/4), 261-263.
206. Bellia, S. et al., 1997. Natural radioactivity in a volcanic island Ustica, Southern Italy. *Appl. Radiat. Isot.*, 48, 287-293.
207. Martinez-Aguirre, A. et al., 1997. Radioactivity impact of phosphate ore processing in a wet marshland in southwestern Spain. *J. Environ. Radioact.*, 34, 45-57.
208. Dickson, B.L., 1995. Uranium-series disequilibrium in Australian soils and its effect on aerial gamma-ray surveys. *J. Geochem. Explor.*, 54, 177-186.
209. Damla, N., Cevik, U., Ihsan Kobya, A., Ataksor, B., Isik, U., 2010. Assessment of environmental radioactivity for Batman, Turkey. *Environ. Monit. Assess.*, 160, 401–412.
210. Mandić, L.J., Dragović, R., Dragović, S., 2010. Distribution of lithogenic radionuclides in soils of the Belgrade region (Serbia). *Journal of Geochemical Exploration* (2010), doi:[10.1016/j.gexplo.2010.03.001](https://doi.org/10.1016/j.gexplo.2010.03.001).

211. Taskin, H., Karavus, M., Ay, P., Topuzoglu, A., Hidiroglu, S., Karahan, G., 2009. Radionuclide concentrations in soil and lifetime cancer risk due to gamma radioactivity in Kırklareli, Turkey. *J. Env. Radioact.*, 100, 49-53.
212. Merdanoglu, B., Altinsoy, N., 2006. Radioactivity concentrations and dose assessment for soil samples from Kestanbol granite area, Turkey. *Radiat. Prot. Dosim.*, 121, 399-405.
213. Selvasekarapandian, S., 2001. Background radiation survey of the Nilgiris Biosphere of Peninsular India, Final report of the DAE/BRNS sponsored project, 1995-1999, Coimbatore, April, 2001.
214. Nageswara, M.V. et al., 1996. Natural radioactivity in soil and radiation levels of Rajasthan. *Radiat. Protect. Dosim.*, 63 (3), 631-642.
215. Mohanty, A.K., Sengupta, D., Das, S.K., Vijayan, V., Saha, S.K., 2004. Natural radioactivity in the newly discovered high background radiation area on the eastern coast of Orissa, India. *Appl. Radiat. Isot.*, 38(2), 153-165.
216. Baranwal, V.C., Sharma, S.P., Sengupta, D., Sandilya, M.K, Bhaumik, B.K., Guin, R., Saha, S.K., 2006. A new high background radiation area in the Geothermal region of Eastern Ghats Mobile Belt (EGMB) of Orissa, India. *Radiat. Measur.*, 41 602 – 610.
217. Mehra, R., Singh, S., Singh, K., Sonkawade, R., 2007. ^{226}Ra , ^{232}Th and ^{40}K analysis in soil samples from some areas of Malwa region, Punjab, India using gamma ray spectrometry. *Environ. Monit. Assess.*, 134 333–342.
218. War, S.A., Nongkynrih, P., Khathing, D.T., Iongwai, P.S., Jha, S.K., 2008. Spatial distribution of natural radioactivity levels in topsoil around the high-uranium mineralisation zone of Kylleng-Pyndensohiong (Mawthabah) areas, West Khasi Hills District, Meghalaya, India. *J. Env. Radioact.*, 99 1665–1670.

219. Sartandel, S.J., Jha, S.K., Bara, S.V., Tripathi, R.M., Puranik, V.D., 2009. Spatial distribution of uranium and thorium in the surface soil around proposed uranium mining site at Lambapur and its vertical profile in the Nagarjuna Sagar Dam. *J. Env. Radioact.*, 100, 831–834.
220. Singh, J., Singh, H., Singh, S., Bajwa, B.S., Sonkawade, R.G., 2009. Comparative study of natural radioactivity levels in soil samples from the Upper Siwaliks and Punjab, India using gamma-ray spectrometry. *J. Env. Radioact.*, 100, 94–98.
221. Rezzoug, S., Fernex, F., Michel, H., Barci-Funel, G., Barci1, V., 2009. Behavior of uranium and thorium isotopes in soils of the Boréon area, Mercantour Massif (S.E. France): Leaching and weathering rate modeling. *J. Radioanal. and Nuc. Chem.*, 279(3), 801–809.
222. Štok, M., Smodiš, B., 2010. Fractionation of natural radionuclides in soils from the vicinity of a former uranium mine Zjirovski vrh, Slovenia. *J. Environ. Radioact.*, 101, 22–28.
223. Dowdall, M., O’Dea, J., 2002. $^{226}\text{Ra}/^{238}\text{U}$ disequilibrium in an upland organic soil exhibiting elevated natural radioactivity. *J. Envir. Radioact.*, 59, 91–104.
224. Blanco, P., Vera Tome, F., Lozano, J.C., 2005. Fractionation of natural radionuclides in soils from a uranium mineralised area in the south-west of Spain. *J. Environ. Radioact.*, 79(3), 315–330.
225. Yeboah, J., Boadu, M., Darko, E. O., 2001. Natural radioactivity in soils and rocks within the Greater Accra Region of Ghana. *Journal of Radioanalytical and Nuclear Chemistry*, 249(3), 629–632.

226. Olley, J. M., Roberts, R.G., Murray, A. S, 1997. Disequilibria in the uranium decay series in sedimentary deposits at allen's cave, nullarbor plain, australia: implications for dose rate determinations. *Radiat. Measur.* 27 (2) 433-143.
227. Perez Del Villar, L., Crespo, M. T., Pardillo, J., Pelayo, M., Galan, M. P., 1996. U and Th Series Disequilibrium in Unaltered and Hydrothermally-altered Granites from the El Berrocal Site (Spain): Weathering Effects. *Appl. Radiat. Isot.* Vol. 47 (9/10), 1115-1119.
228. Andersen, M.B., Erel, Y., Bourdon, B., 2009. Experimental evidence for ^{234}U - ^{238}U fractionation during granite weathering with implications for $^{234}\text{U}/^{238}\text{U}$ in natural waters. *Geochim. Cosmochim. Acta*, 73, 4124–4141.
229. Pekala, M., Kramers, J.D., Waber, H.N., 2010. ^{234}U - ^{238}U activity ratio disequilibrium technique for studying uranium mobility in the Opalinus Clay at Mont Terri, Switzerland. *App. Radiat. Isot.*, 68, 984–992.
230. Dawood, Y.H., 2001. Uranium-series disequilibrium dating of secondary uranium ore from the south Eastern Desert of Egypt. *App. Radiat. Isot.*, 55, 881–887.
231. Airey, P.L., 1986. Radionuclide migration around uranium ore bodies in the alligator rivers region of the northern Territory of Australia-analogue of radioactive Waste repositories - A Review. *Chem. Geo.*, 55, 255-268.
232. Abdelouas, A., 2006. Uranium mill tailings: geochemistry, mineralogy, and environmental impact. *Elements*, 2 (6), 335–341.
233. Schimmanck, W., Klotz, D., Schramel, P., Bunzl, K., 1998. Leaching of natural Radionuclides and heavy metals from uranium mill tailing material as observed in laboratory and outdoor column experiments, In: Merkel, B., Helling, C. (Eds.), *Uranium Mining and Hydrogeology. GeoCongress II Verlag Sven von Loga Köln/FRG* 5: 310–317.

234. Maas, S., Scheier, R., Benslama, M., Crini, N., Lucot, E., Brahmia, Z., Benyacoub, S., Giraudoux, P., 2010. Spatial distribution of heavy metal concentrations in urban, suburban and agricultural soils in a Mediterranean city of Algeria. *Environ. Pollut.*, doi:10.1016/j.envpol.2010.02.001
235. Nael, M., Khademi, H., Jalalian, A., Schulín, R., Kalbasi, M., Sotohian, F., 2009. Effect of geo-pedological conditions on the distribution and chemical speciation of selected trace elements in forest soils of western Alborz, Iran. *Geoderma* 152, 157-170.
236. Reeves, J.B., Smith, D.B., 2009. The potential of mid and near-infrared diffuse reflectance spectroscopy for determining major and trace-element concentrations in soils from a geochemical survey of North America. *App. Geochem.* 24, 1472–1481.
237. Teng, Y., Ni, S., Wang, J., Zuo, R., Yang, J., 2010. A geochemical survey of trace elements in agricultural and non-agricultural topsoil in Dexing area, China. *J. Geochem. Expl.* 104, 118–127.
238. Saby, N.P.A., Thioulouse, J., Jolivet, C.C., Ratié, C., Boulonne, L., Bispo, A., Arrouays, D., 2009. Multivariate analysis of the spatial patterns of 8 trace elements using the French soil monitoring network data. *Sci. Tot. Env.*, 407, 5644–5652.
239. Tijani, M.N., Okunlola, O.A., Abimbola, A.F., 2006. Lithogenic concentrations of trace metals in soils and saprolites over crystalline basement rocks: A case study from SW Nigeria. *Journal of African Earth Sciences*, 46, 427–438.
240. El-Taher, A., 2007. Rare-earth elements in Egyptian granite by instrumental neutron activation analysis. *App. Rad. and Isot.*, 65, 458–464.

241. Middelburg, J.J., Van Der Weijden, C.H., Woittiez, J.R.W., 1988. Chemical processes affecting the mobility of major, minor and trace elements during weathering of granitic rocks. *Chem. Geo.*, 68, 253-273.
242. Donahue, R., Hendry, M.J., Landine, P., 2000. Distribution of arsenic and nickel in uranium mill tailings, Rabbit Lake, Saskatchewan, Canada. *App. Geochem.* 15, 1097-1119.
243. Anders and Grevesse, 1989. Abundances of elements: meteoric and solar. *Geochimica et Cosmochimica Acta*, 53, 197-214.
244. Henderson P., 1984. *Rare Earth Element Geochemistry*. Elsevier, Amsterdam, 510.
245. Unruh, D. M., Budahn, J. R., Siems, D. F., Byers Jr. F. M., 2001. Major and trace element geochemistry; lead, strontium and neodymium isotopic compositions; and petrography of late Cenozoic basaltic rocks from west central Colorado. USGS Open file report 01- 477, 41.
246. Hannigan, R., Dorval, E., Jones C., 2010. The rare earth element chemistry of estuarine surface sediments in the Chesapeake Bay. *Chem. Geo.*, doi:10.1016/j.chemgeo.2010.01.009.
247. Hartányi Z.et. al, 2000. Determination of the trace elements distribution of polluted soils in Hungary by X-ray methods. *Microchem. Journal*, 67, 195-200.
248. Horváth, T., Szilágyi, V., Hartyáni, Zs., 2000. Characterisation of trace element distributions in soils. *Microchem. Journal*, 67, 53-56.
249. Peppas, T.K., Karfopoulos, K.L., Karangelos, D.J., Rouni, P.K., Anagnostakis, M.J., Simopoulos, S.E., 2010. Radiological and INAA determined characteristics of size-fractionated fly ash, *Journal of Hazardous Materials*, doi:10.1016/j.jhazmat.2010.05.005.

250. Giuliano, V., Pagnelli, F., Bornoroni, L., Toro, L., Abbruzzese, C., 2007. Toxic elements at a disused mine district: Particle size distribution and total concentration in stream sediments and mine tailings. *J. Hazard. Mater.*, 45-59.
251. Sterkeman, T., Douay, F., Baize, D., Fourrier, H., Proix, N., Schwartz, C., 2004. Factors affecting trace element concentrations in soils developed on recent marine deposits from northern France. *App. Geochem.*, 19, 89-103.
252. Sierra, M., Martínez, F.J., Sierra, C., Aguilar, J., 2009. Correlations between pedological parameters in relation to lithology and soil type in Almería (SE Spain). *Journal of Arid Environments*, 73, 493–498.
253. Abdel Rahman, R.O., Zaki, A.A., El-Kamash, A.M., 2007. Modeling the long-term leaching behaviour of ^{137}Cs , ^{60}Co and $^{152,154}\text{Eu}$ radionuclides from cement-clay matrices. *J. Hazard. Mater.*, 145, 372-380.
254. El-Kamash, A.M., El-Naggar, M.R., El-Dessouky, M.I., 2006. Immobilisation of cesium and strontium radionuclides in zeolite–cement blends. *J. Hazard. Mater.*, 136, 310–316.
255. Moon, D.H., Dermatas, D., 2006. An evaluation of lead leachability from stabilised/solidified soils under modified semi-dynamic leaching conditions. *Eng. Geol.* 85, 67–74.
256. Nathwani, J.S., Phillips, C.R., 1980. Leachability of Ra-226 from uranium mill tailings consolidated with naturally occurring materials and/or cement: analysis based on mass transport equation. *Water Air Soil Pollut.* 14, 389–402. [21] Popek, E. M., 2003. Sampling and analysis of environmental chemical pollutants, Academic Press, Elsevier, USA.
257. Papadokostaki, K.G., Savidou, A., 2009. Study of leaching mechanisms of caesium ions incorporated in Ordinary Portland Cement. *Journal of Hazardous Materials*, 171, 1024–103.

258. Ogunro, V.O., Inyang, H.I., 2003. Relating Batch and Column Diffusion Coefficients for Leachable Contaminants in Particulate Waste Materials. *Journal of Environmental Engineering*, 129 (10) 930-942.
259. Sokić, M.D., Marković, B., Živković, D., 2009. Kinetics of chalcopyrite leaching by sodium nitrate in sulphuric acid. *Hydrometallurgy*, 95, 273-279.
260. Otero-Rey, J.R., Mato-Fernández, M.J., Moreda-Piñeiro, J., Alonso-Rodríguez, E., Muniategui-Lorenzo, S., Lopez-Mahía, P., Prada-Rodríguez, D., 2005. Influence of several experimental parameters on As and Se leaching from coal fly ash samples. *Anal. Chim. Acta*, 531, 299–305.
261. Brunori, C., Cremisini, C., D' Annibale, L., Massanisso, P., Pinto, V., 2005. A kinetic study of trace element leachability from abandoned-mine-polluted soil treated with SS-MSW compost and red mud. Comparison with results from sequential extraction. *Anal. Bioanal. Chem.*, 381, 1347-1354.

LIST OF PUBLICATIONS

- **Refereed journals**

1. **A. Chakrabarty**, R. M. Tripathi and V. D. Puranik. Occurrences of NORMS and ^{137}Cs in soils of the Singhbhum region of Eastern India and associated Radiation hazard. Radioprotection, vol. 44, no. 1, pp. 55-68 (2009).
2. **A. Chakrabarty**, S. Mohapatra, R. M. Tripathi, V. D. Puranik and H. S. Khushwaha. Quality control of uranium concentration measurements. Accred. Qual. Assur., vol. 15, no. 2, pp. 119-123 (2010).
3. S.K. Sahoo, S. Mohapatra, N.K. Sethy, **A. C. Patra**, A.K. Shukla, R.M. Tripathi and V.D. Puranik. Natural radioactivity in road side soil along Musabani-Jamshedpur road –a mineralised and mining region, Jharkhand and associated risk. Rad. Prot. Dosim., 2010, pp.1-6, doi:10.1093/rpd/ncq111.
4. **A. Chakrabarty Patra**, Sumesh C. G., S. Mohapatra, S. K. Sahoo, R. M. Tripathi and V. D. Puranik. Long term leaching of uranium from different waste matrices. Journal of Environmental Management, vol. 92, pp. 919-925 (2011).
5. **A. Chakrabarty Patra**, S. Mohapatra, S. K. Sahoo, R. H. Pillay, R. M. Tripathi and V. D. Puranik. Gamma spectrometric measurement of Radioactive disequilibrium in uranium deposits of the Singhbhum Shear zone, Eastern India. Submitted to Journal of Radiochimica Acta (2010).
6. **A. Chakrabarty**, V. N. Jha, S. K. Sahoo, R. M. Tripathi and V. D. Puranik. Assessment of Natural Radioactivity and Radioactive Disequilibria in surface soils, Singhbhum Shear Zone, Eastern India. Submitted to Environmental Monitoring and Assessment (2011).

- **Conference proceedings**

1. **A. Chakrabarty**, S. K. Sahoo, V. N. Jha, A. K. Shukla, R. M. Tripathi and V. D. Puranik (2008). Radioactive disequilibria and associated dose in surface soils of the Singhbhum region of Eastern India. Proc. of Indian association of Radiation Protection pp. 324-326.
2. **A. Chakrabarty**, R. M. Tripathi, S. K. Sahoo and V. D. Puranik (2008). Investigations on major and trace elements in rock samples from the Singhbhum belt using INAA technique. Proc. of Indian Analytical Science Congress, pp.108-110.
3. **A. Chakrabarty**, Sumesh C. G., S. Mohapatra, S. K. Sahoo, R. M. Tripathi and V. D. Puranik (2009). Release of uranium from different matrices under environmental conditions (2009). Proc. of Nuclear and radiochemistry Symposium, pp. 615-616.
4. **A. Chakrabarty Patra**, S. Mohapatra, S. K. Sahoo, R. H. Pillay, R. M. Tripathi and V. D. Puranik (2010). Natural Radioactive Disequilibrium in uranium ores and soils from the Singhbhum Shear Zone, Eastern India. Proc. of International Conference on Application of Radiotracers in Chemical, Environmental and Biological Sciences.